SNC - 2708-1
AEC R & D REPORT

SANDERS NUCLEAR CORPORATION
Nashua, New Hampshire

FINAL REPORT

DEVELOPMENT OF THE SIREN CAPSULE

PHASE I

(UNCLASSIFIED TITLE)

AEC CONTRACT NO. AT (29-2) - 2708

BY

ANDERSON, R.W., DESCHAMPS, N.H., REXFORD, H.E., TALBOT, M.

3 OCTOBER 1969

SAN-BWM-69-8935

DISCLAIMER

LEGAL NOTICE

This report was prepared as an account of Government-sponsored work. Neither the United States, nor the Atomic Energy Commission, nor any person acting on behalf of the Commission:

A. makes any warranty or representation, expressed or implied, with respect to the accuracy, completeness, or usefulness of the information contained in the report, or that the use of any information, apparatus, method, or process disclosed in this report may not infringe privately owned rights; or

B. assumes any liabilities with respect to the use of, or for damages resulting from the use of, any information, apparatus, method, or process disclosed in this report.

As used in the above, "person acting on behalf of the Commission" includes any employee or contractor of the Commission, or employee of such contractor, to the extent that such employee or contractor of the Commission, or employee of such contractor prepares, disseminates, or provides access to, any information pursuant to his employment or contract with the Commission or his employment with such contractor.

CONFIDENTIAL

UNCLASSIFIED

SNC - 2708-1

AEC R & D REPORT

FINAL REPORT

DEVELOPMENT OF THE SIREN CAPSULE

PHASE I

(UNCLASSIFIED TITLE)

3 OCTOBER 1969

BY

ANDERSON, R. W., DESCHAMPS, N. H., REXFORD, H. E., TALBOT, M.

SANDERS NUCLEAR CORPORATION
Nashua, New Hampshire

PREPARED UNDER

CONTRACT AT (29-2) - 2708

FOR THE

ALBERQUERQUE OPERATIONS OFFICE

U. S. ATOMIC ENERGY COMMISSION

SAN-BWM-69-8935 (Rev)

TABLE OF CONTENTS

TABLE OF CONTENTS (Cont)

TABLE OF CONTENTS (Cont)

UNCLASSIFIED

UNCLASSIFIED

TABLE OF CONTENTS (Cont)

TABLE OF CONTENTS (Cont)

BLANK

LIST OF ILLUSTRATIONS

LIST OF ILLUSTRATIONS (Cont)

LIST OF ILLUSTRATIONS (Cont)

LIST OF ILLUSTRATIONS (Cont)

LIST OF ILLUSTRATIONS (Cont)

LIST OF ILLUSTRATIONS (Cont)

LIST OF ILLUSTRATIONS (Cont)

BLANK

LIST OF TABLES

LIST OF TABLES (Cont)

LIST OF TABLES (Cont)

BLANK

ABSTRACT

The feasibility of the SIREN isotopic fuel capsule was evaluated by means of analyses and tests of design aspects critical to its successful performance. The feasibility of the SIREN concept was examined from four viewpoints:

- Fabricability and fueling of the capsule
- Ability to perform long-term missions
- Ability to withstand reentry conditions
- Ability to confine the fuel after impact.

Evaluation of the test data and the analyses indicate the SIREN concept could be developed into a successful isotopic fuel system using PuO_2 fuel as either microspheres or solid forms. The status of the technologies required for fabrication of the SIREN capsule are discussed and the areas requiring further development identified.

BLANK

SECTION 1
INTRODUCTION

This program, Development of the Sanders Intact Reentry Encapsulation (SIREN) Fuel Capsule, Phase I, fulfills the terms of Contract AT (29-2)-2708 for the period February 1, 1969 to June 30, 1969.

The objective of Phase I was to evaluate and establish the feasibility of the SIREN fuel capsule concept with the following design criteria:

- Five-year service life after six months of pre-launch storage
- Minimize stresses on the capsule by helium venting
- Minimum of one year fuel containment after impact in soil or water

It is to this end that critical aspects of the SIREN concept have been tested and analyzed.

The SIREN concept is one wherein the fuel capsule contains no metallic components, but rather, uses only high temperature non-metallic materials. The basic capsule is a multi-component structure comprising the following, starting with the innermost component:

- The isotopic fuel source ($Pu^{238}O_2$) - microspheres, sintered oxide, solid-solution oxides or cermets
- The liner - a thin shell of ceramic that provides primary containment; for the solid fuel forms the liner would probably be integral with the fuel

- The dual-purpose structural and heat shield - a shell comprised of many layers of continuously wound graphite yarn impregnated with pyrolytically deposited carbon
- The oxidation protection layer - a coating on the outer surface of the graphite shell

The SIREN type of capsule can be fabricated in a variety of shapes and sizes; the test capsules used in Phase I were spheres 3 inches in diameter. The spherical form was selected for study because such a capsule can be readily fabricated with radially isotropic properties. Methods of analyses and testing were simplified and generally provided more reliable values for evaluation than could be expected from a non-spherical shape.

The following sections of this report discuss the fabrication and testing of the SIREN concept accomplished in Phase I and analyses performed to establish the feasibility of the concept. Since the SIREN capsule is yet in its preliminary stage of development, the test data reported are not necessarily representative of optimized capsule designs.

Particular attention is invited to Paragraph 4.6, Comparative Analysis, in which the program objective is accomplished by bringing together the results of the analyses and tests in an overall evaluation.

SECTION 2
SUMMARY

A series of tests and analyses were performed to evaluate the feasibility of the SIREN concept of an isotopic fuel capsule within the following design criteria:

- "Five-year service life after six-month pre-launch storage."
- "Minimize stresses on the capsule by helium venting."
- "Minimum of one year fuel containment after impact in soil or water."

The feasibility of the SIREN concept was examined from five viewpoints with the realization that the development of the SIREN is yet in the preliminary stage and that specific design and mission requirements were not defined:

(1) The fabricability of the non-fueled SIREN capsule was demonstrated by the successful fabrication of 35 capsules. Analyses of methods for fueling the capsule with PuO_2 indicate fueling can be reasonably performed after some development effort. If the capsules were fueled with PuO_2 as microspheres, development of capsule closure methods would be required. If fueled with solid PuO_2 forms, methods for "hot" fabrication would be required. Development efforts in both cases would involve extension of existing technologies to these specific problems.

(2) Several aspects of the SIREN capsules' ability to perform long-term missions were tested. Specifically, oxidation resistance, helium permeability, and thermal conductivity of the graphite/carbon composite structure were tested.

It was concluded from the test data that the helium permeability and thermal conductivity were definitely within the expected useful range for these design parameters. Depending on specific mission requirements, the graphite/carbon structure may or may not require oxidation protection. If oxidation protection were required, methods of application of such coatings would need additional development.

(3) The ability of the SIREN capsule to survive the environment of a solid propellant fire was demonstrated via test.

(4) The ability of the SIREN capsule to survive the conditions imposed by spinning and non-spinning reentry from orbital and superorbital trajectories was successfully demonstrated via plasma-arc tests.

(5) Impact tests performed with capsules containing solid ceramic cores gave indication that capsules containing solid fuel forms could be safely impacted, i.e., the fuel contained. No tests were performed to assess the ability of the SIREN capsule to contain fuel in the microsphere form. Analysis of impact induced fracture of the graphite/carbon structures resulted in findings expected to yield significant improvement of impact resistance.

SECTION 3
SIREN CAPSULE FABRICATION

3.1 INTRODUCTION

In support of the various testing tasks, a group of 35 test capsules were fabricated. All capsules were fabricated with a 1/2-inch thick shell of carbon impregnated graphite yarn to a finished diameter of 3-1/8-inches. As required by the respective testing tasks, 11 of the capsules were prepared with solid ceramic cores, 22 capsules were prepared with hollow cores (no liner material), and two capsules were prepared with hollow quartz cores. Those capsules requiring oxidation protection were coated with a thin layer of B_6Si as a final operation. To allow correlation of the resulting test data, the graphite/carbon shell on all capsules was fabricated by the same procedures, using the same lots of starting materials, and when possible, processed (impreganted) as a single lot. Figure 3-1 shows a typical test capsule.

3.2 MATERIALS

3.2.1 THE GRAPHITE YARN

The graphitized yarn selected for the initial SIREN study had an ideal texture to provide a close lay that assured identically small voids for later impregnation of the carbon media. The yarn used for the capsules was GSGY-2-5 produced by the Carborundum Company. The yarn was produced from continuous filaments; 480 filaments per each of the five plies giving a total of 2400 filaments for each yarn bundle. Such a pliant yarn was indeed suitable for the great circle nonpolar

SANDERS NUCLEAR CORPORATION

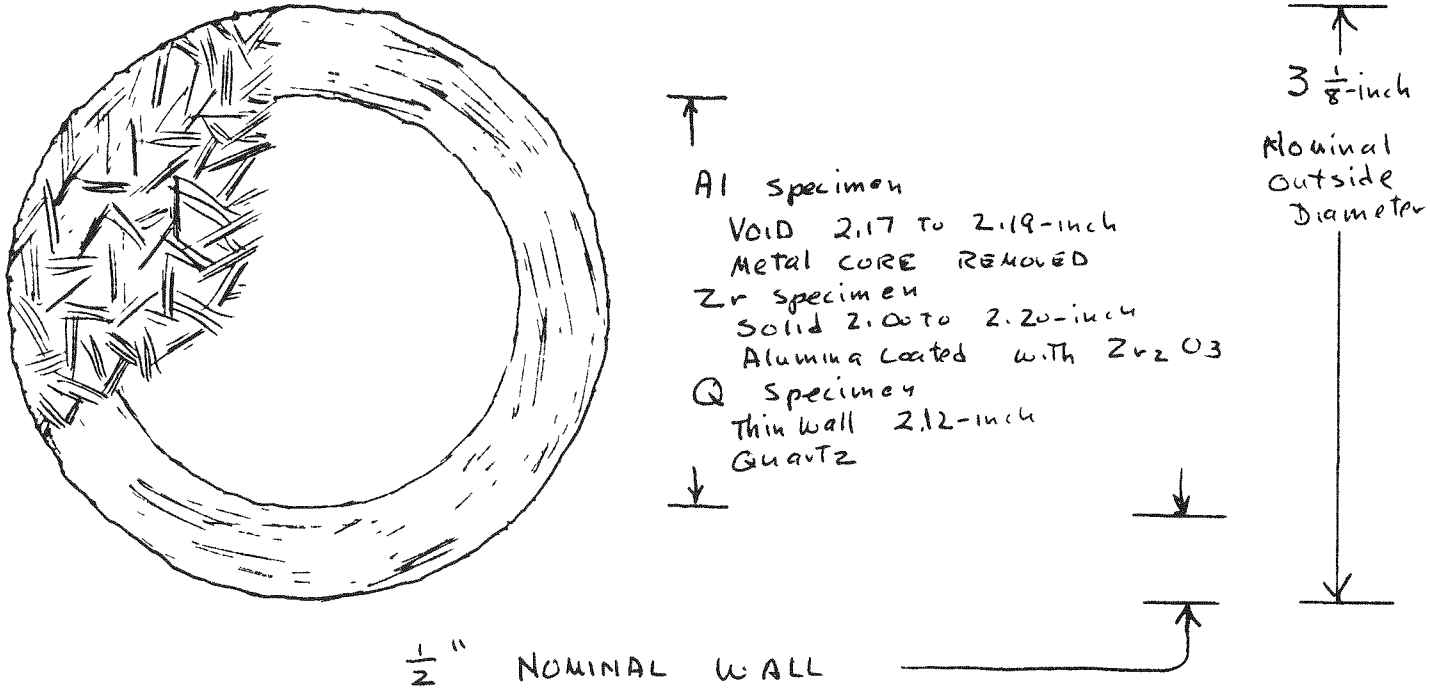

69-H65983-001

Figure 3-1 Typical Test Capsule

winding pattern chosen. The yarn averages 17.6 feet/gram (specified 1750 denier or grams per 9000 linear meters) with a 2.6-inch twist in each ply and a 1.1-inch twist for the assembled five plies as a yarn. Breaking strength averages eight pounds. The yarn was wound on a 2-1/8-inch form to an overall diameter of 3-1/8 inches; this typically required 2200 linear feet at the tension selected for winding.

3.2.2 ZIRCONIA COATED ALUMINA CORE

The cores initially specified were 2-1/8-inch hollow spheres of zirconium oxide with a 0.1 inch wall; procurement could not be made in the time available to complete Phase I and thus selection of an alternate core become essential. Alumina solid spheres were substituted to provide the base for yarn wrapping for those capsules designated for plasma arc and impact testing.

Harbison-Walker Refractories Company of Pittsburgh, Pa. isostatically pressed the 99% pure alumina to provide 2-inch solid cores with an apparent specific gravity of 3.75 and suitable for service temperature to 3500°F. The Harbison-Walker designation (type HW 40-63) is for a 2-inch thermal sphere for use in ball milling. The as received dimensions were of the order of 2.0 to 2.2 inches and the spheres were generally "egg shaped", typical of the product of the isostatic pressing technique. Consequently, it was necessary to abrasively remove material to reduce the out-of-roundness to no greater than 50 mils (0.050 inch) with no surface defect in excess of 30 mils.

To avoid possible interaction between alumina and graphite in the impregnation process, the alumina spheres were flame-sprayed with zirconia to provide a compatible interface. A proprietary process of Metallizing Service Company of Elmwood, Conn. was used. It results in an adherent, dense coating of zirconium oxide with a purity in excess of 90%; the zirconia is stabilized with 5% calcium oxide. Other constituents, each less than 1%, are magnesium oxide, silicon dioxide, and titanium dioxide. After drying the substrate at 200°F for

an overnight cycle, the spheres were plasma flame-sprayed; (this induced a liquefaction of the high temperature solids with subsequent deposition on the sphere). A coating of 4 to 6 mils was confirmed by physical measurement and by weight check. The ZrO_2 coated Al_2O_3 solid core shown in Figure 3-2.

3.2.3 ALUMINUM METAL FORMS

In some of the testing programs it was necessary to provide a SIREN wound container without the usual solid ceramic core. Aluminum was used for the winding form because of the relative ease of removal by chemical means. Hydroforming of 1100 type aluminum by the Roland Teiner Company of Everett, Mass. produced flanged hemispheres which were butt welded as a sphere. To minimize the welding problem, a gas escape hole, 0.05-inch diameter, was drilled in the 0.028-inch container wall and the external weld bead was ground flush. By using available tooling to minimize the delivery time span, a sphere with a 2.125-inch internal diameter with overall outer dimensions that varied from 2.17 to 2.19 inches was produced. The weight of the metal core averaged 25 grams. A typical hollow aluminum sphere is shown in Figure 3-3. After winding, the aluminum was chemically removed.

3.2.4 QUARTZ CORE

Hand blown quartz spheres were used in two of the SIREN capsules as a core having minimum weight but sufficient strength to restrain the peripheral tension of the wrapped yarn. They were somewhat irregular with a diameter of 2-1/8 inches with a 1/16-inch wall. An access hole of 3/8-inch diameter was necessary to facilitate the glass blowing operation. The weight was approximately 16 grams.

3.3 WINDING OPERATIONS

The graphite yarn was successively wrapped around the rigid core in a continually changing polar pattern in a manner similar to the winding of a golf ball. Prior to inserting the core into the winding machine, the surface was

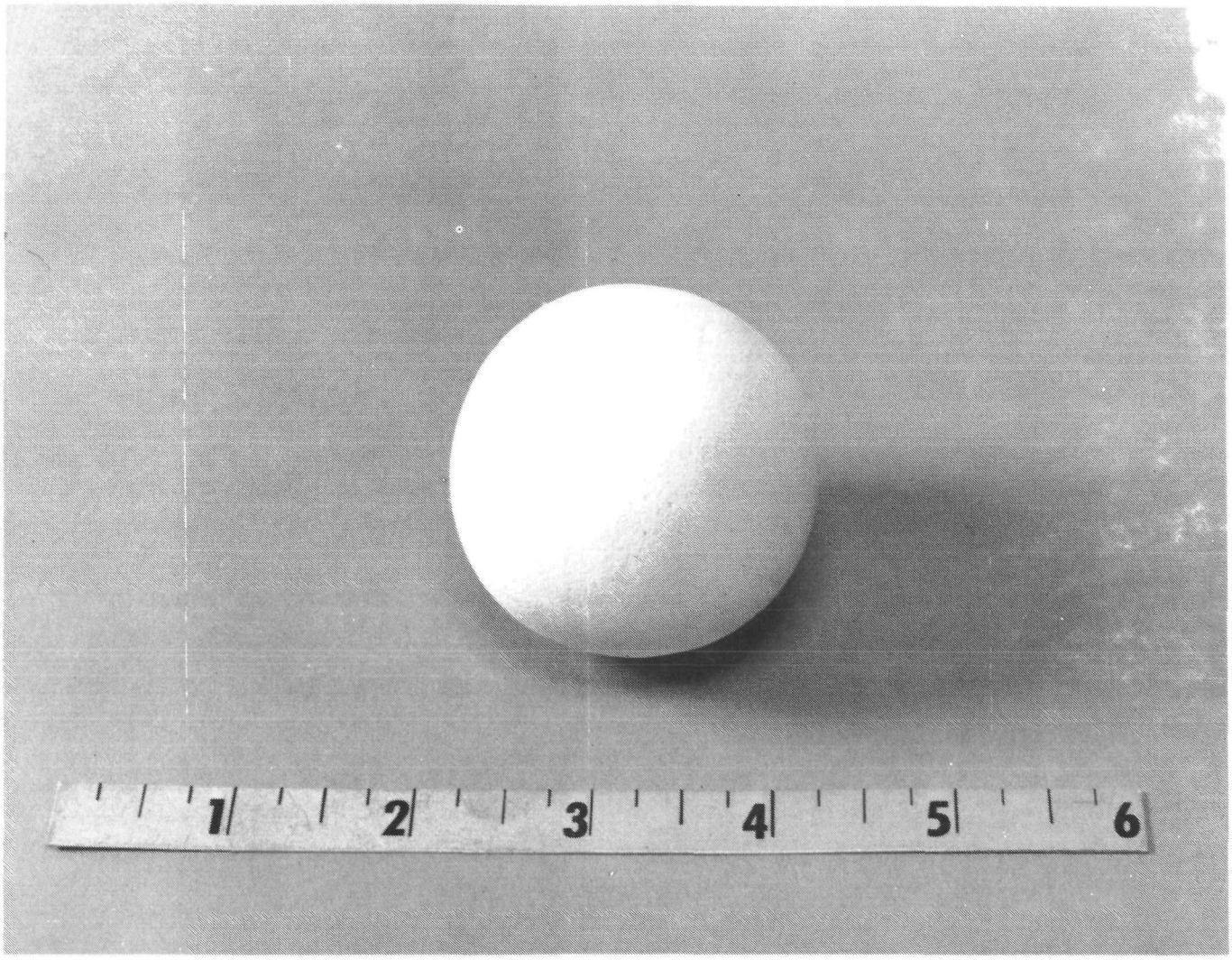

69-311-2

69-H65983-096

Figure 3-2 Solid Al_2O_3 Sphere Coated with ZrO_2.

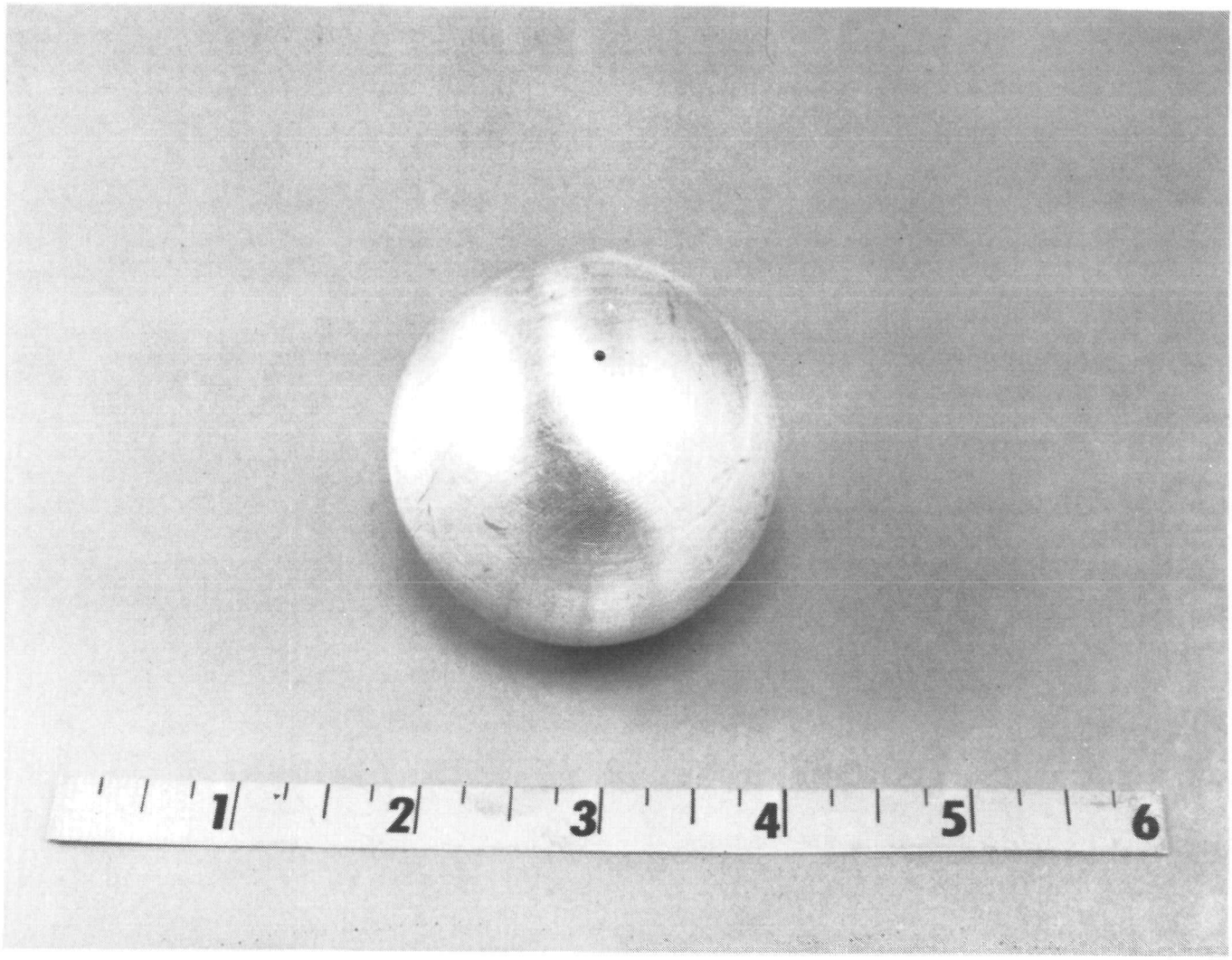

69-311-3

69-H65983-097

Figure 3-3 Typical Hollow Aluminum Sphere Used as a Base for Winding.

cleaned with a solvent and then coated with an organic adhesive to pick up the end of the yarn. As rotation started, the yarn was pulled from the feed spool and was coated with a thin film of adhesive to assure positive placement during winding. During subsequent thermal treatments, the adhesive decomposes leaving a small amount of carbonaceous residue.

The capsule ball winding machine (originally a golf-ball winding machine) had been modified to wind capsules to about 4-inches in diameter. The two winder heads were independently mounted on tracks to oppose each other with adjustable weights used to provide the pressure needed to hold the core in place. A hanging weight of 50 pounds provides a jaw pressure of 40 pounds on the sphere in the jaws. Each head rotates, and within each head a planetary gear drives the three rubber nosed winder jaws as a finger motion to incrementally index the core thus inducing a cross rotation for a great circle wind of the yarn. Pressure imposed on the spheres by the winder head is critical to assure control of yarn slippage. Excessive pressure, however, will cause the rubber jaws to scuff the wound yarn and too little pressure results in improper tracking and unevenness.

The yarn lay rate is governed by the speed of the core rotation in the winder machine. Figure 3-4 illustrates the yarn winding machine. As the yarn is lifted from the end of the 8000-foot capacity spool, it is guided to the adhesive bath of one part Bond Adhesives Company's "Pliobond" (Ht 30) cement to twenty parts of methylethyl ketone. The yarn is totally immersed while passing through a guide tube in the adhesive tank; it then passes through a wiping sponge which spreads the adhesive out evenly over the yarn surface. Quick passage through a 12-inch tubular hot air furnace partially sets the adhesive. The yarn then passes around two General Electric hysteresis tension clutches in series to provide the required wrapping tension. An increase in tension provides an increase in densification of the winding but tends toward unevenness in the surface configuration of the ball. Too low a tension will increase the void dimensions in the lay of yarn and thus prohibit a practical impregnation by the follow-on process. Capsules were wound

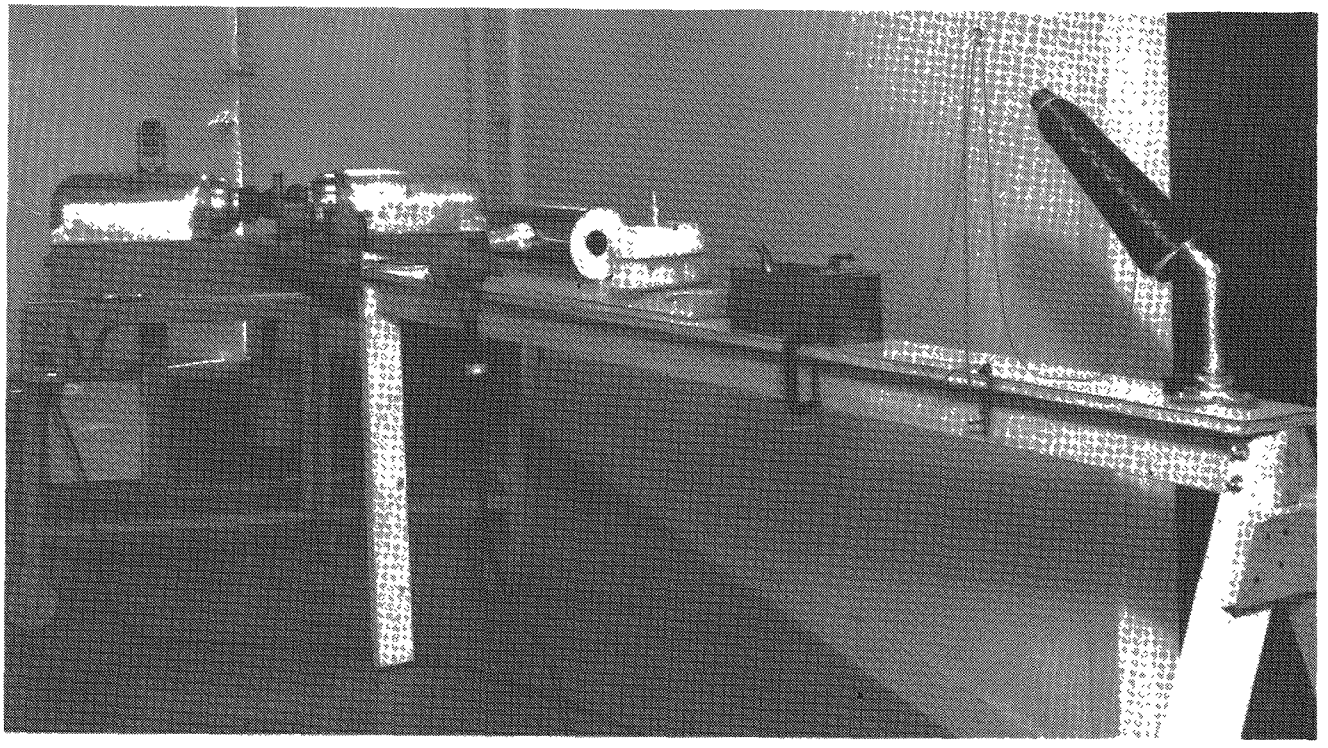

68-0809-1

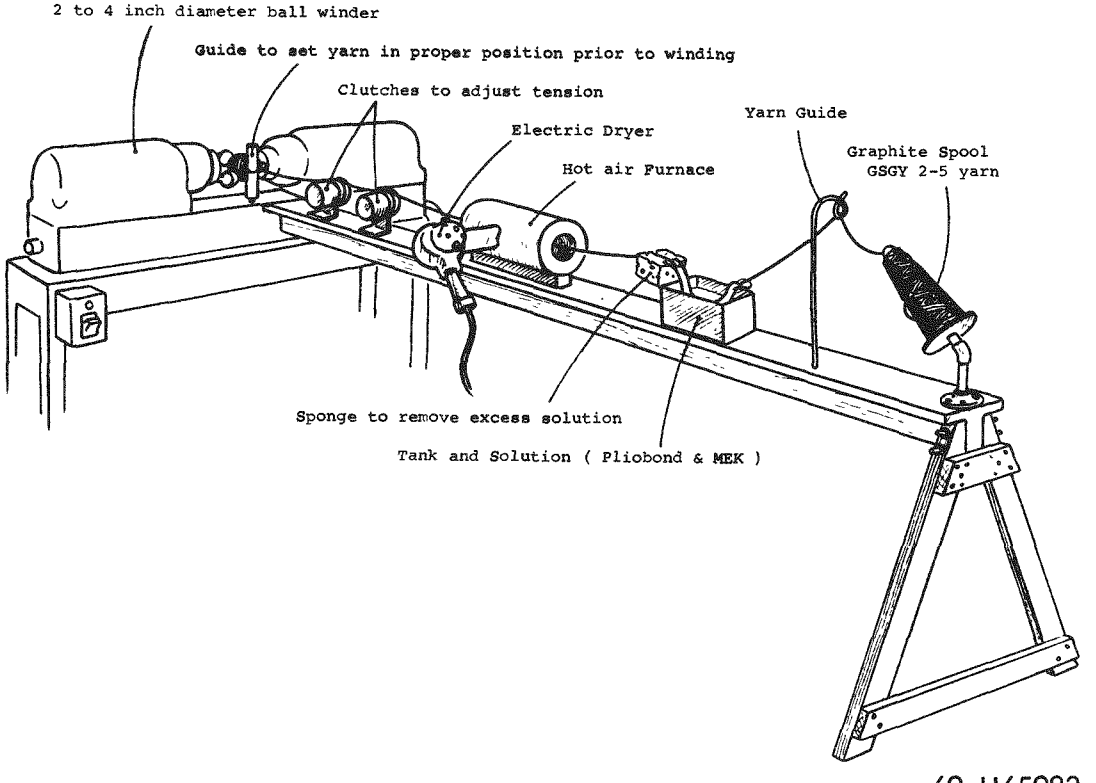

69-H65983-002

Figure 3-4 Yarn Winding Machine.

with a yarn tension of about five pounds. Figures 3-5 and 3-6 show the winding of the capsule at the beginning and end of the winding operation. An "as wound" capsule is shown in Figure 3-7.

In a typical operation, the rigid core is mounted in the winder heads and the yarn is threaded from the spool through the adhesive tank and furnace, over the two clutches and about the vertical guide for several turns about the core. The ball winder motor speed is quickly increased to about 84 RPM and the clutch adjustments are changed as necessary while the winding continues. Furnace temperature is controlled to maintain a tacky condition of the wrapping yarn. The wound SIREN capsule is removed from the machine and placed in a drying oven at about 95°F for two days, or until constant weight is achieved to remove the volatile carrier of the yarn adhesive.

3.4 REMOVAL OF METAL CORE

The aluminum cores of 1100 alloy are used as a rigid member to mount the graphite yarn for wrapping a heavy wall configuration. This metal is removed prior to exposure of the ball to the elevated temperature of the carbon impregnation run. After drilling a 1/4-inch diameter hole in the capsule wall to penetrate the aluminum liner, the unit was weighed to determine the initial process condition. The unit was then positioned in a 1000-ml beaker on a hot plate to contain the overflow of the 15% sodium hydroxide solution that is circulated for the metal removal. This set up (see Figure 3-8) installed in a fume hood, uses a tube funnel inserted in the access hole, with sufficient clearance to permit a reverse flush. The solution, heated to 120°F, is circulated into the capsule and the overflow is contained in the beaker. It is recycled as ncecessary to maintain a flow. A typical schedule is six hours to complete the metal removal reaction. Clear water is then flushed through the capsule for a minimum of two hours prior to air drying at 120°F for two days, or until a constant weight is achieved. The weight differential before and after the dissolution cycle was measured to assure that the process was completed, i.e., that the aluminum sphere was totally reacted and removed.

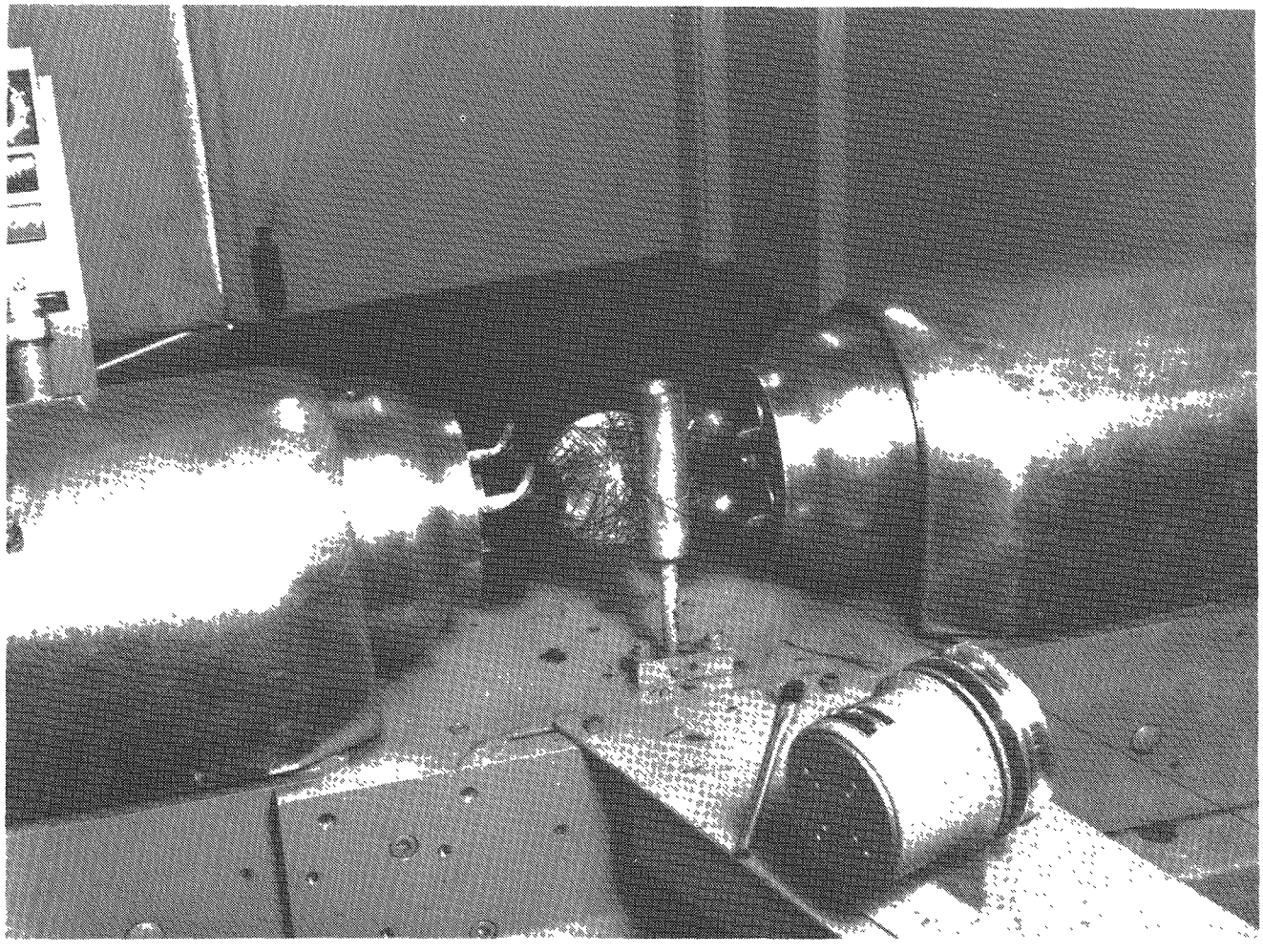

68-0809-3

69-H65983-098

Figure 3-5 Beginning of Capsule Winding Cycle.

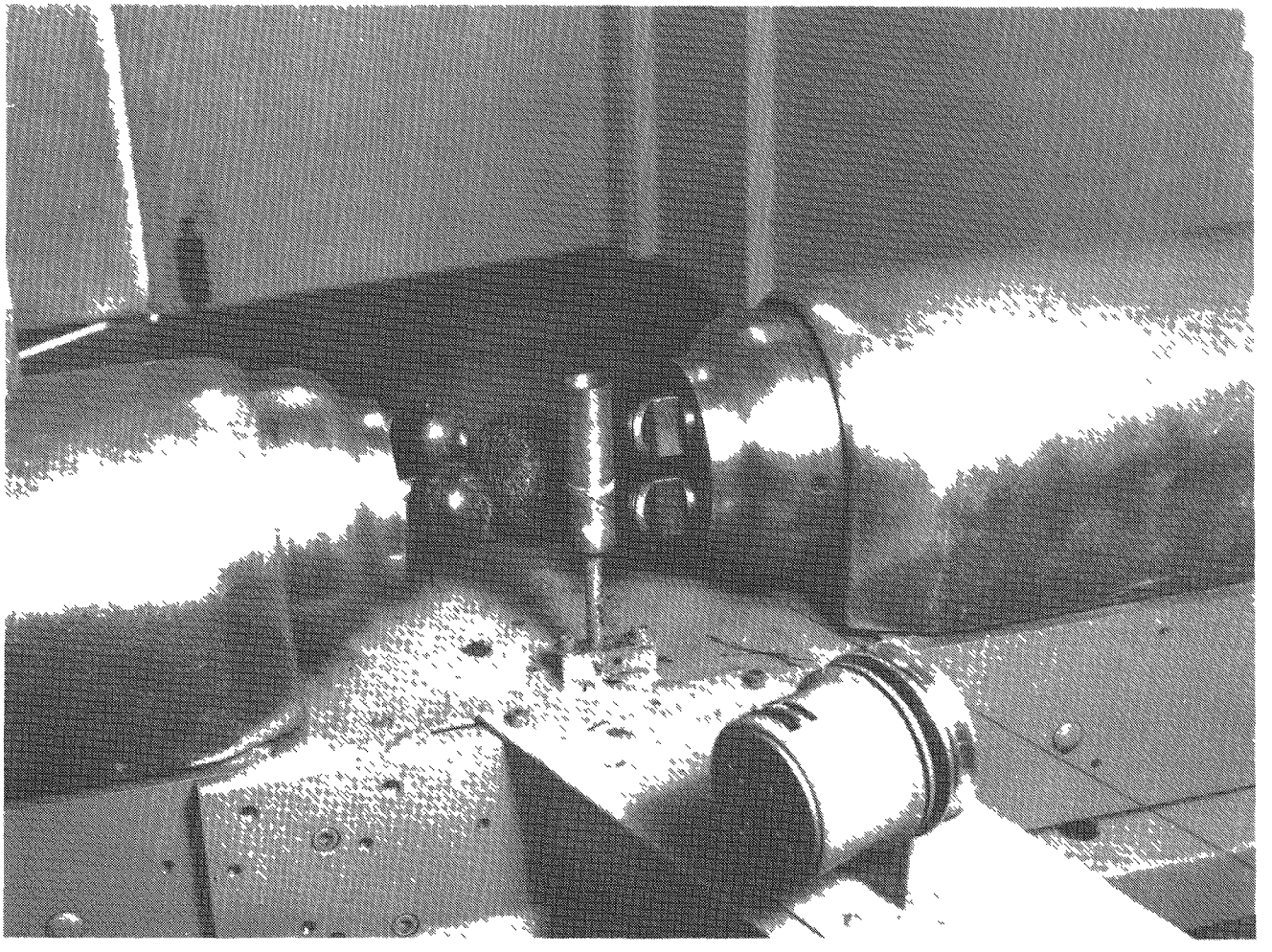

68-0809-2

69-H65983-099

Figure 3-6 Ending of Capsule Winding Cycle.

69-311-1

69-H65983-100

Figure 3-7 "As Wound" Test Capsule.

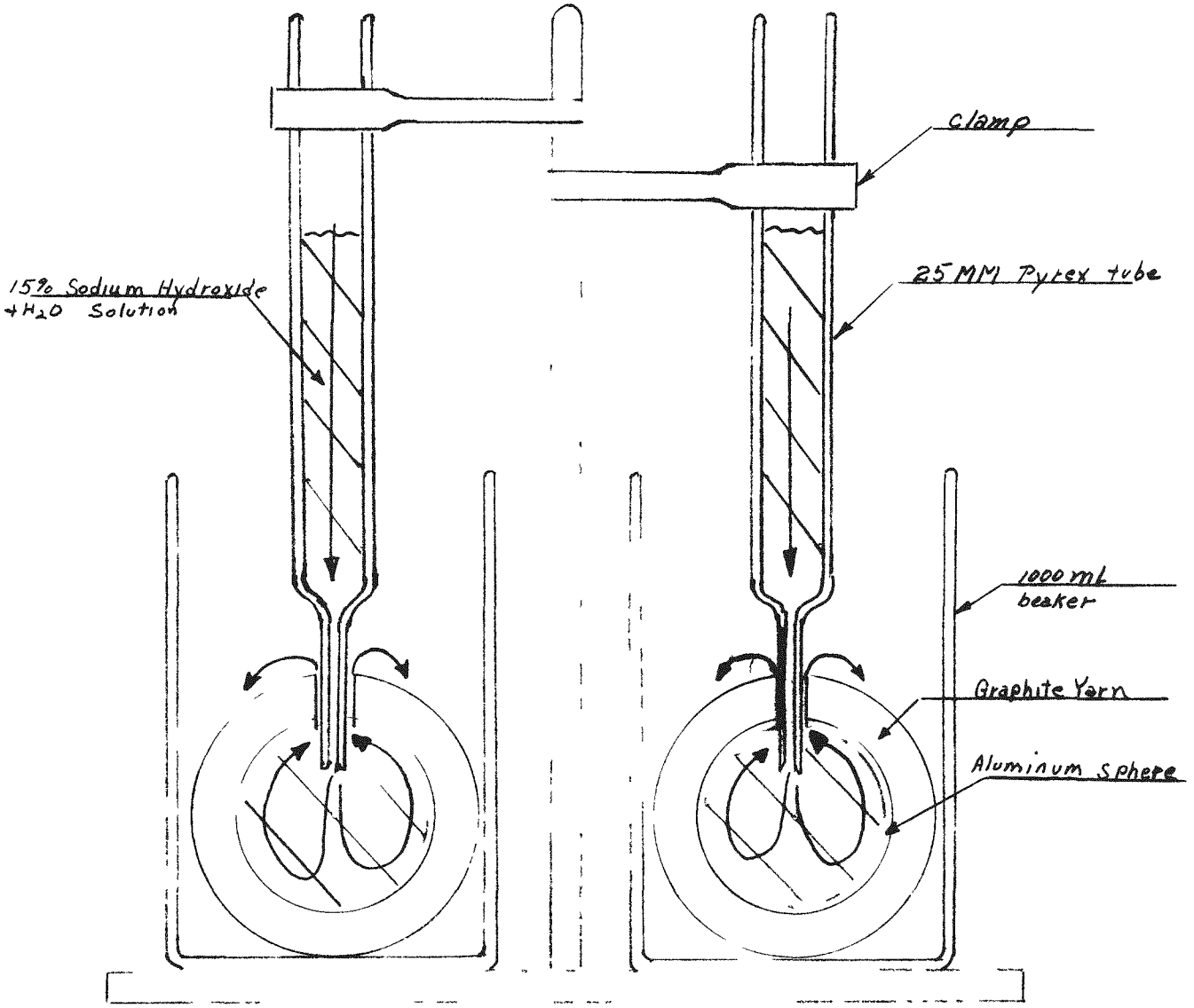

69-H65983-003

Figure 3-8 Aluminum Core Removal Setup.

3.5 CARBON IMPREGNATION

The rigidly wound graphite yarn requires impregnation by a high temperature material to lock the intersecting filaments into a fixed condition. The Pliobond adhesive solids are sufficient to maintain the configuration during the initial phase of the furnace cycle. However, as the impregnation cycle progresses, the adhesive is burned out, and the pyrolytically deposited carbon welds the lay of yarn together and fills the interstices within the wound structure. As the process approaches completion, the density approaches 1.6 grams/cc (100 lb/ft^3) with minimal porosity.

The pyrolizing operation is a proprietary process of Supertemp Corp. of Santa Fe Springs, California. The operation was performed in a vacuum chamber with three shelves (see Figure 3-9) to position the product. Each sphere was supported on a machined graphite jig having three contacts points in a ring configuration to afford the greatest accessibility for the carbonaceous vapor. Identity of the sphere was maintained by a location chart. After the furnace load was secured for processing, the vessel was evacuated to the order of 10^{-3} torr. When the vacuum stabilized, indicating that gas removal was complete, the vessel was back-filled with nitrogen and a purge established. Subsequently, the parts were brought to a temperature of 2050°F and a flush of hydrogen was initiated to clean the graphite by etching. The start up procedure required 24 hours to arrive at stable operating conditions. Natural gas, which is predominantly methane and is the simplest of the saturated hydrocarbons, was then passed over the heated surfaces of the capsules. Upon contact with the hot capsules, the gas was decomposed, resulting in the deposit of carbon. Typically, a carrier gas with a catalyst is employed with the methane, using a total gas pressure of about one-half atmosphere. At the proper temperature and pressure, pyrolysis occurs and the desired material deposits on the yarn in relatively anisotropic layers following the configuration of the substrate yarn. The pyrolytic material can be partially controlled through changes in pressures, temperature

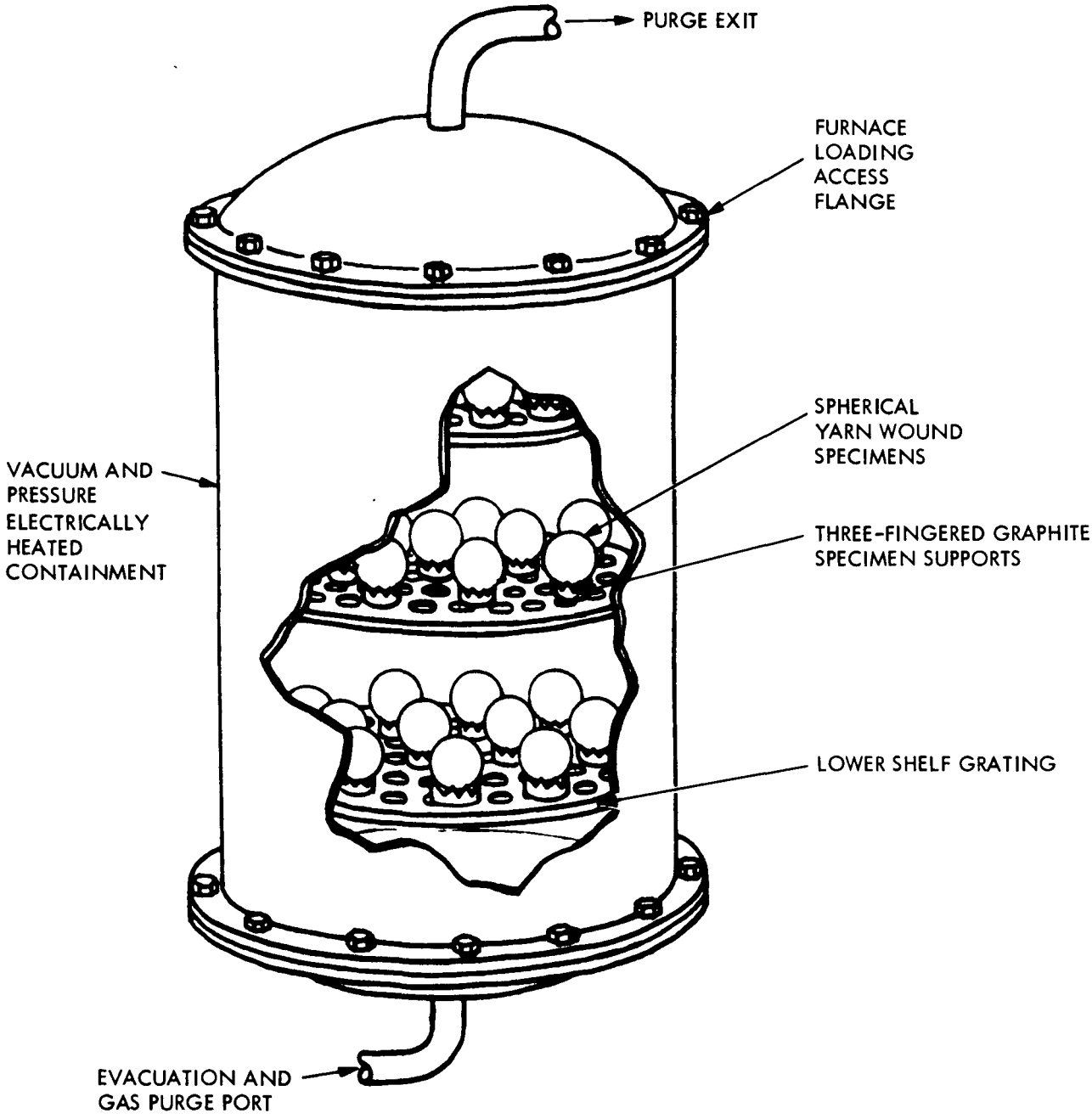

Figure 3-9. Pyrolizing Operation.

and the gas composition input. Typical deposition time is 60 hours at temperature. Approximately 25% of the natural gas is cracked in the furnace to form the pyrolytically deposited carbon. To complete the cycle requires an additional 24 hours for cooling. The SIREN capsules were so prepared in a single furnace loading utilizing a double cycle; the first cycle was 108 hours and the second, 76 hours. Between cycles, samples were removed for evaluation and were found to be satisfactory.

3.6 OXIDATION COATING

The carbon impregnated specimens are subject to oxidation at elevated temperatures. Boron silicide (B_6Si) is a suitable oxidation coating and can be plasma flame-sprayed as described in the section on zirconium oxide coating on the alumina spheres. This process too, is considered proprietary to Metallizing Service Company of Elmwood, Connecticut. The jig for support of the carbon impregnated specimens is also a three-fingered graphite holding tool in a fume hood, with the spraying done by hand. The coating material is subject to temperatures on the order of 20,000°F. Actually the plasma forming gas is blown into a container around an arc before leaving an exit orifice as a hot gas. This gas contacts with the metered flow of ceramic powders to form a molten liquid for deposition on the SIREN specimen. Actual pick up of material was calculated from the weight increase of the sphere. (See Table 3-1.)

3.7 CAPSULE EVALUATION

After the initial furnace cycle was completed, the SIREN specimens were examined to determine what further processing was required. In a cross section of a hollow specimen, wherein the rigid core had been removed by chemical dissolution for special tests, it was noted that the outer 0.4 inch of the 1/2 inch wall was impregnated whereas the collapsed inner windings received very little carbon. (Figure 3-10.) The collapse of the inner windings is graphic evidence that the inner wall was under compression due to the winding tension. The

TABLE 3-1

CAPSULE WEIGHT DATA

CAPSULE IDENTITY	Core Weight (Grams)	After Winding Air Cured (Grams)	Adhesive Set Yarn Weight (Grams)	Density of Wound Structure (Calculated) (Grams/cc)	First Cycle Impregnation Weight (Grams)	First Cycle Density (Grams/cc)	Second Cycle Impregnation Weight (Grams)	Second Cycle Density (Grams/cc)	B_6Si Coating Pickup (Grams/mils)	TEST USE
Note A	Note B	Note C	Note D	Note E	Note F	Note E	Note F	Note E	Note G	
A1 1	24		-							Process Evaluation
2	24	150	126	0.70	219	1.21	None	None	4.5/3.5	FIREBALL
3	25	153	138	0.77	227	1.28	258	1.44	1.6/1.3	OXIDATION
4	24	159	135	0.75	245	1.37	-	-	2.0/1.6	FIREBALL
5	24	154	130	0.72	235	1.31	-	-	-	Process Evaluation
6	24	149	125	0.69	232	1.30	258	1.44	-	OXIDATION
7	24	148	124	0.69	-	-	254	1.42	-	THERMAL COND
8	25	157	132	0.77	-	-	266	1.48	1.1/0.8	OXIDATION
9	26	161	135	0.75	-	-	270	1.50	-	THERMAL COND
10	25	157	132	0.73	-	-	264	1.47	2.5/2.0	OXIDATION
11	26	145	119	0.66	-	-	252	1.40	-	THERMAL COND
12	26	160	134	0.75	-	-	268	1.50	1.9/1.5	OXIDATION
13	24	166	142	0.79	-	-	274	1.53	1.5/1.2	OXIDATION
14	25	156	131	0.73	-	-	266	1.48	3.7/2.9	OXIDATION
15	25	162	137	0.76	-	-	268	1.49	2.2/1.7	OXIDATION
16	26	161	135	0.75	-	-	260	1.45	2.7/2.1	OXIDATION
17	24	156	132	0.73	-	-	258	1.44	1.7/1.3	OXIDATION
18	25	166	141	0.79	-	-	254	1.42	-	PERMEABILITY
19	25	175	150	0.83	-	-	276	1.53	-	PERMEABILITY
20	25	167	142	0.79	-	-	265	1.47	-	PERMEABILITY
21	25	163	138	0.77	-	-	265	1.48	-	OXIDATION
A1 22	25	163	138	0.77	249	1.39	-	-	-	IMPACT

TABLE 3-1

CAPSULE WEIGHT DATA (CONT)

CAPSULE IDENTITY	Core Weight (Grams)	After Winding Air Cured (Grams)	Adhesive Set Yarn Weight (Grams)	Density of Wound Structure (Calculated) (Grams/cc)	First Cycle Impregnation Weight (Grams)	First Cycle Density (Grams/cc)	Second Cycle Impregnation Weight (Grams)	Second Cycle Density (Grams/cc)	B_6Si Coating Pickup (Grams/mils)	TEST USE
Note A	Note B	Note C	Note D	Note E	Note F	Note E	Note F	Note E	Note G	
Zr 1	276	423	147	0.81	223	1.23	247	1.36	2.5/2.0	PLASMA
2	278	426	148	0.81	223	1.23	-	-	2.0/1.6	FIREBALL
3	265	411	146	0.80	-	-	247	1.37	3.2/2.5	-
4	266	410	144	0.79	-	-	249	1.37	3.6/2.9	PLASMA
5	277	415	138	0.76	-	-	239	1.32	-	IMPACT
6	264	408	144	0.79	-	-	251	1.38	-	IMPACT
7	275	412	137	0.75	-	-	240	1.32	-	IMPACT
8	267	415	148	0.81	-	-	246	1.35	-	IMPACT
9	277	423	146	0.80	-	-	243	1.34	-	IMPACT
10	265	420	155	0.85	-	-	251	1.38	-	IMPACT
Zr 11	271	374	103	-	-	-	-	-	-	Not Scheduled
Q 1	11		146	0.81	231	1.29	258	1.44	-	THERMAL COND
Q 2	19		130	0.72	224	1.25	240	1.34	-	THERMAL COND

TABLE 3-1

CAPSULE WEIGHT DATA (CONT)

CHART NOTES

Note A: Three types were identified by their core.

Al - Hollow aluminum metal removed prior to carbon impregnation

Zr - Solid alumina ceramic coated with ZrO_2

Q - Hollow thin wall quartz

Note B: The weight of the core plus the wound yarn with adhesive

Note C: Generally the overall diameter was 3-1/8 inch with a yarn wall of 1/2 inch.

Note D: The Al series had the core removed by etching. While the weight is the adhesive set yarn only, the average weight of the yarn per capsule was 124 grams indicating solids of the adhesive contributed about 12 grams to the gross weight before the furnace impregnating operation.

Note E: Density of wound yarn, calculated based on 180 cc for Al and Q capsules and 182 cc for Zr capsules.

Note F: In Zr and Q capsules the core weight is not included.

Note G: The thickness was calculated from the weight of B_6Si deposited.

Two units received an additional coating as follows:

Al 16 weight increase 10.7 grams - 8.5 mils equivalent thickness

Al 17 weight increase 23.1 grams - 18.2 mils equivalent thickness.

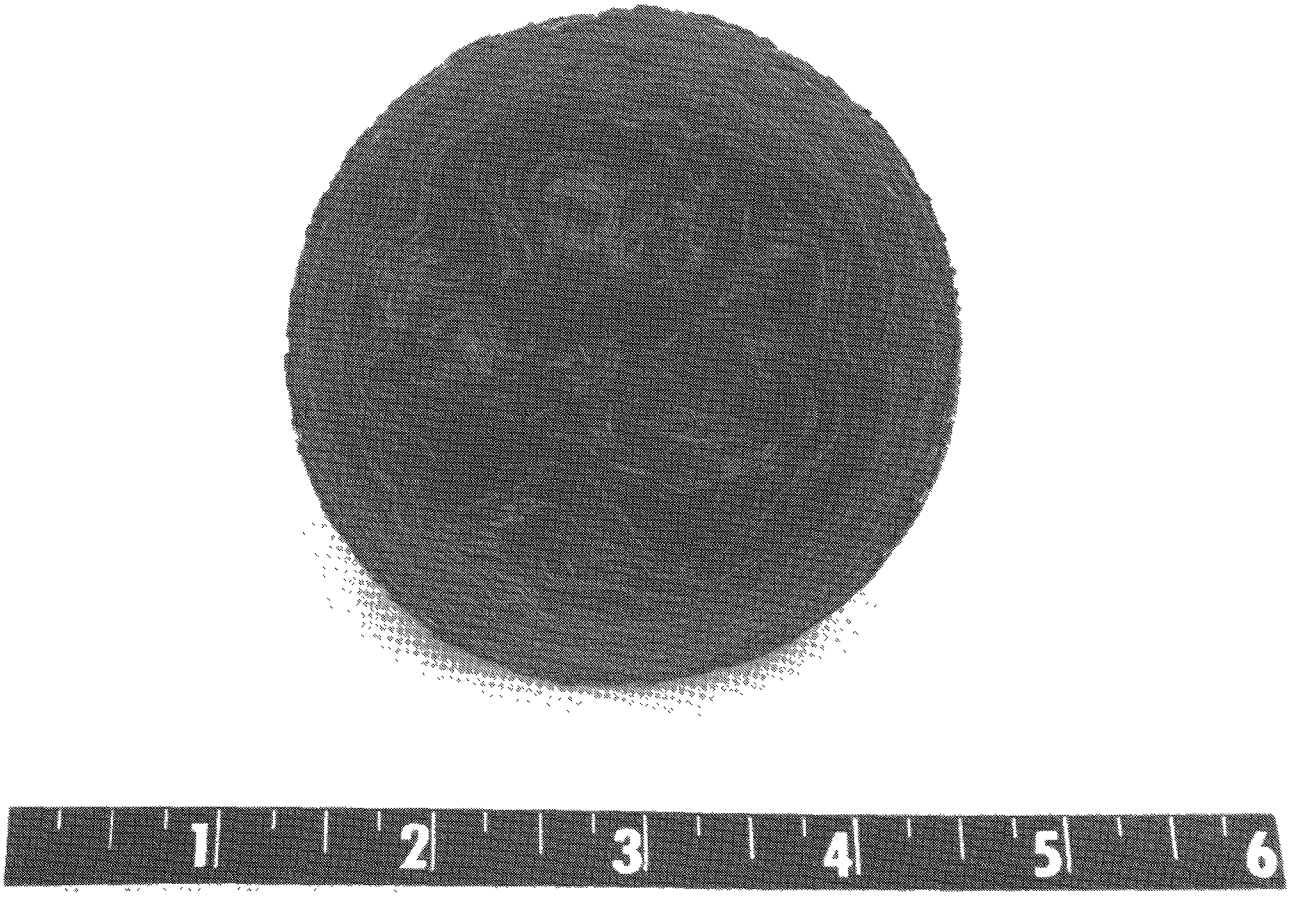

69-404-6

69-H65983-101

Figure 3-10 Cross-Section of "Hollow" Test Capsule After Impregnation.

Pliobond adhesive, that had restrained the tightly wound elongated yarn, apparently burned out during the initial furnace cycle permitting the high loading of the outer windings to collapse the unsupported interior. Subsequent inspection of specimens that were internally supported indicated a higher density near the inner rigid member than near the exterior winding of yarn where the inner windings were restrained. Figure 3-11 is a cross section of a test capsule with a hollow quartz core. In comparison with Figure 3-10, the quartz liner successfully held the inner windings in place. Note the uniformity of impregnation across the graphite structure.

The bulk density of the graphite structures after the second impregnation cycle were quite uniform. The densities averaged 1.43 grams/cc with a standard deviation of 0.06 (about 4 %). Microscopic examination of the cross-sectioned capsule showed that porosity remained throughout the impregnated volume. This porosity was consistent through the outer surface to facilitate further impregnation operations.

3.8 CONCLUSIONS

The fabrication task was successful in providing the required test capsules for the testing tasks. In addition, the fabrication of a lot of 35 capsules has demonstrated the quality and degree of reproducability of the respective fabrication operations. The experience gained provides a valuable background for further development of the SIREN capsule.

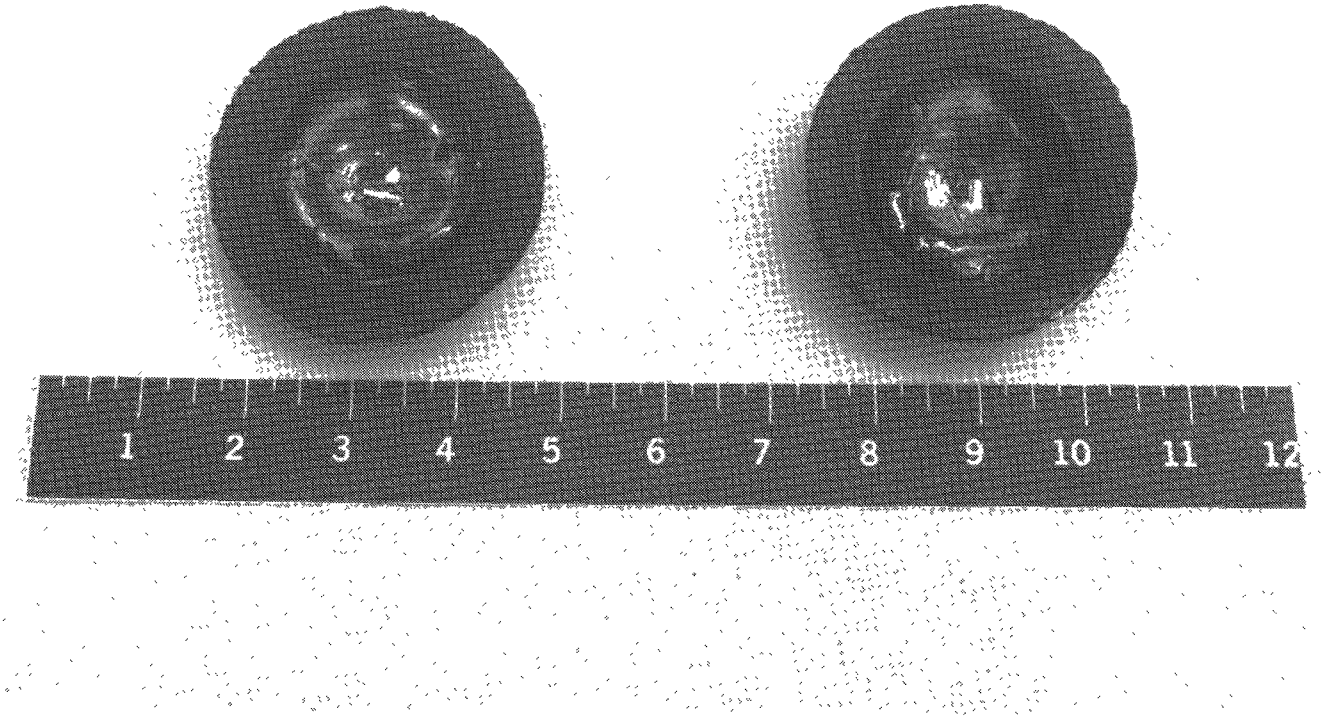

69-462-1

69-H65983-102

Figure 3-11 Cross-Section of Test Capsule With Hollow Quartz Core.

SECTION 4
ANALYSES OF SIREN CAPSULE DESIGN

4.1 INTRODUCTION

As part of the assessment of the feasibility of the SIREN concept, several critical subject areas were analyzed. The objectives of these analyses were to define general design requirements and to evaluate the status of technologies required to meet these requirements. The subjects treated in these analyses are listed below and reports of the analyses are given in the following paragraphs:

4.2 Materials Analysis
4.3 SIREN Capsule Fueling Analysis
4.4 Aerothermal Analysis
4.5 Post Impact Analysis
4.6 Comparative Analysis

BLANK

4.2 MATERIALS ANALYSIS

4.2.1 REFRACTORY COATINGS FOR GRAPHITE

4.2.1.1 Introduction

As an operating unit, the SIREN capsule will be subject to various elevated temperature oxidizing environments during different phases of its mission. Typical oxidation protection requirements would be:

- Pre-Launch Storage – minimum protection required since capsule can be readily cooled and protected in inert atmosphere.
- Launch-Pad Installation – with air-conditioning, maximum expected temperatures would be 500 to 800°F, however, if the cooling system were to fail, the temperature could increase to about 1500°F.
- Earth Atmosphere Reentry – oxidation protection of the graphite would not be required because ablation would be the controlling surface reaction.
- Post-Impact – oxidation protection of the graphite structure may or may not be required depending on the form and properties of the fuel form. For example, retention of the graphite shell about a solid ceramic fuel with a non-active ceramic coating may not be required if the fuel survives impact. However, a capsule containing a particulate or cermet fuel would probably require oxidation protection of the graphite so as to ensure physical containment of the fuel. Conceivably, temperatures ranging to 2000°F or more could be experienced, depending on the impact environment (i.e., sand, rock, swamp, or water).

In view of the diversity of oxidation protection requirements for the graphite structure, a review of existing literature on thermal, mechanical, and physical properties of coatings has been conducted to determine potential coating systems.

4.2.1.2 Discussion

Diffusion of Carbon and Oxygen Through the Coating Material

The rate of diffusion through a coating depends both on the diffusivity and on the concentration of the diffusing species. In order to evaluate prospective coating materials, the permeabilities should be determined under conditions which occur in an actual coating. It is also necessary to determine what degree of oxygen or carbon permeation can be sustained before failure occurs.

If carbon penetrates the coating and reacts on the outside with oxygen, the net effect will be to lose carbon at a rate equal to the permeation rate. Also, the diffusion of oxygen through the coating will produce carbon monoxide at the graphite interface. This condition could cause a build up of pressure which might disrupt the coating from the graphite surface.

A build up of pressure could also occur if, as in a multilayer system, the reaction to produce carbon monoxide occurred at the internal interface. However, this tendency could be avoided by providing a slightly porous inner layer that would allow the carbon monoxide to diffuse through the graphite.

In general, two factors are of importance in producing low permeabilities:

a. A tight binding between the atoms of the solid

b. A tight lattice with small nondiffusing atoms

The failure mechanism of the more commonly applied coatings, however, is probably due to the porosity or nonadherence of the coatings rather than to the diffusion of gases through the coatings. At present, data in this region is so scant that the permeability of a substance under actual coating conditions cannot be estimated.

Chemical Compatibility of Refractory Coatings with Graphite

Refractory Oxides - One of the primary assets of the refractory oxides is their greater resistance to oxidation at elevated temperatures than any other class

of materials.[1] However, the results of experimental data and thermodynamic calculations would seem to indicate that there probably is no oxide that is stable with respect to graphite at 2000°C if one considers the criteria for stability as a CO partial pressure of less than one torr. For example, beryllia, the most stable oxide with respect to carbon, has a CO pressure of 1.52×10^2 torr (0.2 atmosphere)[4] at 2000°C.

TABLE 4-1

REDUCTION OF SEVERAL OXIDES BY GRAPHITE[4]

Reaction between Metal Oxide and Graphite	Free Energy $-\Delta F$ at 2000°C (K cal/g atm O_2)	P_{CO} (atm) at 2000°C	Temperature °C at which P_{CO} = 1 atm
$1/3Al_2O_3+3/2C \rightleftharpoons 1/6Al_4C_3+CO$	6.9	4.6	2473
$BeO+3/2C \rightleftharpoons Be_2C+CO$	-7.1	0.2	2763
$1/3B_2O_3+7/6C \rightleftharpoons 1/6B_4C+C_O$	17.1	44	2103
$MgO+C \rightleftharpoons Mg+CO$	15.0	27	2383
$1/2SiO_2+3/2C \rightleftharpoons 1/2SiC+CO$	23.2	167	1993
$1/2ThO_2+2C \rightleftharpoons 1/2ThC_2+CO$	9.1	7.5	2463
$1/2TiO_2+3/2C \rightleftharpoons 1/2TiC+CO$	29.8	756	1853
$1/2ZrO_2+3/2C \rightleftharpoons 1/2ZrC+CO$	13.1	18	2283

It may be possible to produce an oxide-graphite system if a barrier material is utilized between the graphite and the oxide coating to prevent reduction of the oxide. If this alternative is sought, the barrier material must be chemically and

physically compatible at high temperatures with both the graphite substrate and the oxide coating. Possible barrier materials include metal silicides, nitrides, carbides, and borides since these classes of compounds contain some of the most refractory materials known.

Barrier Materials – Since the most likely approach to graphite oxidation protection at high temperatures is in the utilization of a multilayer coating, the problem is to identify a refractory silicide, nitride, carbide, or boride which is chemically and physically compatible with respect to graphite at these temperatures. The simplest oxidation resistant coating would be that formed from the oxidation of the barrier compounds in that this reaction would preclude the necessity of applying an oxide to the barrier material.

Refractory Silicides

The resistance to oxidation of the metal silicides results from the formation of a coating of silica or a silicate on the exposed surface at high temperatures. However, at low temperatures, below 1093°C, the surface of the majority of the silicides is poorly protected and must be preoxidized in order to provide adequate protection.(1)

Unfortunately, no systematic investigations concerning the silicides listed in Table 4-2 with graphite have been found.

As can be seen from Table 4-2 the silicides of tantalum, titanium, and tungsten offer the best oxidation protection. Chromium silicide, when oxidized, forms a thick, brittle oxide layer which has little stability toward temperature fluctuations. Also $MoSi_2$, which exhibits very little weight gain at high temperatures, does not form an adherent SiO_2 film below 538°C and, therefore, exhibits very poor oxidation resistance at these temperatures.(1)

In contrast to the other silicides, the boron silicides, when exposed to air at high temperatures, undergo a rapid initial oxidation, after which no further oxidation occurs.(6)

TABLE 4-2

POTENTIAL OXIDATION RESISTANT SILICIDES

Silicide	Melting Point, °C (2)	Density, g/cc (2)	Weight Change in Air (1)		
			Temperature, °C	Time, hrs	Weight Gain, mg/cm^2
B_4Si	1093	2.46	1371	3	60
				65	60
B_6Si	1947	2.47	1371	3	50
				65	50
Cr_3Si	1704	6.45	1371	100	15
$MoSi_2$	2010	6.31	1093	19	3
			1649	10	.3
$TaSi_2$	2300	9.14	1649	10	2.4
$TiSi_2$	1499	4.15	1199	4	0.3
			1371	5	2.2
			1371	100	4.4
WSi_2	2110	9.4	1093	19	0.5
			1649	10	2

Refractory Nitrides

Chemically, the nitrides are quite similar to the carbides except for their oxidation resistance which is considerably inferior.

As is illustrated in Table 4-3, Si_3N_4 is the most oxidation resistant nitride with boron nitride slightly less resistant. The nitrides of hafnium, tantalum, titanium, and zirconium have only moderate oxidation resistance.

TABLE 4-3

POTENTIAL OXIDATION RESISTANT NITRIDES

Nitride	Melting Point, °C (2)	Density, g/cc (2)	Oxide Formed	Maximum Service Temperature of Nitride Coating on Graphite, °C (*) (4)
BN	2704	2.25	B_2O_3	982
HfN	3305	13.94	HfO_2	538
Si_3N_4	1900	3.44	SiO_2	1399
TaN	3360	16.3	Ta_2O_5	760
TiN	2930	5.22	TiO_2	538
ZrN	2980	7.09	ZrC_2	538

(*) The temperature at which the rate of attack of air would cause severe erosion or failure of the coated specimen within a few hours. Coating thickness and rate of air flow past the specimen have not been taken into account.

Refractory Carbides

Since metal carbides are among the most refractory materials known and since many of them are compatible with graphite, they are worthy of consideration as possible oxidation protective coatings.

As can be seen by Table 4-4, the most promising carbides, in terms of oxidation resistance, are SiC, HfC, and ZrC.

Refractory Borides

The basis for selecting a boride barrier material are stability with respect to graphite, oxidation resistance, and formation of a metal oxidation product with a high melting point.

TABLE 4-4

POTENTIAL OXIDATION RESISTANT CARBIDES

Carbide	Melting Point, °C (2)	Density, g/cc (2)	Oxide Formed	Maximum Temperature of Stability of Oxide on Carbide, °C (2)	Maximum Service Temperature of Carbide Coating on Graphite, °C (**) (4)
Cr_3C_2	1890	6.68	Cr_2O_3	1130	(830)*
HfC	3885	12.20	HfO_2	1730	1400
SiC	2700	3.21	SiO_2	(1950)*	1650
TaC	3880	13.9	Ta_2O_5	1030	(730)*
TiC	3140	4.93	TiO_2	1230	(930)*
ZrC	3530	6.73	ZrO_2	1730	1400

* Theoretical value, no experimental data available

(**) The temperature at which the rate of attack of air would cause severe erosion or failure of the coated specimen within a few hours. Coating thickness and rate of air flow past the specimen have not been taken into account.

TABLE 4-5

POTENTIAL OXIDATION RESISTANT BORIDES

Boride	Melting Point, °C (2)	Density, g/cc (2)	Oxide Formed	Maximum Temperature of Stability of Oxide on Boride, °C (2)	Maximum Service Temperature of Boride Coating on Graphite, °C (*) (4)
Cr_2B	3300	6.53	Cr_2O_3	-	1500
HfB_2	3062	11.2	HfO_2	2777	1400

(*) The temperature at which the rate of attack of air would cause severe erosion or failure of the coated specimen within a few hours. Coating thickness and rate of air flow past the specimen have not been taken into account.

TABLE 4-5

POTENTIAL OXIDATION RESISTANT BORIDES (Cont)

Boride	Melting Point, °C (2)	Density, g/cc (2)	Oxide Formed	Maximum Temperature of Stability of Oxide on Boride, °C (2)	Maximum Service Temperature of Boride Coating on Graphite, °C (*) (4)
ThB_6	2195	6.4	ThO_2	3300	1500
TiB_2	2900	4.5	TiO_2	1840	1400
ZrB_2	3000	6.09	ZrO_2	2677	1300

(*) The temperature at which the rate of attack of air would cause severe erosion or failure of the coated specimen within a few hours. Coating thickness and rate of air flow past the specimen have not been taken into account.

The preceding table illustrates that any of the selected borides are possible candidates for use in the protection of graphite. In fact, unlike their corresponding carbides, the borides are relatively stable in the presence of moisture which gives them an added advantage as an oxidation protective material.

Mechanical Compatibility of Refractory Coatings with Graphite

A great deal of information on the mechanical and thermal properties of prospective coating materials at high temperatures is available. However, such large discrepancies have been found in much of the data that only verified data is presented in this report. This information, however, is of limited use in solving the mechanical problems within a given system for it must be remembered that the properties of the coating material may change markedly during prolonged service at high temperatures. This may be due to grain growth, annealing, carbon diffusion, chemical reactions of the coating material with either carbon or oxygen, or any combination of these factors. Even if these factors do not appear, the physical properties of the coating may be entirely different from those measured on the bulk material.

Thermal shock resistance of a coating material must also be considered. This depends on the bond strength, thickness, thermal conductivity of the coatings, and the differences between the thermal expansion of the coating and the substrate. These factors will be discussed in the following paragraphs.

Linear Thermal Expansions Between 21 - 2204°C - By far, the most important criteria for predicting the mechanical compatibility of a system is a close match of the thermal expansions of both the substrate and the coating. Tables 4-6 through 4-9 list the average coefficients of linear thermal expansion of various silicides, nitrides, carbides, and borides in the 21 - 2204°C range. Table 4-10 lists the average coefficients of linear thermal expansion of various carbon and graphite filaments and Figures 4-1 and 4-2 give a comparison of the more chemically feasible coatings with these graphites.

TABLE 4-6

AVERAGE COEFFICIENTS OF LINEAR THERMAL EXPANSION OF VARIOUS SILICIDES(1)

Silicide	Temperature Range, °C	Thermal Expansion Coefficient in/(in) (°C) x 10^{-6}
B_4Si	21 - 999	5.94
B_6Si	21 - 999	5.4
Cr_3Si	21 - 1071	10.44
$MoSi_2$	21 - 1071	8.28
$TaSi_2$	320 - 1070	10.8
$TiSi_2$	20 - 1070	10.44
WSi_2	421 - 1071	7.92

TABLE 4-7

AVERAGE COEFFICIENTS OF LINEAR THERMAL EXPANSION OF VARIOUS NITRIDES(1)

Nitride	Temperature Range, °C	Thermal Expansion Coefficient in/(in) (°C) x 10^{-6}
BN	21 - 1093	7.56
HfN	24 - 1371	6.48
Si_3N_4	21 - 982	2.48
TaN	21 - 704	3.6
TiN	593 - 1427	9.0
ZrN	593 - 1427	7.74

TABLE 4-8

AVERAGE COEFFICIENTS OF LINEAR THERMAL EXPANSION OF VARIOUS CARBIDES(1)

Carbide	Temperature Range, °C	Thermal Expansion Coefficient in/(in) (°C) x 10^{-6}
Cr_3C_2	816 - 1982	10.44
HfC	816 - 2204	7.92
SiC	538 - 2204	5.4
TaC	21 - 2204	7.46
TiC	816 - 2204	9.9
ZrC	816 - 2204	9.0

TABLE 4-9

AVERAGE COEFFICIENTS OF LINEAR THERMAL EXPANSION OF VARIOUS BORIDES[1]

Boride	Temperature Range, °C	Thermal Expansion Coefficient in/(in) (°C) x 10^{-6}
Cr_2B	21 - 2204	8.64
HfB_2	21 - 2204	7.56
ThB_6	21 - 2204	8.28
TiB_2	21 - 2204	8.64
ZrB_2	21 - 2204	8.28

TABLE 4-10

AVERAGE COEFFICIENTS OF LINEAR THERMAL EXPANSION OF VARIOUS CARBON AND GRAPHITE FILAMENTS AT ROOM TEMPERATURE

Filament	Thermal Expansion Coefficient in/(in) (°C) x 10^{-6}	
Carbon/Graphite[4]	(c)	2 - 9
Graphite[8]	(ab)	2.22
	(c)	3.77
Pyrolytic Graphite[7]	(ab)	0.18
	(c)	7.2

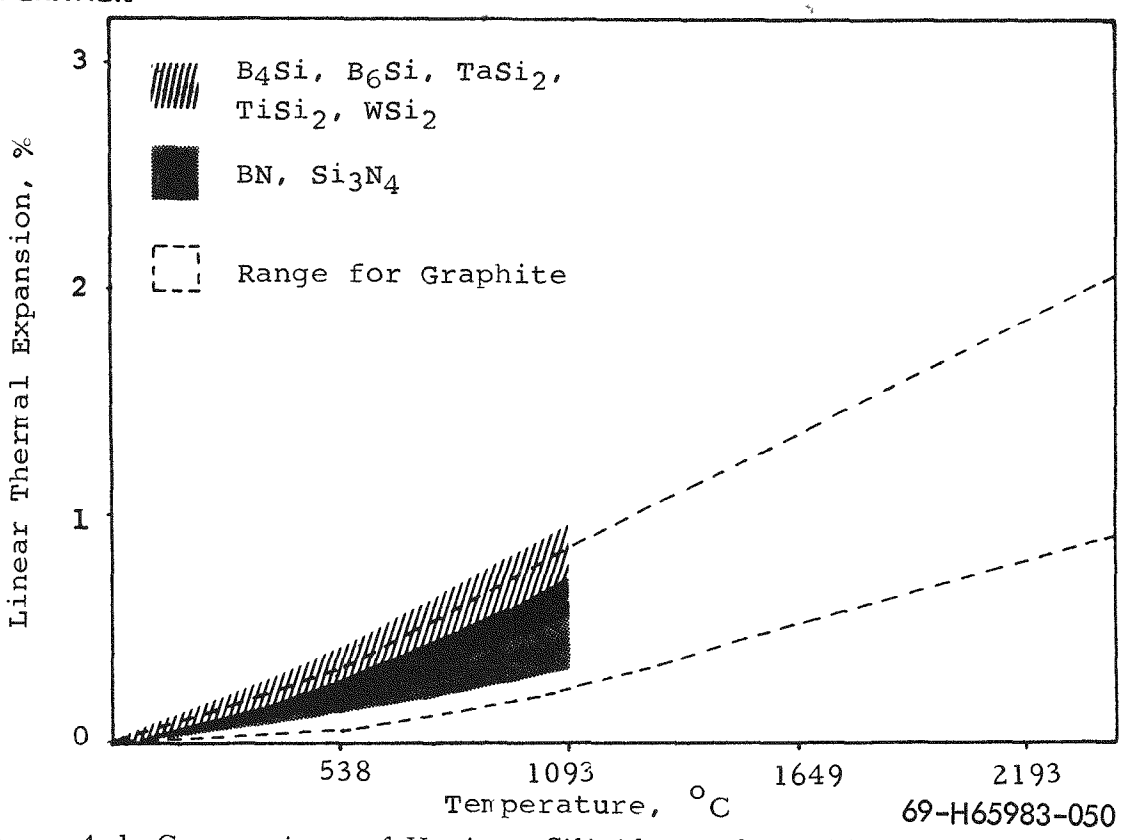

Figure 4-1 Comparison of Various Silicides and Nitrides with Graphite.

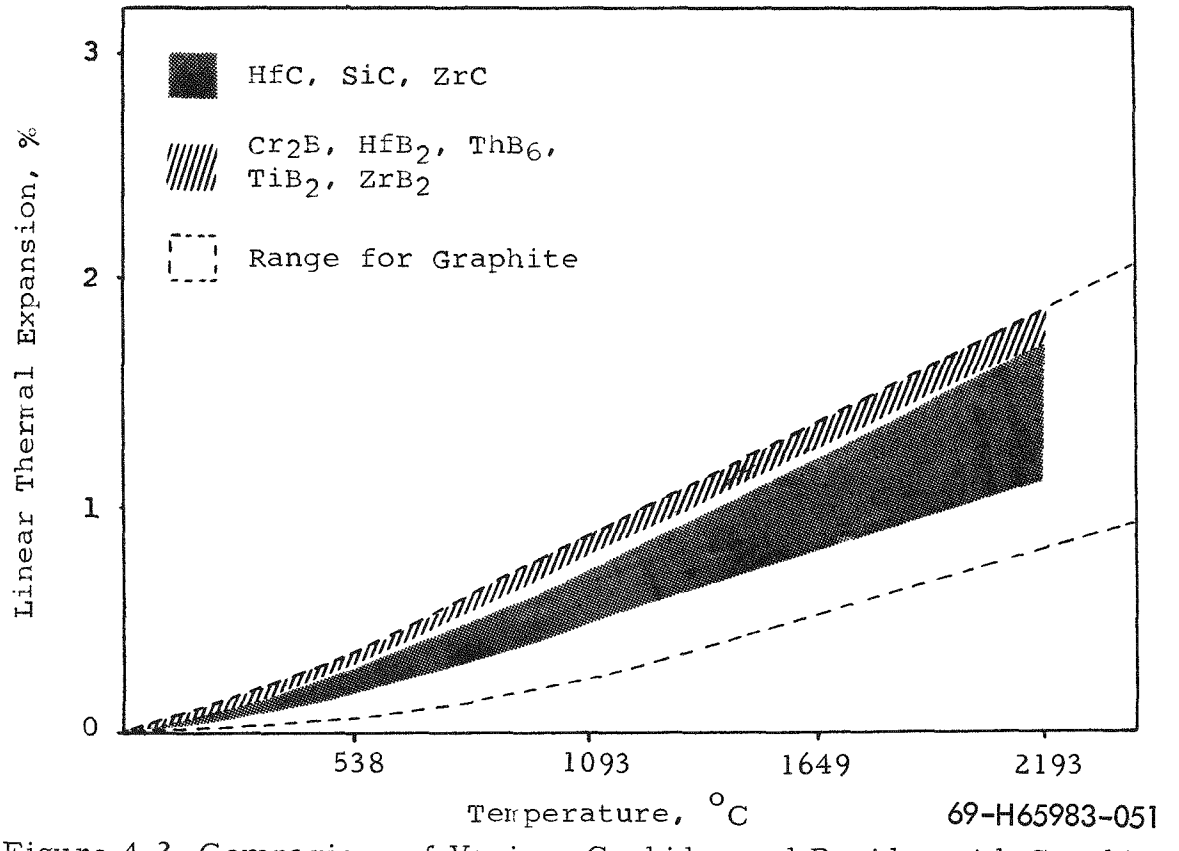

Figure 4-2 Comparison of Various Carbides and Borides with Graphite.

Strength Data at 1093°C - Limited strength data for the silicides, nitrides, carbides, and borides have been reported for the 1093°C range. These are listed in Tables 4-11 through 4-14.

TABLE 4-11

MECHANICAL PROPERTIES OF VARIOUS SILICIDES(1)

Silicide	Modulus of Rupture, 10^3 Kg/cm^2 1093°C	Tensile Strength 10^3 Kg/cm^2 1093°C	Youngs Modulus 10^6 Kg/cm^2 1093°C
Cr_3Si	5.39	-	-
$MoSi_2$	3.57-6.02	2.1	2.8
$TaSi_2$	2.1	-	3.43
$TiSi_2$	2.1	1.4	-
WSi_2	3.57	-	2.1

TABLE 4-12

MECHANICAL PROPERTIES OF VARIOUS NITRIDES(1)

Nitride	Modulus of Rupture, 10^3 Kg/cm^2 1093°C	Tensile Strength 10^3 Kg/cm^2 1093°C	Youngs Modulus 10^6 Kg/cm^2 1093°C
BN	0.21	0.042	0.07
Si_3N_4	0.77-4.9	-	0.56-2.17

TABLE 4-13

MECHANICAL PROPERTIES OF VARIOUS CARBIDES(1)

Carbide	Compressive Strength, 10^3 Kg/cm^2 1093°C	Modulus of Rupture, 10^3 Kg/cm^2 1093°C	Tensile Strength 10^3 Kg/cm^2 1093°C	Youngs Modulus 10^6 Kg/cm^2 1093°C
Cr_3C_2	6.3	5.6	-	-
HfC	-	2.24	-	-
SiC	-	1.47	-	3.5
TaC	-	3.01	-	-
TiC	-	4.2	0.07	-
ZrC	-	2.45	1.05	3.5

TABLE 4-14

MECHANICAL PROPERTIES OF VARIOUS BORIDES(1)

Boride	Modulus of Rupture, 10^3 Kg/cm^2 1093°C	Youngs Modulus 10^6 Kg/cm^2 1093°C
TiB_2	2.8	3.85
ZrB_2	0.049	3.85

Specific Heats and Thermal Conductivities at 1093°C - The specific heats and thermal conductivities of the silicides, nitrides, carbides, and borides have been reported for the 1093°C range. These properties are listed in Tables 4-15 through 4-18.

TABLE 4-15

THERMAL PROPERTIES OF VARIOUS SILICIDES[1]

Silicide	Specific Heat g · Cal/(g) (°C) 1093°C	Thermal Conductivity g · Cal · cm/(hr) (cm²) (°C) 1093°C
$MoSi_2$	0.14	148.8
$TaSi_2$	0.058	-
$TiSi_2$	0.24	-
WSi_2	0.058	252.96

TABLE 4-16

THERMAL PROPERTIES OF VARIOUS NITRIDES[1]

Nitride	Specific Heat g · Cal/(g) (°C) 1093°C	Thermal Conductivity g · Cal · cm/(hr) (cm²) (°C) 1093°C
BN	0.47	133.92
HfN	0.08	133.92
Si_3N_4	0.3	22.32
TaN	0.1	-
TiN	0.21	230.64[3]
ZrN	0.13	171.12

TABLE 4-17

THERMAL PROPERTIES OF VARIOUS CARBIDES[1]

Carbide	Specific Heat g · Cal/(g) (°C) 1093°C	Thermal Conductivity g · Cal · cm/(hr) (cm²) (°C) 1093°C
Cr_3C_2	0.21	-
HfC	0.07	223.20
SiC	0.31	163.68
TaC	0.08	-
TiC	0.21	357.12[3]
ZrC	0.13	297.60[3]

TABLE 4-18

THERMAL PROPERITIES OF VARIOUS BORIDES[1]

Boride	Specific Heat g · Cal/(g) (°C) 1093°C	Thermal Conductivity g · Cal · cm/(hr) (cm²) (°C) 1093°C
HfB_2	0.095	401.76
TiB_2	0.3	401.76
ZrB_2	0.18	282.72

4.2.1.3 Summary

It would appear from the preceding investigation that the most satisfactory coating, from both a chemical and mechanical point of view, for the high temperature oxidation protection of graphite is silicon carbide. This coating will afford protection to graphite for substantial periods to a maximum of 1650°C.[4]

Silicon carbide is the only compound of silicon and carbon known to occur in the condensed state, and it exists in several crystalline forms.[1] Beta silicon carbide is considered to be an unstable phase that can exist at all temperatures below its melting point, but above 1650°C it slowly transforms to the alpha phase. This phase is generally characterized by a hexagonal structure but it actually has many modifications, including both hexagonal and rhombohedral forms.

Silicon carbide can be prepared as a coating by use of one of the following gas-phase reactions:

a. Direct deposition of the carbide on a heated surface via vapor deposition

b. Carburization of the silicon in a hydrocarbon-containing atmosphere

c. Decomposition of the volatile metal halide vapor on the substrate at a temperature high enough to cause interdiffusion of the carbon and the silicon

d. Direct carbide deposition by the pyrolysis of an organometallic compound.

The first process generally gives the highest deposition rates and yields the purest deposits, since the metal-to-carbon ratio can be controlled.[5]

The main advantages of using a silicon carbide coating are hardness, chemical and oxidative resistance, thermal conductivity, strength, and other properties which are needed for high performance structural components.

Also, a number of the borides, Si_3N_4, BN, SiC, HfC, ZrC, and both B_4Si and B_6Si are suitable for use at lower temperatures. In a multilayer coating system these materials could be used as an initial coating to provide protection to the graphite during handling operations.

Other refractory materials, which cannot be utilized directly because of their mismatch of thermal expansions with graphite, can be used as alloys and therefore, should be considered for low temperature applications.

4.2.2 IMPREGNATION MATERIALS

4.2.2.1 Introduction

There has been considerable interest for the last several years in the application of pyrolytic or refractory anisotropic materials in aerospace components. Several of the properties that make these materials so attractive are:

a. A high melting point

b. A high strength-to-weight (density) ratio at high temperatures

c. A high resistance to oxidation.

In addition, most of these materials have low gas permeabilities and possess a low thermal conductivity perpendicular to the plane of deposition together with a high surface emissivity.

The characteristics of pyrolytic carbon, graphite, boron nitride, and boron pyrolytic graphite are presented in this report together with their anisotropic thermal and mechanical properties.

4.2.2.2 Discussion

Methods of Deposition

High temperature gas-phase reactions are employed in the processing of pyrolytic materials. It is the particular process chosen which leads to the formation of these materials with a high degree of anisotrophy. In practice, the process is performed by passing the vapors of a compound over a substrate maintained at an elevated temperature. Here the compound is decomposed and the crystals nucleate and grow in a preferred direction. In this fashion the deposit is built up gradually at a controlled rate. However, various discrete aspects of the process such as the effects of furnace geometry, intermediate reaction rages, diffusion rates, and accommodation coefficients all play a part in producing a deposit with a given property.

4.2.2.3 Properties of Pyrolytic Materials

Although pyrolytic carbon has been known for some time, an interest in this material has developed only after it was demonstrated that anisotropy could be obtained in this material owing to a tendency of the basal graphite planes to deposit parallel to the deposition surface. Emphasis on the highly oriented form led to the use of the term "pyrolytic graphite" among workers in the United States. Workers outside the United States, however, have a preference for "pyrolytic carbon" even when referring to the more oriented forms. Because of an equal interest in less oriented types of the material, those who have been engaged in the development of nuclear fuel particle coatings have also used the more general term "pyrolytic carbon". (5)

In pyrolytic graphite, a parallel arrangement of the basal plane of the hexagonal cells is maintained. However, the basal planes are not necessarily oriented with respect to each other in successive layers, but are randomly stacked. Thus, a hexagonal graphitic structure requires that the basal planes be 3.35 angstrom units apart. In defining the direction of the graphite structure, the direction parallel to the basal plane is termed the "a" or "ab" directions and the direction perpendicular to the basal plane, the "c" direction.

Because the bonding of the carbon atoms in the plane, "ab" direction, is essentially covalent, while the interplanar attraction, "c" direction, is largely electrostatic, nearly all of the properties of interest in pyrolytic carbon and graphite reflect this strong in-plane bonding and weak interplanar attraction.

The structure of boron nitride is nearly identical to that of pyrolytic graphite because of the similarity in their crystal structure. Although pyrolytic boron nitride is not as strong as pyrolytic graphite, it is considerably more resistant to oxidation at temperatures up to 2000°C. (5)

Alloys of pyrolytic graphite have been produced by the addition of substitutional and interplanar foreign atoms to the lattice. These additions are made in

order to change some of the mechanical, thermal, or electrical characteristics of pyrolytic graphite, while retaining the basic properties of this material. In general, the addition of boron to form boron pyrolytic graphite increases the strength of the material, and its resistance to oxidation, with little change in its thermal and mechanical properties.(17)

In the early history of pyrolytic graphite production the presence of residual stress in the product, as a result of an isotropic thermal contraction in cooling from the deposition temperature was recognized, and this factor was thought to be a limitation. It was later recognized, however, that in addition to these stresses, those resulting from annealing during deposition must be taken into consideration. Because each succeeding layer of deposited material has less time to anneal, the net effect depends on the thermal history of each differential element of the total structure. Other factors contributing to the stress patterns are:

a. Soot or tar inclusions in the structure and

b. The temperature drop through an internally heated deposit.

Oxidation Resistance - The oxidation rate of pyrolytic materials has been measured and is presented in Figure 4-3 for comparison.

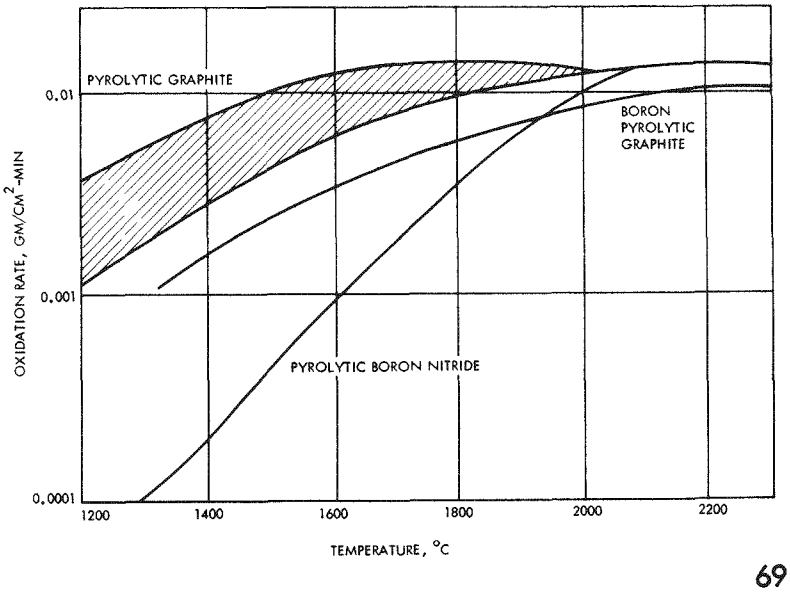

69-H65983-052

Figure 4-3 Oxidation Resistance of Pyrolytic Materials.(5) (16)

A wide range of values is seen for the oxidation rate of pyrolytic graphite. This is due to the various processing conditions experienced by the material and also to the reaction mechanism which becomes diffusion controlled at high temperatures.

Of the represented materials, pyrolytic boron nitride oxidizes at the lowest rate. At 1200°C pyrolytic graphite oxidized at a rate 15 times that of pyrolytic boron nitride, while boron pyrolytic graphite oxidized at an intermediate rate.

Specific Heats - The specific heats of pyrolytic graphite and pyrolytic boron nitride as a function of temperature are shown in Figure 4-4.

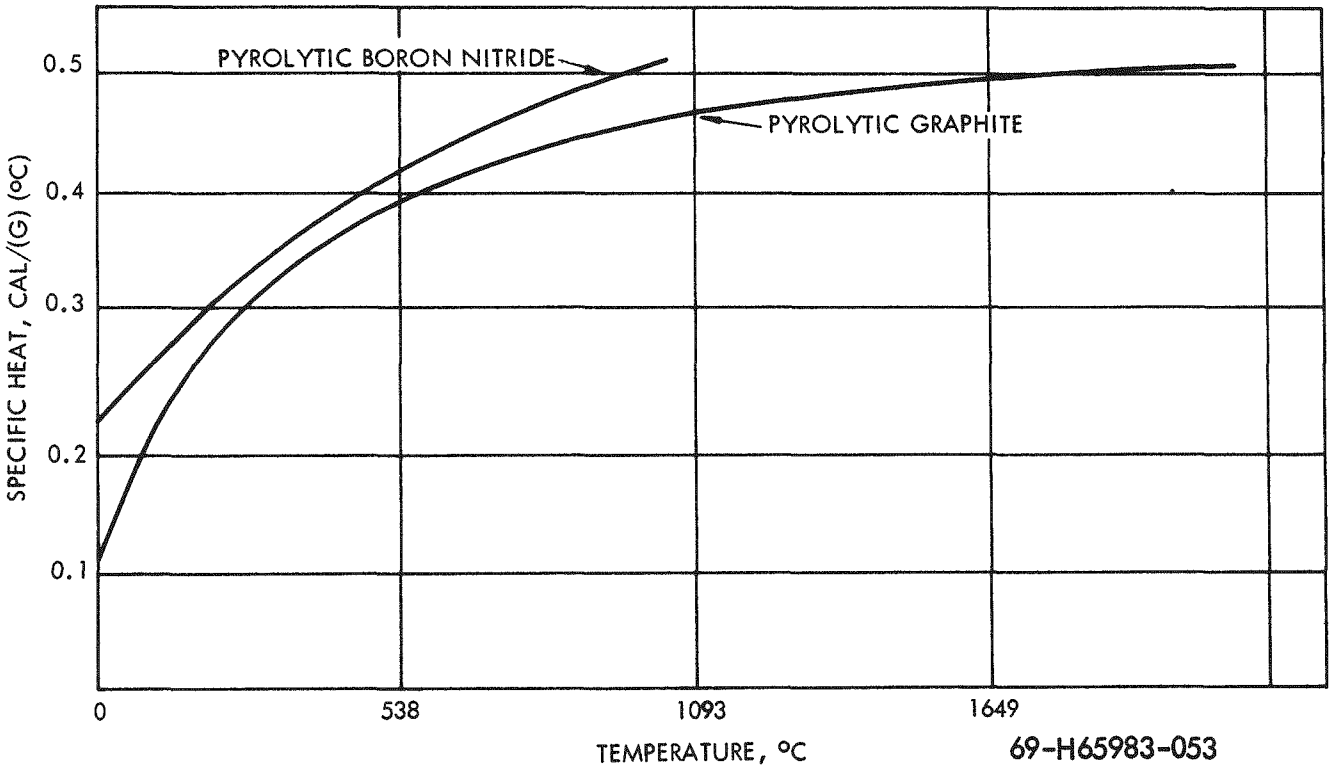

Figure 4-4 Specific Heats of Pyrolytic Materials.[5] [19]

The specific heat of pyrolytic graphite is seen to increase to a maximum in the temperature range 1371 to 1649°C.

Strength Data - The tensile strengths of pyrolytic graphite and pyrolytic boron nitride as a function of temperature are shown in Figure 4-5.

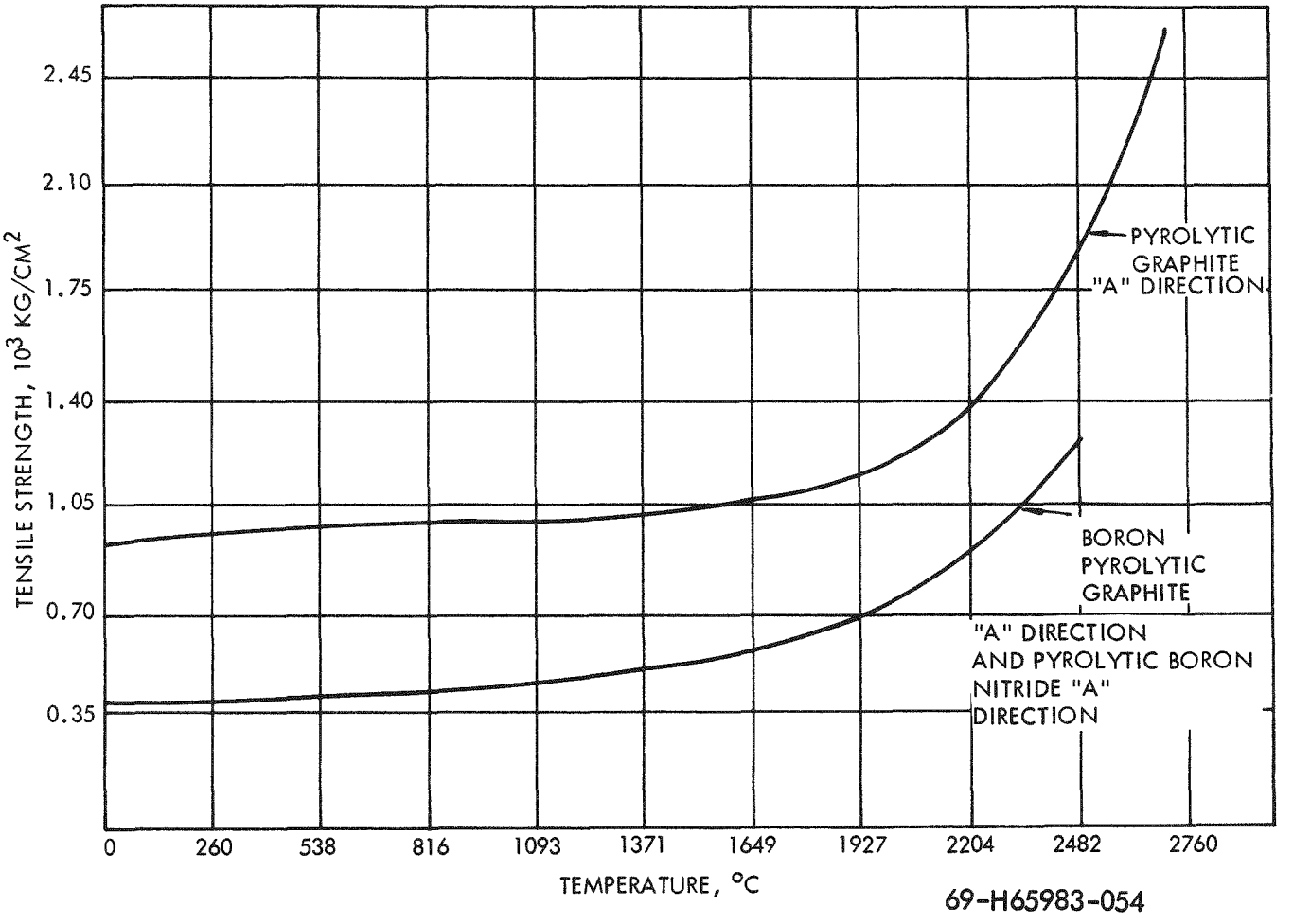

Figure 4-5 Tensile Strengths of Pyrolytic Materials.[5] [16] [18]

The increase in the tensile strengths of the above materials with temperature is one of the unique properties of these materials. As can be seen, the tensile strengths of both boron pyrolytic graphite and pyrolytic boron nitride are below that of pyrolytic graphite.

Experimental data[30] on the strength of composites of graphite yarn impregnated with pyrolytic graphite indicate the strength of the impregnant is the controlling parameter. As shown in Figure 4-6, two composites were prepared with

the same graphite impregnant, but one composite was wound with a low strength yarn (CY2-5) and the other with a high strength yarn (Thornel-50). In comparison, the strength curves for the two materials were essentially coincident and thereby show no effect of the higher strength yarn. These results suggest that the bonding between the yarn and impregnant was minimal and that full advantage of the strength of the yarn could be realized if greater bonding were promoted.

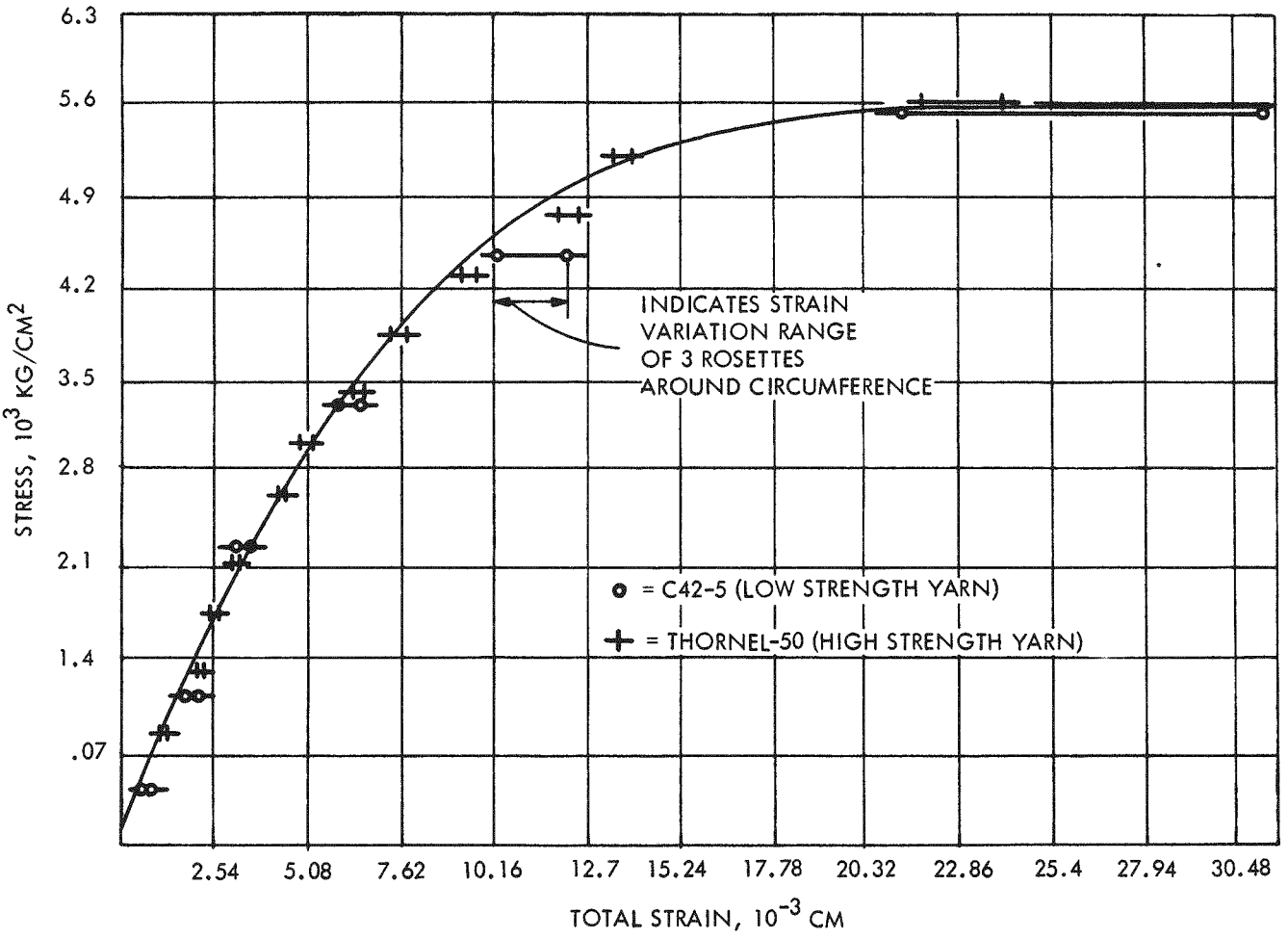

69-H65983-055

Figure 4-6 Stress versus Total Strain in Carbon and Graphite Yarns.[10]

Thermal Conductivities - The thermal conductivities of pyrolytic materials in the direction parallel to the deposition surface as a function of temperature are given in Figure 4-7.

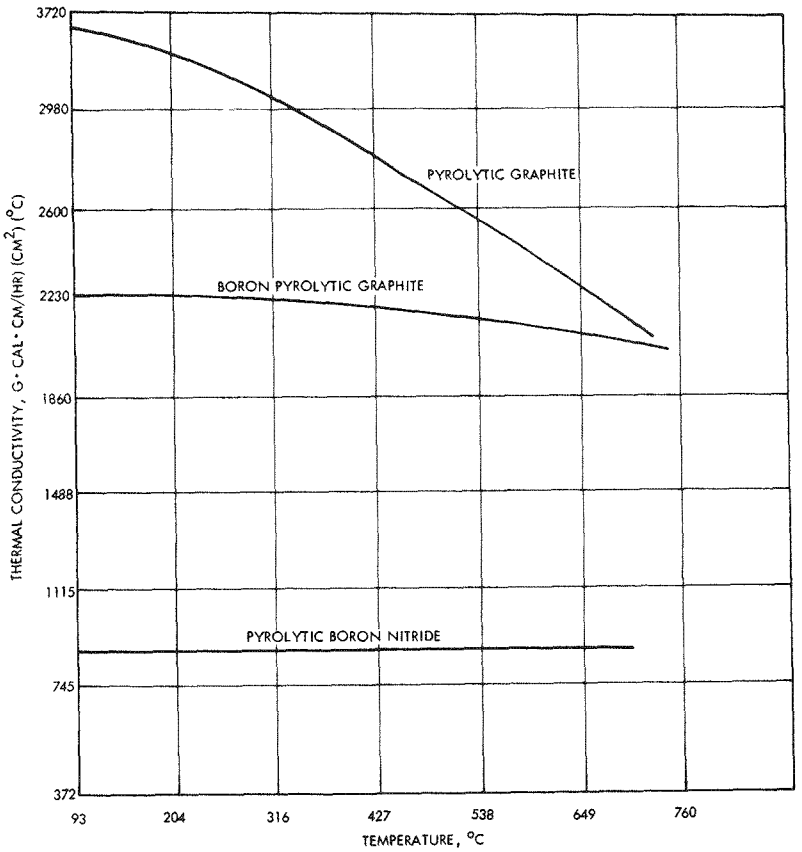

69-H65983-056

Figure 4-7 Thermal Conductivities of Pyrolytic Materials in the "a" Direction. (16) (18)

The corresponding "c" axis thermal conductivities of pyrolytic materials are presented in Figure 4-8.

The thermal conductivities of pyrolytic materials define these materials to be excellent heat conductors in the "a" direction and excellent insulators in the "c" direction.

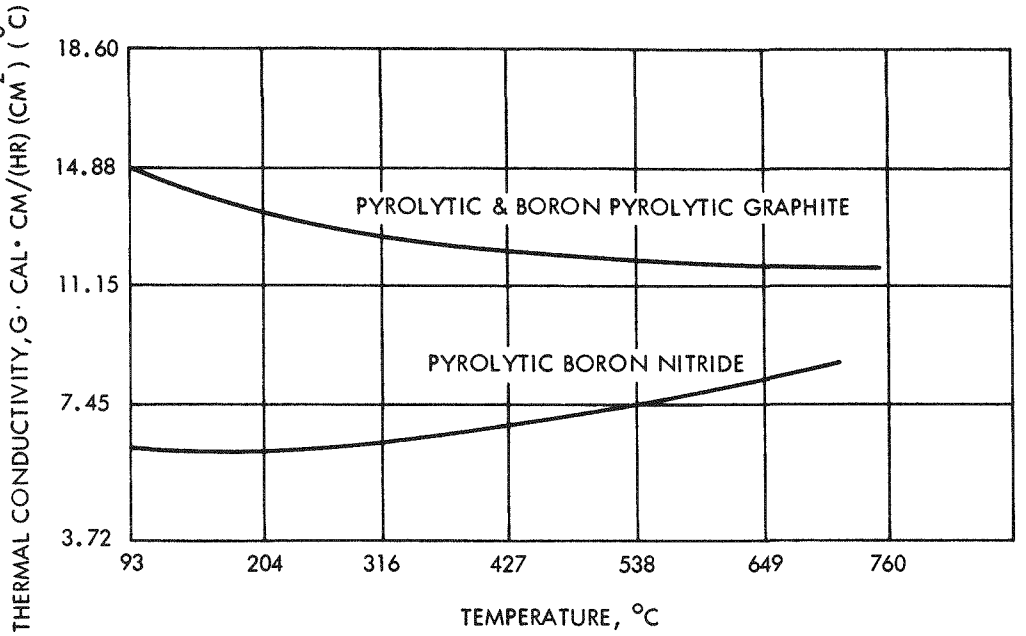

69-H65983-057

Figure 4-8 Thermal Conductivities of Pyrolytic Materials in the "c" Direction.(16) (18)

Thermal Expansions - Figure 4-9 represents the "a" and "c" direction thermal expansion coefficients of pyrolytic graphite and pyrolytic boron nitride as a function of temperature.

4.2.2.4 Summary

The unique properties of the pyrolytic materials make them particularly attractive for use in aerospace components. Pyrolytic graphite is known to be the highest temperature structural material available and on a strength-to-density basis pyrolytic graphite would provide the lightest structure possible for very high temperature applications.

However, the oxidation resistance of pyrolytic graphite is inferior to that of either pyrolytic boron nitride or boron pyrolytic graphite up to 2000°C.

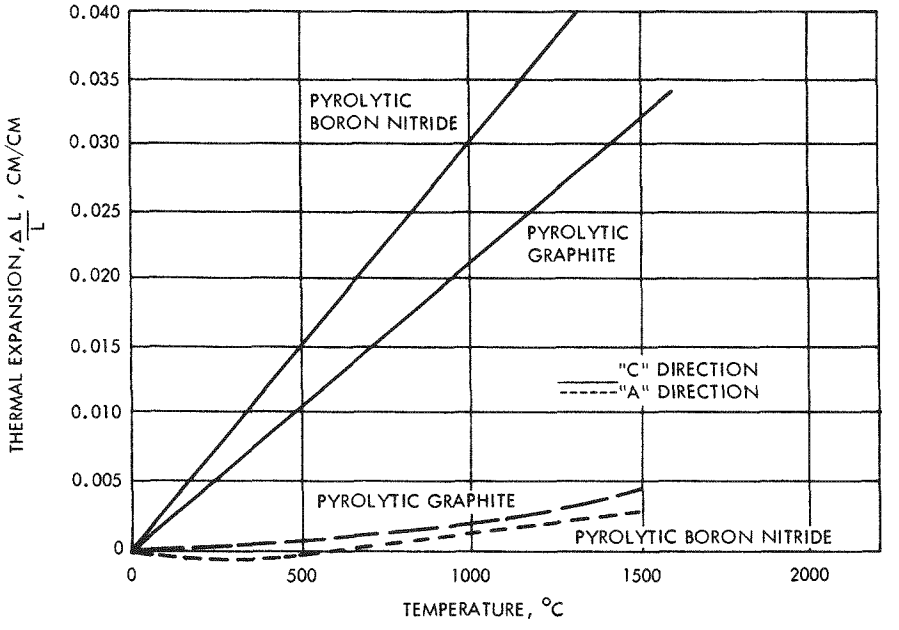

69-H65983-058

Figure 4-9 Thermal Expansion Coefficients of Pyrolytic Materials in the "a" and "c" Directions.

The high thermal conductivity of both pyrolytic graphite and boron pyrolytic graphite in the "a" direction is particularly advantageous since it serves to distribute the heat of reentry over a larger radiating surface area. In contrast to this, the thermal conductivity of these materials in the "c" direction is sufficiently low to enable the material to serve as an effective heat shield.

As the development of pyrolytic materials is still continuing and as significant property improvements have already been realized, it is expected that in the near future it will be possible to tailor the properties of these materials for a specific application. However, much additional research into the mechanisms of the matrix-fiber bonding is required in order to reach a level of understanding whereby materials with specific properties can reliably be produced.

4.2.3 HIGH TEMPERATURE WINDING MATERIALS

4.2.3.1 Introduction

Because of their high strengths, ceramic and graphite fibers, whiskers, and matrix materials, which for many years have been only laboratory curiosities, are today being seriously considered as components for aerospace applications.

One of the primary advantages in utilizing these materials for structural components is their low density and high inherent strength and modulus. These properties arise from the fact that the best available fabrication methods, together with the shape and size of the fiber, all tend to favor a higher degree of perfection within the fibrous material than can be attained in a bulk material.

Although many high modulus, low density materials are not easily fiberized, various ingenious techniques have been employed to overcome this deficiency. However, at this time, these methods are extremely slow and expensive. Also of considerable importance in selecting these materials is both the strength retention of these fibers at elevated temperatures and the chemical compatibility between these fibers and the various matrix materials.

This report attempts to cover some of the more important aspects of fibrous materials such as their tensile strength, modulus of elasticity, temperature resistance, chemical stability, forming methods, and other relevant data.

4.2.3.2 Discussion

Factors Affecting Fiber Strength

In general, the apparent strengths of most fibers fall considerably short of their theoretical values. This can be explained by considering the following factors:

a. Compositional Factors - These include molecular structure, resistance to chemical degradation, hardness, and such time dependent properties as creep, stress-rupture, and stress-corrosion.

b. Processing Factors - These play an important role in determining the internal and external structure of the material. They also determine whether or not a material will be a single crystal, a polycrystalline material, or an amorphous material.

c. Structural Factors - These factors include both the micro- and macroscopic structure of the material, the type, number, and location of lattice defects, the nature of the internal stresses, and the dimensions.

d. Testing Factors - Because the test method chosen determines how the load is transmitted to the fiber, it can also affect the state of stress within the fiber prior to fracture. It is this interaction between the stresses and the lattice defects that determines the values obtained for the strengths. Another factor that affects the apparent strength is the condition of the surface; i.e., if it has been exposed to oxygen, water vapor, or wetted by some other material.

Fabrication Processes

Carbon and Graphite Materials — The most common method of producing high strength, high modulus carbon and graphite fibers is by the pyrolysis of an organic precursor filament. Numerous compositions have been tried for this purpose, but viscose rayon and polyacrylonitrile are the most commonly used precursors.[9] These thermally converted fibers are commonly referred to as either partially carbonized, carbonized, or graphitized. In fact, all three terms are commonly used to describe the same material. The main difference in the use of these terms seems to be the following:

a. Fibers prepared at temperatures under 927°C are referred to as partially carbonized or carbonized. Graphite fibers, although synthesized from the same precursor materials, are processed at temperatures as high as 3000°C.

b. Fibers having a carbon content up to 90 w/o are often described as partially carbonized. Those having a carbon content above 98 w/o are referred to as graphitized.

c. During graphitization, crystallite size increases from 50 Å to ca 1000 Å while interlayer spacing decreases from the 3.44 Å typical of carbon to the 3.35 Å accepted for the graphitic structure.[31]

In producing these fibers other considerations must be taken into account besides the maximum temperature attained and the carbon content. Means of applying tension to the precursor fibers during heat treatment must be available as this is important in aligning the crystal structure. This in turn determines the elastic modulus; the greater the degree of orientation, the higher the elastic modulus.[9] Tension may also be applied to the precursor fibers prior to pyrolysis provided that it is maintained throughout the cycle.

High modulus fibers have been produced by both processes. This leads to a fiber with a diameter of about seven microns, and either a circular or irregular cross section, depending on the precursor material. Usually the finished fibers are supplied as a yarn rather than as a single filament.[9]

Although the carbon fibers have poor oxidation resistance, their strength retention at very high temperatures makes them an attractive material for use in structural components.

Glass and Fused Silica Materials

Glass fibers, because of their sensitivity to degradation by mechanical abrasion and corrosion, are usually protected by the application of sizings, lubricants, and finishes after the drawing process. Unless the surface of these glass fibers is protected from abrasion and other environmental influences, the strength is sharply reduced. Also any interaction between the glass fibers and the protective agent adversely affects the strength.

Recently, high strength fused silica fibers have been produced by using a chemical inhibitor prior to drawing the fibers through a molten metal such as aluminum. Average tensile strengths in excess of 56×10^3 Kg/cm^2 have been obtained with this method. Other metals which have been coated on fused silica

fibers include zinc, antimony, and lead. Unsuccessful attempts have also been made to coat fused silica fibers with copper, nickel, and stainless steel.

Provided the surface of the fibers is protected from mechanical abrasion, it has been found by several investigators that variations in the drawing process such as composition, nozzle diameter, and drawing speed do not affect the mean fiber strength. However, a profound change in the structure of glass fibers can be experienced during the cooling cycle. It has been postulated that rapid cooling favors an orientation of the weak bonds normal to the axis of drawing and results in higher strengths.[10]

Environmental effects such as moisture and temperature also influence the strength of glass fibers. It has been found that glass strength decreases significantly upon exposure to moisture and high temperature heat treatments.

Matrix Materials

The potential of using fiber-reinforced ceramics for aerospace components seems to be more limited than that of either resin or metal matrix composites. The reasons for this are:

a. Excessive fiber-matrix interactions

b. Microcracking caused primarily by the mis-match of thermal expansions between the fiber and the matrix

c. Oxidation of the fiber material.

In addition, the very high elastic moduli and the low fracture strains of most ceramics do not fully utilize the reinforcing potential of the fibers.

The systems that have received the most attention are:

Fiber	Matrix
Molybdenum	Al_2O_3, ThO_2, UO_2, ZrO_2
Nickel	Al_2O_3, UO_2, ZrO_2

Fiber	Matrix
Niobium	ThO_2, UO_2
Tungsten	Al_2O_3

In order to incorporate these metal fibers into a ceramic matrix the metal fiber is coated with a ceramic paste and allowed to dry. Several plies of this ceramic coated fabric are then stacked and hot pressed at 1399°C to form a dense, well sintered matrix around the reinforcement. This technique appears to keep the reaction between the constituents to a minimum.

Because of the relatively low temperature applications of fiber-reinforced resins they will be considered only briefly in this report. The most commonly used resins are the polyesters, epoxies, and phenolics although much progress has been made in developing more thermally stable resins such as the polyimides and the polybenzimidazoles. It would appear from the literature that the maximum useful temperature of these materials is in the 200-260°C range, far below the needs of the present program.

In comparison to the other matrix materials some of the potential advantages of employing fiber-reinforced metals and alloys are:

- They exhibit superior strength at elevated temperatures
- A major improvement in the specific strength is evident,
- A higher degree of anisotrophy is achieved.

Many problems still remain to be solved in order to realize the full potential of these materials. Among these problems are composite fabrication and chemical compatibility, as the fabrication processes are complex and varied and hence, the properties of the final material are greatly affected.

Some of the materials that can now be purchased in sample quantities for testing and evaluation are:

Matrix	Reinforcement
Aluminum	Beryllium, Boron, Silicon Carbide
Aluminum Alloys	Silicon Carbide coated Boron
Magnesium	Boron, Silicon Carbide
Nickel	Boron, Silicon Carbide, Tungsten
Titanium	Silicon Carbide coated Boron

Among these materials boron/aluminum, silicon carbide coated boron/aluminum alloys, silicon carbide/nickel, and silicon carbide coated boron/titanium form strong, compact composites.[9] Also, silicon carbide coated boron matrix materials were found to have superior resistance to degradation at elevated temperatures compared to that of other materials.[12] In summary, it should again be emphasized that all of the above materials are chemically and mechanically quite complex. Much progress has been made, but much remains to be accomplished before reproducible and reliable matrix materials can be obtained.

Other Ceramic Materials

As the strength of a material is highly dependent on its microstructure, which in turn is directly related to the forming process, a comparison of the various forming processes is of importance.

Continuous fibers can be formed by a ceramic extrusion technique in which finely divided oxide particles are mixed with an organic binder and then extruded through platinum orifices. However, considerable care must be taken in controlling the thermal treatment during processing in order to prevent excessive grain growth of the originally small oxide particles.

Another technique that is commonly employed is vapor deposition. This consists of reducing or decomposing a volatile compound of the desired coating material onto a heated substrate, usually a fine wire or other conductive filament. However, this decomposition must be accomplished below the melting points of the coating material and the substrate material.

Filaments produced by the vapor deposition technique are, by the very nature of the process, composite materials containing a metallic core surrounded by a ceramic coating. By closely controlling the processing parameters, high strength filaments have been produced by this method.

Among the numerous other processes which have been used to form polycrystalline materials are plasma deposition, drawing of the material from a melt, and fused salt electrolysis.

Whisker Materials

The dependence of whisker strength on size has been well documented.[7] It has been demonstrated by several workers that the high strength dependency of whiskers is primarily due to the greater probability of fewer internal or external flaws being present in whiskers than are present in other materials.

It has also been demonstrated that any outgrowths which produce stress concentrations can seriously decrease the whisker strength, but that this can be partially corrected by etching of the outer surface of the whisker.[10]

A variety of techniques has been employed for growing whiskers, especially for the metallic variety. These have been grown spontaneously from plated metals and in eutectic alloys. Whiskers have also been grown by condensation from the vapor phase, by electrolysis, by rapid cooling of aqueous solutions, by changes in pressure, and by the high temperature reduction of metallic salts in a hydrogen atmosphere. This latter method is the most widely used industrial process for the production of whisker materials.

In order to assure a supply of uniformly high-strength whiskers very careful control must be maintained over all the processing parameters as the variations in these parameters strongly influence the strength of whisker materials.

Methods of Evaluation – The three methods most commonly used for determining the strengths of a fiber are:

a. The tensile test

b. The bend test

c. The loop test

Each of these methods has its limitations, but it is generally considered that the tensile test yields the most precise values since the stress is evenly distributed throughout the entire fiber. With the other two methods, only the outer parameter of the fiber at the point of maximum curvature is stressed to the maximum value.

The tensile test is based essentially on pulling a fiber apart by gripping the ends and applying a load along the fiber's axis. The stress value obtained is determined by simply dividing the breaking load by the fiber's cross sectional area.

Three of the most common difficulties in using this type of test are·

a. Maintaining a firm grip on the fiber without damaging the fiber in the grip area,

b. Ensuring proper alignment of the load along the fiber's axis

c. Determining the true cross sectional area of the fiber.

In contrast to the tensile test, the bend and loop tests depend essentially on imparting a symmetrical curvature to the fiber. This places the outer surface of the fiber at the point of maximum curvature under maximum stress.

One of the most common errors that is encountered in using these tests is in the precise measurement of the diameter of the material, especially for the very minute fibers and whiskers. Other sources of error would occur if:

a. The fiber does not have a uniform or symmetrical cross sectional area throughout

b. The fibers are not homogeneous and isotropic

c. The elastic modulus in tension is not equal to that in compression for the particular material.

As can be seen from the above discussion, when strength data is of critical importance, tests on specific lots of material should be performed.

Properties of Reinforcing Fibers

Chemical Properties – The melting points and densities of both continuous and whisker materials are tabulated in Table 4-19.

TABLE 4-19

CHEMICAL PROPERTIES OF REINFORCING FILAMENTS

Filament	Melting Point °C(7)	Density (Theoretical) g/cm³(7) (11)
1. Continuous		
A. Glass		
E-glass	840	2.55
E/HTS	840	2.55
YM31A	840	2.77
S-994	840	2.49
29-A	900	2.66
SiO_2	1,660	2.19
B. Graphite		
Carborundum Co.	3,650	1.49
Courtaulds, Ltd.		1.94
Hitco		1.8
Morganite, Ltd.		1.9
Union Carbide		1.63
C. Metal		
Be	1,285	1.85
B	2,200	2.35
Mo	2,622	10.2
W	3,410	19.3

TABLE 4-19

CHEMICAL PROPERTIES OF REINFORCING FILAMENTS (CONT)

Filament	Melting Point °C(7)	Density (Theoretical) g/cm^3(7) (11)
D. Non-Metal		
C	3,700	1.86
TiB_2	2,940	4.5
ZrB_2	3,060	6.1
TiC	3,095	4.92
WC	2,750	15.7
ZrC	3,400	6.56
BN	2,982	2.1
2. Whiskers		
A. Ceramic		
Al_2O_3	2,000	3.98
BeO	2,550	3.01
B_4C	2,490	2.52
Graphite	3,650	2.1
SiC	2,700	3.22
Si_3N_4	1,900	3.19
B. Metals		
Cu	1,083	8.92
Cr	1,890	7.2
Fe	1,540	7.85
Ni	1,455	8.98

Linear Thermal Expansions and Strength Data – Room temperature thermal expansions and strength data of a variety of continuous, whisker, and matrix materials are reported in Table 4-20, and the mechanical properties of various graphite filaments are listed in Table 4-21.

Figure 4-10 shows a comparison of the mechanical properties as a function of deposition temperature from two studies on carbon fibers[28].

4.2.3.3 Summary

Of the various types of composite materials, the fiber-composites are receiving widespread attention. These materials offer the greatest potential where high strength, high modulus, and low density are prime requisites. In addition, a wide range of properties is available because high performance fibers and matrix materials can be arranged in many configurations varying from uniaxial alignment to one of complex weaves.

Because many of these new fibers are more refractory and more chemically and mechanically stable than glass fibers the development of new, high temperature composites is being realized.

As a result of these research and development efforts an ever increasing volume of information is being generated but to date, no data has been compiled which would aid in predicting which characteristics would produce the best overall properties such as impact resistance, matrix-fiber bonding, and fabricability for a given system.

Of the many materials available, those employing fibers of boron, especially silicon carbide coated boron filaments, silicon carbide, or graphite appear to be the most promising from a strength to density basis. However, these materials are still in the developmental stage and further documentation of their properties is needed before these materials can be fully utilized.

TABLE 4-20

MECHANICAL PROPERTIES OF REINFORCING FILAMENTS

Filament	Approximate Thermal Expansion Coefficient in/(in)(°C) × 10^{-6} at Room Temp. (1) (7) (14) (15)	Experimental Tensile Strength, 10^3 Kg/cm^2 at Room Temp. (7) (9) (13)	Youngs Modulus, 10^6 Kg/cm^2 at Room Temp. (7) (9) (13)
1. Continuous			
A. Glass			
E-glass	5.0	17.5	0.074
E/HTS		35	0.074
YM31A		35	1.12
S-994		45.5	0.088
29-A		56	1.01
SiO_2	0.56	59.5	0.074
B. Graphite*			
Carborundum Co.	3.77	19.6	3.5
Courtaulds, Ltd.		17.5-26.2	1.96-4.2
Hitco		10.5-21	1.75-3.5
Morganite Ltd.		14-31.5	2.45-4.55
Union Carbide		12.6-28	1.75-3.5
C. Metal			
Be	13-18	15.4	2.94
B	8.3	24.5	4.55
Mo	5.43	22.4	3.64
W	4.6	28	4.13

* See Table 4-21

TABLE 4-20

MECHANICAL PROPERTIES OF REINFORCING FILAMENTS (CONT)

Filament	Approximate Thermal Expansion Coefficient in/(in) (°C) × 10^{-6} at Room Temp. (1) (7) (14) (15)	Experimental Tensile Strength, 10^3 Kg/cm^2 at Room Temp. (7) (9) (13)	Youngs Modulus, 10^6 Kg/cm^2 at Room Temp. (7) (9) (13)
D. Non-Metal			
C	–	12.6	0.42
TiB_2	9	1.33	3.78-5.39
ZrB_2	7.5	2.3	4.48
TiC	9-10.2	4.75	3.15-4.2
WC	5	3.5	5.18-7.14
ZrC	9	1.96	4.13-4.2
BN	7.56	15.4	0.91
2. Whiskers			
A. Ceramic			
Al_2O_3	6-9	11.2-182	4.2
BeO	8-13	140-196	4.2
B_4C	4.3	65.4	4.9
Graphite	4	210	10.15
SiC	5.4	7-115.5	4.55
Si_3N_4	2.48	105	2.8

TABLE 4-20

MECHANICAL PROPERTIES OF REINFORCING FILAMENTS (CONT)

Filament	Approximate Thermal Expansion Coefficient in/(in) (^{o}C) x 10^{-6} at Room Temp. (1) (7) (14) (15)	Experimental Tensile Strength, 10^{3} Kg/cm^{2} at Room Temp. (7) (9) (13)	Youngs Modulus, 10^{6} Kg/cm^{2} at Room Temp. (7) (9) (13)
B. Metals			
Cu	16.6	29.9	1.26
Cr	6.2	90.5	2.45
Fe	11.7	133	2.02
Ni	13.3	39.2	2.17
C. Matrix Materials			
Al/Al_2O_3		4.75	1.82
Al/B		11.4	2.24
Al/SiC		6.43	2.31
B/SiO_2		24.5	3.64
B/W		28	3.84
Mg/B		9.63	2.19
Ni/B		13.15	2.28
Ni/SiC		10.65	3.08
Ni/W		15.5	2.95
Ti/SiC		9.1	2.1
W/SiC		25.3	4.69
C/Epoxy		6.3	1.54
SiC/Epoxy		7.2	2.03
B/Polyimide		9.5	2.84

CONFIDENTIAL

TABLE 4-21

MECHANICAL PROPERTIES OF VARIOUS GRAPHITE FILAMENTS*

Designation	Tensile Strength, 10^3 Kg/cm^2 at Room Temperature	Youngs Modulus, 10^6 Kg/cm^2 at Room Temperature
Carborundum Co.		
GSC42	7-12.6	0.21-0.35
GSG42	7-12.6	0.21-0.35
Courtaulds, Ltd.		
Type A	19.2-22.8	1.96-2.3
Type B	17.5-21	3.5-4.2
Type C	22.8-26.2	2.45-2.8
Hitco		
HMG25	10.5	1.75
HMG40	17.5	2.8
HMG50	21	3.5
Morganite Ltd.		
Type I	14-21	3.85-4.55
Type II	24.5-31.5	2.45-3.15
Union Carbide		
Thornel 25	12.6	1.75
Thornel 40	24.5	2.8
Thornel 50	28	3.5

*Data obtained from manufacturer's brochures

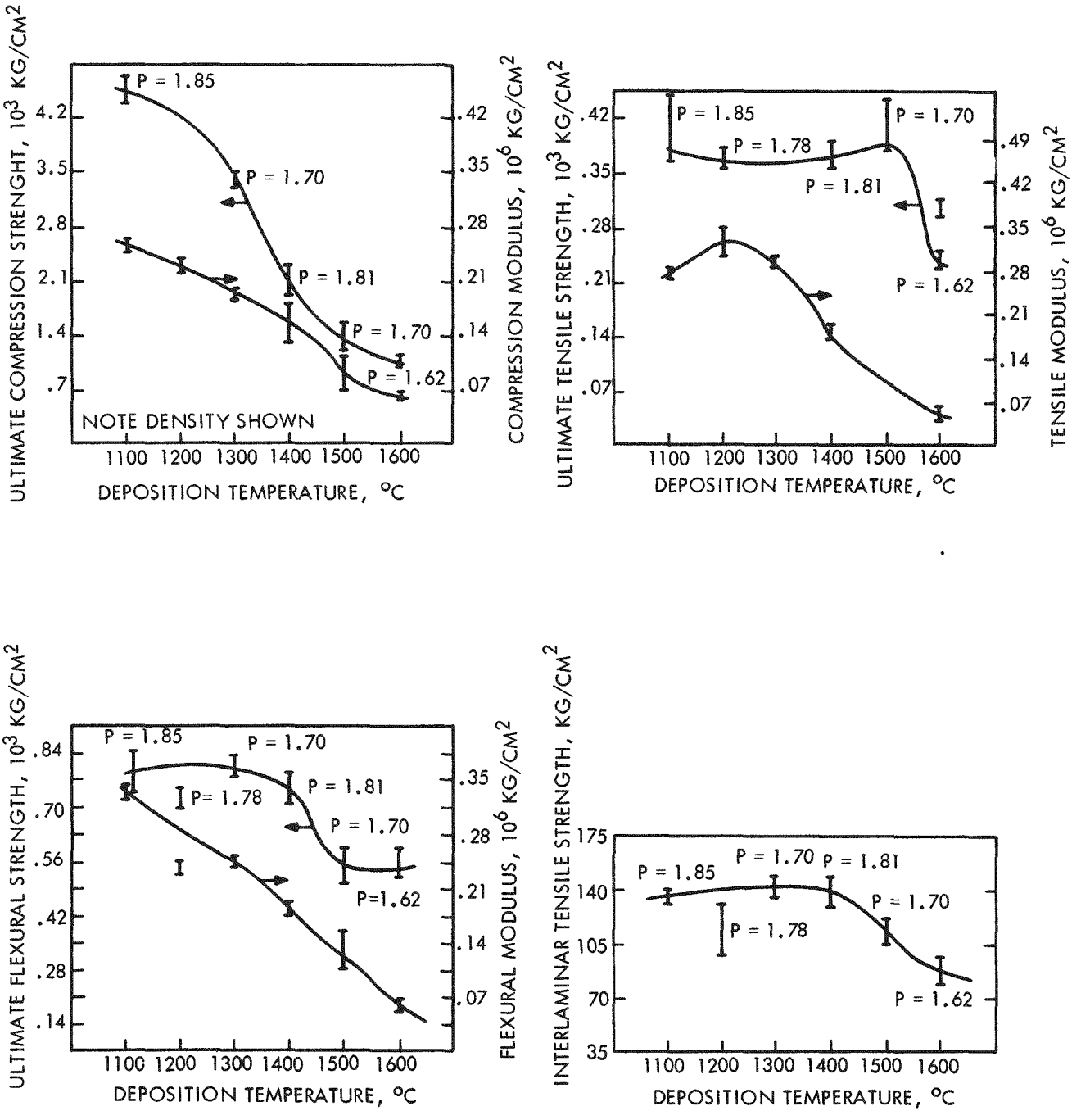

69-H65983-059

Figure 4-10 Comparison of Mechanical Properties of Carbon Fibers as a Function of Deposition Temperature[28].

4.2.4 REFRACTORY LINER MATERIALS

4.2.4.1 Introduction

A number of refractory elements and compounds have been evaluated as possible liner materials for fuel capsules. Two specific groups, the refractory metals and oxides, appeared to fulfill the initial requirements of high temperature stability and suitable compatibility behavior in direct contact with $Pu^{238}O_2$. The refractory borides, carbides, nitrides, and mixed oxides have also been evaluated for use as possible liner materials, although a barrier material is required between these compounds and the fuel.

This section presents the thermal, mechanical, and physical properties of these materials together with existing reaction data of these materials with both graphite and $Pu^{238}O_2$.

4.2.4.2 Discussion

Chemical Compatibility of Refractory Materials

Compatibility between two materials in contact is governed by both the physical and chemical properties associated with each material. These properties include melting points, densities, strengths, thermal expansions, specific heats, thermal conductivities, and any tendencies for compound or solid solution formation.

Of the candidate refractory liner materials only the refractory metals iridium, molybdenum, niobium, rhenium, tantalum, and tungsten and the oxides beryllia, hafnia, magnesia, thoria, and zirconia have been considered for possible use in direct contact with $Pu^{238}O_2$. Other refractory compounds such as the borides, carbides, nitrides, and mixed oxides, because of their expected interaction with $Pu^{238}O_2$, can not be considered for use in direct contact with the fuel but can be utilized as a possible liner material, provided an adequate barrier material is placed between the fuel and these refractory materials.

With PuO_2 - Some research has been conducted concerning the compatibility of various refractory metals and oxides with $Pu^{238}O_2$. Table 4-23 lists possible refractory oxides and their reaction temperatures with PuO_2. Of these oxides, complete solid solution has been established in the binary systems involving PuO_2 with ThO_2 and ZrO_2 above 1500°C.[28] However, it has been found that ThO_2 and ZrO_2 do not show solid solution formation at 1250°C.[23] Although beryllia appears to be the most chemically stable candidate and indicates less tendency toward interaction in the temperature range to 2135°C, handling difficulties are encountered as a result of its high neutron output. Hafnia has been completely eliminated as a possible candidate because of its interaction with PuO_2 at essentially all temperatures above 1000°C.[28] Therefore, the most likely oxides for use with $Pu^{238}O_2$ would appear to be MgO, with a reaction temperature somewhat above 1500°C, and ThO_2 or ZrO_2, with a reaction temperature above 1250°C.

Prior compatibility results for PuO_2 have indicated a fair degree of stability with refractory metals.[28] Data from compatibility trials indicate a general absence of severe reaction with molybdenum at all temperatures, a slight surface pitting and compound formation with both rhenium and iridium which increases with increasing temperature, and a very well defined attack with tungsten which increases in penetration with increasing temperature.[23] [28]

It should be emphasized, however, that these studies have been mainly cursory in nature in that only a limited number of experiments have been undertaken. It has been found, though, that in nearly all the materials tested, fuel impurities have been evident in the reaction product with little or no involvement of the $Pu^{238}O_2$.[25]

While data based on the standard free-energy change for plutonium oxide-metal reactions indicates that a reaction between these materials is not favored, there exists a driving force in a closed system which precipitates a reaction. Cubic plutonia, which can exist as a single phase over a composition range from PuO_2 to $PuO_{1.61}$, must be considered as a two-component system which exhibits

a bivariant behavior. As a closed system, the degree of dissociation of the plutonia would depend on the amount of void volume in the system or the affinity of the encapsulant material. However, if there is a "sink" for the oxygen, chemical as well as geometrical considerations enter into the degree of dissociation.

As the chemical potential of oxygen in PuO_2 is higher than that in the metal oxides then by the second law of thermodynamics the chemical potential of any species must have the same value in all phases when equilibrium is established and thus oxygen will be transported from the plutonia to the metal until a metal oxide is formed. It is via this mechanism that molybdenum is more compatible with $Pu^{238}O_2$ than any of the other refractory metals in that it is necessary for the oxygen potential to fall to that of $PuO_{1.88}$ before molybdenum oxide is formed.[28] Table 4-25 lists the reaction temperatures of the refractory metals with PuO_2.

With Graphite – Because of the high cost of test specimens and the inability to produce a realistic environmental simulation, compatibility data for graphite-refractory materials is difficult to correlate. The approaches taken in property measurements were essentially deterministic with little consideration for the statistical character of the tests. Also because the applications of coated graphite are so varied and specialized there was little, if any, effort being directed towards standardization of test procedures.[32]

a. Refractory Zirconates

The compatibility data for the refractory zirconates is listed in Table 4-22. Calcium zirconate is compatible with graphite to a temperature greater than 1704°C.[1] No data has been found for the compatibility of barium zirconate.

b. Refractory Oxides

The compatibility data for the refractory oxides is listed in Table 4-23. Of the represented oxides magnesium oxide is the most compatible with graphite.

TABLE 4-22

COMPATIBILITY OF REFRACTORY ZIRCONATES[1]

Zirconate	Melting Point, °C[1]	Density g/cc[1]	Temperature of Reaction, °C With Graphite
$BaO \cdot ZrO_2$	2649	6.26	-
$CaO \cdot ZrO_2$	2344	4.76	> 1704

TABLE 4-23

COMPATIBILITY OF REFRACTORY OXIDES[4][21][22][23][24][25][28]

Oxide	Melting Point, °C[2]	Density g/cc[2]	Temperature of Reaction, °C	
			With Graphite	With PuO_2
BeO	2530	3.01	1300	2135
HfO_2	2812	9.68	1730	> 1000
MgO	2800	3.58	1800	1500
ThO_2	3050	9.86	1600	1500
ZrO_2	2590	5.75	1400	1500

c. Refractory Nitrides

The compatibility data for the refractory nitrides is listed in Table 4-24. Data has been found for only two of the nitrides and it would appear from this information that boron nitride is the most compatible with graphite.

TABLE 4-24

COMPATIBILITY OF REFRACTORY NITRIDES[1]

Nitride	Melting Point, °C[2]	Density g/cc[2]	Temperature of Reaction, °C With Graphite
BN	2704	2.25	1982
HfN	3305	13.94	-
TaN	3360	16.3	-
TiN	2930	5.22	> 1649
ZrN	2980	7.09	-

d. Refractory Metals

The compatibility data for the refractory metals is listed in Table 4-25. Although iridium is the most compatible metal with graphite its interaction with plutonia limits its usefulness.

TABLE 4-25

COMPATIBILITY OF REFRACTORY METALS[4][21][22][23][28]

Metal	Melting Point, °C[15]	Density g/cc[15]	Temperature of Reaction, °C	
			With Graphite	With PuO_2
Ir	2410	22.42	> 2110	> 1250
Mo	2610	10.22	1200	> 1750
Nb	2468	8.57	1400	> 1593
Re	3180	21.02	-	< 1500
Ta	2996	16.6	1000	> 1704
W	3410	19.3	1400	1593

e. Refractory Carbides

The compatibility data for the refractory carbides is listed in Table 4-26. Of the represented carbides it would appear from the limited data found that boron carbide is the most compatible with graphite.

TABLE 4-26

COMPATIBILITY OF REFRACTORY CARBIDES(1)

Carbide	Melting Point, °C(2)	Density g/cc(2)	Temperature of Reaction, °C With Graphite
B_4C	2350	2.52	>2204
HfC	3885	12.20	-
NbC	3500	7.6	<2235
SiC	2700	3.21	>1288
TaC	3880	13.9	<2235
TiC	3140	4.93	-
ZrC	3530	6.73	-

f. Refractory Borides

The compatibility data for the refractory borides is listed in Table 4-27. Data has been found for only two of the borides and it would appear from this information that hafnium boride is the most compatible with graphite.

Mechanical Properties of Refractory Materials

Linear Thermal Expansions Between 21 - 2204°C - Tables 4-28 through 4-33 list the average coefficients of linear thermal expansion of the refractory zirconates, oxides, nitrides, metals, carbides, and borides.

TABLE 4-27

COMPATIBILITY OF REFRACTORY BORIDES[4]

Boride	Melting Point, °C[2]	Density g/cc[2]	Temperature of Reaction °C With Graphite
Cr_2B	3300	6.53	-
HfB_2	3062	11.2	> 2500
NbB_2	2900	6.97	-
ThB_4	2510	7.5	-
TiB_2	2900	4.5	-
ZrB_2	3000	6.09	> 2420

TABLE 4-28

AVERAGE COEFFICIENTS OF LINEAR THERMAL EXPANSION OF VARIOUS ZIRCONATES[1]

Zirconate	Temperature Range, °C	Thermal Expansion Coefficient in/(in) (°C) $\times 10^{-6}$
$BaO \cdot ZrO_2$	25 - 999	8.46
$CaO \cdot ZrO_2$	25 - 999	10.45

TABLE 4-29

AVERAGE COEFFICIENTS OF LINEAR THERMAL EXPANSION OF VARIOUS OXIDES(1)

Oxide	Temperature Range, °C	Thermal Expansion Coefficient in/(in) (°C) × 10^{-6}
BeO	1204 - 2093	13.5
HfO_2	982 - 2204	11.9
MgO	982 - 2204	17.2
ThO_2	1427 - 2204	12.85
ZrO_2	1316 - 2204	15.75

TABLE 4-30

AVERAGE COEFFICIENTS OF LINEAR THERMAL EXPANSION OF VARIOUS NITRIDES(1)

Nitride	Temperature Range, °C	Thermal Expansion Coefficient in/(in) (°C) × 10^{-6}
BN	21 - 1093	7.56
HfN	24 - 1371	6.48
TaN	21 - 704	3.6
TiN	593 - 1427	9.0
ZrN	593 - 1427	7.74

TABLE 4-31

AVERAGE COEFFICIENTS OF LINEAR THERMAL EXPANSION OF VARIOUS METALS[15]

Metal	Temperature Range, °C	Thermal Expansion Coefficient in/(in) (°C) x 10^{-6}
Ir	0 - 100	6.5
Mo	20 - 1593	6.65
Nb	0 - 1000	7.88
Re	20 - 1000	6.7
Ta	20 - 1500	8.0
W	0 - 500	4.45

TABLE 4-32

AVERAGE COEFFICIENTS OF LINEAR THERMAL EXPANSION OF VARIOUS CARBIDES[1]

Carbide	Temperature Range, °C	Thermal Expansion Coefficient in/(in) (°C) x 10^{-6}
B_4C	871 - 2204	6.08
HfC	816 - 2204	7.92
NbC	21 - 2204	7.38
SiC	538 - 2204	5.4
TaC	21 - 2204	7.46
TiC	816 - 2204	9.9
ZrC	816 - 2204	9.0

TABLE 4-33

AVERAGE COEFFICIENTS OF LINEAR THERMAL EXPANSION OF VARIOUS BORIDES(1)

Boride	Temperature Range, °C	Thermal Expansion Coefficient in/(in) (°C) x 10^{-6}
Cr_2B	21 - 2204	8.64
HfB_2	21 - 2204	7.56
NbB_2	21 - 1649	8.64
ThB_4	20 - 982	5.94
TiB_2	21 - 2204	8.64
ZrB_2	21 - 2204	8.28

Strength Data at 1093°C - Tables 4-34 through 4-38 list the mechanical properties of the refractory oxides, nitrides, metals, carbides, and borides.

TABLE 4-34

MECHANICAL PROPERTIES OF VARIOUS OXIDES(1)

Oxide	Modulus of Rupture, 10^3 Kg/cm^2 1093°C	Tensile Strength 10^3 Kg/cm^2 1093°C	Youngs Modulus 10^6 Kg/cm^2 1093°C
BeO	1.96	0.21	3.5
MgO	1.05	0.35	2.59
ThO_2	-	-	2.03
ZrO_2	0.70	0.84	1.05

TABLE 4-35

MECHANICAL PROPERTIES OF VARIOUS NITRIDES[1]

Nitride	Modulus of Rupture 10^3 Kg/cm^2 1093°C	Tensile Strength 10^3 Kg/cm^2 1093°C	Youngs Modulus 10^6 Kg/cm^2 1093°C
BN	0.14	0.035	0.07

TABLE 4-36

MECHANICAL PROPERTIES OF VARIOUS METALS[15][20][27]

Metal	Modulus of Rupture, 10^3 Kg/cm^2 1093°C	Tensile Strength 10^3 Kg/cm^2 1093°C	Youngs Modulus 10^6 Kg/cm^2 1093°C
Ir	-	3.15	-
Mo	1.4	1.4 - 2.1	2.73
Nb	0.91	0.91 - 1.19	-
Re	-	8.69	-
Ta	0.43	1.05 - 1.4	1.54
W	0.91	3.5 - 5.25	3.5

TABLE 4-37

MECHANICAL PROPERTIES OF VARIOUS CARBIDES[1]

Carbide	Modulus of Rupture, 10^3 Kg/cm^2 1093°C	Tensile Strength 10^3 Kg/cm^2 1093°C	Youngs Modulus 10^6 Kg/cm^2 1093°C
B_4C	2.09 - 2.42	-	-
HfC	2.24	-	-

TABLE 4-37

MECHANICAL PROPERTIES OF VARIOUS CARBIDES[1] (Cont)

Carbide	Modulus of Rupture, 10^3 Kg/cm^2 1093°C	Tensile Strength 10^3 Kg/cm^2 1093°C	Youngs Modulus 10^6 Kg/cm^2 1093°C
SiC	1.47	-	3.5
TaC	3.01	-	-
TiC	4.2	0.07	-
ZrC	2.45	1.05	3.5

TABLE 4-38

MECHANICAL PROPERTIES OF VARIOUS BORIDES[1]

Boride	Modulus of Rupture, 10^3 Kg/cm^2 1093°C	Youngs Modulus 10^6 Kg/cm^2 1093°C
TiB_2	2.8	3.85
ZrB_2	0.049	3.85

Specific Heats and Thermal Conductivities at 1093°C - Tables 4-39 through 4-43 list the thermal properties of the refractory oxides, nitrides, metals, carbides, and borides.

TABLE 4-39

THERMAL PROPERTIES OF VARIOUS OXIDES[1]

Oxide	Specific Heat g · Cal/(g) (°C) 1093°C	Thermal Conductivity g · Cal · cm/(hr) (cm²) (°C) 1093°C
BeO	0.5	148.8
HfO_2	0.11	22.3
MgO	0.33	5.95
ThO_2	0.07	2.23
ZrO_2	0.16	2.23

TABLE 4-40

THERMAL PROPERTIES OF VARIOUS NITRIDES[1]

Nitride	Specific Heat g · Cal/(g) (°C) 1093°C	Thermal Conductivity g · Cal · cm/(hr) (cm²) (°C) 1093°C
BN	0.47	133.92
HfN	0.08	133.92
TaN	0.1	-
TiN	0.21	230.64[3]
ZrN	0.13	171.12

TABLE 4-41

THERMAL PROPERTIES OF VARIOUS METALS[15][27]

Metal	Specific Heat g · Cal/(g) (°C) 1093°C	Thermal Conductivity g · Cal · cm/(hr) (cm²) (°C) 1093°C
Mo	0.057	1041
Nb	0.075	-
Re	0.033	-
Ta	0.038	-
W	0.038	1120

TABLE 4-42

THERMAL PROPERTIES OF VARIOUS CARBIDES[1]

Carbide	Specific Heat g · Cal/(g) (°C) 1093°C	Thermal Conductivity g · Cal · cm/(hr) (cm²) (°C) 1093°C
B_4C	0.51	119
HfC	0.07	223.20
NbC	0.13	-
SiC	0.31	163.68
TaC	0.08	-
TiC	0.21	357.12[3]
ZrC	0.13	297.60[3]

TABLE 4-43

THERMAL PROPERTIES OF VARIOUS BORIDES[1]

Boride	Specific Heat g · Cal/(g) (°C) 1093°C	Thermal Conductivity g · Cal · cm/(hr) (cm^2) (°C) 1093°C
HfB_2	0.095	401.76
NbB_2	0.2	163.1
ThB_4	0.12	-
TiB_2	0.3	401.76
ZrB_2	0.18	282.72

4.2.4.3 Summary

Thermodynamic considerations eliminated all but a few materials for use in direct contact with PuO_2 at temperatures above 1500°C because of compatibility problems. The experimental evaluation of these few showed that molybdenum and magnesia were compatible with $Pu^{238}O_2$ at temperatures of 1750°C and 1500°C, respectively. At these temperatures little or no evidence of reaction was observed on molybdenum materials whereas some interaction was observed in the MgO specimens under the same conditions. For lower temperatures, up to 1250°C, both ThO_2 and ZrO_2 can be considered for use as it has been demonstrated that these oxides do not show solid solution formation at this temperature.

Of the liner materials that have been considered for indirect use, boron nitride, boron carbide, and hafnium boride appear to be worthy of further investigation, particularly for use with molybdenum.

4.2.5 REFERENCES

1. Lynch, J.F., Ruderer, C.G., and Duckworth, W.H., Engineering Properties of Selected Cermaic Materials, American Ceramic Society, (1966).

2. Weast, R.C., Handbook of Chemistry and Physics, Chemical Rubber Co., (1967).

3. Taylor, R.E., and Nakata, M.M., "Thermal Properties of Refractory Materials", Report No. WADD-TR-60-581, Part IV, Contract 33(657)-7136, Atomics International, (Nov. 1963).

4. Criscione, J.M., et al, "High Temperature Protective Coatings for Graphite", Report No. ML-TDR-64-173, Part I & II, Contract AF33(657)-11253, Union Carbide Corp., (June; Oct. 1964).

5. Powell, C.F., Oxley, J.H., and Blocker, J.M. Jr., Vapor Deposition, John Wiley & Sons, Inc., (1966).

6. Colton, E., "Introducing Boron Silicide", Nuclear Engineering, (Aug. 1961), pp. 324 - 325.

7. Fiber Composite Materials, American Society for Metals, (1965).

8. Greenstreet, W.L., "Mechanical Properties of Artificial Graphites - A Survey Report", Contract W-7405-eng-26, Oak Ridge National Laboratory, (Dec. 1968).

9. Rauch, H.W., Sr., Sutton, W.H., McCreight, L.R., "The Fabrication, Testing and Application of Fiber-Reinforced Materials - A Survey", Report No. AFML-TR-68-162, General Electric Co., (Sept. 1968).

10. McCreight, L.R., Rauch, H.W., Sr., and Sutton, W.H., "A Survey of the State-of-the-Art of Ceramic and Graphite Fibers", Report No. AFML-TR-65-105, General Electric Company, (May 1965).

11. Fleck, J.N., Jablonowski, E.J., "New World of Composites: What We Can Expect in the 1970's", Metal Progress, pp. 99 - 103, (March 1969).

12. Kreider, K.G., Schile, R.D., Breiman, E.M., Marciano, M., "Plasma Sprayed Metal Matrix Fiber Reinforced Composites", Report No. AFML-TR-68-119, United Aircraft Corp., (July, 1968).

13. Henry, E.C., "Research on Refractory Composites and Coatings", Presented at Thirteenth Meeting of Refractory Composites Working Group, (July 1967).

14. Shand, E. B., Glass Engineering Handbook, McGraw-Hill Book Co., Inc., (1958).

15. Hampel, C. A., Rare Metals Handbook, Reinhold Publishing Corp., (1967).

16. Schiff, D., "Pyrolytic Materials for Reentry Applications", Metals Engineering Quarterly, pp. 32 - 42 (Nov. 1962).

17. Garber, A. M., "Pyrolytic Materials for Thermal Protection Systems, "Aerospace Engineering, pp. 126 - 137, (Jan. 1963).

18. Garber, A. M., Nolan, E. J., Scala, S. M., "Pyrolytic Graphite - A Status Report", Transactions of the Eighth Symposium on Ballistic Missile and Space Technology, Vol. I, (Oct. 16 - 18, 1963).

19. Nolan, E. J., Scala, S. M., "Aerothermodynamic Behavior of Pyrolytic Graphite During Sustained Hypersonic Flight", ARS Journal, pp. 26 - 35, (Jan. 1962).

20. Chelius, J., "Nonferrous Refractory Metals", Metals Reference Issue, p. 85, (Dec. 14, 1967).

21. Barth, V. D., and Rengstorff, G. W. P., "Oxidation of Tungsten", DMIC Report 155, (July 17, 1961).

22. Selle, J. E., "A Summary of the Phase Diagrams and Compatibility of PuO_2 with Various Materials", MLM-1589, Mound Laboratory, (April 21, 1969).

23. Pardue, W. M., et al, "Mid Year Report for the Program to Develop Composite Fuel Forms of $Pu^{238}O_2$", BMI-1860, Battelle Memorial Institute, (March 1969).

24. Pardue, W. M., et al, "Summary Report on Development Program for Fabrication of Composite Fuel Form of $Pu^{238}O_2$", BMI-1849, Battelle Memorial Institute, (Sept. 16, 1968).

25. "Mound Laboratory Isotopic Power Fuels Programs: Oct. - Dec., 1968", MLM-1528, Mound Laboratory, (Jan. 31, 1969).

26. Lyman, T., Metals Handbook, Vol. I, American Society for Metals, (1961).

27. Pobereskin, M., "Mid Year Report on Development Program for Fabrication of Composite Fuel Form of $Pu^{238}O_2$", BMI-1831, Batelle Memorial Institute, (March 11, 1968).

28. Stoller, H. M., Frye, E. R., "Carbon-Carbon Materials for Aerospace Applications", Sandia Corporation.

29. Frye, E. R., SCTM-69-123.

30. Mantell, C. L., Carbon and Graphite Handbook, John Wiley & Sons, (1968).

31. Wurst, J. C., "Review of Testing and Standards for High Temperature Coatings", 1st Progress Report of the Committee on Coatings, National Research Council, (1968).

4.3 SIREN CAPSULE FUELING ANALYSIS

4.3.1 INTRODUCTION

The purpose of the SIREN Capsule Fueling Analysis is to determine, for future verification, techniques for fabricating and/or fueling using those $Pu^{238}O_2$ isotopic fuel forms currently available and under development.

The fuel forms considered in the Fueling Analysis are:

- Microsphere
- Solid solution
- Cermet
- Sintered oxide

Each of the $Pu^{238}O_2$ fuel forms requires a different approach to the technical aspects of fabrication and/or fueling. The compatibility of materials must also be factored in so that suitable liner materials can be chosen for each fuel form based on the best information currently available.

Health safety is given prime consideration in determining the fueling techniques for "cold" fabricated and "hot" fabricated capsules. The general philosophy which will prevail in the analysis is that all "cold" fabricated fueling and/or "hot" fabricated capsules will be performed in a "surgically clean" manner, insofar as possible, to reduce the magnitude of contamination and associated health hazards.

Cost estimates, based on direct labor, materials and equipment necessary for each approach, are made and presented.

4.3.2 COLD FABRICATION AND MICROSPHERE FUELING OF SIREN

4.3.2.1 Fuel Description

Mound Laboratories, Monsanto Research Corporation, Miamisburg, Ohio is the present supplier of $Pu^{238}O_2$ microspheres.[1,2]

This fuel, as supplied for use in space isotopic power programs, consists of microspheres ranging in size from 50 to 250 μ. Health safety requirements currently require that the fine content below 47 μ be drastically reduced. Mound has reported that $Pu^{238}O_2$ particulate less than 47 μ is particularly biologically hazardous from the airborne (inhalation) standpoint.

The fuel specifications for SNAP 27[2], by way of example, require that the upper limit of fines from each 200-gram batch shall not be more than 1×10^{-3} weight percent of particulate less than 47 μ diameter. This amounts to 2 mg of fines per 200-gram batch. Mound Laboratories reportedly is able to reduce the fine content to a lower level.

Some of the salient features of this fuel form are:

- Thermal stability of the microspheres is reasonably good
- Power density is approximately 2.7 watts/cc, assuming a reasonable packing fraction (30% void volume)
- Thermal conductivity is 0.003 cal/sec cm $^{\circ}C$ (528$^{\circ}C$, Helium atmosphere)
- Coefficient of expansion ($10^{-6}/^{\circ}C$) ranges from 8.06 to 14.4 (100°to 1000$^{\circ}C$)
- Biological hazard due to airborne particulate is quite high.

4.3.2.2 Capsule Description

The SIREN capsule is composed of a hollow inner sphere over which is wound many layers of graphite yarn in the fashion of a golf ball. The wound spherical assembly is then impregnated with pyrolized graphite. A detailed description of the fabrication of the SIREN capsule is given in Section 3.

The purpose of such a structure is to take advantage of the strength characteristics observed in filament-wound composite structures. Similar materials

such as pyrolytic graphite impregnated felt have abnormally high strength characteristics normal to the face of the felt, but poor strength in the plane parallel to the face. With the SIREN concept, the capsule is designed so that the forces of impact are directed perpendicular to the plane having high tensile strength and low compressive strength and parallel to the plane having high compressive and impact strength.

The liner over which is wound the graphite yarn provides a fuel/capsule interface. The liner must be compatible with the fuel form and the capsule in order to fulfill its primary purpose. The liner material, then, must meet these requirements:

- Compatibility with fuel at the maximum anticipated temperature
- Must not permit significant fuel diffusion at the operating temperature or during reentry heating
- Must allow helium permeation from fuel to graphite
- Must be compatible with graphite at the maximum anticipated temperature
- Must have high compressive strength and resist impact forces imposed
- Must not melt or undergo significant differential expansion during maximum reentry temperature
- Must be resistant to thermal shock.

Candidate liner materials for the microsphere fuel form as presently envisioned are ThO_2, ZrO_2, molybdenum (using powdered metallurgy techniques) and molybdenum cermet of the aforementioned refractory oxides. If molybdenum is used, a suitable over-layer such as flame sprayed ZrO_2 is required to eliminate incompatibility problems with the graphite and to provide some oxidation protection for the molybdenum.

Access to the interior void volume of the unfueled, wound and impregnated capsule is accomplished by drilling a hole of appropriate size through the graphite to the liner, thus exposing the liner. The fueling port is opened into the liner by drilling or other techniques as appropriate for the liner material used.

Figure 4-11 shows a cross-section of a completed and fueled SIREN Capsule (conceptual).

4.3.2.3 Fueling Requirements

Fueling of the cold fabricated capsule generally follows the approach used in fueling metallic capsules, in that the capsule is fabricated and prepared for fueling prior to any exposure to radioactive fuels. This is where the similarity ends, for unlike multiple encapsulated metallic capsules where each encapsulation is sequentially performed, the fabrication of the two primary encapsulations for the SIREN capsule is completed prior to fueling. The third "encapsulation" or oxidation resistant coating is applied after final closure.

The major problem, from the fueling standpoint is to prevent contamination of the SIREN capsule by $Pu^{238}O_2$ fines. Contamination prevention is emphasized for SIREN rather than decontamination with the view that the former drastically reduces or eliminates the latter and because the SIREN outer structure would be difficult to decontaminate.

It is recognized that low contamination levels in a glove box used for $Pu^{238}O_2$ microsphere fueling are next to impossible to maintain. However, glove box design and arrangement as well as fueling apparatus can be a major factor in preventing contamination of the SIREN capsule.

The glove box construction should meet the following requirements in addition to the usual radiological safety requirements of effuelent filtration, monitoring, and shielding:

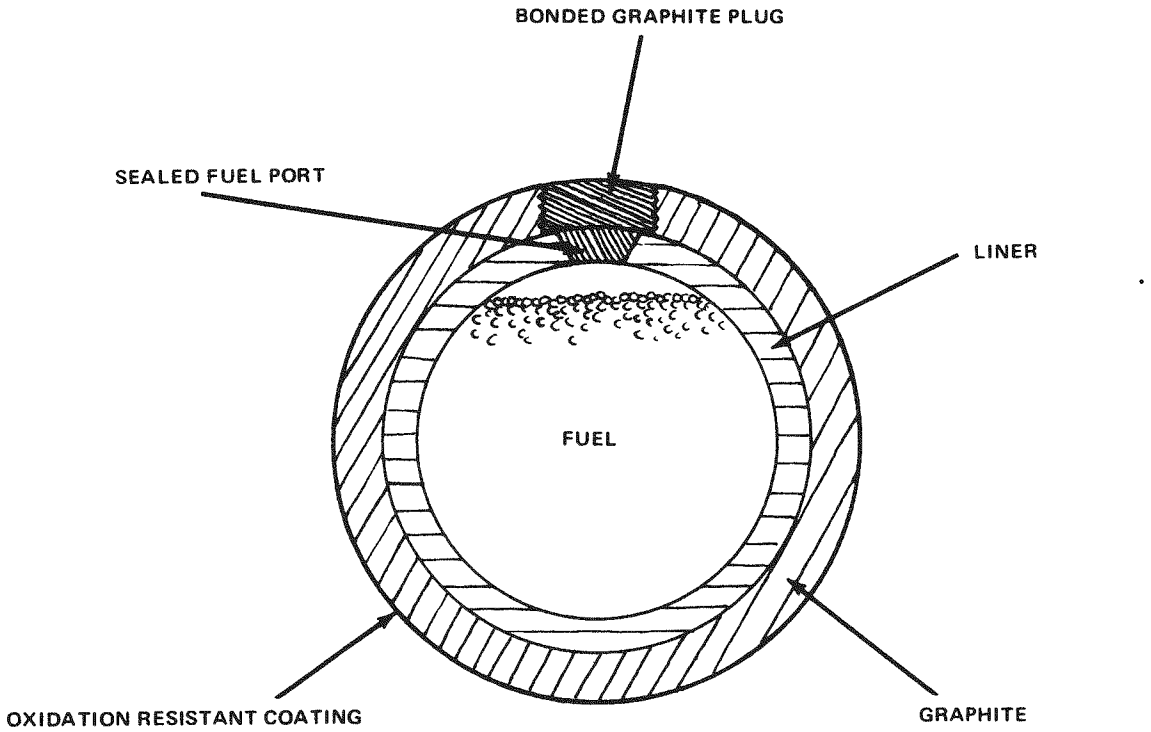

69-H65983-039

Figure 4-11 Fueled SIREN Capsule (Conceptual).

- Atmosphere controlled (helium, less than 100 PPM O_2)
- Easily decontaminated surfaces
- Contain no equipment or facilities not essential to operation
- Contain sealed compartments for contaminated article storage after use
- Transfer ports to open into glove boxes of successively lower contamination level.

With regard to radiological safety, the quantity of microsphere type fuel for a typical capsule (approximately 186 watts) presents a minor problem with regard to shielding. The approximate gamma and neutron dose rate, as derived from the Mound Laboratories Pu^{238} Data Sheets are summarized below (based on two feet from the source center line):

- Gamma dose rate (mrem/hr) - 2.1
- Neutron does rate (mrem/hr) - 14.5.

While the gamma and neutron dose rates are negligible for occasional (a couple of hours per week) operation, prolonged or repetitive operations require some shielding. The tenth-value layer for water (considering energies involved) is approximately 8 inches. A water window of 8-inch thickness or its equivalent in plexiglass is recommended.

The neutron dose rate at 6 inches from the capsule will give problems, however, and it now becomes necessary to either limit the time the fueling operator's hands are close to the capsule (after fueling) or to provide some additional shielding (plexiglass, for example) to reduce the dose rate.

Assuming, for the moment, that no shielding is used and the entire operation takes two hours, it is estimated that the total exposure dose (γ + n) will be 23.4 mrem. On this basis, three or four capsules per week, per operator, could be fueled without exceeding an exposure of 100 mrem/week (whole body).

The number of capsules per operator will depend upon the radiation exposure to the operator. Master-slave manipulation can be used to reduce the dose rate hazard to the extremities.

The subject of fines requires further consideration. The SNAP 27 fines requirement[2] was 10^{-3} weight percent of fines per 200-gram batch of $Pu^{238}O_2$ fuel (10 PPM). Should this level prove to be a hazard or otherwise unsatisfactory, Mound Laboratories has reported[3] that the contamination level can be reduced by at least 4 orders of magnitude (roughly 1 dpm per microsphere).

4.3.2.4 Fueling Techniques

Many techniques have been examined for use in fueling of the cold fabricated capsule. Some of these techniques show promise while others are less suitable for a variety of reasons. Each technique is identified by a subparagraph. The advantages and/or disadvantages of each technique are summarized for each case.

It cannot be overemphasized that the final form of fueling tools or technique(s) chosen for evaluation in the next phases of the program may change drastically during actual evaluation with simulated and/or real fuel. The techniques and tools, then, have to be proven and represent possible approaches to the problems of fueling the cold fabricated capsule and effecting a reliable seal or closure.

Contamination Prevention Cooling Fixture

Figure 4-12 shows the contamination prevention/cooling fixture as it is presently envisioned for use with most of the approaches to the fueling problem. This fixture is assembled prior to insertion into the glove box.

Prior to insertion of the capsule into the fixture, a threaded sleeve with a silicone rubber gasket attached to one end is screwed into the graphite opening. The gasket seals the area between the sleeve and capsule liner. The bore of the sleeve is plated and highly polished for ease of decontamination and serves to prevent contamination of the porous graphite outer structure. The exterior of the

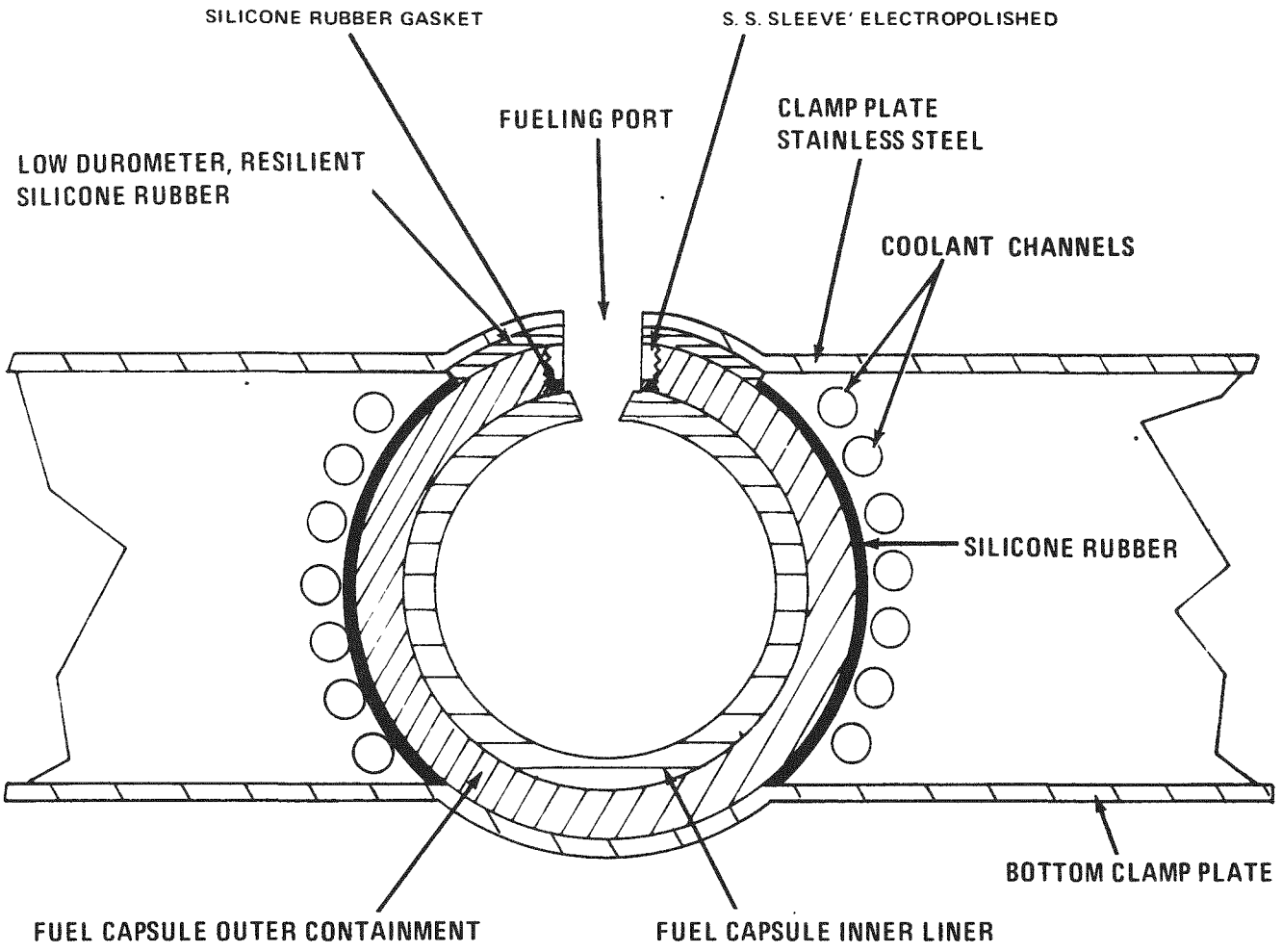

69-H65983-040

Figure 4-12 Combination Cooling/Contamination Prevention Fixture.

capsule, including the opening in the graphite, is sealed, (save for the fueling port in the liner) from exposure to the glove box environment. The sleeve and area immediately adjacent to the port (underneath the upper clamping plate) is sealed with a low durometer (30 to 40) highly resilient silicone rubber gasket. Clamping pressure applied between the upper and lower clamp plates causes the silicone rubber gasket to conform to the surface imperfections of the SIREN capsule as well as seat against the sleeve.

Cooling of the capsule can be accomplished by one of two methods:

- Direct contact with chilled, distilled water
- Contact to a split, spherical, water-cooled chill block with thin silicone rubber contacting surface.

The latter of these two methods is depicted in Figure 4-12. The former is feasible because of the non-wetting characteristics of the graphite surface, and because the structure of the graphite layer has exhibited low porosity. If the direct contact method is used, appropriate monitoring and disposal (possibly recovery of $Pu^{238}O_2$ in the event of a spill) of the water must be provided for. The chill water coils, because they are a closed system, should not have to be monitored.

The type of opening in the ceramic liner as shown in Figure 4-12 is designed for a particular fueling tool. This opening will change as appropriate for specific fueling tools, techniques and liner or port materials.

Compression Seal Fueling Tool

The compression seal fueling tool shown in Figure 4-13 is designed to be used with the tapered opening in the ceramic liner shown in Figure 4-12.

This tool has been tested with SiO_2 microspheres containing a substantial quantity of fines of unknown size and microspheres ranging in size from 30 to 125 microns. In contrast with the $Pu^{238}O_2$ microspheres, the SiO_2 microspheres are hollow with an average wall thickness of 2 microns. A 14-gage (0.082 in. O.D.,

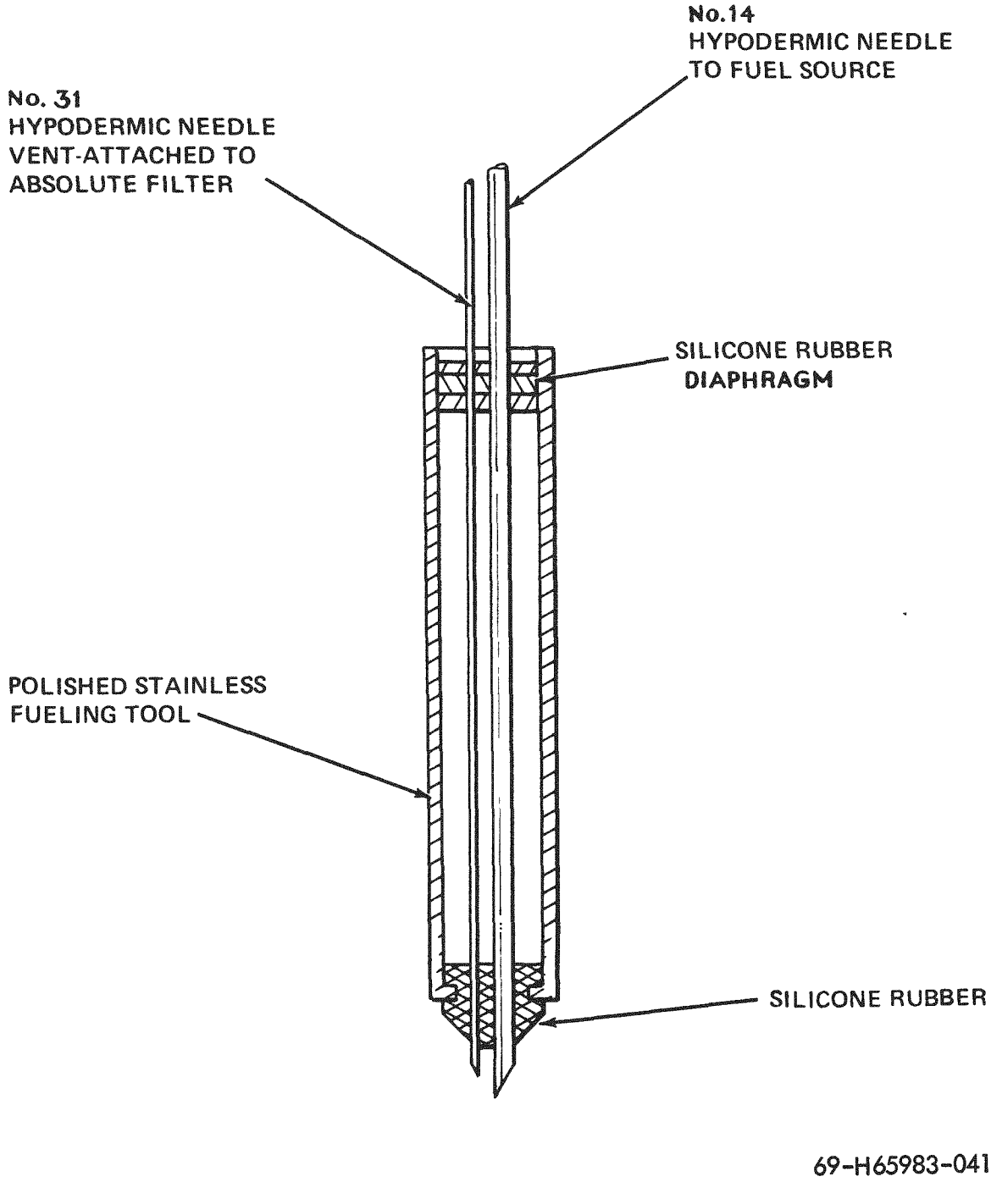

Figure 4-13 Compression Seal Fueling Tool.

0.063 in. I.D.) needle approximately one foot long was successfully used in conjunction with a 35 cc disposable plastic laboratory syringe to transfer the SiO_2 microspheres into a SIREN capsule, using the compression seal fueling tool. A No. 31 needle (0.010 in. O.D., 0.005 in. I.D.) was used as a vent to equalize pressure differences caused by displacement of air by the microspheres.

Figure 4-14 shows the fueling tool together with the associated fueling apparatus being put in place. A tool holding jig (not shown) would be necessary for proper placement.

Figures 4-15, 4-16 and 4-17 show the sequence of operations through fueling and removal of the fueling assembly.

The nose of the fueling tool is forced into contact with the tapered hole in the liner. The vacuum pump is actuated and the valve is turned on sufficiently to obtain a slight negative pressure within the capsule (the amount of negative pressure will have to be determined experimentally). The fuel is then admitted by opening the fuel reservoir valve. A metal, water-cooled, syringe is next operated to force the microspheres into the capsule cavity. A vibrator operating at some frequency which is sufficient to agitate the microspheres to a fluidized condition is used to enhance transfer of the fuel. Upon completion of fuel transfer, a "wash" of ZrO_2 microspheres is similarly forced into the capsule to remove as much as possible of any fuel remaining in the hypodermic needle and fuel container and to form a protective cover (from the standpoint of fines migration) over the fuel within the capsule. The combination cooling and contamination prevention fixture may also have to be vibrated to settle and level out the fuel in the capsule. Upon completion of these two operations, the vacuum pump is shut down and the pressure differential equalized by venting. Both needles are then withdrawn into the silicone rubber sealed cavity within the tool barrel and the assembly withdrawn from the capsule, capped and set aside. Up to this point no fuel has been exposed to the interior of the glove box.

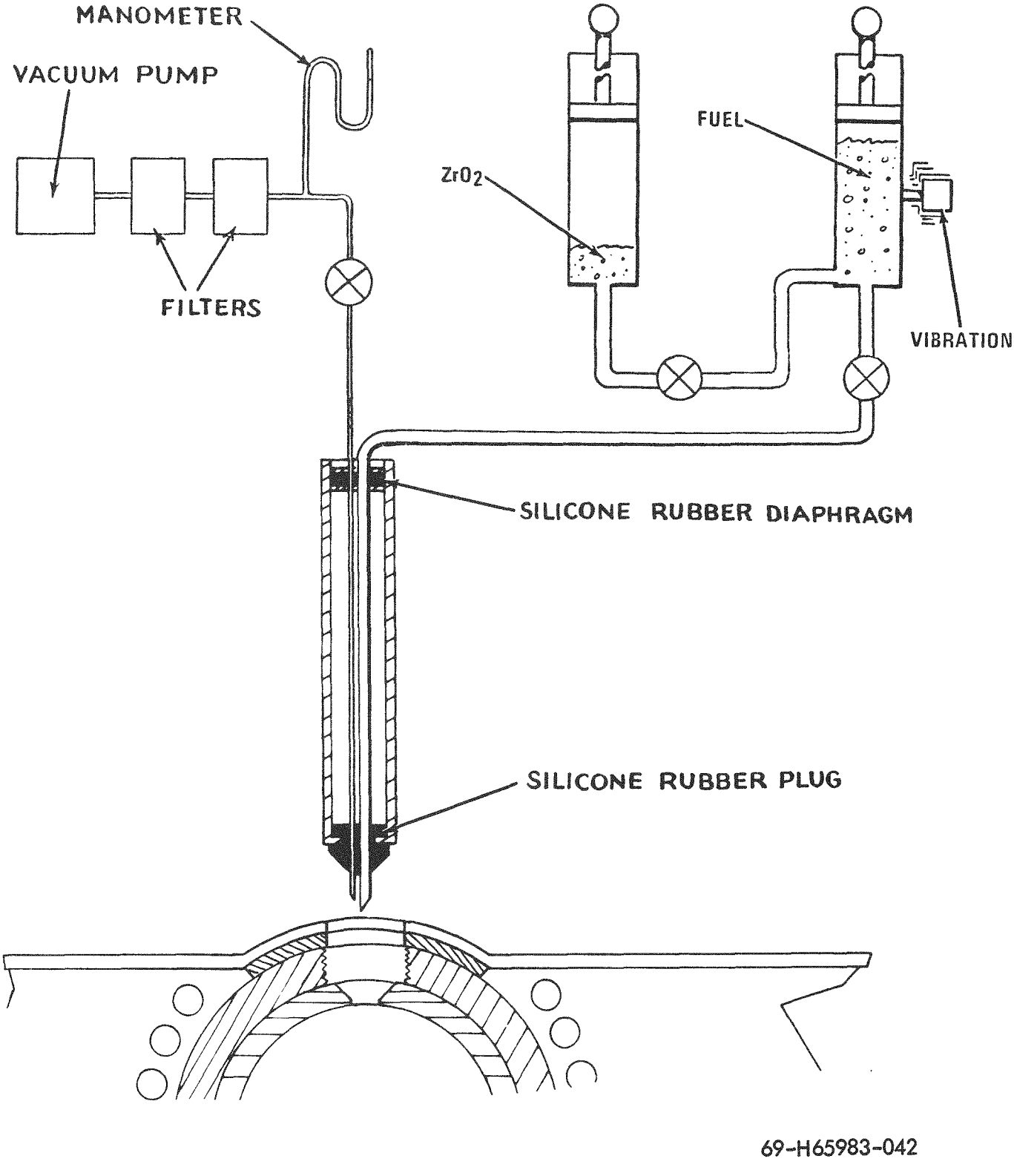

Figure 4-14 Tool Being Put In Place.

SANDERS NUCLEAR CORPORATION

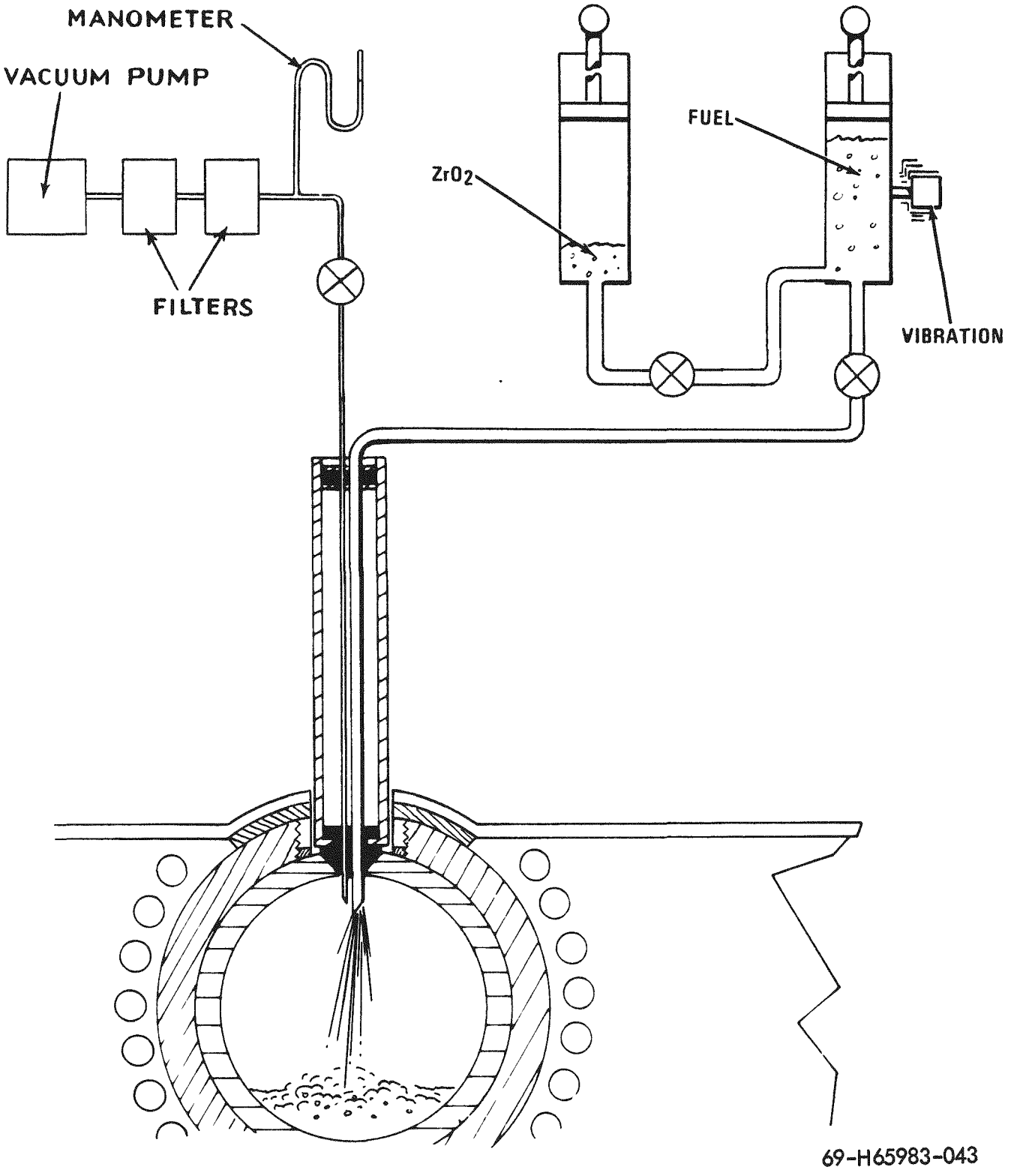

Figure 4-15 Fueling Tool in Place and Fueling.

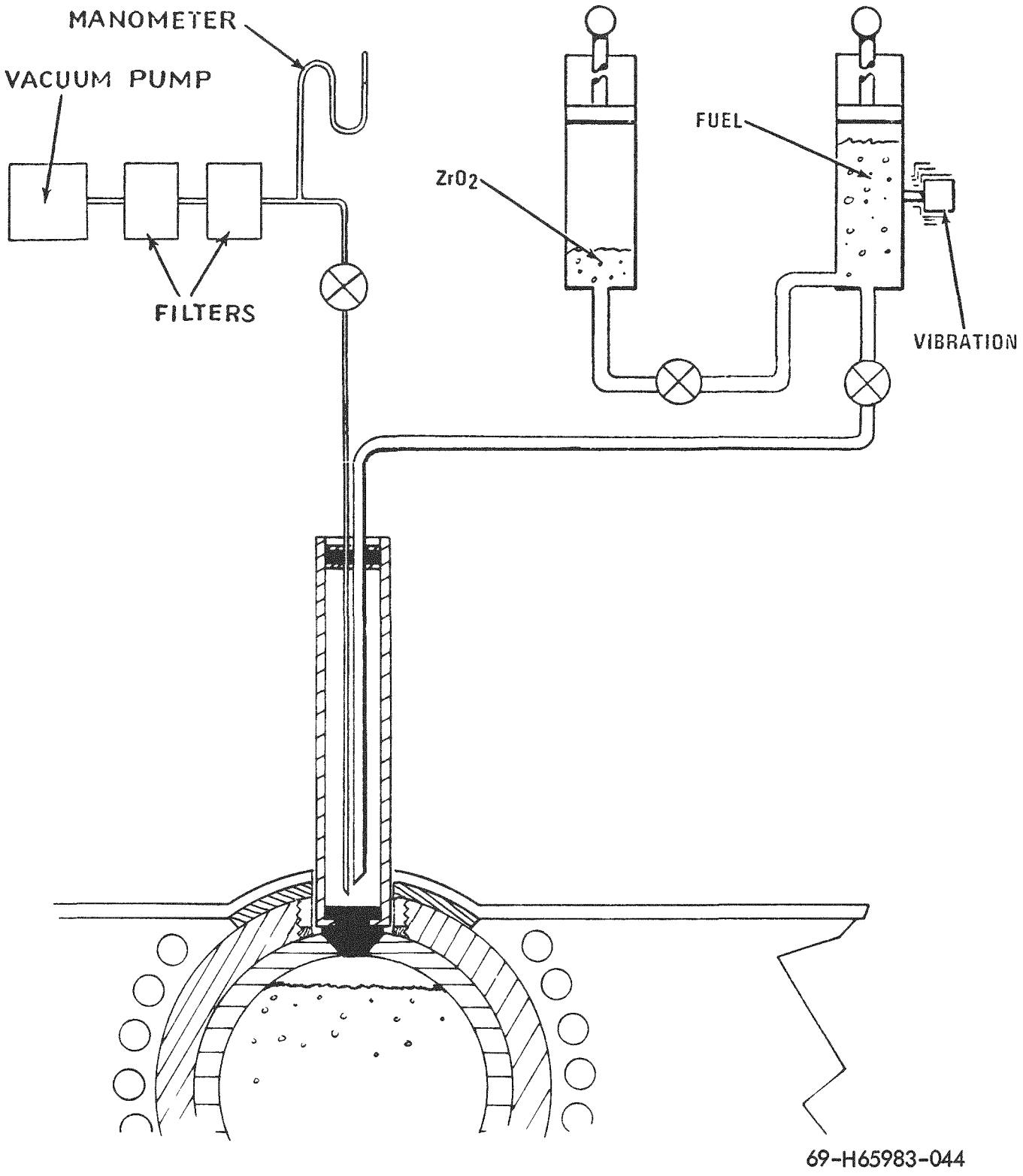

Figure 4-16 Needle Withdrawn After Fueling, ZrO_2 in Place.

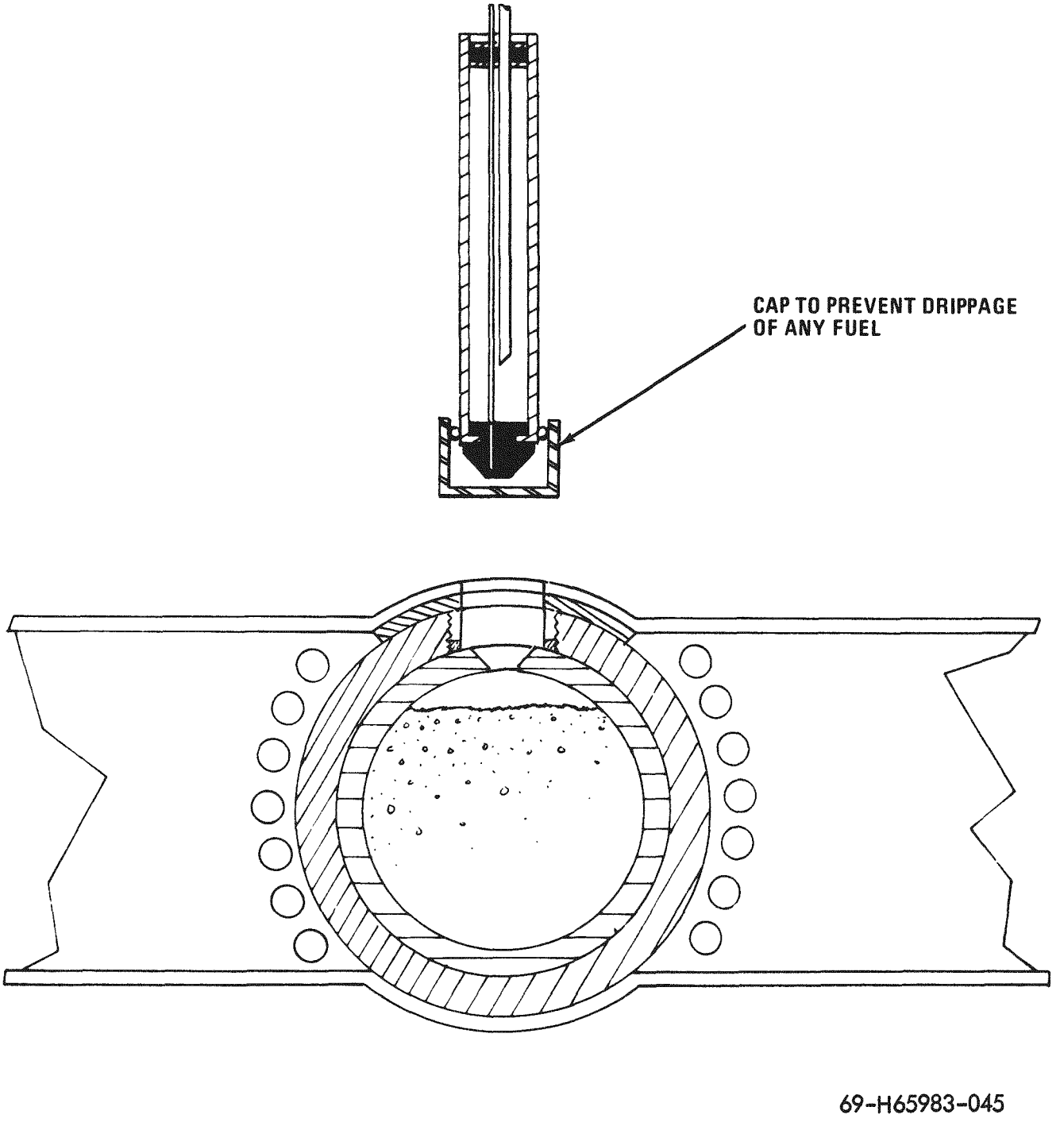

Figure 4-17 Fueling Tool Withdrawn and Drip Cap in Place.

Closure of the capsule can be accomplished by implanting a mating plug of the same liner material as shown in Figure 4-18. The plug is coated with a thin ZrO_2 base slurry which when fused, completes the seal. The temperature of the capsule is allowed to rise sufficiently to dry the cement and fusing is accomplished through the use of a pulsed laser to avoid thermal shocking the ZrO_2 liner as depicted in the artist's sketch (Figure 4-19).

A smear of the exposed area of the sealed liner and sleeve is now taken and counted as shown in Figure 4-20. Decontamination to acceptable levels can be performed using moistened swabs if the contamination level is excessive.

The cooling and support fixture is now decontaminated and moved into an adjoining glove box where the top clamp plate is removed to permit removal of the contamination prevention sleeve and sealing of the graphite section.

A graphite plug is wetted with furfuryl alcohol or other high carbon content binder and screwed into place as shown in Figures 4-21 and 4-22.

The capsule is next removed from the cooling and support fixture, the oxidation coating applied and finally inspected (calorimetry, contamination, etc.).

The postulated advantages of this technique are:

- Fueling is performed with a completely closed system
- Small hole size (on the order of 1/8 in.) required in liner should reduce the effects of convection currents spreading contamination into the port area.

An alternative technique for firing the slurry is to remove the capsule from the combination fixture after decontamination and heat the capsule with an induction heater under inert atmosphere.

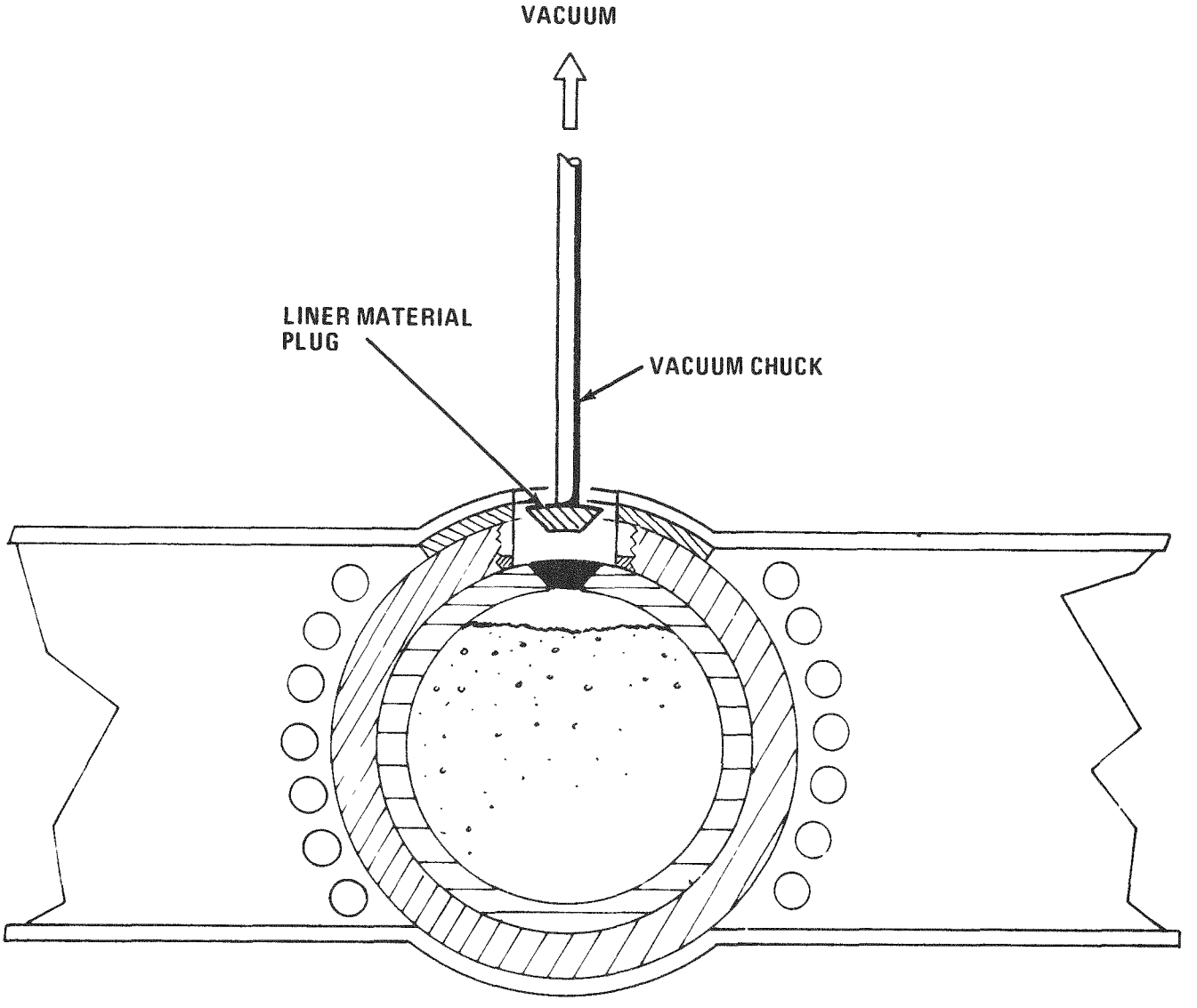

69-H65983-046

Figure 4-18 Implanting Liner Plug.

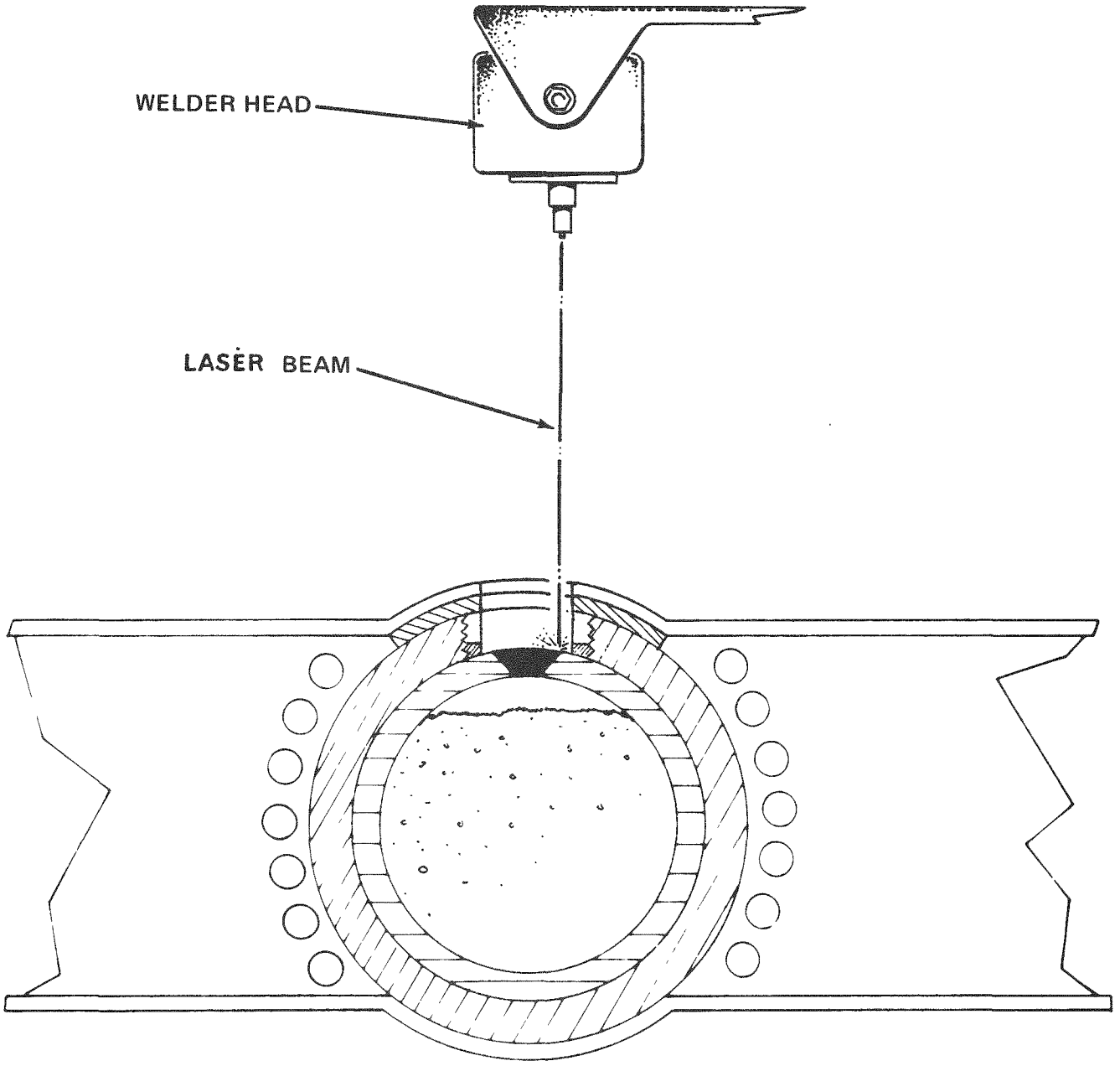

Figure 4-19 Laser Welding Plug in Place.

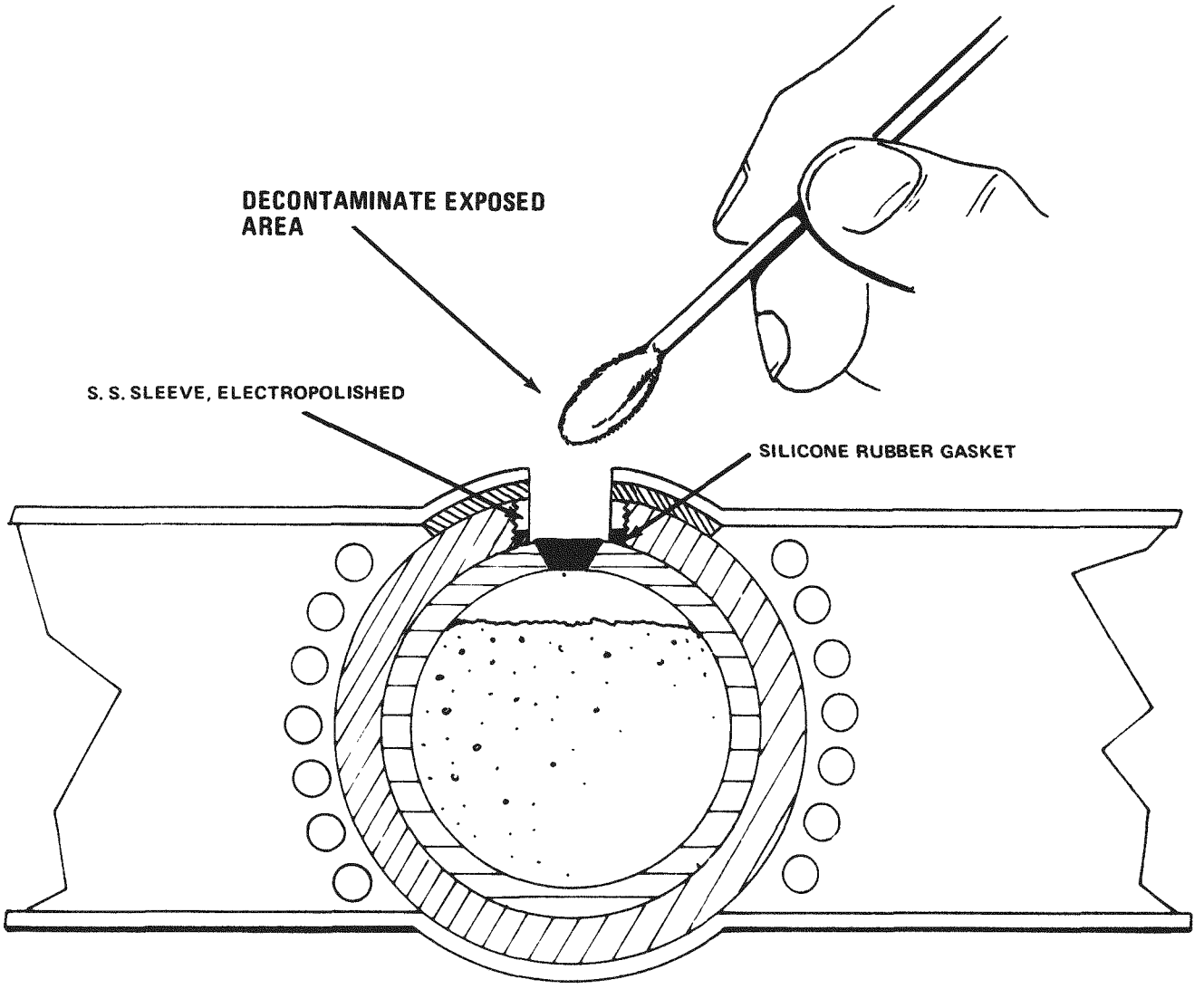

69-H65983-048

Figure 4-20 Decontamination of Exposed Area.

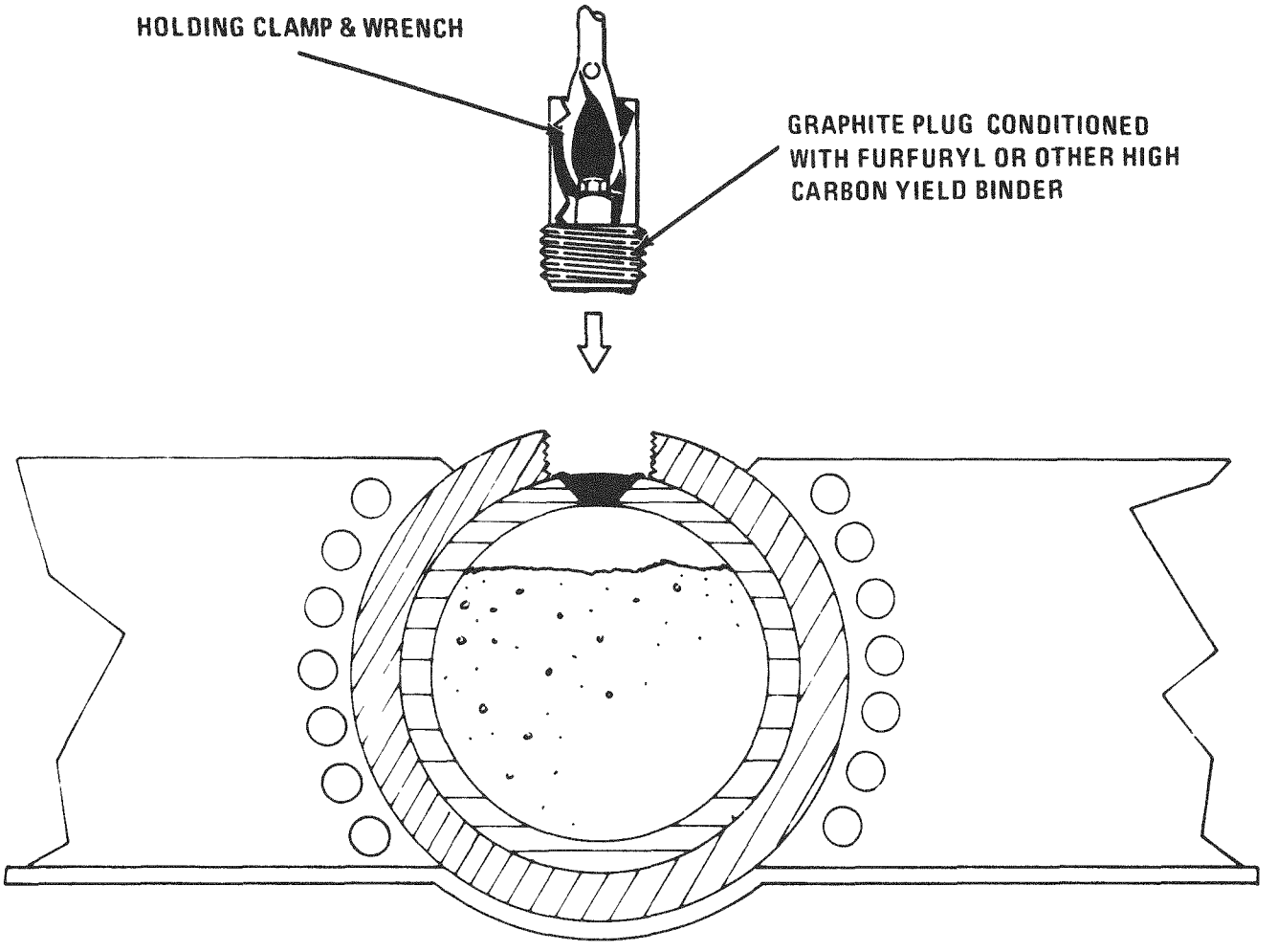

Figure 4-21 Preparing to Implant Outer Plug.

SANDERS NUCLEAR CORPORATION

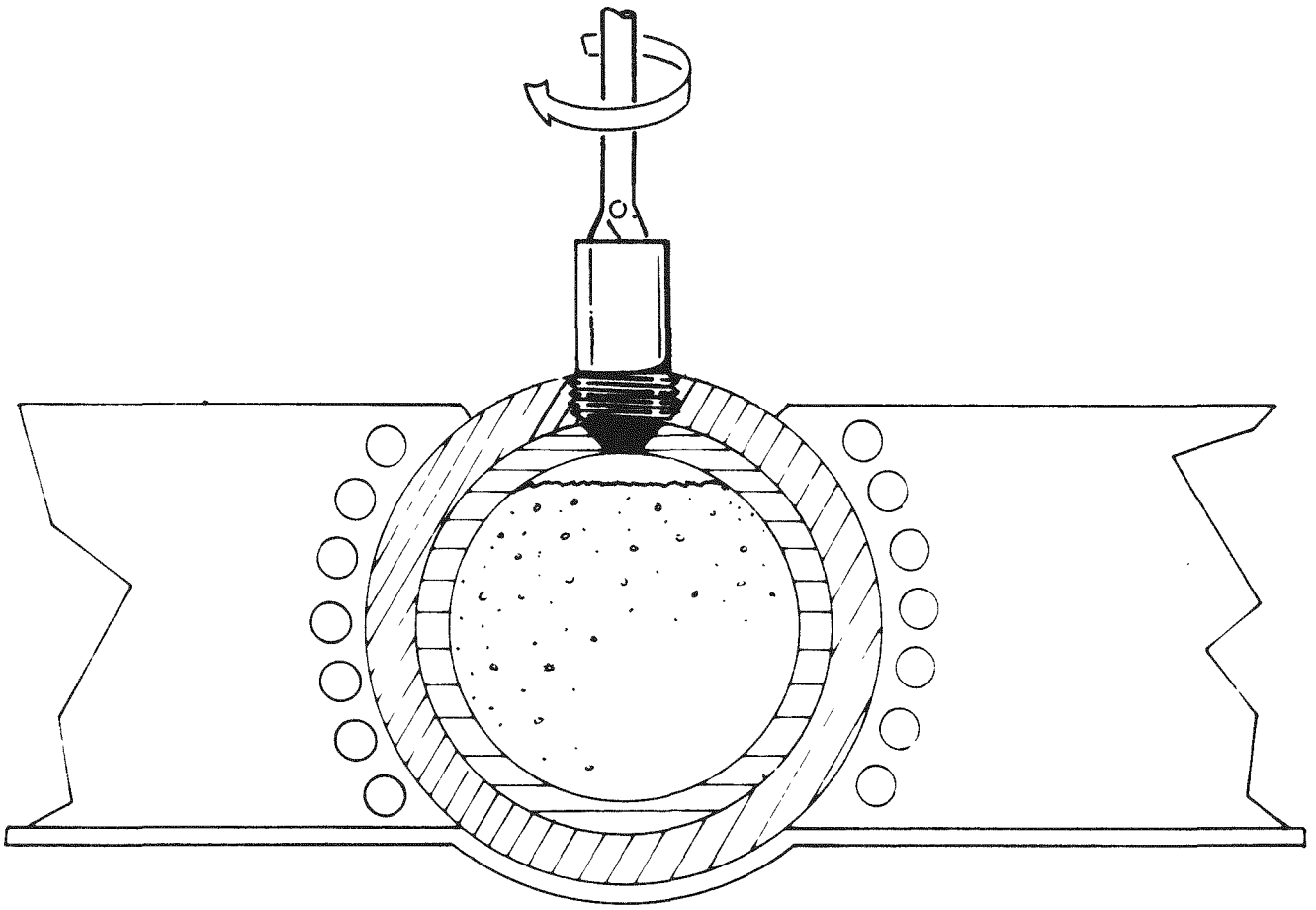

69-H65983-085

Figure 4-22 Outer Plug in Place.

The obvious disadvantages are:

- The fuel is briefly exposed to the glove box environment after removal of the fueling tool, thus presenting the possibility of contamination despite the small opening
- The sealing technique requires development.

Inflated Seal Technique

Figure 4-23 shows an inflated seal technique which has been tried in the laboratory (using ZrO_2 microspheres of 100 to 400 micron size in lieu of actual fuel) with some degree of success.

The fueling tool utilizes an inflatable silicone rubber bladder which is bonded to the outside of a stainless steel barrel. The barrel is equipped with two silicone rubber captive seal plugs to permit the insertion of two hypodermic needles into the fuel capsule interior. The needles are of two different diameters: one 14-gage (0.082 in. O.D., 0.063 in. I.D.) and one 31-gage (0.010 in. O.D., 0.005 in. I.D.). The smaller needle is connected to a small absolute filtered vacuum pump so that the gas pressure inside the capsule promotes the flow of the microspheres into the capsule through the larger fuel-carrying needle. The remainder of the fueling apparatus is essentially that described in the preceding subparagraph.

Initially, both needles are adjusted to protrude through the tool nose. The bladder is sufficiently inflated to provide a good seal against the entire capsule fueling port. Upon completion of fuel loading, a "wash" of dry zirconia microspheres is deposited through the fueling needle to provide a protective cover over the fuel. The pressure differential between the inside and outside of the capsule is equalized, the needles withdrawn to a position between the two seal plugs, bladder deflated and tool withdrawn. Sealing of the capsule can then proceed.

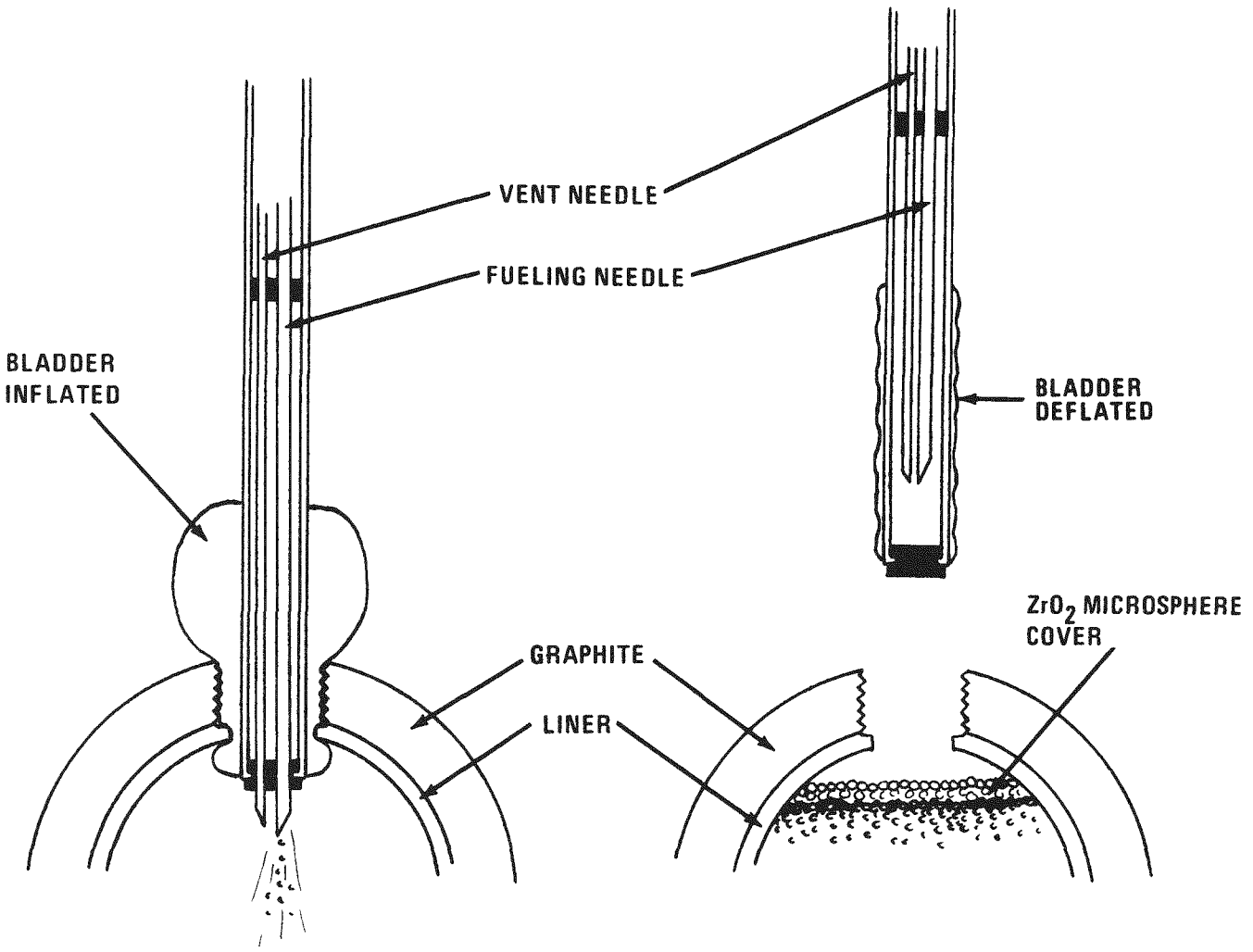

Figure 4-23 Inflated Seal Fueling Tool.

This technique has at least two major disadvantages as indicated below:

- $Pu^{238}O_2$ microspheres landing on the bladder can cause puncture (experience has shown this to happen to the gloves in the glove boxes)
- Migration of fines inside capsule adjacent to port after removal of fueling tool and prior to sealing the liner can cause contamination of the port area.

Disposable Plug Technique

Figure 4-24 shows a disposable plug technique. The fueling method and containers are essentially the same as described in the two preceding subparagraphs and will not be described here.

The capsule liner used in this technique would be fabricated from molybdenum (powered metallurgy fabrication) and flame sprayed with an oxide coating prior to winding and impregnation. It is felt that an oxide liner, e.g., ZrO_2, or ThO_2 is not applicable for this technique.

The loading plug and needles would be fabricated from molybdenum for fuel compatibility. The threads on the plug would be reasonably tight fitting with the liner in keeping with the contamination prevention philosophy.

Upon completion of the fuel loading, the tubing is heated sufficiently to permit crimping off adjacent to the top of the plug and the fueling equipment stored.

A molybdenum closure plug is then mated with the fueling plug and the two screwed as a unit into the capsule. The fueling plug will enter the capsule interior and remain there. The closure plug can then be laser or TIG welded to enhance fuel particulate containment. (Welding must be done under high purity cover gas with less than 50 PPM oxygen.)

After obtaining a satisfactory smear of the fueling port, a light slurry of ZrO_2 base cement can be applied over the exposed molybdenum area, dried according to the manufacturer's directions and final closure of the graphite completed.

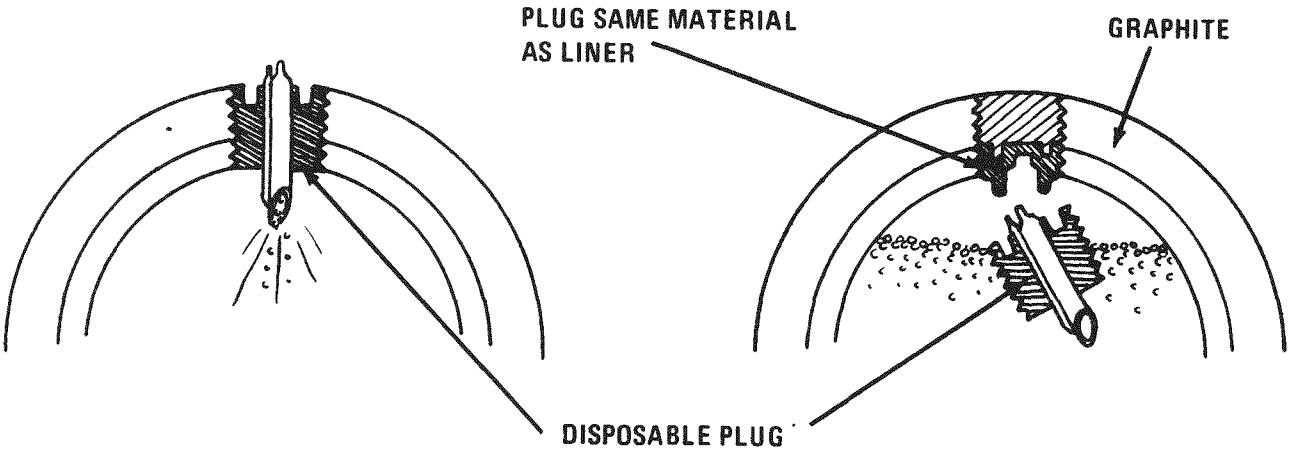

69-H65983-087

Figure 4-24 Disposable Plug Fueling Technique.

This technique has some problem areas which will require development and has some disadvantages. These are:

- Fabrication of the hypodermic tubing into the fueling plug
- Crimping of the tubing
- Adjustment of fit of threaded parts to prevent premature seizure of mating parts
- Final weld of closure plug to prevent stress induced cracking of area around plug
- The loose fueling plug may tend to break up some of the microspheres during normal prelaunch handling and launch shock and vibration conditions, thus producing a quantity of fines
- The loose plug might produce a hammer effect and may fracture the liner on impact or during launch conditions.

Since similar problems were encountered and solved in sealing the SNAP 11 TZM fuel capsule,[4] it is felt that the problem as stated herein can also be solved.

A variation of the technique stated herein would utilize a smaller plug (fueling and closure), permitting the final welding operations to be accomplished somewhat easier. It should be noted that if the thread fit can be sufficiently close, diffusion welding would take place during mission operating temperatures, thus improving the integrity of the seal.

Combination Fueling and Liner Sealer, Technique "A"

A variation of the compression fueling tool is shown in Figure 4-25. The differences between this tool and the one depicted in Figure 4-13 lie primarily in needle size and position. Only one needle is used.

The tool is coupled to the fuel container by a Swagelok type of coupling just above the outer barrel. The hypodermic needle is originally pointed to permit

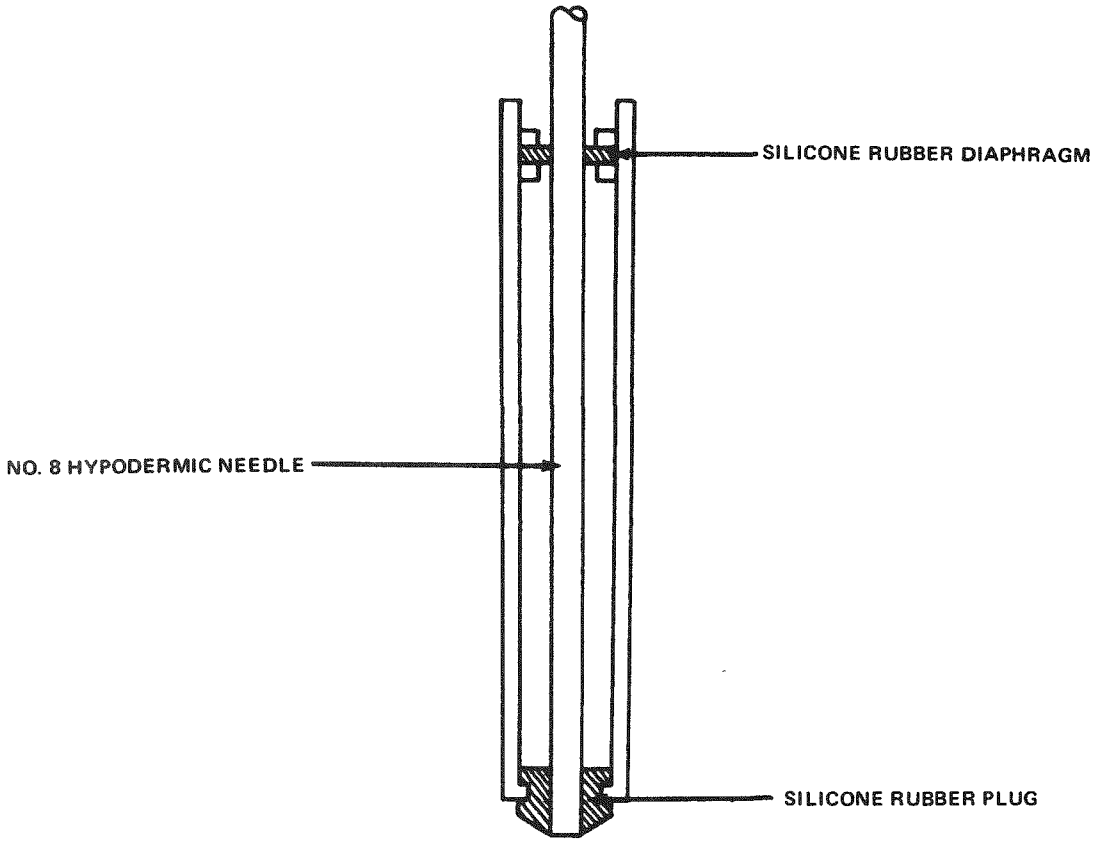

Figure 4-25 Combination Fueling and Liner Sealing Tool.

penetration of the diaphragm and plug. The end is then cut, chamfered, smoothed and withdrawn to approximately 1/16 inch inside the rubber plug. Connection is then made to the fueling apparatus and the unit inserted in the capsule fueling port as shown in Figure 4-26. Note that the hole in the liner has a double taper. The maximum diameter of the smaller taper is approximately 0.130 inch.

The cavity of the capsule and fuel carrying needle is then evacuated to a point very near the sealed fueling container. The fueling container has been previously purged and backfilled with helium. The fueling valve is then opened and fuel forced into the capsule. Several such evacuations and filling operations may be necessary to completely fuel the capsule. A final wash of ZrO_2 is then used to remove as much particulate as possible from the needle and adjacent opening into the capsule.

The capsule is now pressure-equalized with helium (if still negative with respect to the glove box) and the connection broken at the coupling. The tool is maintained in place.

A molybdenum tapered plug which has been matched to the smaller portion of the double-tapered opening is now dropped into the needle and rammed in place by a trigger spring operated ram (this operates in much the same manner as Starrett adjustable stroke prick punch). See Figure 4-27. Such precautions are necessary to avoid breaking the liner.

The remainder of the fueling tool is now removed and stored to prevent spread of any residual contamination and the fueling port checked for contamination. Inasmuch as the operations to this point have been more or less "surgically clean", the fueling should be "clean" and contamination nil or very low.

The next step involves fusing the top edge of the molybdenum plug to the ZrO_2 liner using a pulsed laser to avoid thermal shock. A disc of Nb, 0.001 to 0.004 inch thick (thickness arbitrary at this point) and of appropriate diameter is placed in the tapered hole and pulse laser welded into place, fusing the entire

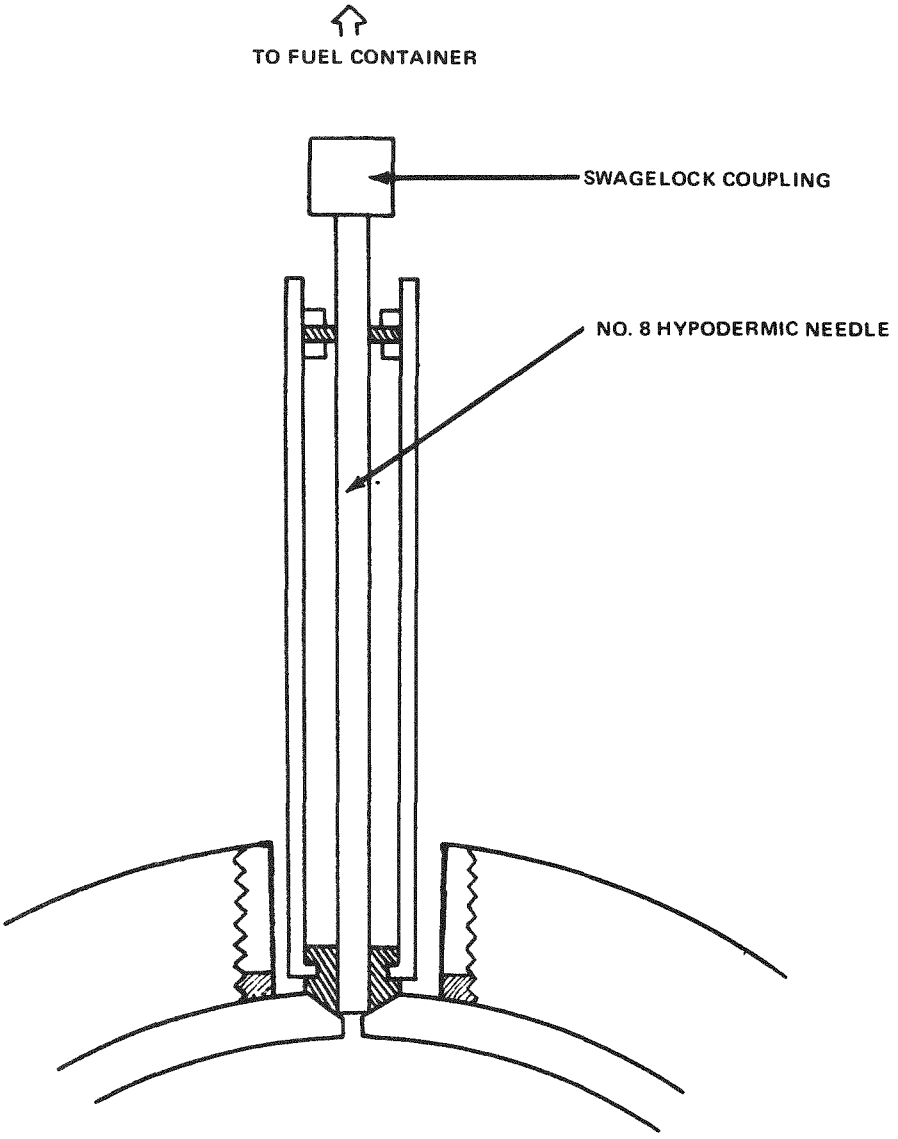

Figure 4-26 Fueling Configuration for Combination Fueling and Liner Sealing Tool.

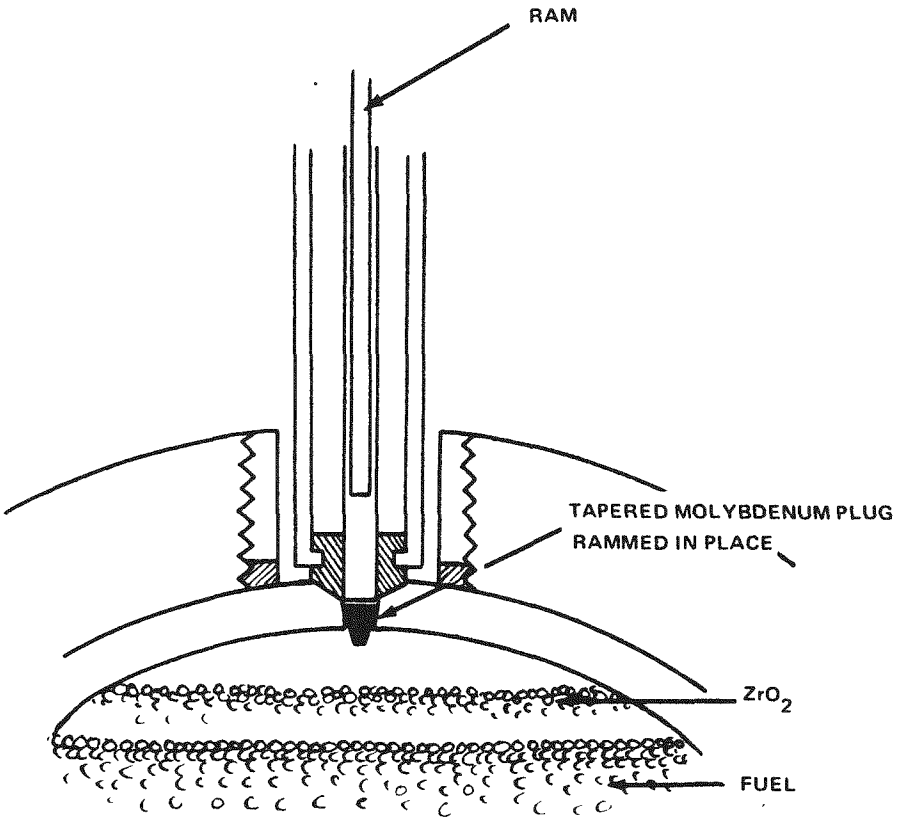

69-H65983-090

Figure 4-27 Liner Sealing Operation.

wafer to the substructure. Additional discs are added, and the process repeated until the liner thickness is reached. The capsule is now ready for final closure of the graphite and application of the oxidation resistant coating.

Development areas for this technique include:

- Development of the plug and disc sealing technique (determine feasibility)
- Determination of the workability of fueling technique
- Determine the practicality of using double tapered holes in thin liners.

Combination Fueling and Liner Sealer, Technique "B"

The same basic technique described in the preceding subparagraph is used, including the fueling tool. The prime difference lies in the sealing port used in the refractory oxide liner. Figure 4-28 shows the completed and sealed fueling port.

Upon completion of the fueling process and subsequent removal of the fueling apparatus (except for the tool itself), a plug is dropped into the needle and rammed into place as indicated in the preceding subparagraph. The tool is now removed, bagged and stored, and a smear taken and counted. If the contamination level is acceptable, the secondary plug is screwed into place and the contamination prevention sleeve assembly removed. A weld is now made around the periphery of the secondary plug, completing the seal.

A final smear survey of the area can now be made and closure and coating of the graphite effected.

The liner is a refractory metal oxide, probably ZrO_2. The insert (molybdenum, iridium, platinum/rhodium, etc.) is brazed to the liner before the graphite covering is fabricated.

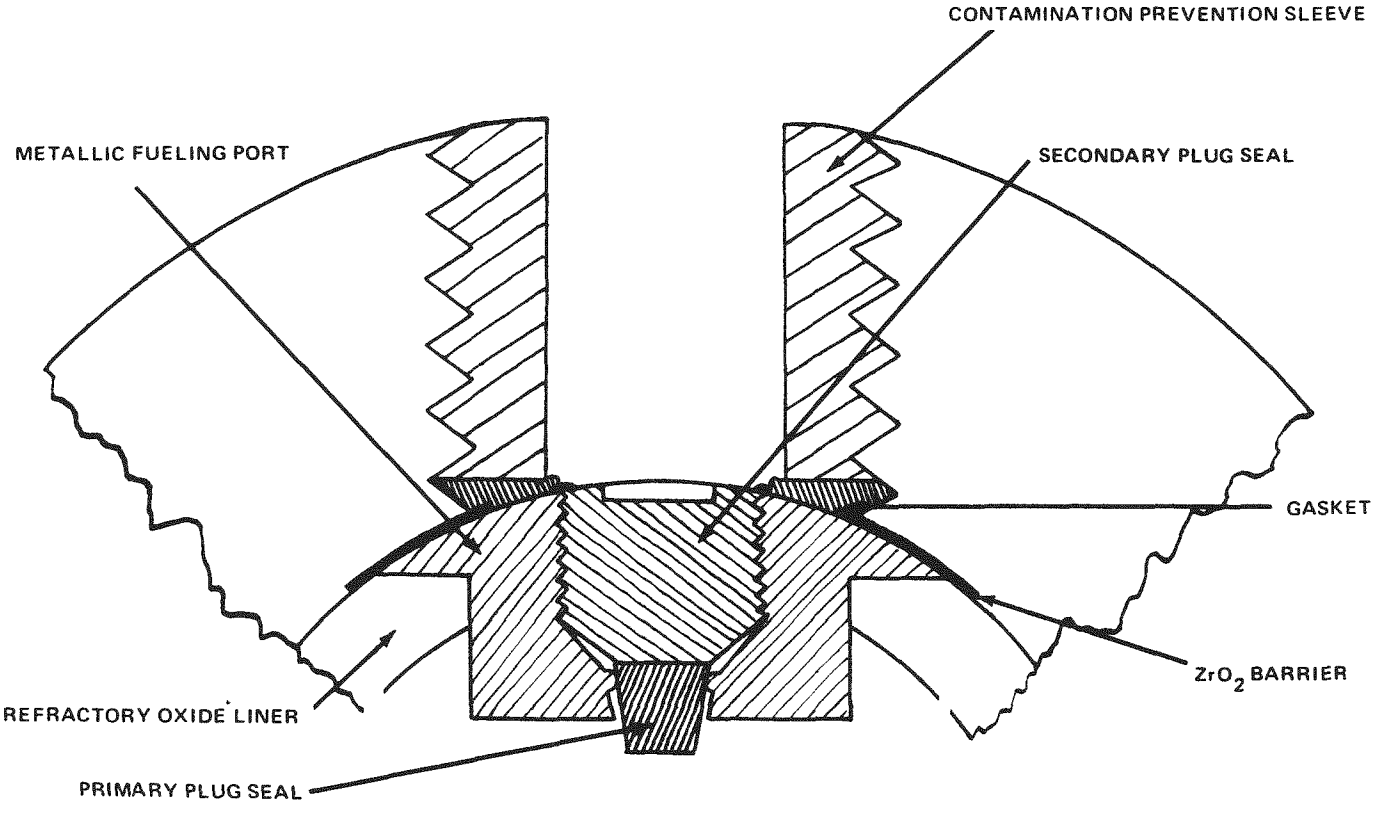

69-H65983-091

Figure 4-28 Metallic Fueling Port.

Problem areas include determining the feasibility of the technique due to high stresses involved between the ZrO_2 liner and the metal plug caused by the differences in coefficient of expansion. A ZrO_2/molybdenum cermet liner may alleviate the problem. In any case a detailed stress analysis will be required to determine the feasibility of the design and other ramifications involving compatibility with graphite and fuel.

Combination Fueling and Liner Sealer, Technique "C"

The tool used for this technique is similar to that shown in Figure 4-25 except that the silicone rubber plug at the fuel exit end (nose) is flat instead of tapered. The hole in the liner is straight and smaller in diameter than the hypodermic needle. Pressure contact seals the tool to the liner and fueling is accomplished as before. Upon decoupling the fueling apparatus, but with the tool still in place, a slurry of ZrO_2 base cement is injected into the hole in the liner via a separate hypodermic needle and syringe, forming a "blob" inside the liner, and completely filling the hole. A borescope would be used to verify sufficiency of fill before removing the fueling tool.

Subsequent drying and firing of the slurry plug can be carried out in a furnace (maintaining differential pressure between the capsule interior and the furnace essentially zero) or other suitable technique.

"Egg-Timer" Fueling Technique

Figure 4-29 shows an "egg-timer" approach to fueling the SIREN capsule

In this case the capsule is not initially attached to a cooling/contamination prevention fixture. The fueling process is quite simple in that after the fueling tool and capsule are screwed together, the assembly is inverted, the valve is opened and fuel transferred to the capsule and the valve closed. The disadvantages become apparent when separation of the capsule and fueling device takes place. There is no opportunity to cover the fuel with zirconia as in the cases previously described, so that the fueling port becomes directly accessible to the fuel when the tool is removed. In summary, the disadvantages are:

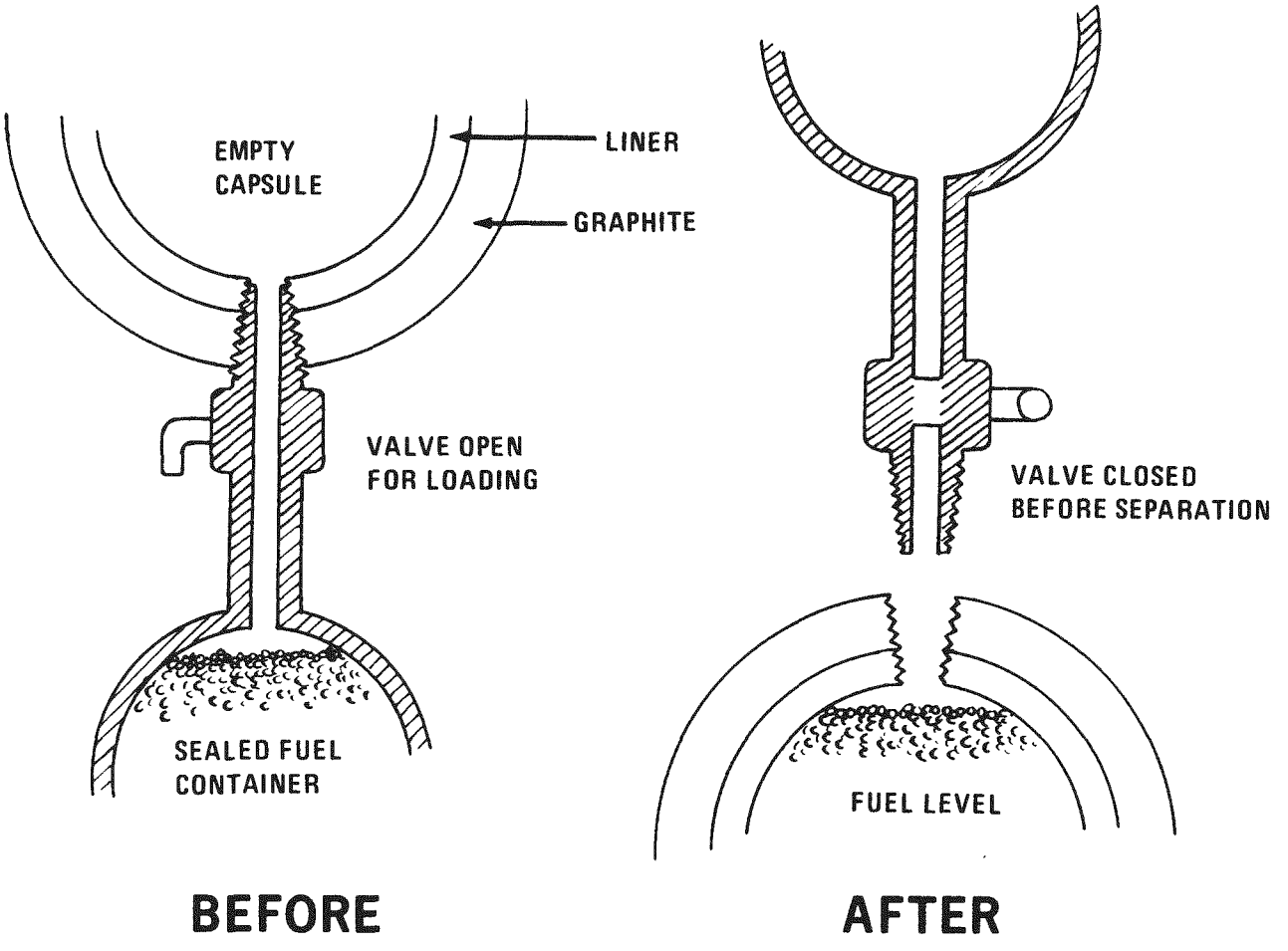

69-H65983-092

Figure 4-29 "Egg Timer" Fueling Tool.

- Migration of fines to the fueling port making decontamination difficult or impossible
- Closure of ceramic liner becomes more difficult because of the geometry at the liner/graphite junction
- Cooling/contamination prevention fixture would be more complex (and perhaps useless) in that it must be applied after the fact.

Conical Valve Fueling Tool

Figure 4-30 depicts a conical valve fueling tool. This fueling technique has some merit if modified to provide a gasket seal to the liner.

The outstanding merit of this tool lies in the use of a larger opening for the fuel to pass into the capsule void volume. It is anticipated, however, that upon removal of the tool, severe migration and/or diffusion of the fines will result in contamination of the port area prior to closure of the liner. Up to the point of removal, it should provide for contamination free transfer of the fuel when used in conjunction with the cooling fixture described previously.

Other Techniques

A closure technique which may have merit involves the use of a blind type pop-rivet using a ductile metal such as platinum, or other precious metal alloy. If iridium could be used, for example, a platinum or platinum-rhodium braze could effect the final liner seal to a premetalized area around the hole in the liner after popping the rivet into place. Such a rivet may be designed to use the fueling tool described in the subparagraph on Technique "C".

Summary

Some of the fueling techniques described exhibit more merit than others when viewed in light of the contamination prevention philosophy. It is obvious that the closure method will have a direct bearing on the fueling technique to be used as well as on the practicality and feasibility of the fueling techniques to be used. It is with these thoughts in mind that this next section has been written.

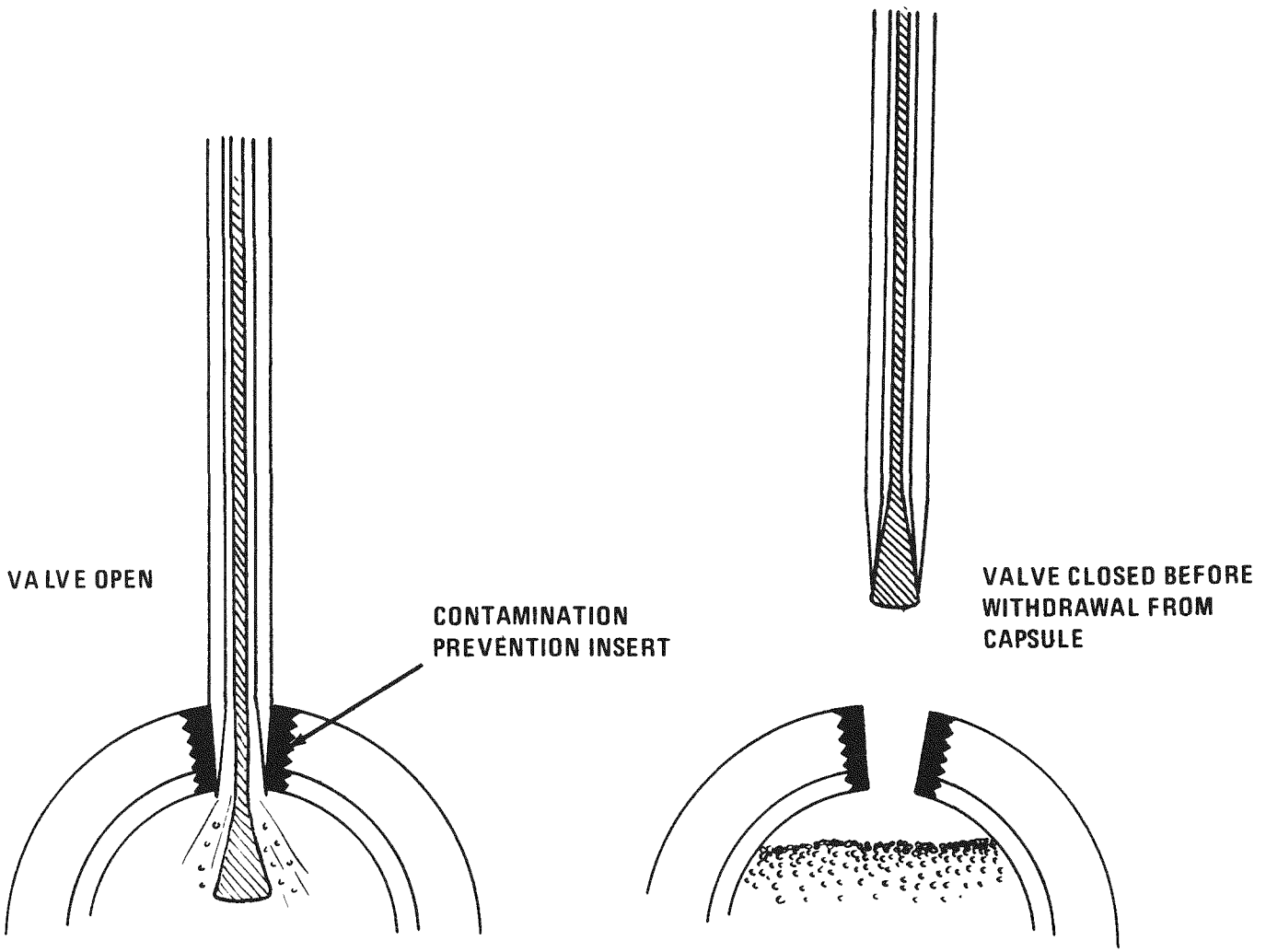

Figure 4-30 Conical Valve Fueling Tool.

4.3.2.5 Capsule Closure

The method of closing the SIREN capsule, aside from getting the fuel into the capsule without contaminating it, is perhaps the most important operation for it must insure that the fuel will remain within the liner after the capsule has been exposed to one or more of the following operating conditions:

- Storage
- Launch abort
- Launch pad fire
- Environment imposed by the mission (including mission duration)
- Reentry temperatures
- Impact
- Burial (land or water).

An additional requirement of the closure is compatibility with the fuel and graphite outer structure.

Table 4-44 is a summary of candidate liner and closure techniques and materials which, while they exhibit a quantity of unknowns, may be feasible to use. Some of the material combinations and techniques appear, at the outset, to be more promising than others.

Case 1 involves an all ZrO_2 (or ThO_2) liner and plug. The plug and mating hole are fabricated after impregnation to avoid deposition of carbon within the liner. Sealing of the mating parts is accomplished with a slurry of ZrO_2 base cement. Firing of the sealant can be accomplished by atmosphere controlled furnace, induction heating of the entire capsule, or laser heating. The first two are quite useful if the differential pressure (furnace to inside capsule) is essentially zero, otherwise gas seeping from within the capsule may carry out fines.

The atmosphere furnace or induction heating in a controlled atmosphere (using the graphite outer structure as the susceptor) technique requires removal of the capsule from the combination cooling/contamination prevention fixture after

Table 4-44

SIREN CANDIDATE LINER AND CLOSURE TECHNIQUES AND MATERIALS SUMMARY

CASE	CLOSURE TYPE AND MATERIAL	LINER MATERIAL	SUGGESTED METHOD OF CLOSURE	REMARKS
1	Tapered Plug ZrO_2	ZrO_2	ZrO_2 Base Slurry Furnace or Laser Fired	Compatibility ZrO_2 Base Slurry and PuO_2 Unknown. Technique to be established.
2	Tapered Plug ZrO_2	ZrO_2	Induction Brazed Seal, Niobium or precious metal	Technique to be established.
3	Molybdenum Insert, Molybdenum Plug and Screw	ZrO_2	Insert Brazed to Liner with Nb, Screw TIG or Laser Welded, or Braze of Above	Coefficient of Expansion between molybdenum and ZrO_2 differ by factor of 2+ stresses of whole assembly must be examined to determine feasibility. Compatibility problem may exist also.
4	Same as Case No. 3	ZrO_2	Iridium Braze	Compatibility of Braze with PuO_2 (should be better than Pt but needs examination).
5	Same as Case No. 3	ZrO_2/Mo Cermet	Same as Case No. 3	Differential Expansion Problem may be significantly reduced by decreased expansion of cermet.
6	Same as Case No. 3	ThO_2/Mo Cermet	Same as Case No. 3	Differential Expansion Problem should be lessened over Case No. 5 because ThO_2 has lower coefficient of expansion than ZrO_2.
7	Tapered Plug of Molybdenum, Nb Discs	ZrO_2	Liner Metallized at Fuel Port, Nb Discs Laser Welded in Place	Laser welding techniques require development, differential expansion differences may be a problem.
8	Same as Case No. 7	ThO_2/Mo or ZrO_2/Mo Cermet	Same as Case No. 7	Laser welding techniques require development, differential expansion problem lessened because of lower expansion of cermet.
9	Same as Case No. 7 but Mo Discs	Molybdenum	Mo Plug and Discs Laser Welded in Place	Laser welding techniques require development.
10	Molybdenum Plug	Molybdenum Powder, pressed & sintered	TIG or Laser Weld	Oxidation resistant coating interface required between molybdenum and graphite.
11	Niobium Plug and screw	Molybdenum Powder, pressed & sintered	TIG or Laser Weld, Induction Braze	Oxidation resistant coating interface required between molybdenum and graphite.
12	ZrO_2 Base Cermet	ZrO_2	Injected Slurry, furnace or induction firing	Technique requires further analysis and test to assess feasibility.

the plug with its slurry has been put in place. The rise in temperature will have to be sufficiently slow (including the allowance for self-heating from the fuel) that complete drying of the slurry has taken place without the generation of pin holes or cracks, and without entrapment of moisture within the capsule liner. There also may be some interaction between the ZrO_2 liner and graphite, and/or ZrO_2 and PuO_2 (solid solution formation) at the firing temperatures.

The laser fired seal may present problems in terms of lack of depth of penetration, resulting in a weak seal, microcrack generation, etc.

Case 2 utilizes the same materials and fabrication technique for liner and plug, but both plug and fueling port are premetallized with niobium or other appropriate braze material. Sealing can be by the furnace or induction heating technique as in Case No. 1. However, there will be some interaction between graphite and ZrO_2 (carbide formation), and ZrO_2 and PuO_2 (solid solution formation), at the brazing temperature. Because the brazing cycle is short, the extent of the reaction should be minimal. RF heating of the braze should be relatively easy to accomplish on a localized basis and should provide a fast method for obtaining the seal. The possibility of pin holes does exist, however, and the sealing reliability of the technique would have to be proven.

The molybdenum insert for Cases 3 and 4 is reasonably simple in principle, but differential expansion problems leave doubt with regard to maintaining the seal with the ZrO_2 and insert. The technique may be workable, however, if a cermet such as ZrO_2/Mo or ThO_2/Mo is used as indicated by Cases 5 and 6. Because the coefficient of expansion of these cermets is lower than either oxide alone, the stresses generated as a function of temperature may be tolerable.

Case 7 uses a double-tapered opening in the ZrO_2 liner. A molybdenum plug is inserted at the end of the fueling process before the fueling tool is removed to provide a temporary seal and thus contain the $Pu^{238}O_2$ fines. The port opening is premetallized to enhance the sealing of niobium discs into place using either localized induction heating or a laser technique. This method has considerable merit if the stresses developed after bonding do not break the braze or the discs.

Case 8 uses the same closure as Case 7, except the liner is a ZrO_2/Mo or ThO_2/Mo cermet. Again, the two problems of matching coefficients of expansion and laser welding technique require detailed analysis and development, respectively.

Case 9 is similar to Case 7, except that the discs and liner are molybdenum. The liner is fabricated by powdered metallurgy techniques. The section through the port area will require the liner wall to be somewhat heavier to accommodate the plug and liner. The laser welding technique will require development. A refractory oxide barrier; e.g., ZrO_2, will be required at the interface of the graphite and molybdenum.

Cases 10 and 11 are an extension of existing metal capsule technology wherein the liner is molybdenum fabricated by powdered metallurgy techniques to achieve the necessary porosity for helium release.

Case 12 involves the injection of a suitable consistency slurry of ZrO_2 base cement into a small fueling hole in the ZrO_2 liner by means of a hypodermic needle and syringe. Firing of this slurry can be achieved by any of the methods previously described. If the seal technique can be perfected, several advantages may be realized:

- The small sized hole required tends to reduce the magnitude of a possibly weak area in the liner
- Relative ease of fabrication and maintenance of contamination prevention philosophy.

The use of a tapered hole in the fueling port of the capsule liner (Cases 1 and 2) presents problems with respect to fines migration control prior to effecting closure, as well as the technique to be used in securing a satisfactory closure. With regard to the former, it would appear that the smaller the opening in the liner, the less effect convection currents (caused by the hot $Pu^{238}O_2$) will have on movement of fines into the port area during the period of time the port may be exposed prior to closure.

The subject of electron-beam welding has been avoided thus far for several reasons. The evacuation of the environment around the capsule may stress the seal sufficiently to open it such that gas escaping from the capsule interior will carry fines into the welding chamber; and the highly localized, continuous heating that electron-beam welding affords, subjects refractory oxides to substantial thermally induced stresses and subsequent microcrack generation. This tool is a valuable one however, and must not be overlooked where its application may permit (e.g., Cases 5, 6, 10, and 11).

The closure methods described herein each merit further investigation and subsequent selection of the most promising candidates. Additional factors involved in their selection are:

- Effect of expansion differences between closure and liner and resulting stress as a function of temperature
- Effect of compatibility on sealants and closure materials with fuel and graphite
- Thermal shock resistance
- Impact resistance
- Helium venting.

References

(1) Mound Laboratories AEC R & D Report, "Plutonium-238 Isotopic Fuel Form Data Sheets", October 31, 1968, Report No. MLM-1564

(2) Mound Laboratories Report, "The Separation and Determination of Fines in Plutonium Dioxide Microspheres", August 16, 1968, Report No. MLM-1524.

(3) Personal Communication, Mr. C. Henderson, Manager, Technical Coordination, Mound Laboratories

(4) Personal Communication, Mr. W. J. Fretague, Sanders Nuclear Corporation regarding work done on SNAP 11 by Martin Nuclear Division & ORNL

4.3.3 "HOT" FABRICATION OF SIREN

The massive fuel forms (solid solution, cermet, and sintered oxide) require complete fabrication of the fuel loading into a spherical or oblate spheroidal shape and the addition of an appropriate primary encapsulation. It must be noted, however, that if the microsphere fuel form is encapsulated in a suitable liner so that it outwardly resembles the encapsulated massive fuel forms, the capsule can be hot fabricated in the same manner as the massive fuel forms.

This paragraph discusses the fuel forms identified above, the fabrication process and requirements associated with their use in SIREN.

4.3.3.1 Fuel Description

Solid Solution Fuel Form

The Los Alamos Scientific Laboratory is developing a solid solution $Pu^{238}O_2$ fuel form for use at 900°C.[1,2] Their work, however, has extended to cover temperatures over 1800°C.

LASL has observed that a continuous solid solution fuel form of a refractory oxide and $Pu^{238}O_2$ appear to provide a more stable fuel form. Oxides selected for use as diluents are ZrO_2 and ThO_2. The results of their work has shown that:

- The melting point of the PuO_2 solution increases with increasing amounts of ZrO_2 or ThO_2
- Power density can be varied with minimal change in other fuel properties
- The specific radioactivity of a given size respirable particle of $Pu^{238}O_2$ is reduced by diluent

Salient physical properties are:

- Massive fuel form

- Power density ranges from 1 to 4.5 watts/cm^3, depending on diluent to PuO_2 ratio (usable range probably 3.5 to 4)
- Thermal conductivity greater than bulk microspheres and variable with diluent to PuO_2 ratio and specific diluent
- Biological hazards (airborne) practically nil. (Addition of oxide or cermet encapsulation should reduce this to zero with normal precaution still to be taken for an alpha emitting material.)

Cermet Fuel Form

The development work on the cermet form of $Pu^{238}O_2$ is being carried out by Battelle[3,4] (Columbus). The goal is a fuel form (massive) for 1500°C operation for 5 years. The postulated advantages of this fuel form are:

- Enhanced thermal conductivity
- Enhanced mechanical strength
- Enhanced fuel retention and stability
- Capabilities for gas control (helium release).

Advanced composite technology such as this has been in existence through AEC work (dating back some 15 years) on dispersion reactor fuels; thus the effort performed by BMI has been greatly aided in terms of material selection.

Compatibility tests performed by BMI have shown the $Pu^{238}O_2$-molybdenum and $Pu^{238}O_2$-ThO_2 composites (refractory metal and a ceramic) to be promising. The approximate physical properties for the PuO_2-Mo cermet are summarized below:

- Density 8.66 to 10.91 g/cc
- Coefficient of expansion (10^{-6}/°C)

  7.5 to 12 (high density PuO_2-Mo)
- Thermal conductivity

  0.0285 to 0.0322 cal/sec cm°C (high density PuO_2-Mo @ 1500°C)

- Power density to approximately 3.7 watts/cm^3.

The reports to date[2] indicate that the goals are being achieved, although much work still remains to be accomplished.

The addition of a refractory metal such as molybdenum or ceramic oxide coating will greatly enhance the fuel retention characteristics, thus reducing the airborne biological hazard to zero.

Sintered Oxide

The sintered oxide form of $Pu^{238}O_2$ is fabricated from PuO_2 powder. Fuel form geometry is accomplished through the use of dies and firing of the compacted mass. The bulk properties of the sintered mass have essentially the same thermophysical properties of individual microspheres. The power density (4.58 w/cc) is much increased over the bulk microsphere form by virtue of the elimination of the void volume.

Because this fuel form is in the early development stage at Mound Laboratories[6,7], the precise physical properties are not actually known. Values quoted (e.g., power density) are based upon 80% Pu^{238} in the element plutonium and inferred from microsphere data.[5]

4.3.3.2 Fabrication

Fabrication of the SIREN capsule using any one of the massive fuel forms described in subparagraph 4.3.3.1 or encapsulated microspheres will require that the fuel form be fabricated with an integral liner. In view of this requirement, compatibility of various liner materials with graphite and PuO_2, a description of the liner itself, and decontamination requirements will be necessary. The following aims to present sufficient information to permit a preliminary selection of liner material/fuel forms to be made.

Compatibility

Table 4-45 summarizes the compatibility of the most likely group of liner material candidates. Not reported in the table is work being done by LASL[1,2] on the compatibility of solid solution of ZrO_2/PuO_2 and ThO_2/PuO_2 with TZM at 900°C. Results to date indicate good compatibility, i.e., no interaction.

There are marked similarities in the postulated compatibility behavior of the liner candidates listed and the three massive fuel forms or encapsulated microspheres. If liner materials were to be chosen at this point in time, it is felt that the following fuel form/liner combination show good promise:

- For solid solution of ZrO_2/PuO_2 or ThO_2/PuO_2; ZrO_2 or ZrO_2/Mo cermet, ThO_2 or ThO_2/Mo cermet
- For PuO_2/Mo cermet; ZrO_2/Mo cermet or ThO_2/Mo cermet and molybdenum
- For PuO_2 sintered oxide; ZrO_2, ThO_2, ZrO_2/Mo or ThO_2/Mo cermet; molybdenum
- For microsphere, ZrO_2, ThO_2, and cermets of each.

These choices have been made based upon the apparent limited interaction between the fuel form and liner material, and liner material and graphites. As stated previously, some of these combinations have yet to be proven sufficiently to warrant a positive commitment of their use.

Encapsulation

This section will consider several types of liner materials and fabrication techniques for use with $Pu^{238}O_2$ massive fuel forms and SIREN.

Refractory Oxide Liner

The fabrication of a ZrO_2 or ThO_2 liner for use with any of the three massive fuel forms described in subparagraph 4.3.3.1 can be accomplished in at least three ways:

TABLE 4-45

COMPATIBILITY OF GRAPHITE AND CANDIDATE LINER MATERIALS WITH PuO_2 FUEL FORMS

Fuel Form	Liner Material	Remarks
Solid Solution		
ZrO_2 or ThO_2 with $Pu^{238}O_2$	ZrO_2	Liner forms solid solution with PuO_2 resulting in substoichometric PuO_x. Graphite reduces ZrO_2 to form carbides at interface ($T > 1600^{\circ}C$) and stops unless a new surface is exposed.
	ThO_2	Essentially the same as ZrO_2.
	ZrO_2/Mo Cermet	ZrO_2 and Mo react forming substoichometric MoO_x. Graphite reacts at interface and then stops. Reaction of cermet and PuO_2 expected to be of limited nature.
	ThO_2/Mo Cermet	Essentially the same as ZrO_2/Mo.
	Mo	Interface reaction with graphite at high temperature unless barrier put between.
	MgO	MgO is reduced by the graphite, reaction with PuO_2 [3,4] above $1500^{\circ}C$.
Composite		
PuO_2/Mo	ZrO_2/Mo	PuO_2 forms solid solution with ZrO_2; expect reaction of PuO_2/Mo cermet with ZrO_2/Mo cermet; ZrO_2-Mo also reacts; combination requires further analysis.

TABLE 4-45

COMPATIBILITY OF GRAPHITE AND CANDIDATE LINER MATERIALS WITH PuO_2 FUEL FORMS (Cont)

Fuel Form	Liner Material	Remarks
Composite (Cont)		
PuO_2/Mo	ThO_2/Mo	Essentially the same as ZrO_2/Mo cermet.
	Mo	Expect no reaction with liner PuO_2 at 1500°C, may be usable to 2200 or 2300°C; Mo/graphite reaction of limited nature unless ZrO_2 barrier interposed, then should be the same as above.
PuO_2/MgO	MgO	Reduced by graphite forming carbides --- limited type reaction; reacts with PuO_2 above 1500°C.
PuO_2/ThO_2	Mo	Mo/graphite reaction and potential solution as noted above.
Sintered Oxide		
$Pu^{238}O_2$	ZrO_2	Expect possible solid solution reaction with ZrO_2 and ThO_2 with fuel
	ThO_2	
	ZrO_2/Mo Cermet	Expect same as for Composite Fuel
	ThO_2/Mo Cermet	
	MgO	

TABLE 4-45

COMPATIBILITY OF GRAPHITE AND CANDIDATE LINER MATERIALS WITH PuO_2 FUEL FORMS (Cont)

Fuel Form	Liner Material	Remarks
Microspheres		
$Pu^{238}O_2$	ZrO_2	Probably more reaction with these liner candidates then sintered oxide due to larger available surface area.
	ThO_2	
	ZrO_2/Mo Cermet	
	MgO	
	ZrO_2	
	ThO_2	
	ZrO_2/Mo Cermet	
	ThO_2/Mo Cermet	
	MgO	

- Precast hollow liner
- Slip liners
- Chemical deposition

The precast hollow liner would range in thickness from 0.030 inch to 0.125 inch and be fabricated from high purity material (ZrO_2 would be stabilized) mating with the external configuration of the PuO_2 fuel form. The liner would initially be in two halves as shown in Figure 4-31. The halves would then be pressed over the fuel form and subsequently bonded in a furnace (furnace contained in appropriate controlled ventilation alpha glove box). Bonding slip would be a new ZrO_2 base material being developed by Zirconium Corporation of America.[8] This material exhibits low porosity, low shrinkage and high strength akin to that of stabilized ZrO_2. (A similar ThO_2 based slip is a possibility for the ThO_2 liner.) The firing temperature is 2000°F. The result is a fuel form completely isolated by the refractory oxide liner as shown in Figure 4-32.

The precast hollow liner has one problem area which may impart major significance to its usefulness. Unless the inside geometry of the liner almost exactly matches that of the fuel form, the fuel form may "rattle" thus causing doubt of liner integrity following subjection to the launch environment or on impact due to the "hammer effect" of the fuel on the liner. A possible solution would be to cement the fuel to the liner with a ceramic slip.

An additional technique which requires mentioning in the use of metallized bonding techniques using a niobium* braze. A butt joint would be appropriate for the metallized seal. Sealing temperatures could be achieved through RF induction heating in controlled atmosphere.

A slip liner would be fabricated by submerging the PuO_2 fuel form into a slip mixture retrieving it when the refractory oxide has built up a sufficient layer, and

*Note that the possibility of previous metal brazes such as platinum rhodium, or iridium could be used once compatibility with all materials is established or appropriate interface provided.

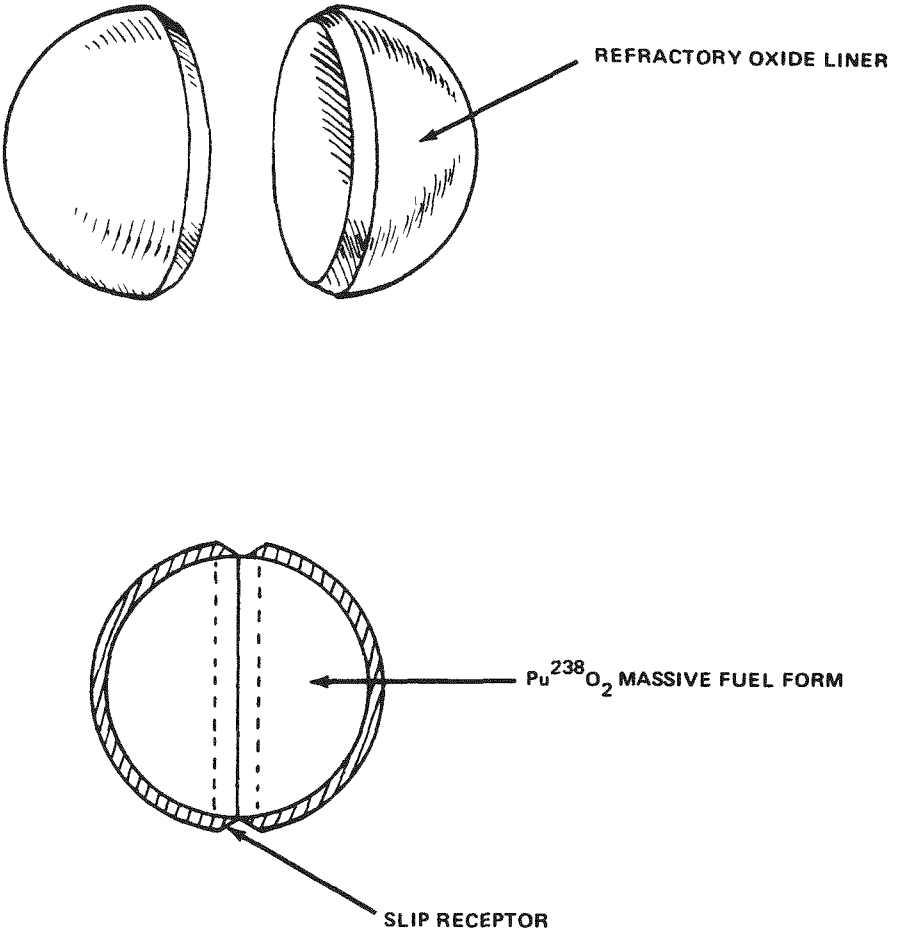

69-H65983-094

Figure 4-31 Mating of Liner to $Pu^{238}O_2$ Massive Fuel Form.

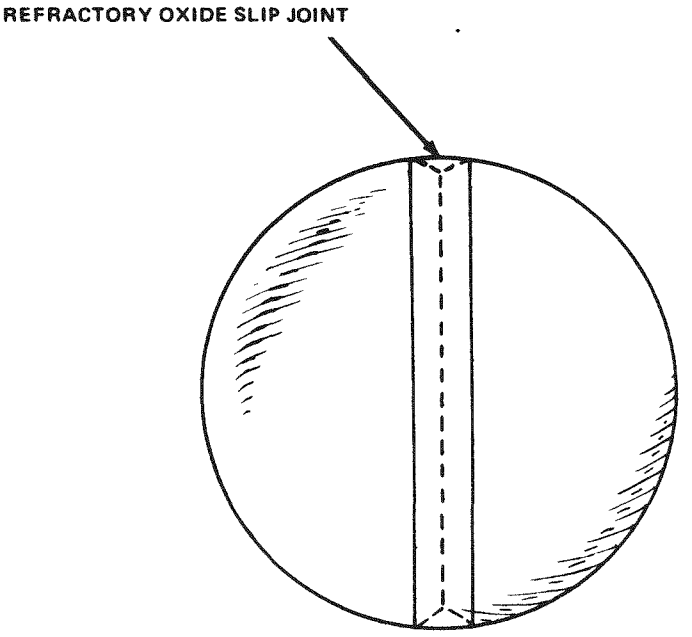

69-H65983-095

Figure 4-32 Liner in Place Around Massive Fuel Form.

then performing the heat treating operation. Since the still air temperature of these fuel forms (assuming approximately 2 inch O. D., and 242 watts (t) for solid solution or cermet; 313 watts for sintered oxide) will be quite high, precooling will be necessary to avoid premature curing and crack and pore generation.

The ZrO_2 base slip previously described[8] can also be sprayed onto the fuel form and subsequently fired. This process could be repeated until the desired liner thickness was achieved.

When fired to maturity, the slip type of liner coating is now integral with the fuel form, exhibiting good thermal shock resistance and minimal shrinkage.

Chemical deposition can also be used to coat the massive fuel form using ZrX or ThX, decomposing the deposition material and oxidizing it, all in a manner similar to the coating techniques described in the BMI reports.[3,4,11] The coating thickness would probably only be of the order of a few mils.

Cermet Liners

Another technique of supplying a liner for the fuel form, is an unproven but very interesting concept for eliminating the problems which will be encountered in the techniques described in the preceding subparagraphs and other problems normally associated with liners for radioisotopic fuels. Although this technique lends itself ideally to the PuO_2/Mo cermet fuel form, it may be possible to use it with the solid solution or sintered oxide fuel form as well. To employ this liner technique, the $Pu^{238}O_2$ cermet fuel would be pressed and processed to the desired shape and compactness. ZrO_2 microspheres plated with molybdenum (in the same manner as PuO_2 microspheres are coated with molybdenum)[3,4] would then be arranged in an annulus between the fuel form and a high pressure mold. Applying pressure to the extremeties would cause the coated ZrO_2 microspheres to conform to the shape of the fuel form resulting in a ZrO_2-cermet liner of desired thickness. The ZrO_2-cermet would have approximately the same thermal expansion characteristics as the PuO_2 cermet, thus eliminating the mechanical interface problem.

Assuming that the oxidation characteristics of the ZrO_2 cermet are similar to that of $Pu^{238}O_2$ cermet, the long term fuel containment capabilities of the ZrO_2 cermet liner are also apparent. Thermal shock resistance is enhanced by the use of ZrO_2/Mo cermet. Results of a water quench from 1000°C in air showed the ability of PuO_2 cermet ($Pu^{239}O_2$ standin) to withstand the thermal shock without evidence of matrix failure.

Additional work done by BMI[4] utilized plasma sprayed molybdenum on a male hemispherical mold. The preformed shells were then fitted into hemispherical graphite punches containing a plasma sprayed barrier layer of tantalum. Fuel was loaded into the mated configuration through a hole in one of the hemispheres, the hole closed with powder metallurgy Mo plug and the assembly hot pressed at 1725°C. The punch broke, fracturing the top Mo hemisphere before sufficient time and pressure was applied to promote bonding. This process has been reported to be feasible with further development effort required.

The general technique of chemical vapor deposition of molybdenum from MoF_6 by hydrogen reduction on the microsphere fuel form and the composite fuel form has been investigated by BMI[3]. This technique is quite applicable to all three of the massive fuel forms. The use of a molybdenum liner requires a refractory oxide interface with the graphite in order to eliminate interaction. The ZrO_2 base slip previously described may satisfactorily provide the barrier.

BMI has also investigated duplex coating; Type I (thoria over molybdenum) and Type II (molybdenum over thoria). Type I was a thoria/plutonia cermet, and Type II a molybdenum/plutonia cermet. Reentry tests by Sandia[11] in the arc tunnel have shown both Type I and Type II to be promising as potential protective coatings for the fuel form.

Liners for Microsphere Fuel Form

The liner for the microsphere fuel form will follow from the analysis of paragraph 4.3.2. Suffice it to say that one of the liner and closure techniques

which has proven feasible in follow-on work, is used to provide fuel containment and meet the requirements as summarized in paragraph 4.3.2.5.

Decontamination

Both the solid solution and cermet forms of $Pu^{238}O_2$ appear to have excellent fuel retention. The microspheres and particulate (contamination) seem to be sufficiently tied up in the solid solution and cermet matrix that contamination prior to cladding is a minor problem.

At this writing, more information is available on the cermet fuel form than either the solid solution or sintered oxide, however, some inference may be taken from the cermet test results.[3,4]

At the conclusion of oxidation tests performed on PuO_2/Mo cermet and PuO_2/MgO cermet, the following observations were made:

- $Pu^{239}O_2$/Mo cermet - bulk of fuel form unaffected, and although $Pu^{239}O_2$ was exposed at the surface, apparently none of it had vaporized or powdered off. Loss of Mo from the matrix was inhibited by necessity for diffusion of O_2 into the channels between particles and outward diffusion of MoO_3
- $Pu^{239}O_2$/MgO cermet - no external changes noted.

Samples of both cermets subjected to thermal cycling and thermal shock (1000°C to water quench) exhibited excellent stability.

BMI has reported[5] that no attempt has been made thus far to ascertain the degree of surface contamination. However, the contamination is felt to be very small. For example, the equipment used to coat the microspheres with the molybdenum has shown no trace of contamination upon completion of the coating process. Of course, one can speculate that the contamination, if any, remains on the coating vessel walls, clad with molybdenum.

LASL has reported[10] that contamination on the encapsulated solid solution fuel source should not present a problem and that the source could be delivered for "Hot" winding in a contamination-free state.

In view of the good fuel retention characteristics of the cermet, it is reasonable to require that surface contamination on the encapsulated fuel be of the order of 50 dpm/m^2 or less (ideally, it should be zero).

It is felt that the contamination requirements noted above should be imposed on the sintered oxide and the solid solution as well. The amount of free particulate available from these two fuel forms is not known at this writing, but due to the nature of the materials, is felt to be small.

Recognition must be made of the possibility of having to decontaminate a microsphere fueled liner to a satisfactory level in the event a cooling contamination prevention fixture cannot be used or does not provide the necessary protection for some reason. In that case, it might be advisable to fabricate the capsule with a metallic coating which can be readily chemically removed after fueling and closure. Such a material might be copper, or other easily vapor deposited material. In addition, the use of a strippable coating becomes a real possibility if the capsule temperature can be maintained below the melt temperature of the coating. It is further possible that a plating of metal, coated with Thermo-Cote I* which melts at 350 - 375°F (or other special high melting formulation) could be used to prevent contamination of the fuel capsule proper. The coating would entrap hot $Pu^{238}O_2$ particulate which may come in contact with it. After initial closure, the coating could be stripped away, followed by chemical machining of the metallic coating after the final sealing is performed.

"Hot" Winding

A massive fuel form with its primary encapsulation will exhibit quite high "still" air temperature. For example, assuming a 2-inch O. D. sphere (fuel), the approximate temperatures are:

*Trademark Thermo Cote, Inc.

- Solid solution or cermet - 3.5 w/cc - 242 w(t) ≈ 830°F
- Sintered oxide - 4.6 w/cc - 313 watts (t) ≈ 1360°F
- Microsphere - 2.7 w/cc - 186 watts (t) ≈ 700°F

It can be seen that these temperatures will place some special requirements on the "hot" winding process.

Despite the excellent fuel retention characteristics of the massive fuel forms and despite the encapsulation of the massive fuel forms on the microsphere fuel forms, Health Physics requirements will dictate that appropriate precautions must be taken for the alpha-emitting fuel. This means that the hot winding operation will take place within a glove-box system housing the entire winding apparatus.

Gamma and neutron dose rates for the fuel have been derived from the Mound Laboratories Pu^{238} data sheets.[6] The approximate dose rates two feet from the center line of the source are summarized below:

● 186 w(t) microsphere	2.1 mrem/hr (γ)	14.5 mrem/hr (n)
● 242 w(t) solid solution; cermet	2.7 mrem/hr (γ)	18.8 mrem/hr (n)
● 313 w(t) sintered oxide	3.4 mrem/hr (γ)	24.3 mrem/hr (n)

The maximum permissable dose for the total body is 100 mrem/week. Past experience has shown that the normal winding process takes approximately 15 minutes, including loading and unloading. If one now makes the assumption that the hot winding operation will require twice that amount of time, the whole body exposure will approximate 14 mrem (γ + n) (sintered oxide fuel). The hands will receive more than this because of loading operations. The hand exposure dose rate (assuming six inches) is approximately 540 mrem (γ + n)/hr. An assumption of five minutes exposure to the hands yields throughout the entire operation an exposure dose of approximately 38 mrem for each wound capsule.

It is anticipated that little shielding will be required for winding one or two capsules per week. Higher production rates, however, will require shielding and perhaps remote handling at the operating side of the glove box. Other sides of the glove box requiring access because of yarn conditioning, winding tension adjustment, etc., would not necessarily require shielding because the source-to-operator distance is probably sufficient to reduce the dose rates to tolerable levels.

Shielding of the glove box can take the form of plexiglass or a water window. The half-value layer of plexiglass (lucite) is 6 cm; water is 4.6 cm. An 8-inch thick water window approximates a tenth value layer, thus reducing the neutron dose rate to 2.4 mrem/hr (at two feet).

For hot winding of a microsphere capsule, the shielding becomes proportionally less due to the reduced power density and neutron and gamma dose rates.

The suggested atmosphere for the glove box to be used in "Hot" winding is argon.

Because of the high "still air" temperature involved, it will be necessary to cool the capsule prior to loading it into the winding machine. To accomplish this, the capsule could be subjected to a cooling gas stream such as Freon 12* (or another of the Freon series), or simply immersed in a container of water or other satisfactory liquid. Once the capsule temperature has been reduced to near ambient, the capsule can then be loaded into the winding machine.

The winding machine presently has rubber tipped ball grippers; these could be changed to metal (e.g., stainless). Cooling during the winding process could be accomplished by using a ring of gas jets located below the capsule with Freon 12 or other suitable Freon gas used to maintain a reasonable working temperature.

Handling of the capsule would be either remote (master-slave manipulators) or by use of suitable length tongs.

*Trademark E. I. Dupont

The winding process, assuming now that the capsule is sufficiently cooled, could be started in the following manner:

a. Load the capsule into the winding head.

b. Place a smear of carbonaceous glue (e.g., Pliobond) on capsule

c. Pick up loose end of yarn and lay over glue area, holding in place with tongs

d. When attached, (self-heating will aid glue drying) release end of yarn and start winder slowly until loose end is secure and winding operation is satisfactory.

e. Increase speed of winder and start cooling the capsule again. The operator may now step back and observe winding with an optical system. He need not approach winding setup unless adjustments are necessary or when capsule dimensions need be ascertained.

f. When capsule has reached the required diameter, the yarn is cut and the loose end pulled underneath several layers using a curved upholsterer's needle of appropriate size. (The needle will have to be threaded by hand, but the attachment of the loose end can be done with surgeon's forceps.) This operation is now complete and the capsule temperature can be allowed to rise (after removal from the winding machine) to remove volatiles and to convert the "glue" used on the yarn to enhance the winding characteristics to carbon.

The capsule is now ready for impregnation and can be moved remotely to the pass-through port and thence to the impregnation furnace.

"Hot" Impregnation and Coating

The wound capsule is transferred via a pass-through port into the impregnation furnace.

The impregnation or pyrolizing furnace requires evacuation prior to initiation of the pyrolizing operation. Both the evacuation effluent and pyrolyzing gas which exit the furnace must pass through an absolute filter assembly similar to that used in the glove-box system. Inasmuch as the pyrolizing gas may be hot, water cooling of the exhaust piping may have to be used to avoid destroying the filter. The effluent gas, as in the case of the glove-box system described in the preceding subparagraph will have to be monitored for possible alpha release.

The impregnation process preparation involves evacuation, as stated before, then backfilling and purging with nitrogen, evacuation and backfilling with hydrogen, and then evacuation followed by backfilling range with methane. The temperature of the furnace is raised to approximately 2000°F for periods upward of 180 hours to permit decomposition of the methane and deposition of carbon within the graphite wound structure.

It must be emphasized that although it is not anticipated that release of Pu^{238} will occur during the impregnation process, precautions must still be taken for containment in that eventuality. For this reason, the furnace access port must open into a glove box.

Upon completion of the impregnation operation, the oxidation resistant coating must be applied (presently the coating is B_6Si). As presently envisioned, the coating will be plasma flame sprayed thereby requiring an additional controlled atmosphere glove box operating in the same fashion as the systems described previously. The optimum coating thickness is between 3 and 15 mils. Upon completion of the plasma spray operation, the B_6Si coating must be fired and then oxidized. This can be accomplished by using an induction heater to raise the capsule temperature to between 1000 and 1500°C in an inert atmosphere (Ar or He) for upwards of one hour. The capsule is then cooled to between 700 to 800°C and exposed to an oxygen atmosphere for conversion of the B_6Si to the glassy phase (surface reaction only). The B_6Si coating process is covered by U.S. Patent No. 3,275,467.[12]

References

(1) Los Alamos Scientific Laboratory Quarterly Status Report on "Pu^{238} Space Electric Power Fuel Development Program", July 1 - September 30, 1968, Report No. LA-4068-MS

(2) Los Alamos Scientific Laboratory Quarterly Status Report on "Pu^{238} Space Electric Power Fuel Development Program", October 1 - December 31, 1968, Report No. LA-4089-MS

(3) Battelle Memorial Institute "Midyear Report on Development Program for Fabrication of Composite Fuel Form of $Pu^{238}O_2$", March 11, 1968, Report No. BMI-1831

(4) Battelle Memorial Institute "Summary Report on Development Program for Fabrication of Composite Fuel Form of $Pu^{238}O_2$", September 16, 1968, Report No. BMI-1849

(5) Personal Communication with Mr. M. Poberskin, Technical Editor, Composite Fuel Development Program, BMI,and Mr. WM. Pardue, Program Manager

(6) Mound Laboratories Plutonium - 238 Isotopic Fuel Form Data Sheets, October 31, 1968, Report MLM-1564

(7) Personal Communication with Mr. C. Henderson, Manager, Technical Coordination, Mound Laboratories

(8) Personal Communication with Dr. King, Director of Research, Zirconium Corporation of America

(9) Personal Communication with Mr. M. Poberskin, Technical Editor, Composite Fuel Development Program, BMI

(10) Personal Communication with Mr. J. Leary, LASL

(11) Battelle Memorial Institute "Midyear Report on Development Program for Fabrication of Composite Fuel Form of $Pu^{238}O_2$", March 11, 1968, Report No. BMI-1860

(12) Patent 3,275,467, "Coating Graphite and Method of Coating" by E. Colton, Assigned to Allis-Chalmers Manufacturing Company, Milwaukee, Wisconsin

4.3.4 COMPARISON OF FABRICATION TECHNIQUES

It becomes appropriate at this stage of analysis to compare cold and hot fabrication techniques including estimated fabrication costs (in terms of man-hours and equipment) for each configuration for only by such a comparison can each technique be placed in proper perspective. The comparison does not end there, however, for what may be economical and feasible, may not be practical. Future growth of fuel form technology (massive forms) will also tend to alter any conclusion reached as a result of this analysis.

4.3.4.1 "Cold" vs "Hot" Fabrication

In summary of the analyses presented in paragraphs 4.3.2 and 4.3.3, the following $Pu^{238}O_2$ fuel form - SIREN fabrication relationships have been established:

Fuel Form	Fabrication Technique
Microsphere	"Cold" fabrication prior to fueling "Hot" fabrication subsequent to fueling
Solid Solution	"Hot" fabrication subsequent to fueling
Cermet	"Hot" fabrication sebsequent to fueling
Sintered Oxide	"Hot" fabrication subsequent to fueling

The foregoing indicates that "hot" fabrication techniques can be used with all the proposed fuel forms, while "cold" fabrication lends itself only to the microsphere type.

The microsphere fuel form will present a significant problem from the standpoint of contamination. This problem will be more pronounced for the "cold" fabricated and fueled SIREN than for the "hot" fabricated SIREN because of the greater difficulty of decontaminating the wound structure should the contamination prevention philosophy not be as successful as anticipated.

Contamination prevention or decontamination of the SIREN capsule is not the limiting factor, however, the type of closure and securing a reliable seal of that closure subsequent to closure are probably the most important problem areas requiring solution. In general, the primary and secondary plug techniques (see Figure 091) appears at this writing to be the most promising from the standpoint that a primary seal (in the form of a plug) is made before breaking the gasket seal between the fueling tool and liner. Even if that technique is successful to the point of contamination free fueling and closure, the space available to perform the final weld is severely restrictive making TIG welding of the screw plug to the insert almost impossible. Electron-beam or laser techniques are needed, along with considerable development to produce the degree of weld integrity and repeatability required.

The contents of Table 4-46 are intended to summarize the major problem areas for comparing "hot" versus "cold" fabrication. If a choice were to be made on the basis of problem complexity alone, it is felt that the hot winding technique will offer the greatest chance of success and adaptability to other fuels and fuel forms.

TABLE 4-46
COMPARISON OF "HOT" VS. "COLD" FABRICATION

"Cold" Fabrication	"Hot" Fabrication
1. Technique usable only with microsphere type fuel	1. Technique usable with all $Pu^{238}O_2$ fuel forms discussed
2. Requires development of closure and closure techniques	2. Sophistication of winding, impregnation, and oxidation resistant coating equipment increased due to radiological and atmosphere control requirements

TABLE 4-46

COMPARISON OF "HOT" VS. "COLD" FABRICATION (Cont)

"Cold" Fabrication	"Hot" Fabrication
3. Requires development of fueling tools and technique	3. "Hot" winding techniques require further development
4. Contamination problem is significant due to difficulty in decontaminating the wound structure	4. Strippable coatings (metallic and/or inorganic) may be used as an aid to decontamination during liner fueling and closure operations for microspheres.

4.3.4.2 Fabrication Cost Analysis

A precise cost analysis for fueling the SIREN capsule contains many variables thus making such an analysis extremely difficult. An intitial approximation of the costs for cold and hot fabrication are presented in Tables 4-47 and 4-48, respectively. Each of these analyses are based on the following assumptions to allow a common ground for evaluation:

- Fuel is GFE
- Fueling gloves boxes and other required jigs and tools exist
- The liner/closure combinations listed are workable
- Development costs are not included
- Tooling is a non-recurring cost, probably covered in development effort
- Labor costs are based on $4.28/hr for technician(s) (cost rounded off to nearest dollar)

Table 4-47

SIREN FABRICATION COST ANALYSIS (ESTIMATED)

COLD FABRICATED AND MICROSPHERE FUELED

1. Liner*	Liner Mat'l	Liner Cost ($)	Closure Liner & Graphite Type	Mat'l Cost ($)	Fab Cost ($)	Supplies & Mat'ls Cost ($)	Closure Oper. Cost ($)	Tool Tooling Cost ($)	Other Labor ($)	Cost Summary Mat'l ($)	Cost Summary Labor ($)	Cost Summary Total ($)
Case No. 1	ZrO_2	41	ZrO_2 Plug - Slip Sealed	41	171	50	35	200		132	206	338
Case No. 2	ZrO_2	41	ZrO_2 Plug/Nb Braze	41	171	10	35	200		92	206	298
Case No. 3	ZrO_2	41	Mo Insert Nb Braze; Plug & Screw	50	257	10	70	300		101	327	428
Case No. 4	ZrO_2	41	Mo Insert Ir Braze, Plug & Screw	50	257	25	70	300		126	327	453
Case No. 5	ZrO_2/Mo	160	Same as Case No. 3	50	257	10	70	300		220	327	547
Case No. 6	ThO_2/Mo	200	Same as Case No. 3	50	257	10	70	300		260	327	587
Case No. 7	ZrO_2	41	Mo tapered plug; Nb discs	35	171		70	400		76	241	317
Case No. 8	ThO_2/Mo or ZrO_2/Mo	160 to 200	Same as case No. 7	35	171		70	400		235	241	476
Case No. 9	Mo	100	Mo Plug & discs	15	171		70	800		115	241	356
Case No. 10	Mo	100	Mo Plug & Screw	30	257		70	800		130	327	457
Case No. 11	Mo	100	Nb Plug & Screw	30	257		70	800		130	327	457
Case No. 12	ZrO_2	41	ZrO_2 Base Slip	50	70	50	70	150		141	140	281
2. Winding									7		7	
Graphite Yarn						10						
Other Supplies						10				10		
3. Impregnation						100			171	100	171	271
4. Fueling Operation						50			70	50	70	120
5. Oxidation Resistant Coating (assumed done by Mound Laboratories)						110		250	171	110	171	281

*Refer to Table 4-44 for more information

**Estimated tooling given for reference only-not included in total cost since it would most likely be covered in development costs.

Liner cost range $281 to $ 587
Items 2-5 699 699
Total Range $980 to $1285

TABLE 4-48

SIREN FABRICATION COST ANALYSIS (ESTIMATED)
"HOT" FABRICATION

	Item	Mat'l Cost ($)	Fab Cost ($)	Total ($)
1.	Hot Winding			
	Graphite Yarn	10	10	20
	Coolant	25		25
	Misc	10		10
2.	Impregnation	100	171	271
3.	Oxidation Resistant Coating	110	171	281
Total		$255	$352	$607

- Engineering, supervision and health physics support are provided but not costed.

Special facilities and equipment are listed below (in addition to those in existence):

	Cost
• Induction heater with atmosphere controlled heat zone (all cases)	$ 15 K
• Pulsed laser welder, Cases 3 - 11	25 K
• Fueling equipment (all cases)	15 K
• Plasma spray equipment (all cases)*	35 K
• Special glove box for plasma spray*	25 K
• Special glove box for all heat treatments*	10 K
TOTAL	$ 96.5 K

The total cost per SIREN capsule (fueled, but fuel cost not included) can be summarized as follows:

Liner	$ 281 to $ 587
Remaining fabrication	699 to 699
TOTAL	$ 980 to $ 1285

On the basis most promising liner/fueling port/closure technique, (Case 10) the estimated cost would be:

Liner	$ 457
Remain of fabrication	699
TOTAL	$ 1156

*Costs are order of magnitude - Mound Laboratories

The assumptions and conditions for the hot fabrication (all $Pu^{238}O_2$ fuel forms) are as follows:

- All fuel forms supplied with appropriate line material, ready for hot fabrication - GFE
- Capsule is contamination free
- Development costs not included
- Engineering, supervision and health physics support provided but not costed
- Labor costs are based on $4.28/hr for technician(s) (cost rounded off to nearest dollar)

Special facilities and equipment are listed below (in addition to those already in existence).

	Estimated Cost
• Glove-box system for hot winding*	$ 16 K
• Glove-box system for impregnation	4.8 K
• Glove-box system for plasma spray	25 K
• Glove-box system for heat treatment	10 K
• Ball winder-modified	15 K
• Impregnation furnace and induction heater (10-inch × 15-inch hot zone)	40 K
• Pass boxes (5)	4 K
• Plasma spray equipment	$ 35 K

*Glove-box estimates are only order of magnitude - Mound Laboratories. Note that this price does not include ventilation, instrumentation and other radiation monitoring equipment that may be required.

	Estimated Cost
• Extra shielding and fabrication	$ 3 K
• Atmosphere controlled induction heated furnace	15 K
TOTAL	$ 167.8 K

The total cost per SIREN capsule fabricated on GFE fuel and liner is estimated at $607, consistent with the assumption and conditions stated previously.

If one were to now make the assumption that microsphere fuel only was to be supplied, the liner cost would be approximately $457 (Case 10, previous cost analysis); the fueling $120, for a total cost of approximately $1184.

Summarizing, it would appear that the cost per capsule, on a production basis (under the assumptions and conditions previously stated) is of the order of $1200. The necessary technical and Health Physics support, etc., will alter this figure considerably.

4.3.5 PROBLEM AREAS

During the course of discussion of possible fueling and/or fabrication techniques, the following problem areas were uncovered.

4.3.5.1 Microsphere Fueling

The discussion of the fueling of a cold fabricated capsule with the $Pu^{238}O_2$ microsphere fuel form has shown that no matter what technique is used, there are problem areas which require solution. Moreover, while most of the problems are solvable, the requirement to develop and/or fully utilize new technology is clearly evident (the pulsed laser to weld the closure, for example).

The major problem areas associated with microsphere fueling are listed below in order of increasing importance:

- Application and implementation of the contamination prevention philosophy to microsphere fueling

- Adequate fuel fines control
- Fueling tools, transfer plumbing, and technique for microspheres
- Liner materials selection
- Closure method and technique.

All of these problem areas are very much interrelated and require almost simultaneous solution starting with the liner material and closure method.

4.3.5.2 "Hot" Fabrication

The problem areas associated with hot fabrication of the SIREN are quite similar to those of the cold fabricated (before fueling) version except that the capsule is already fueled. The major problem areas relating to hot fabrication are listed below:

- Method of microsphere fueling and decontamination
- Method of cooling the capsule before and during winding
- Hot winding technique (including machine modification)
- Impregnation of hot wound structure
- Application of oxidation resistant coating
- Heat treatment of oxidation resistant coating.

As in the case of the cold fabricated and fueled SIREN, the problem areas are interrelated, although perhaps not to the same degree. The complex nature of the fabrication equipment required because the capsule is hot and is radioactive is well within the scope of modern engineering practice.

4.3.6 RECOMMENDATIONS

Upon reviewing the analyses, comparison of fabrication techniques, and problem areas, it would appear that hot fabrication of the SIREN offers the greatest potential. The reasons for making this statement are delineated below:

- Hot fabrication is applicable to the $Pu^{238}O_2$ fuel form presently developed or those under development
- The outer structure (SIREN) is not perturbed by the addition of a potention trouble spot (the fueling port)
- The problems associated with decontamination of the outer structure are eliminated
- Fabrication of a closure for atmosphere fueled capsule (before hot fabrication) is made much easier and simpler
- Closure (before hot fabrication) can be performed more easily and with a greater chance for success
- Hot fabrication is independent (for the most part) of the fuel form
- The hot fabrication process is more readily adaptable to advances in material technology (yarn, impregnant, etc.).

It is, therefore, recommended that the development of SIREN technology be oriented in the direction of hot fabrication.

It is also recommended that where microsphere fueling will be used that the techniques discussed in paragraph 4.3.3 be adapted for fueling of an appropriately selected liner on which the SIREN will be fabricated.

Facilities mockups should be made when the process is finally established to provide a good basis for establishment of final facilities and equipment requirements and cost estimation.

4.4 AEROTHERMAL ANALYSIS

4.4.1 INTRODUCTION

A body approaching the earth possesses a large amount of energy - potential energy because of its position above the earth's surface and kinetic energy because of its velocity. A satellite in a circular orbit at 200 miles altitude possesses a kinetic energy of about 13,000 B/lb and a potential energy of approximately 1200 B/lb. An object approaching the earth from deep space possesses a kinetic energy of approximately 26,000 B/lb. These energies compare with 1000 B/lb required to vaporize water and 25,000 B/lb to vaporize carbon. Carbon has one of the highest heats of vaporization known at present.

To withstand these extreme reentry environments a body must be capable of either absorbing the high surface heat flux without exceeding its degradation temperature or be capable of sustaining the equilibrium reradiation temperature. The SIREN capsule incorporates both techniques in order to survive reentry.

The SIREN heat source consists of a 3.0-inch outside diameter sphere with a 0.5-inch graphite carbon wall thickness (Figure 4-33). Reentry and internally generated heat are radiated from the high temperature outer graphite surface.

Since the SIREN heat source concept is a new development it is desirable to evaluate the ability of this design to withstand reentry and to contain the fuel before and after impact. The purpose of this study is to provide pertinent reentry data which will allow for comparison with existing space nuclear power supplies.

Ablation analyses are performed by: (1) computing theoretical trajectories, (2) determining heating rates, and (3) using thermal balances at the surface to determine temperature - time history. Naturally, no closed solution exists for use in ablation analyses, and all problem solutions are obtained through the use of iterative computational methods and high speed computers. In this study use was made of charts prepared by Lovelace[5], which depict kinematic and heating parameters for ballistic reentries at speeds of 26,000 to 45,000 ft/sec.

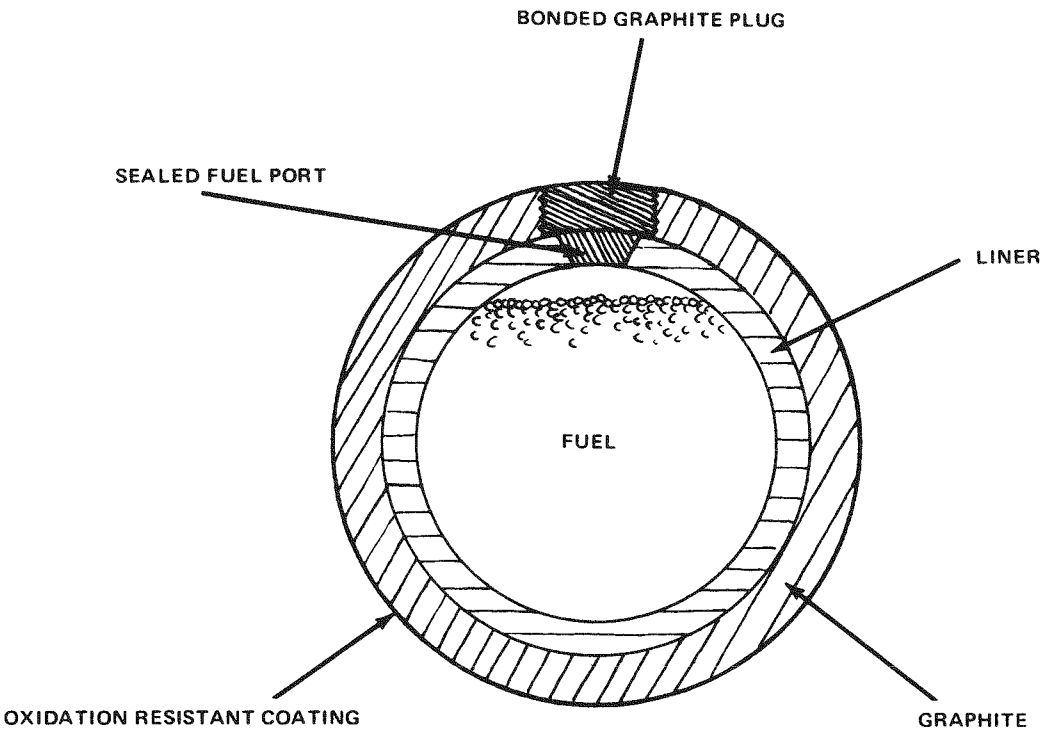

69-H65983-010

Figure 4-33 Fueled SIREN Capsule.

Works of Scala, Sinclair, and Gilbert[2] as well as Metzger, Engle and Diaconis[3] were used to determine the capsule surface recession during reentry.

Six initial reentry conditions were investigated: 0.01°, 1°, 2°, and 90° at 26,000 ft/sec; 6° at 36,000 ft/sec; and, 8° at 45,000 ft/sec. For these initial conditions, aerodynamic heating, capsule surface temperature and surface recession were determined for rotating and non-rotating reentry modes. In addition, terminal velocity for a non-ablated 3.0-inch capsule was determined.

The selection of these specific initial reentry conditions was based on the following reasoning:

- Desire to determine mass loss during trajectories causing most severe integrated heat load
- Desire to obtain sufficient data at orbital velocities for comparison with existing heat source capsule data
- Desire to know maximum surface temperature during a reentry or abort of a planned earth orbit.

The orientation of a spherical heat source during reentry is not well defined, so local heating rates were bracketed by analyzing sources which were stable and sources which spun about an axis perpendicular to the flow. Results are based on an initial altitude above the earth's surface of 300,000 feet for an initial velocity of 26,000 ft/sec and 400,000 feet for initial velocities of 36,000 and 45,000 ft/sec.

4.4.2 AERODYNAMIC FLOW REGIMES

Bodies reentering the earth's atmosphere may experience aerodynamic flow that can be divided into three distinguishable flow regimes. They are: free molecule flow, transitional flow, and continuum flow. This study deals only with laminar hypersonic flow in the three flow regimes since all appreciable heating during reentry occurs during hypersonic flight. The one exception is in the determination of terminal velocity, which deals with subsonic flow.

Aerodynamic heating of a body passing through the three flow regimes can be calculated with a good degree of accuracy when considering only the free molecular and continuum stagnation heating rate theories and neglecting the transitional flow regime. This is accomplished by choosing a suitable boundary between continuum and free molecular flow theory.

The variation of stagnation Stanton number versus Knudsen number for spheres[4] is shown in Figure 4-34. Straight line approximations to the variation of the Stanton number in the continuum and free molecular regimes are also noted in Figure 4-34, with intersection of the lines occurring at a Knudsen number, $K_N = \lambda/D = 0.30$. This indicates that a reasonable approximation to the calculations of aerodynamic heating may be obtained by using free molecular heating theory when the Knudsen number is greater than 0.30 while using continuum flow theory when the Knudsen number is less than 0.30. The location of the $K_N = 0.30$ boundary in the velocity - altitude plan is shown in Figure 4-35. A sphere diameter of three inches (D = 3) was used.

The flow regime correlation function[3] which is shown in Figure 4-36 provides an additional means of locating the boundary separating free molecule and continuum heating. For Reynolds number, $Re_S = \rho_\infty V_\infty D/\mu_2$, below about 10, the Stanton number decreases rapidly below the high Reynolds number value. A Reynolds number of 10 was chosen as boundary between continuum and free molecular flow and its locations in the velocity-altitude plane for a three-inch diameter sphere is shown in Figure 4-35. The Reynolds number was evaluated as follows:

$$Re_S = \frac{\rho_\infty V_\infty D}{\mu_2} = \frac{\rho_2 \rho_\infty V_\infty D}{\rho_2 \mu_2} = \frac{\rho_2 \rho_\infty V_\infty D}{P_2 \left(11 \left(\frac{h^x}{100} \right)^{-0.3640} \times 10^{-7} \right)} \qquad (1)$$

where

ρ_2, ρ_∞, are in lbm/ft^3

P_2 is in atm

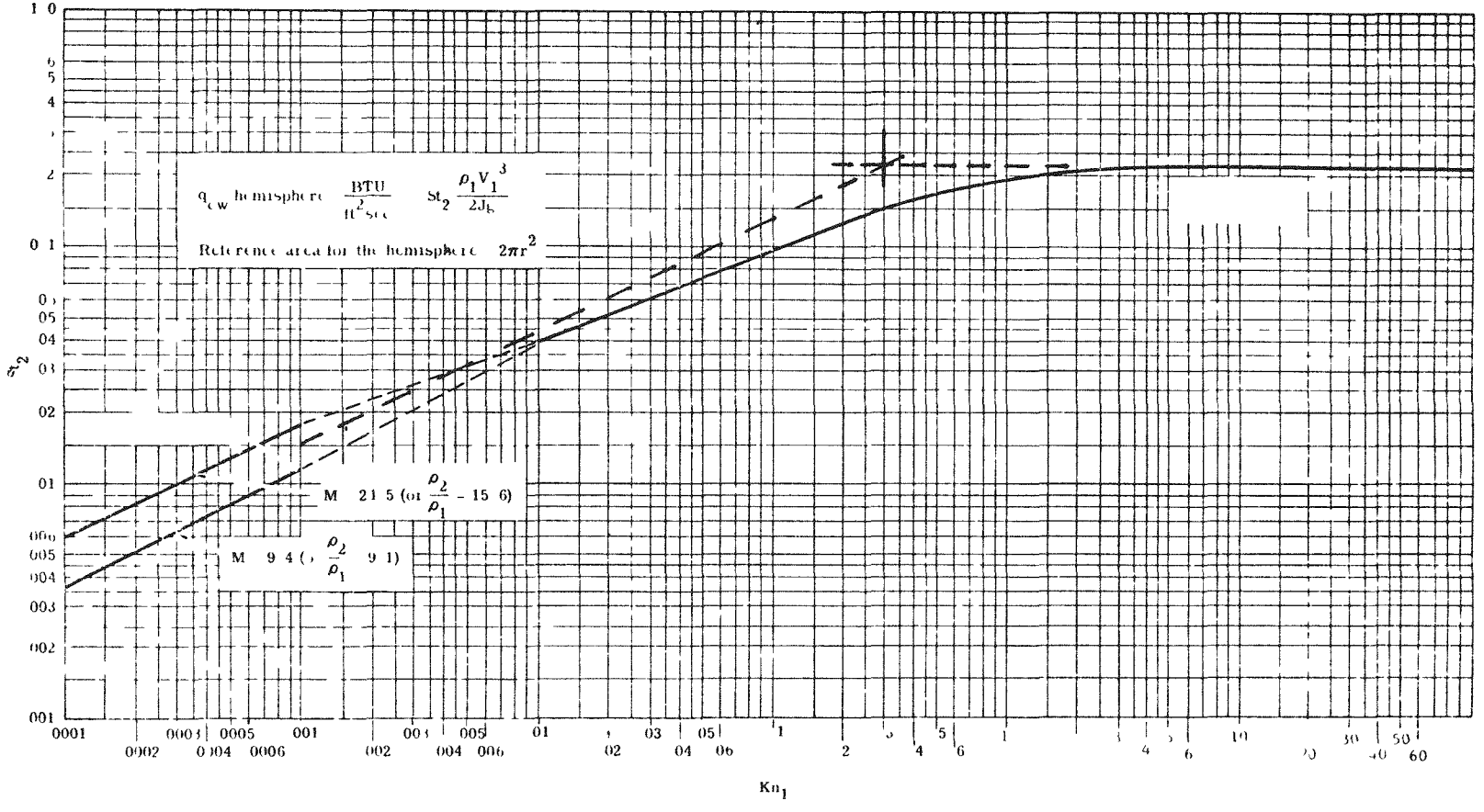

69-H65983-011

Figure 4-34 Area-Averaged Stanton Number Behind the Shock vs. Knudsen Number for Hemisphere in Hypersonic Flow.

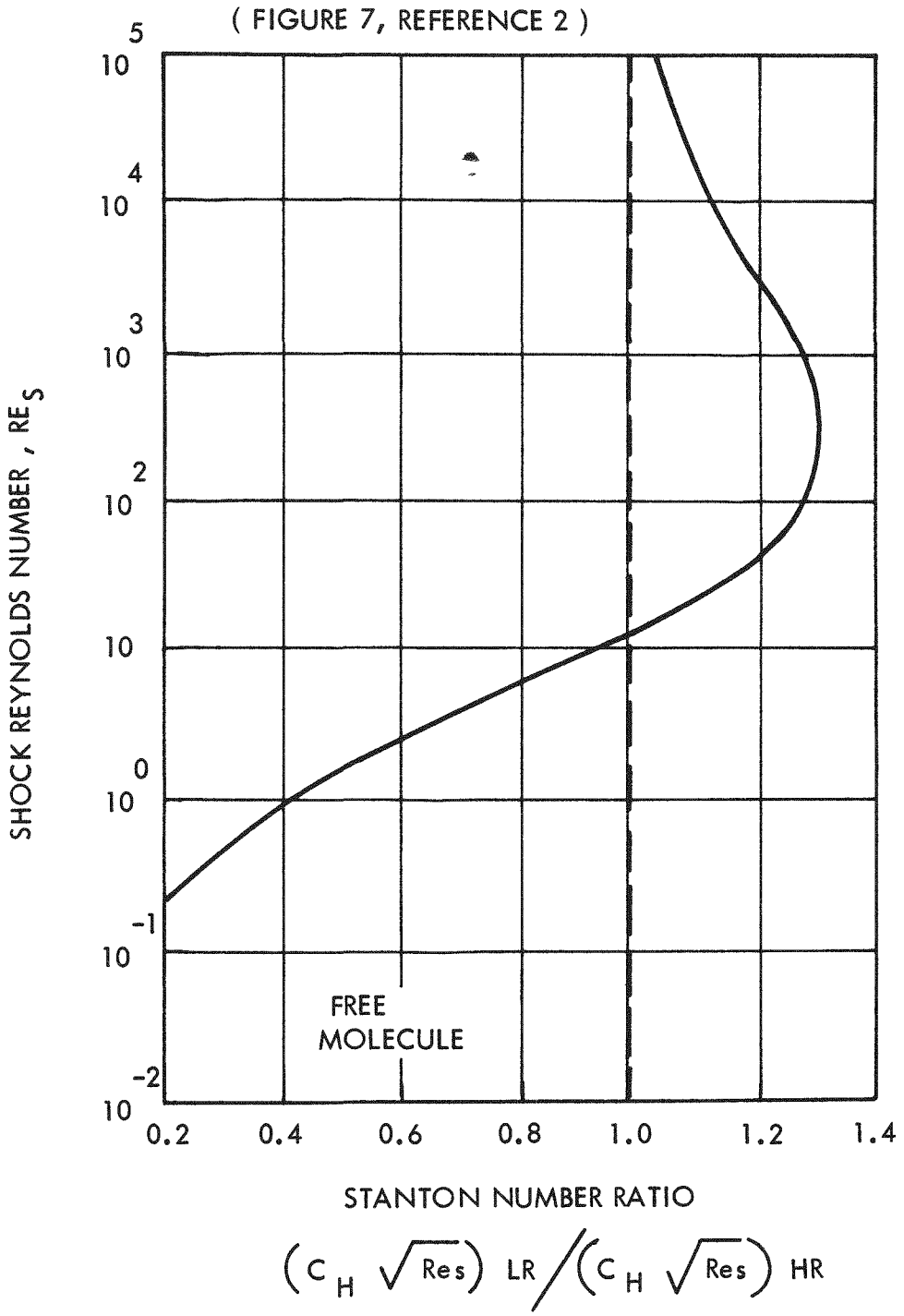

Figure 4-35 Flow Regime Correlation Function.

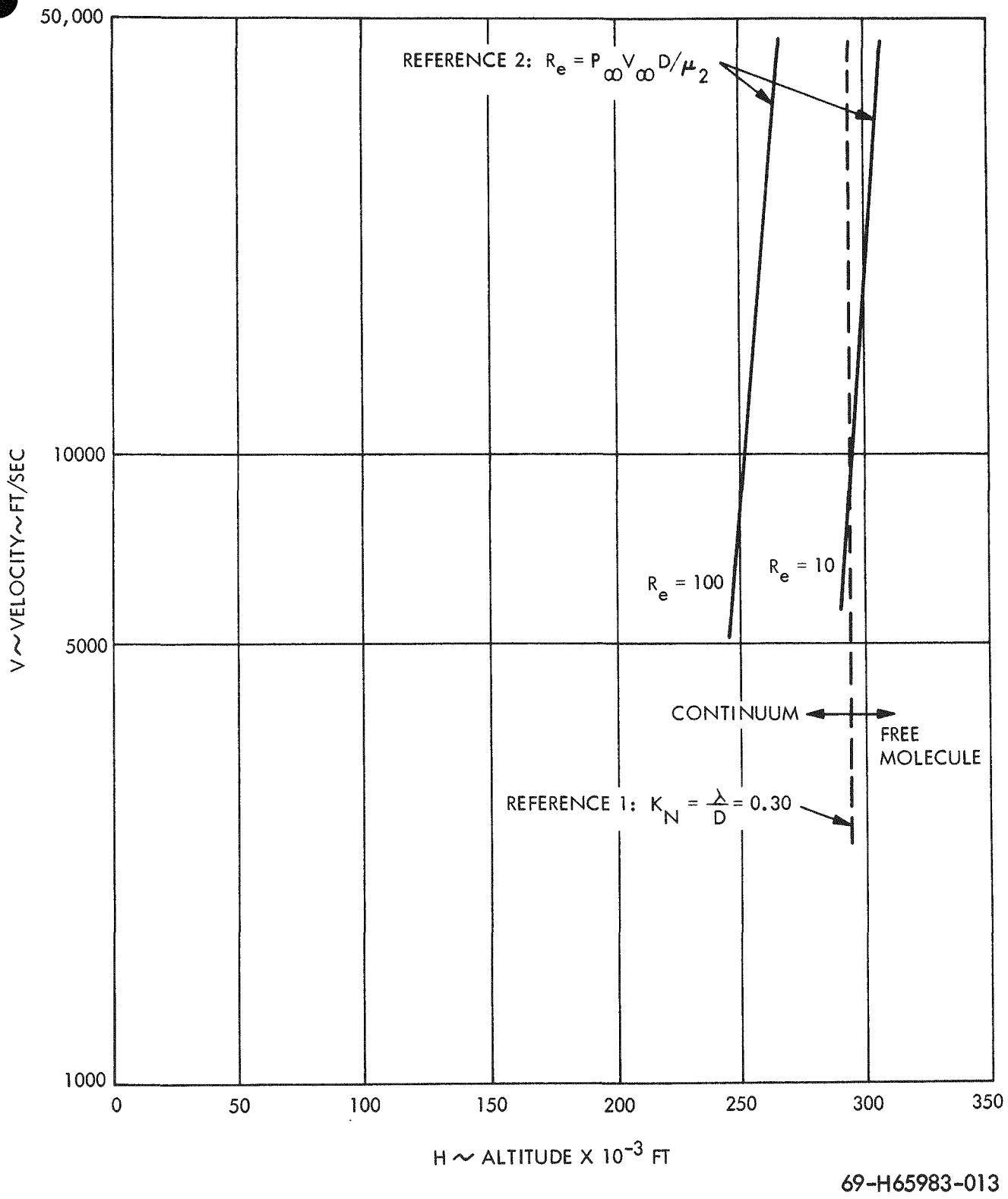

Figure 4-36 Continuum - Free Molecular Boundary.

$\frac{h^x}{100}$ is in BTU/lb

and a straight line approximation to the variation[8] of density and viscosity with reference enthalpy was used (Figure 4-37).

$$\frac{\rho_2 \mu_2}{P_2} = 11 \left(\frac{h^x}{100}\right)^{-0.3640} \times 10^{-7} \frac{lb^2}{(ft)^4 sec} \qquad (2)$$

The free stream density, ρ_∞, was obtained from the 1962 Standard Atmosphere and $\rho_2 = (\rho_2/\rho_\infty)\,\infty$ from the Avco Everett Research Laboratory Hypersonic Gas Dynamic Charts for Equilibrium Air. The boundary for Reynolds number equal to 100 is also shown for informative purposes.

The boundary locations predicted in two different ways, (i.e., $K_N = 0.30$ and $Re_S = 10$) are in close agreement. Continuum heating theory is applicable below about 300,000-foot altitude for all velocities.

4.4.3 DRAG COEFFICIENTS

Figure 4-38 (taken from Reference 4) shows the variation of drag coefficients with flow regime for a sphere. With a 3.0-inch diameter sphere the transition between molecular and continuum flow occurs at an altitude of about 280,000 feet. For the purpose of this study a drag coefficient of 0.92 was assumed constant over the entire hypersonic reentry analysis. In addition, the ballistic coefficient was assumed constant, even though a small change in the value occurred because of ablation.

4.4.4 TRAJECTORY ANALYSIS

Before reentry heating rates and mass loss can be determined it is necessary to determine the theoretical trajectory of the reentry capsule. The trajectory yields necessary data such as velocity, altitude, and range versus time during the reentry. From these data it is then possible to determine heating rates, capsule suface temperature, stagnation pressure, and mass loss as a function of time.

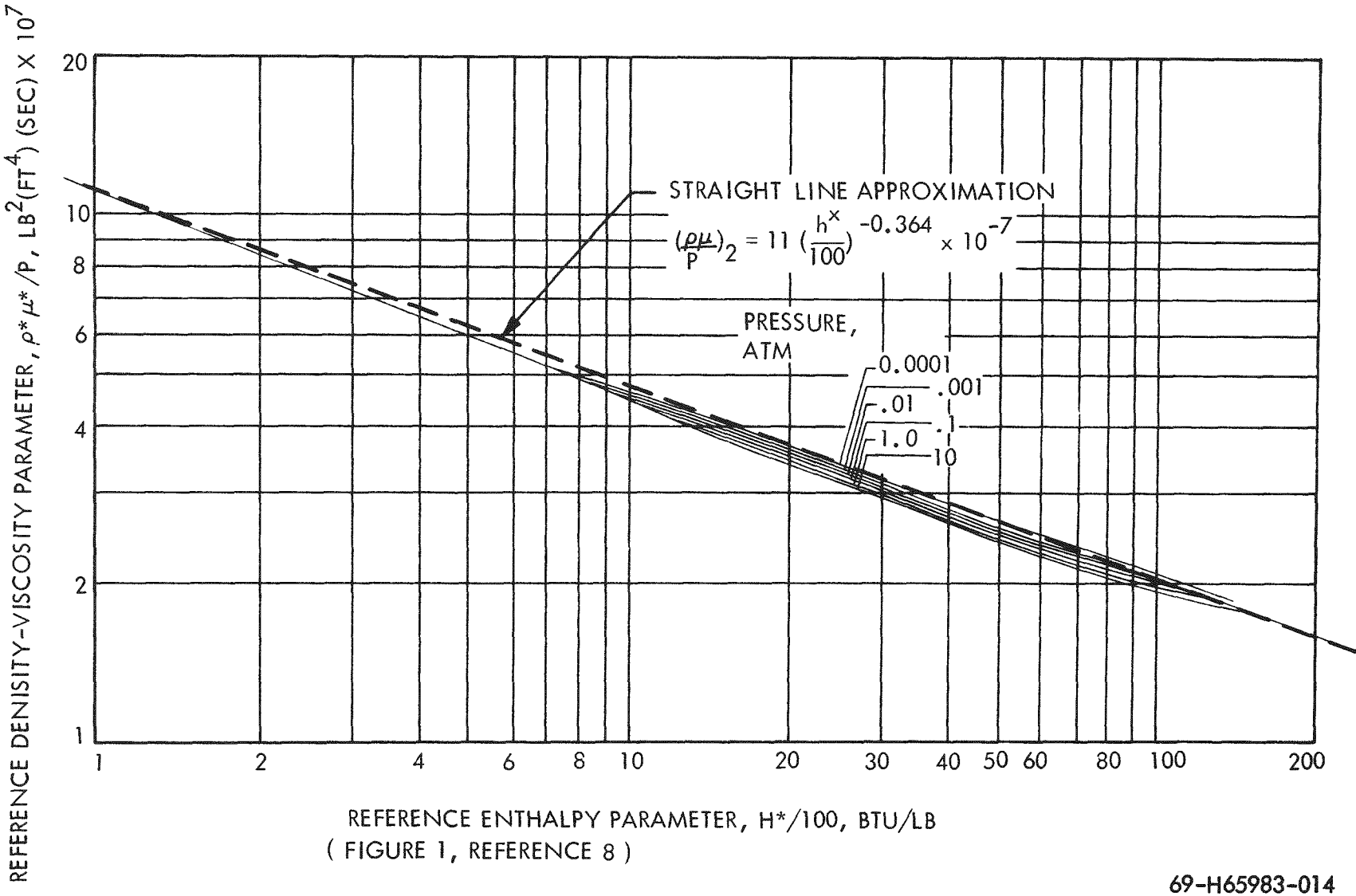

Figure 4-37 Variation of Product of Reference Density and Viscosity $\rho^*\mu^*$ with Reference Enthalpy as a Function of Pressure.

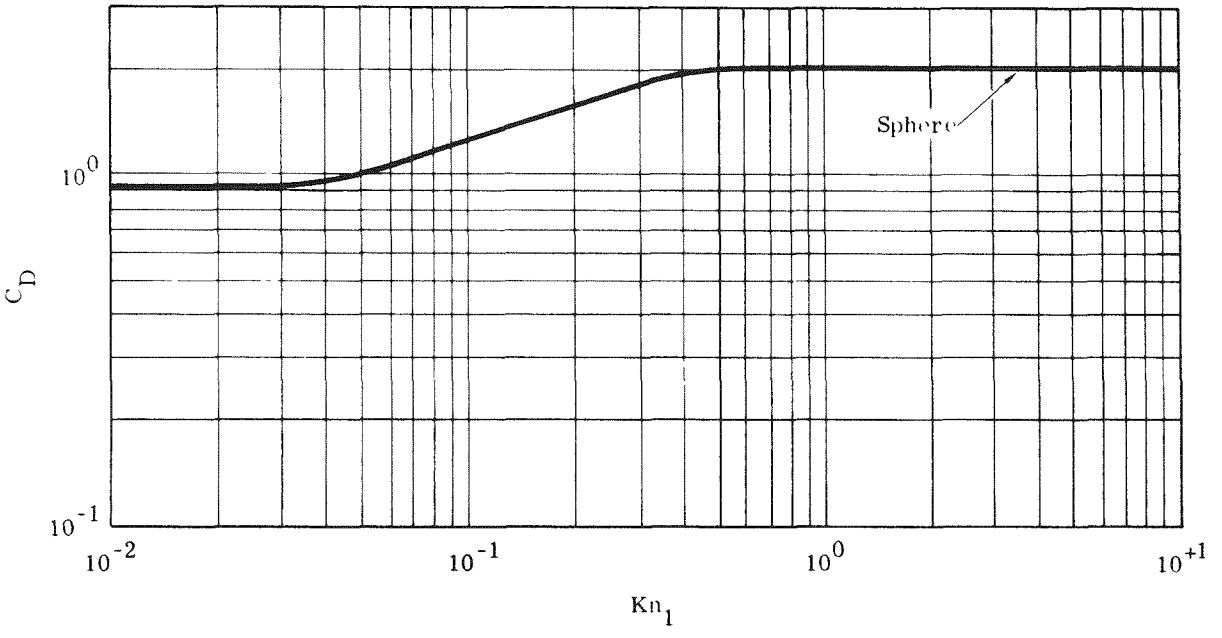

69-H65983-015

Figure 4-38 Drag Coefficient vs. Knudsen Number for a Sphere in Hypersonic Flow.

The reentry motion of an object within the atmosphere is a resultant of its mass, size, shape and orientation, and of its rotational and translational rates. Kinematic motion of a point mass body with given aerodynamic parameters have been solved in References 6 and 7 for steep and shallow reentries.*

The basic equations of motion used are shown below:

$$-\frac{d^2y}{dt^2} = g + \frac{D \sin \phi}{m} - \frac{L \cos \phi}{m} - \frac{u^2}{r} \tag{3}$$

$$\frac{d^2x}{dt^2} = -\frac{uv}{r} - \frac{D}{m}\left(\cos \phi + \frac{L}{D} \sin \phi\right) \tag{4}$$

where:

x = Direction tangent to earth's surface - ft.

y = Direction normal to earth's surface - ft

t = Time - seconds

g = Acceleration of gravity - ft/sec^2

D = Drag - lbs.

L = Lift - lbs

ϕ = Local flight path angle - degrees

m = Mass of fuel capsule - slugs

u = Horizontal velocity component - ft/sec

v = Vertical velocity component - ft/sec

r = Distance from center of the earth to capsule - ft

w = Local angular velocity - radians/sec

*Classical free body diagram shown in Figure 4-39.

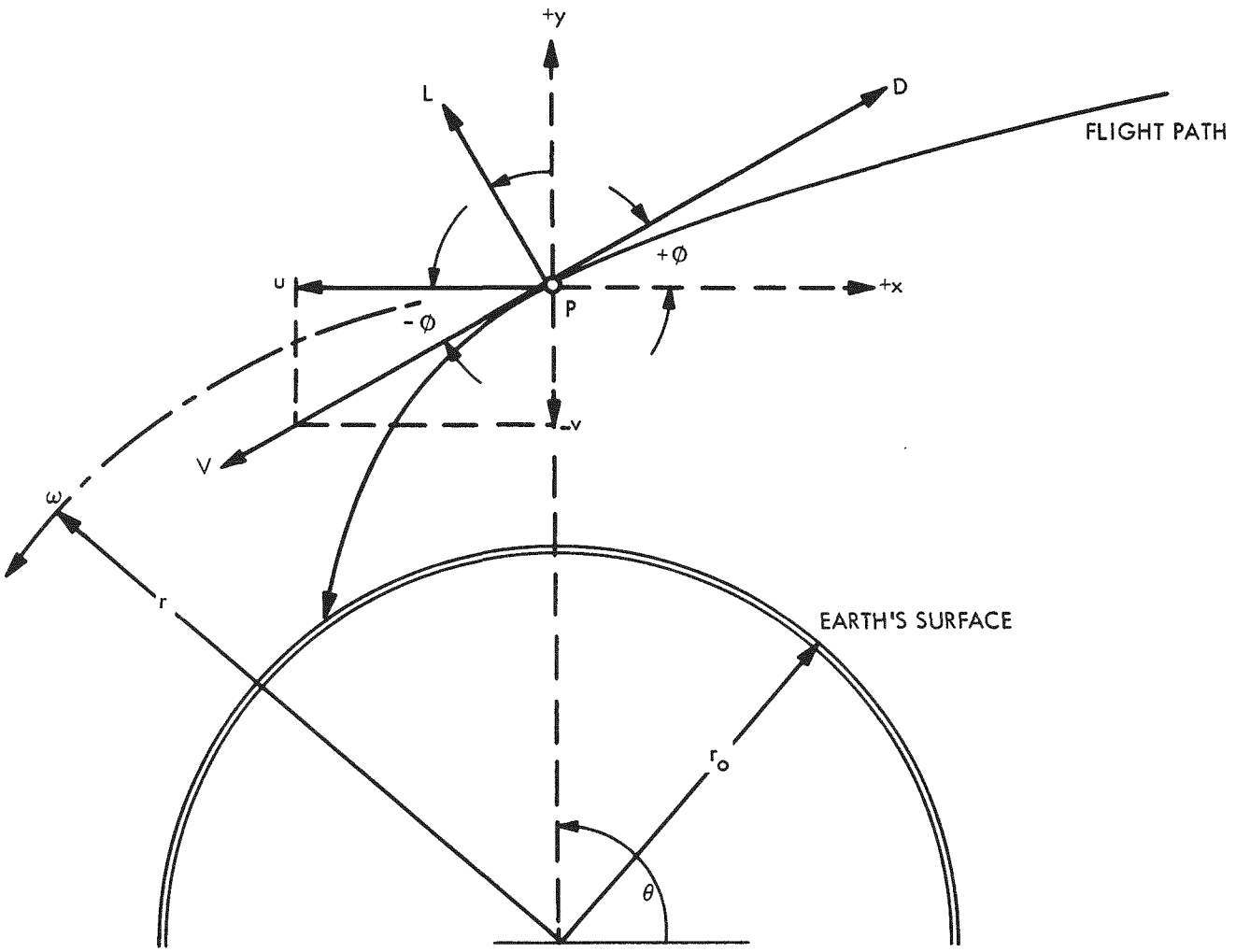

69-H65983-016

Figure 4-39 Free Body Diagram for a Point, Mass "P", Moving in the Atmoshpere and Influenced by Central Inverse Square Gravity Field.

The simplifying assumptions made in solving the exact nonlinear differential equations of References 6 and 7 are:

- Atmosphere and earth are spherically symmetric
- Variation in atmospheric temperature and molecular weight with altitude are negligible compared to the variation in density
- Peripheral velocity of the earth is negligible compared to the velocity of the reentry body.

Figure 4-40 gives reentry trajectories for a reentry velocity of 26,000 ft/sec. Figure 4-41 indicates the trajectory for a reentry velocity of 36,000 ft/sec and a reentry angle of 6° which is the minimum reentry angle at this velocity. Likewise, for 45,000 ft/sec, the trajectory is given for the minimum reentry angle without skip which is 8° (Figure 4-42).

4.4.5 AERODYNAMIC HEATING

During the reentry phase the SIREN sphere heat balance can be written as follows:

$$Q_{SR} = Q_C + Q_i + Q_{GR} (B/ft^2 sec) \qquad (5)$$

where

Q_{SR} = Surface radiation heat flux

Q_C = Convective heating rate (including combustion)

Q_i = Internal heat source

Q_{GR} = Gas radiation heat flux

4.4.5.1 Surface Radiation

The anticipated temperatures on the surface of the sphere during reentry are between $1000^{\circ}K$ and $4000^{\circ}K$. Temperatures of this magnitude cause the sphere to

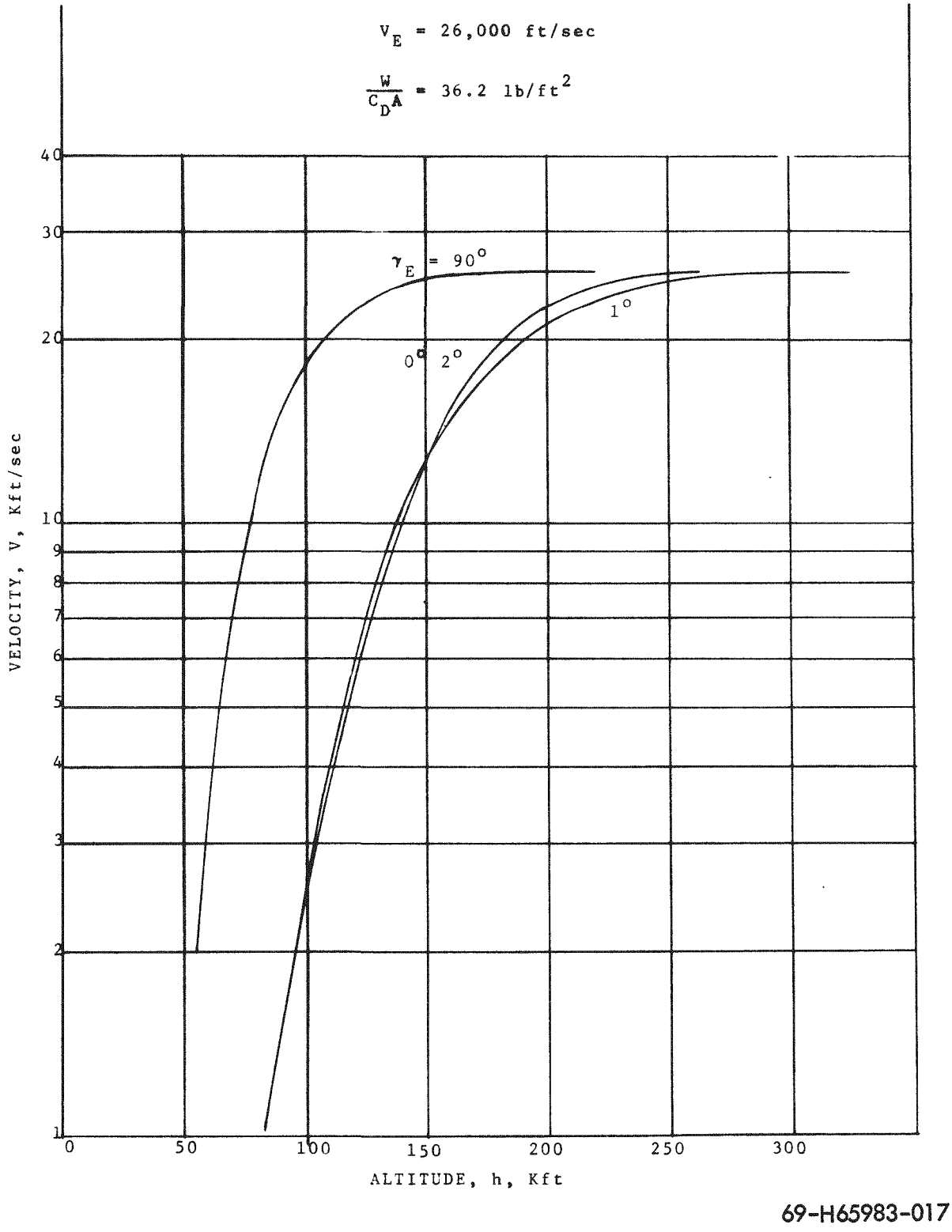

Figure 4-40 Reentry Trajectory, Velocity = 26,000 ft/sec.

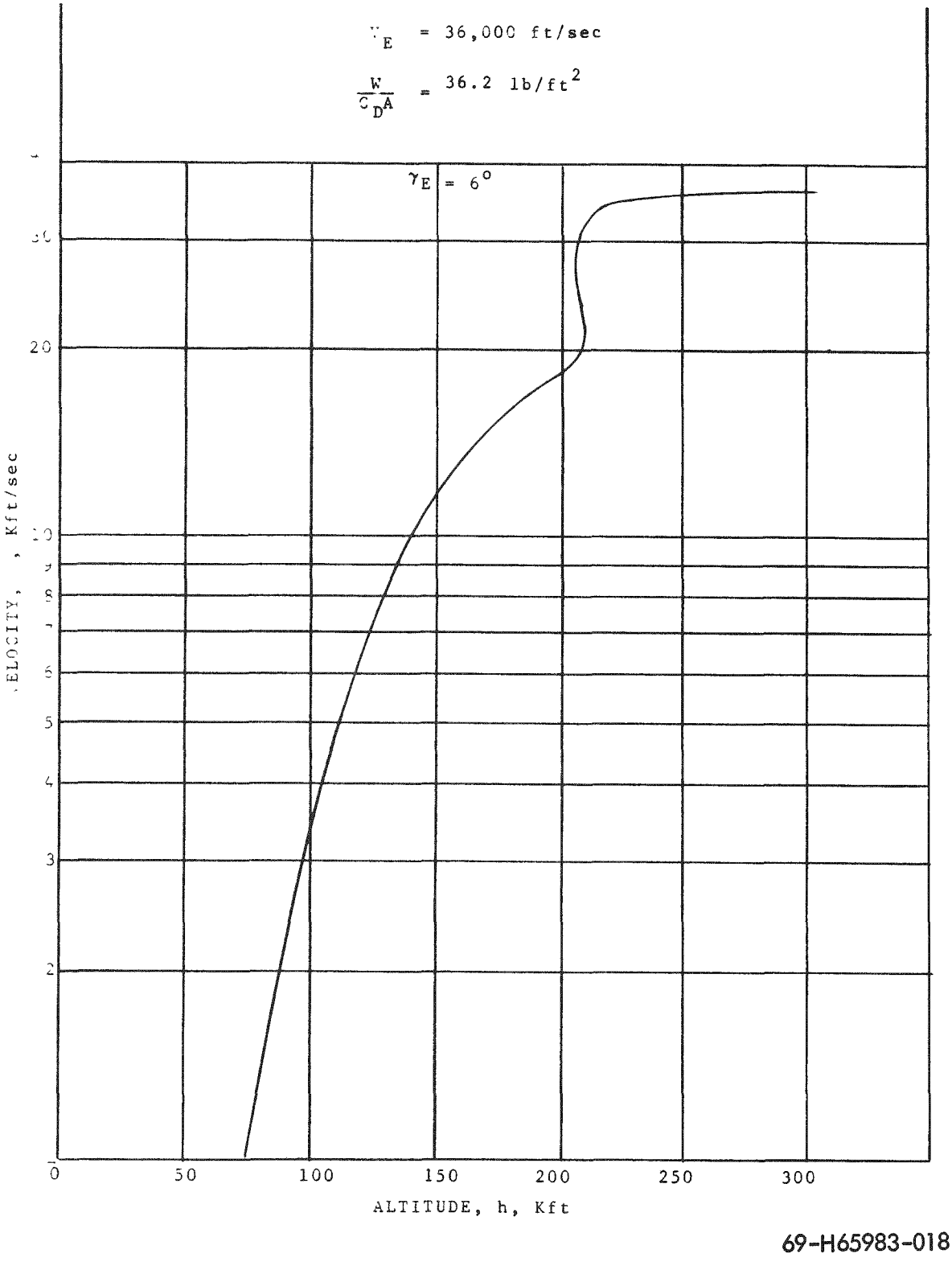

Figure 4-41 Reentry Trajectory, Velocity = 36,000 ft/sec.

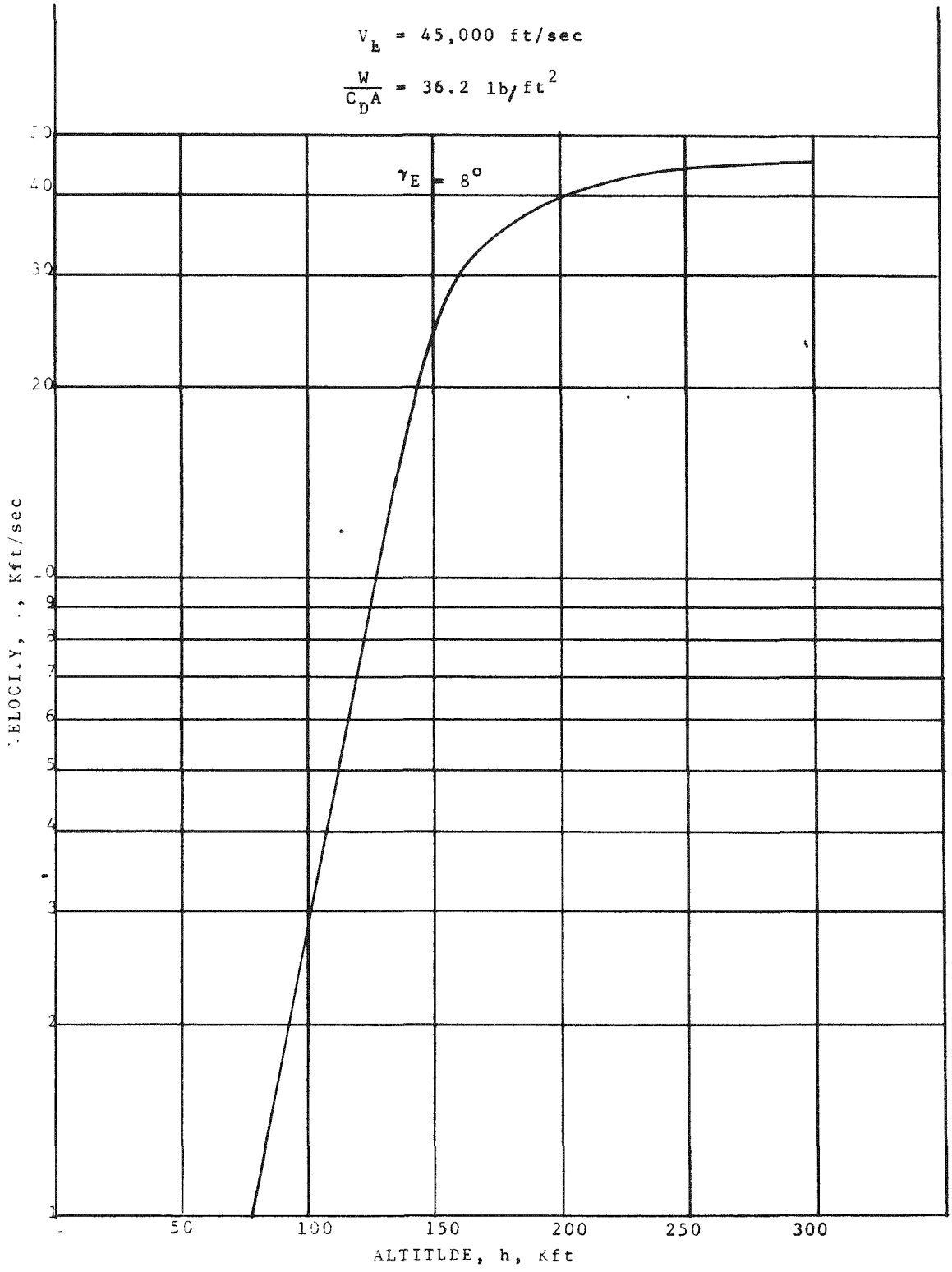

Figure 4-42 Reentry Trajectory, Velocity = 45,000 ft/sec.

dissipate its energy via radiation from the exterior surface. The radiation heat rate is given as:

$$Q_{SR} = \int_A \sigma \epsilon T_W(A)^4 \, dA, \ B/sec \tag{6}$$

where

$T_W(A)$ = Local wall temperature, K

ϵ = Emissivity, assumed 0.85

$\sigma = 5.0388 \times 10^{-12}$ $B/ft^2 sec\ K^4$

4.4.5.2 Viscous Aerodynamic Heating

The aerodynamic convective heat transfer rate is based on results from Reference 1 for a reentry in the continuum flow regime. As the surface temperature ($T_W > 1000^oK$) increases during reentry, the exothermic oxidation reactions exceed the mass transfer effect in the boundary layer due to blowing, and thus, results in a net increase in heat transfer to the stagnation point and along the surface of the graphite sphere. Based on analysis in References 2 and 3 the stagnation point heating is:

$$Q_C = \left(\frac{P_o}{R_N}\right)^{1/2} [33.3 + 0.0333 (H_s - h_w)] \ BTU/ft^{3/2} atm^{1/2} \tag{7}$$

where

P_o = Stagnation pressure, atm

R_N = Nose radius, 0.125 ft

H_s = Stagnation enthalpy, B/lb

h_w = Wall enthalpy, B/lb

Stagnation enthalpy is a function of the velocity and is given as:

$$H_s = 100 + 13{,}500 \left(\frac{V}{V_s}\right) \tag{8}$$

where:

V = Velocity of the sphere, ft/sec

V_s = Satellite velocity, ft/sec

Stagnation pressure can be written:

$$P_s \approx 0.975 \times 759 \left(\frac{\rho}{\rho_o}\right)\left(\frac{V}{V_s}\right)^2 \text{ atm} \tag{9}$$

where:

ρ = Ambient density, lb/ft^3

ρ_o = Density at sea level, lb/ft^3

Substituting equations 8 and 9 into equation 7, we obtain:

$$Q_C = a\ 76.94 \left(\frac{\rho}{\rho'_o}\right)^{1/2} \left\{ [33.3 - 0.0333\ (h_w - 100)] \left(\frac{V}{V_s}\right) + 449.55 \left(\frac{V}{V_s}\right)^3 \right\} \tag{10}$$

where:

a = 1 for stagnation condition, i.e., the sphere is nonrotational

a = 0.1375 for rotating sphere (Reference 4)

4.4.5.3 Internal Heat Source

Internal heat generated by the fuel capsule is $Q_i = 2.7$ watt/cm^3; this is an equivalent of:

$$Q_i = 0.892 \text{ BTU/ft}^2\text{sec} \tag{11}$$

4.4.5.4 Gas Radiation Heating

Reference 5 presents an approximate equation for radiation heating under an equilibrium condition:

$$Q_{GR} = A R_N \left(\frac{\rho}{\rho_o}\right)^{1.78} \left(\frac{V}{10^4}\right)^B \text{ BTU/ft}^2\text{sec} \tag{12}$$

where:

A = 0	B = 0	V < 25,000
A = 6.8	B = 12.5	25,000 < V < 30,000
A = 0.003	B = 19.5	30,000 < V < 35,000
A = 20.4	B = 12.5	35,000 < V

Furthermore, it is assumed that the standard atmosphere density variation can be approximately obtained by:

$$\left(\frac{\rho}{\rho_o}\right) = e^{-h/23,500} \tag{13}$$

Substituting equations (6), (10), (11), (12) and (13) into equation (5) we obtain the heat balance equation. This equation is a function of three parameters, namely: velocity, V, surface temperature, T_W and altitude, h.

Solution of equation (5) is presented for a nonrotating sphere ($a = 1$) in Figure 4-43. In this set of calculations internal heat generation and gas radiation heating are neglected. Figure 4-44 shows calculations for a rotating sphere ($a = 0.1375$), with internal heat source and gas radiation heating included.

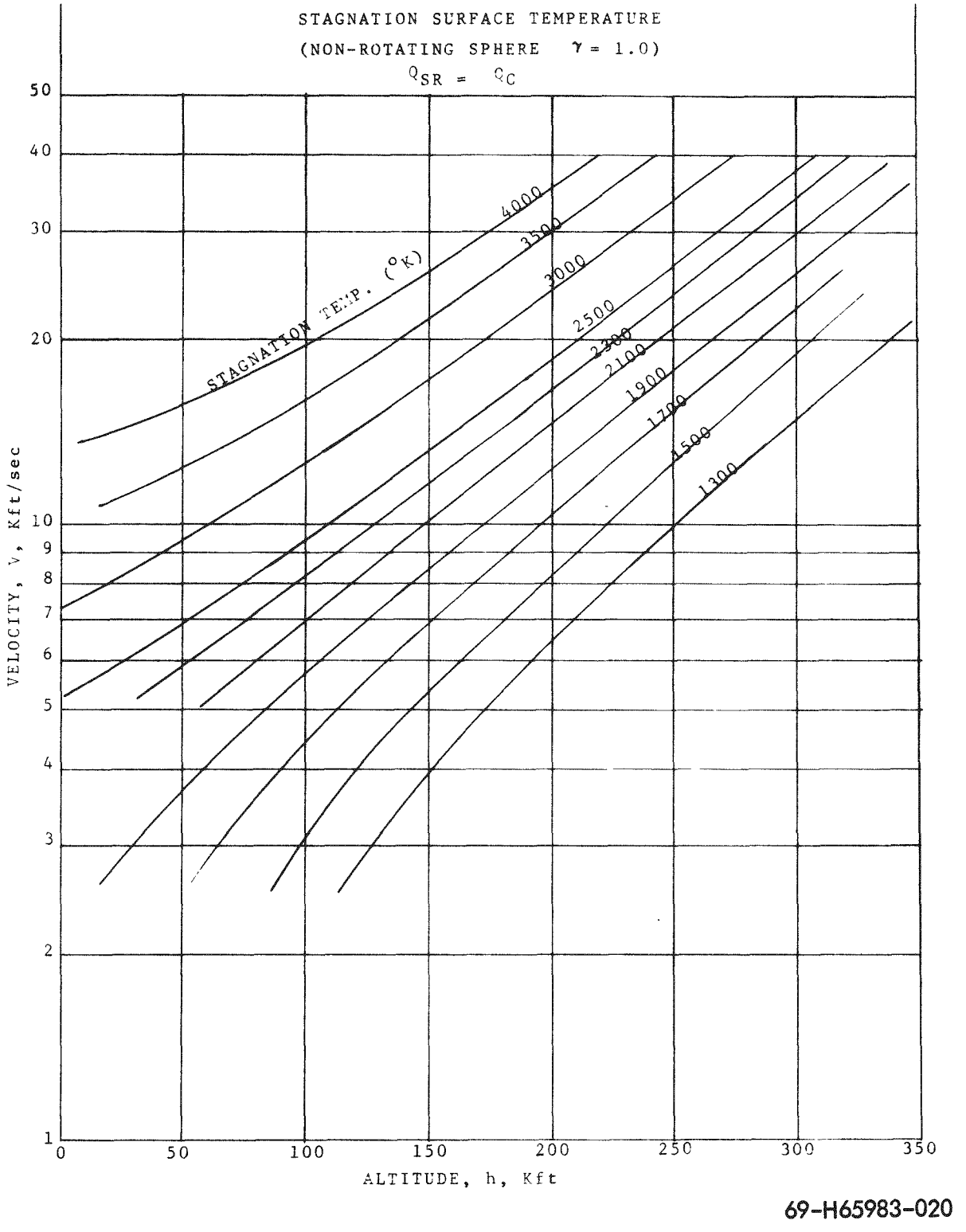

Figure 4-43 Velocity vs. Altitude as a Function of Stagnation Surface Temperature (Non-rotating Sphere).

SANDERS NUCLEAR CORPORATION

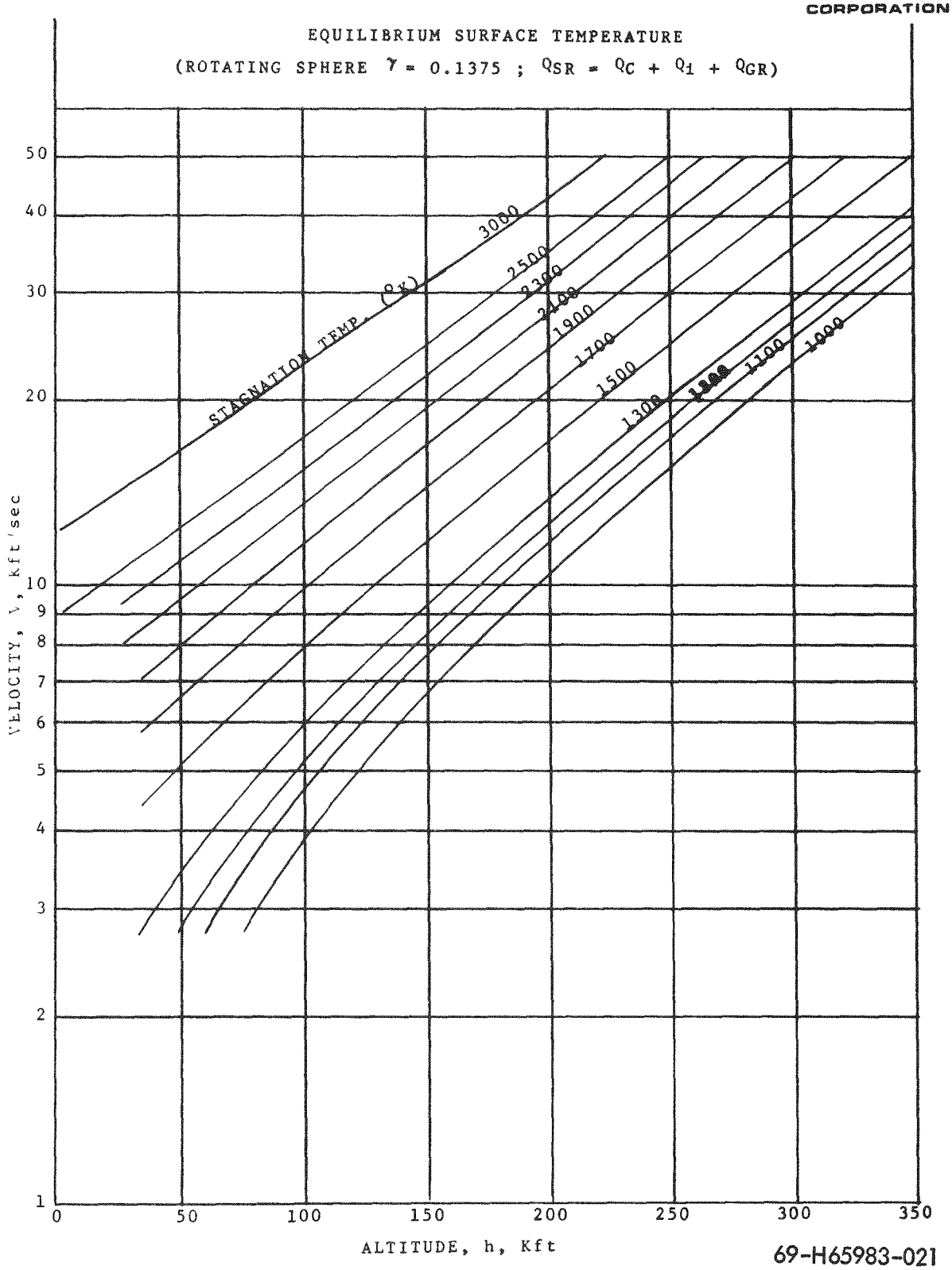

Figure 4-44 Velocity vs. Altitude as a Function of Stagnation Surface Temperature (Rotating Sphere).

4.4.6 MASS LOSS RESULTING FROM ABLATION

A superposition of the reentry trajectory (Figures 4-40 through 4-42) over the isotherms (Figures 4-43 or 4-44) will yield the temperature profile during the reentry. Figures 4-45 through 4-50 show the temperature variation along the trajectory of a rotating sphere as a function of the time elapsed. Time is measured from the initiation of reentry: t = 0 is at an altitude h = 300,000 feet for the V_E = 26,000 ft/sec case, approximately at the altitude where continuum theory is applicable; and h = 400,000 feet for V_E = 36,000 and 45,000 ft/sec cases. The free molecule-continuum boundary is marked on Figures 4-49 and 4-50.

Based on analysis in References 2 and 3, the mass loss rate due to graphite oxidation is:

$$\frac{dm}{dt} = \frac{\beta}{\sqrt{(2116)}} \frac{F(T_W)\sqrt{P}}{\sqrt{R_N}} \left(\frac{lb}{ft^2 sec} \right) \tag{14}$$

where:

m = ablated mass, lb/ft^2

β = proportional constant due to rotation = 1/4

p = air pressure, atmospheres

$$F(T_W) = \frac{(0.21)^{1/2} k_o e^{-E/RT_W}}{\left\{ \left(\frac{1}{R_N} \right) + 0.21 \left[\left(\frac{k_o}{C} \right) e^{-E/RT_W} \right]^2 \right\}^{1/2}} \tag{15}$$

where:

k_o = effective collision frequence = 9.65×10^5 $lb/ft^2 sec\ atm^{1/2}$

E = activation energy = 44,000 cal/mole

R = gas constant = 1.987 cal/mole ^oK

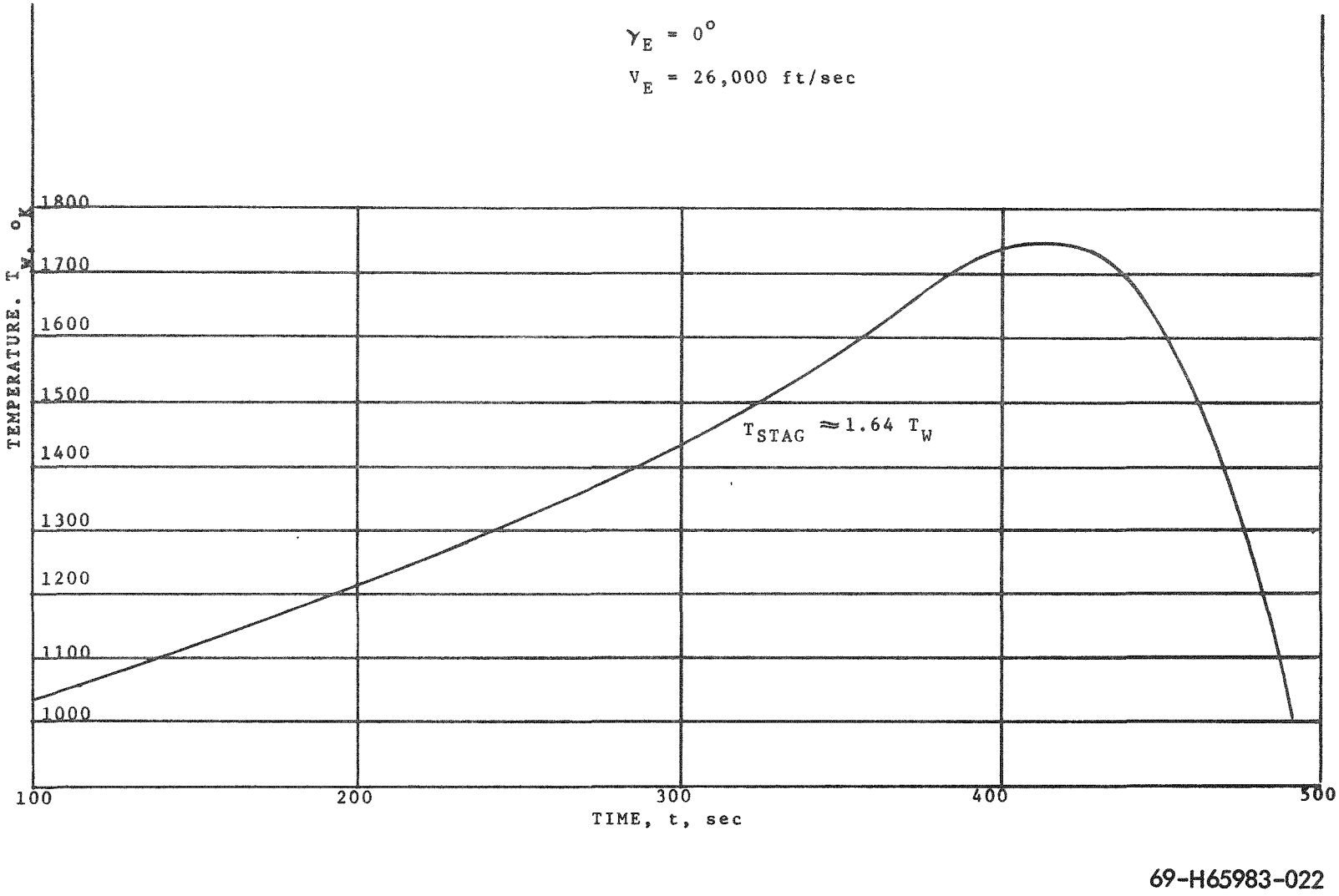

Figure 4-45 Surface Temperature of Spinning SIREN Heat Source ($\gamma_E = 0^\circ$, V_E = 26,000 ft/sec).

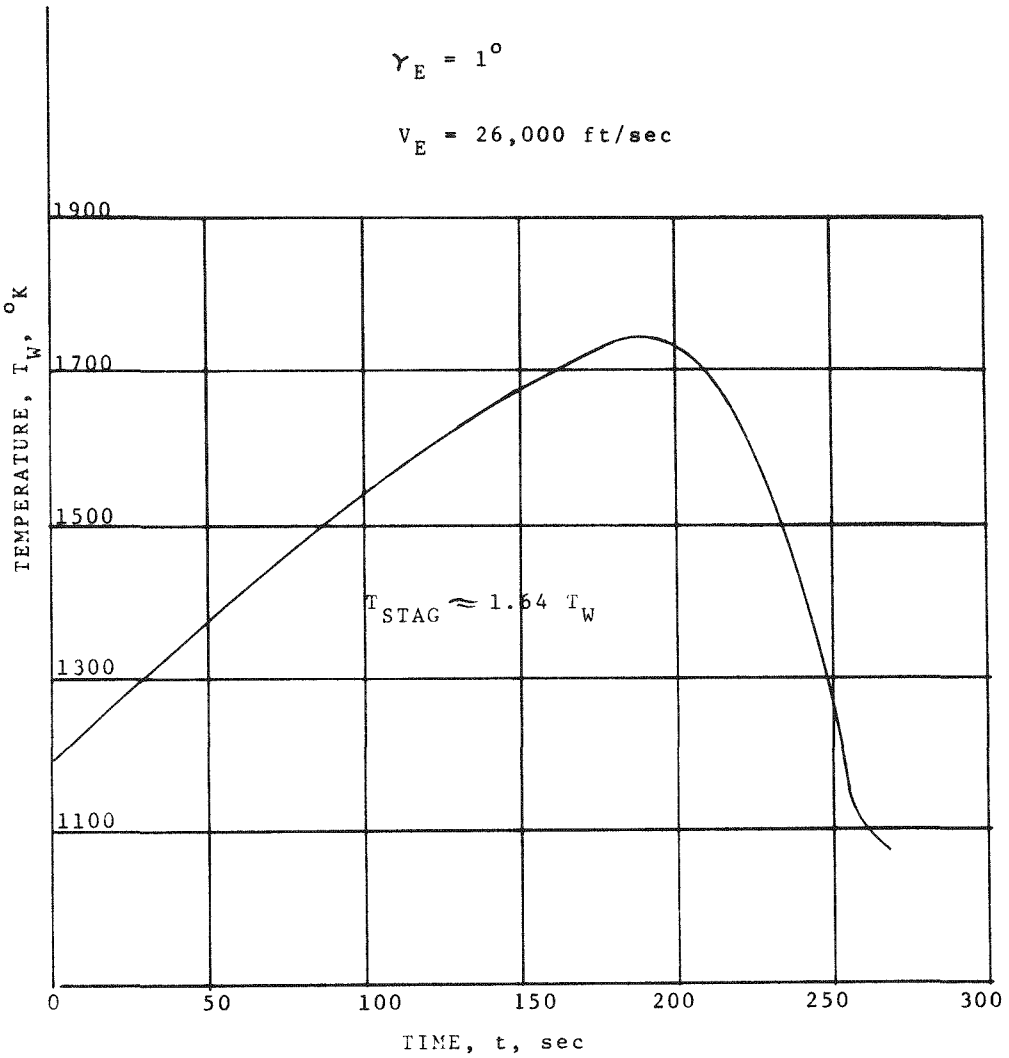

69-H65983-023

Figure 4-46 Surface Temperature of Spinning SIREN Heat Source ($\gamma_E = 1^o$, $V_E = 26{,}000$ ft/sec).

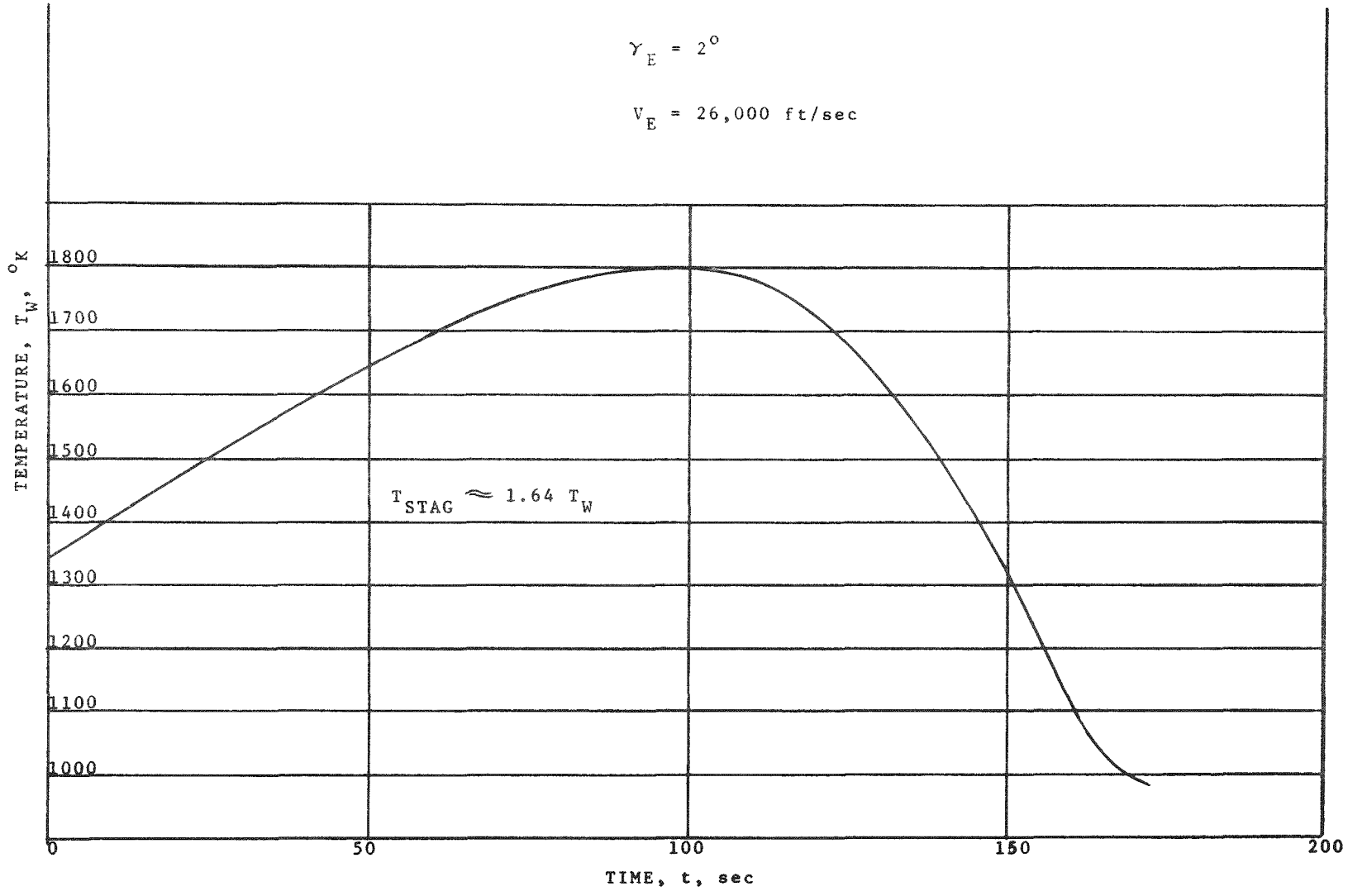

Figure 4-47 Surface Temperature of Spinning SIREN Heat Source ($\gamma_E = 2^o$, $V_E = 26{,}000$ ft/sec).

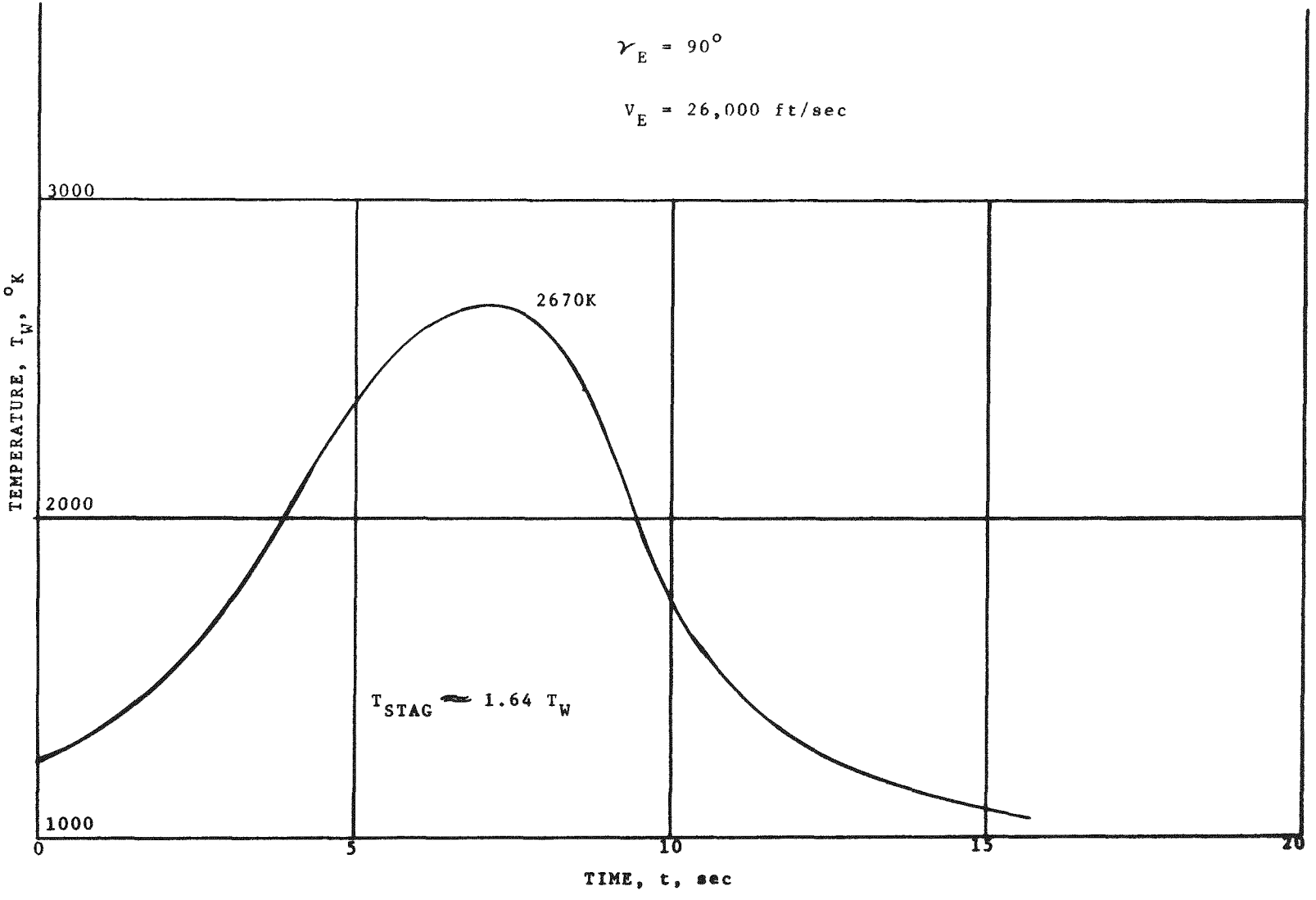

Figure 4-48 Surface Temperature of Spinning SIREN Heat Source ($\gamma_E = 90^\circ$, $V_E = 26{,}000$ ft/sec).

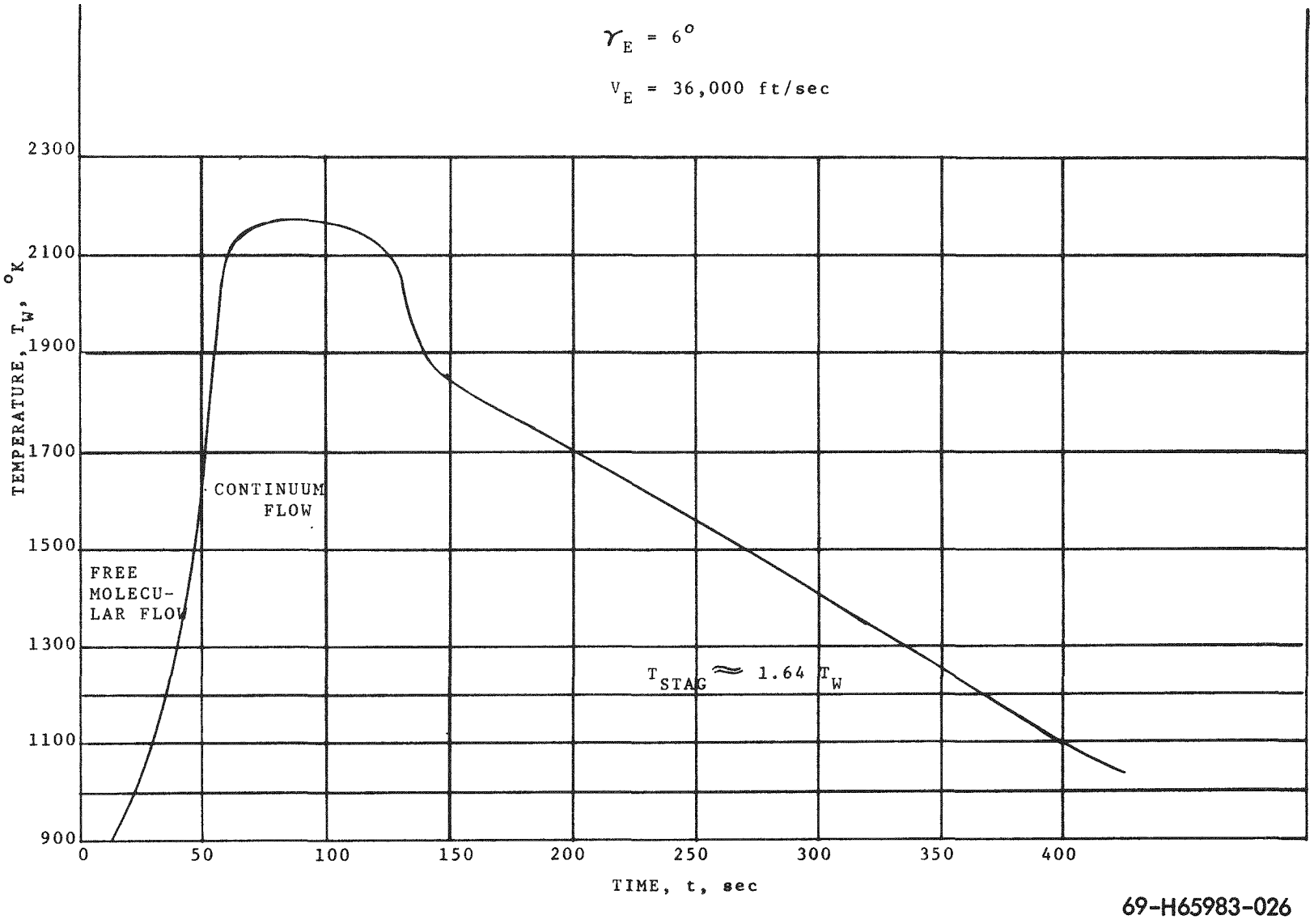

Figure 4-49 Surface Temperature of Spinning SIREN Heat Source ($\gamma_E = 6^o$, $V_E = 36{,}000$ ft/sec).

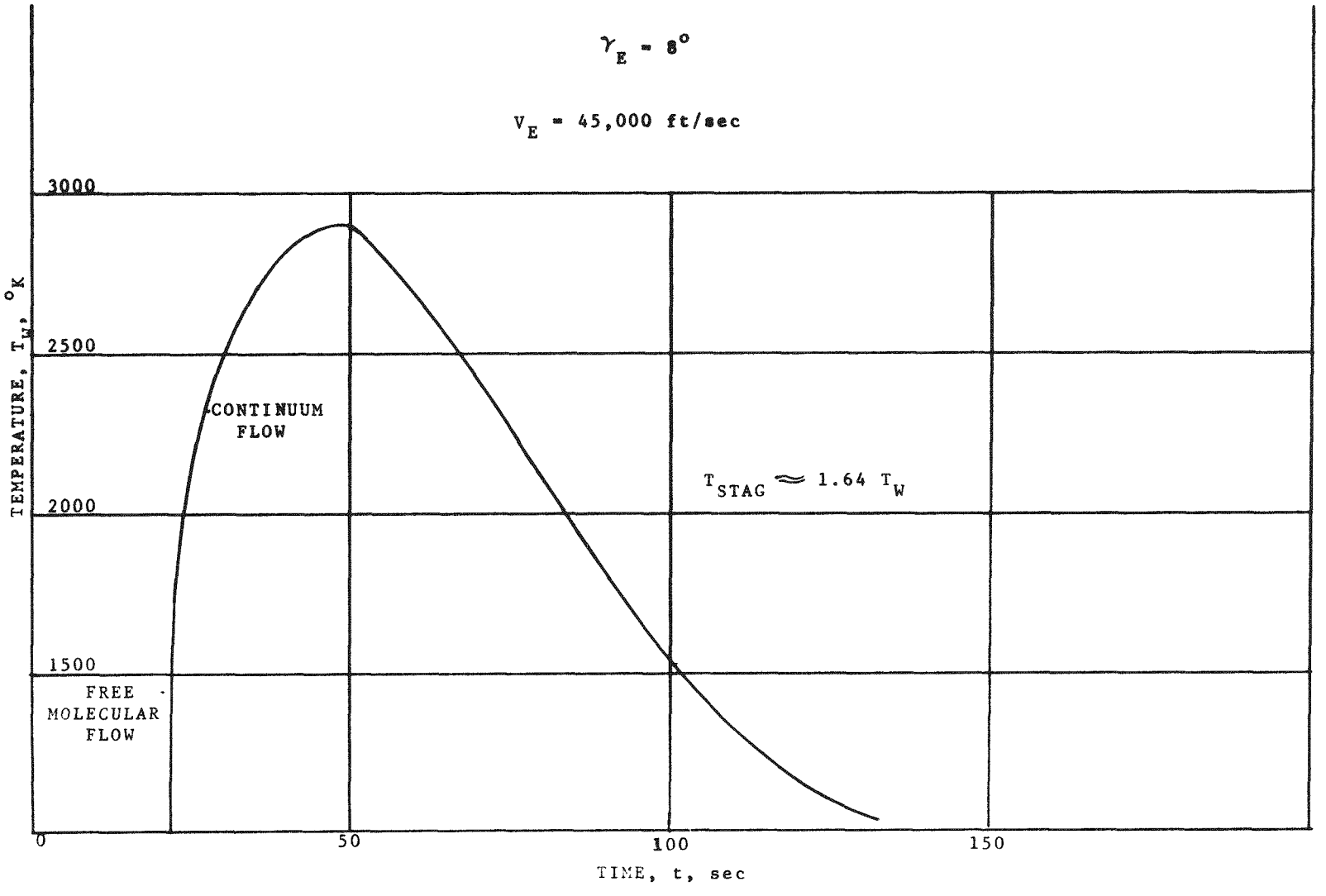

Figure 4-50 Surface Temperature of Spinning SIREN Heat Source ($\gamma_E = 8°$, $V_E = 45{,}000$ ft/sec).

C = Diffusion controlled mass transfer constant

$= 6.35 \times 10^{-3}$ lb/sec $ft^{3/2}$ $atm^{1/2}$

Equation (15) is plotted in Figure 4-51 as a function of wall temperature T_W. Since the temperature pulse is known, $F(T_W)$ can be obtained as a function of time, and ultimately $F(T_W)P^{1/2}$ as a function of time.

4.4.7 TERMINAL VELOCITY

Estimates of the terminal or impact velocity of the SIREN capsule at sea level vary widely with various assumptions about the drag coefficient. Unfortunately, the capsule flies through the Reynolds number range in which the flow changes from subcritical to supercritical and the drag coefficient may change from $C_D \approx 0.5$ to $C_D \approx 0.1$. The actual magnitude of the change in C_D and the Reynolds number at which it occurs depends on the surface roughness.

It is worth noting, as in Reference 9, that the terminal velocity of a falling body tends to be somewhat higher than the equilibrium velocity for which the weight equals the drag. However, in our case the difference is at most 5% and will be neglected in view of the other, larger, uncertainties for the sake of a simpler computation.

Drag data on spheres in subsonic flight have been summarized by Hoerner[10] and are shown in Figure 4-52 for both smooth and rough spheres. The roughness investigated in these tests was granular (e.g., sandpaper) and in the roughness parameter k/D, k is the grain size.

The behavior of the drag curve is seen to depend critically on the degree of roughness. For k/D = 0.003 (k = 0.009 inch on the 3-inch sphere), transition to supercritical flow occurs sooner than on the smooth sphere and the supercritical drag coefficient may be a little higher. For k/D = 0.03 (k = 0.09 inch on the 3-inch sphere) there is no transition and C_D remains high throughout. Intermediate values of k/D will presumably produce intermediate behavior.

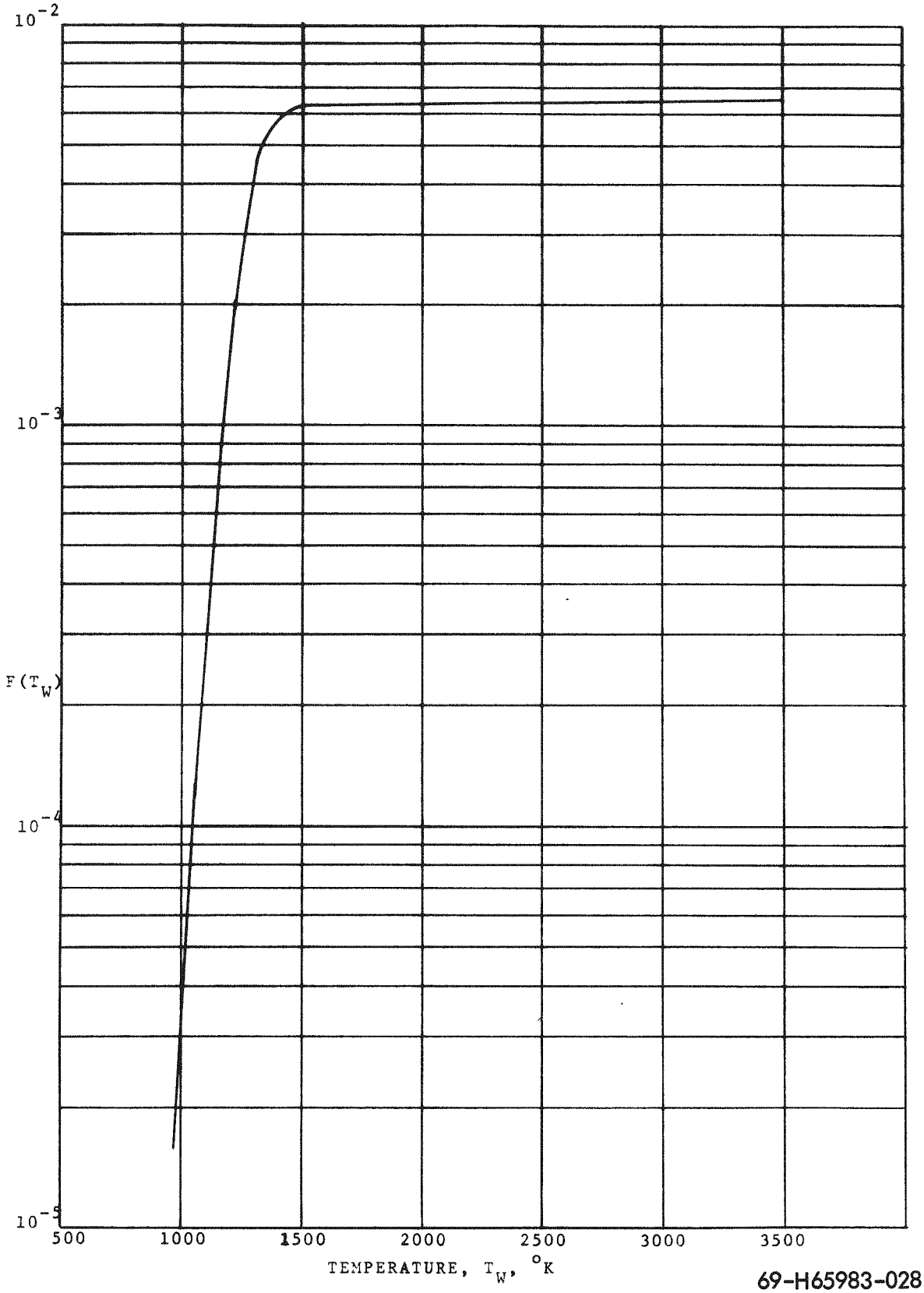

Figure 4-51 Temperature Dependent Oxidation Parameter.

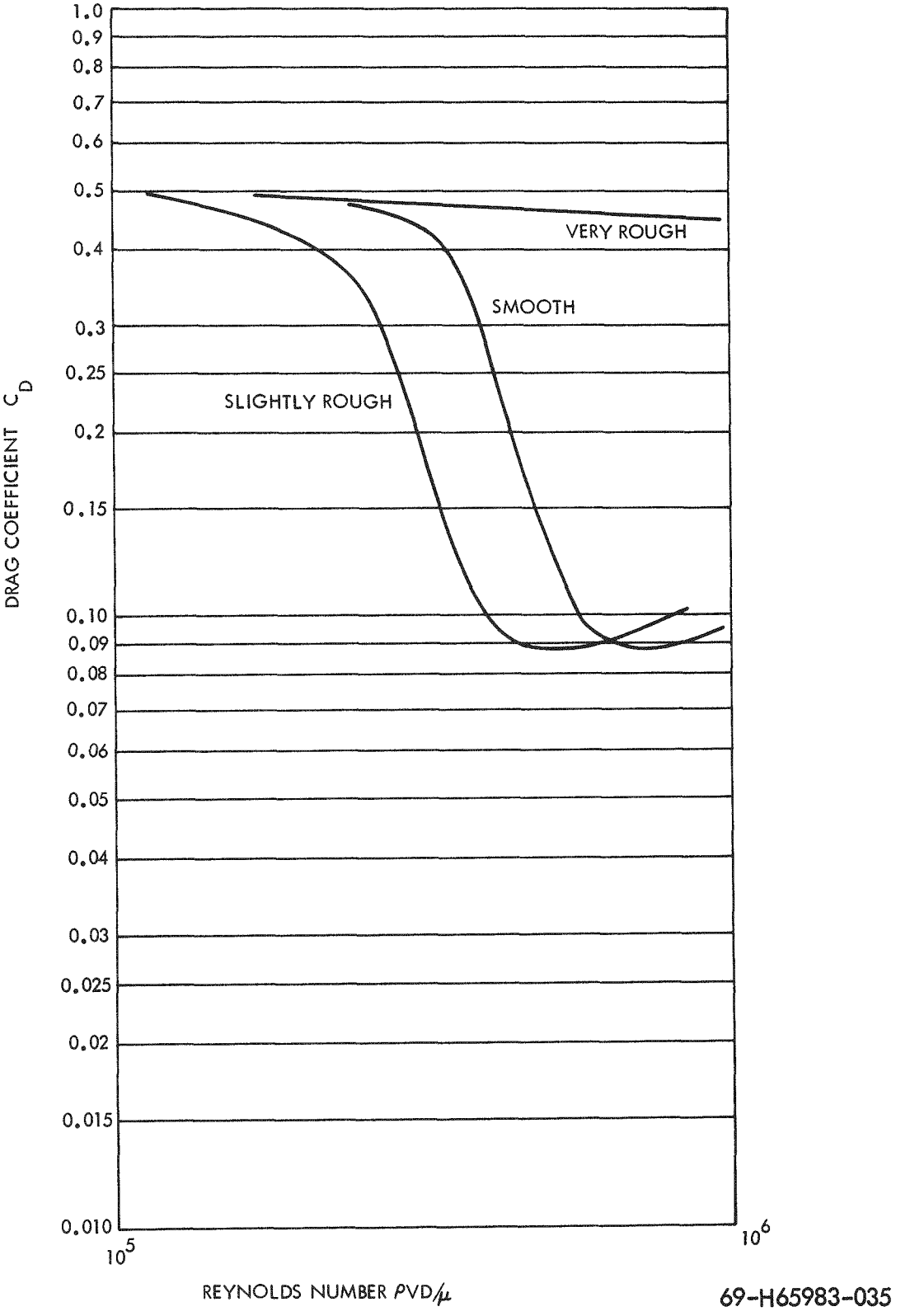

Figure 4-52 Drag Data on Spheres in Subsonic Flight.

Equilibrium velocities at any altitude may be computed from the formula:

$$V_{EQ} = 29(W/\sigma C_D A)^{1/2} \quad (16)$$

where:

σ is the density ratio ρ/ρ_{SL}

Values are shown in Figure 4-53 for the representative subcritical and supercritical drag coefficients.

$$C_{D_1} \approx 0.47$$

$$C_{D_2} \approx 0.10$$

using the parameters of the current capsule design;

d = 3 inches

W = 1.635 lbs

Also shown is the Reynolds number regime:

$$3.5 \times 10^5 < Re < 5.5 \times 10^5$$

in which the transition from subcritical flow occurs on a smooth sphere.

Using these data, probable velocity-altitude histories of smooth, slightly rough, and very rough capsules have been sketched. Actual trajectories could of course be obtained by integration of the equations of motion for any assumed variation of C_D with Re. Checks were made, on the basis of the solutions given in Reference 9, to insure that the transition altitude (17,000 ft) is high enough for the capsule to accelerate to the new equilibrium speed.

4.4.8 RESULTS

Time-temperature plots of the SIREN outer surface during reentry are given in Figures 4-45 through 4-50. In arriving at these equilibrium temperatures it was

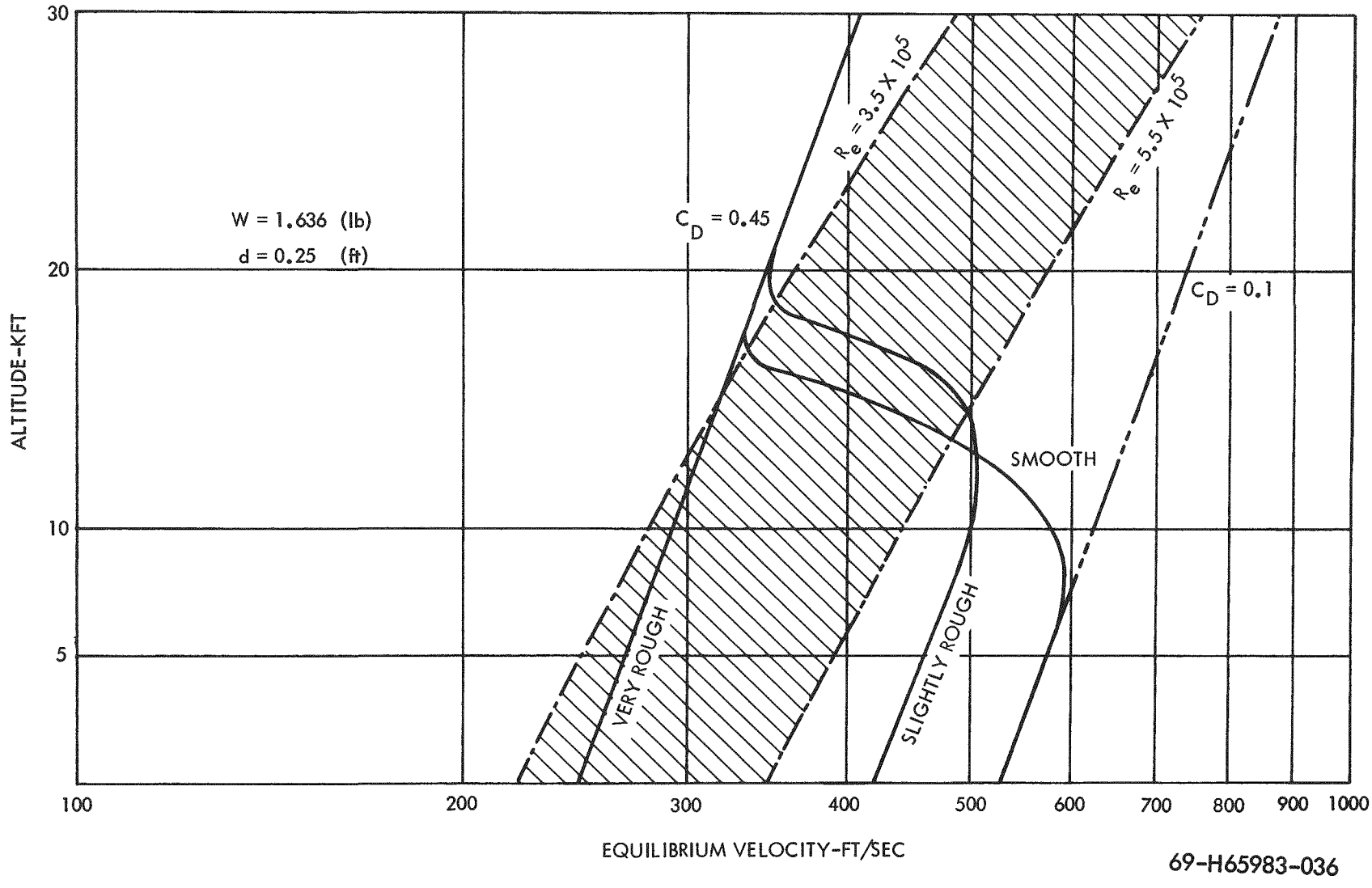

Figure 4-53 Equilibrium Velocities.

assumed that $T_W(A)$ of equation (6) was constant over the entire surface of the capsule. This assumption is indicative of a spinning reentry.

Radiative heat transfer, Q_{GR}, and internal heat generation, Q_i, had only a secondary influence on the equilibrium surface temperature. For instance, the maximum stagnation point temperature for the 45,000 ft/sec, 8° reentry when accounting for Q_i and Q_{GR} in equation (5) is 4650°K whereas it is 4500°K without consideration of these two factors. It is therefore possible to use Figures 4-45 through 4-50 to obtain stagnation point temperature by using the relationship:

$$T_{STAG} \approx \left(\frac{1}{0.1375}\right)^{0.25} T_W \qquad (17)$$

which is arrived at by substituting equation (10) into equation (6) for Q_{SR}.

The reentry thermal analysis assumes that the capsule has no thermal capacity and therefore represents a thermal balance of heat flux at the capsule outer surface. The condition of thermal flux balance established the initial reentry surface temperature.

Maximum spinning-capsule surface temperature for the reentry conditions under investigation was 2900°K and occurred with the superorbital condition of 45,000 ft/sec at minimum reentry angle of 8° (Figure 4-50). The maximum stagnation point wall temperature for this reentry condition was 4750°K.

Figures 4-54 through 4-59 give the mass loss rate was a function of time for the reentering SIREN capsule in a spinning mode. Mass loss rate is then integrated over the reentry interval to yield total ablated mass per unit area:

$$m = \int_o^t \frac{dm}{dt}\, dt = \int_o^t \beta \frac{F(T_W)}{\sqrt{R_N}} P_e^{1/2}\, dt \qquad (18)$$

and the recession:

$$(\Delta r) = 12000 \frac{m}{\rho_g} \text{ (mils)}$$

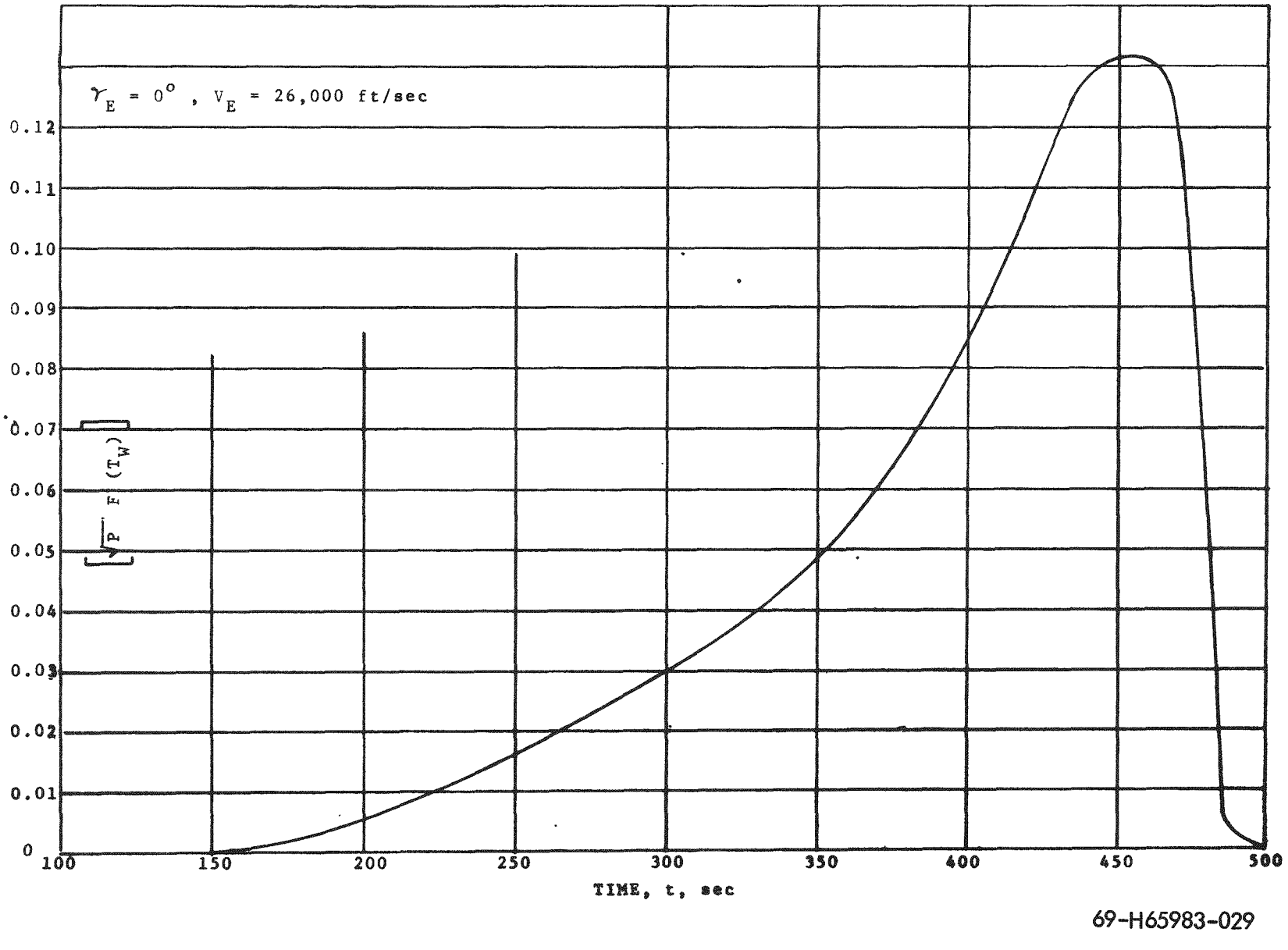

Figure 4-54 Maximum Loss Rate for Spinning SIREN Capsule ($\gamma_E = 0^\circ$, V_E = 26,000 ft/sec).

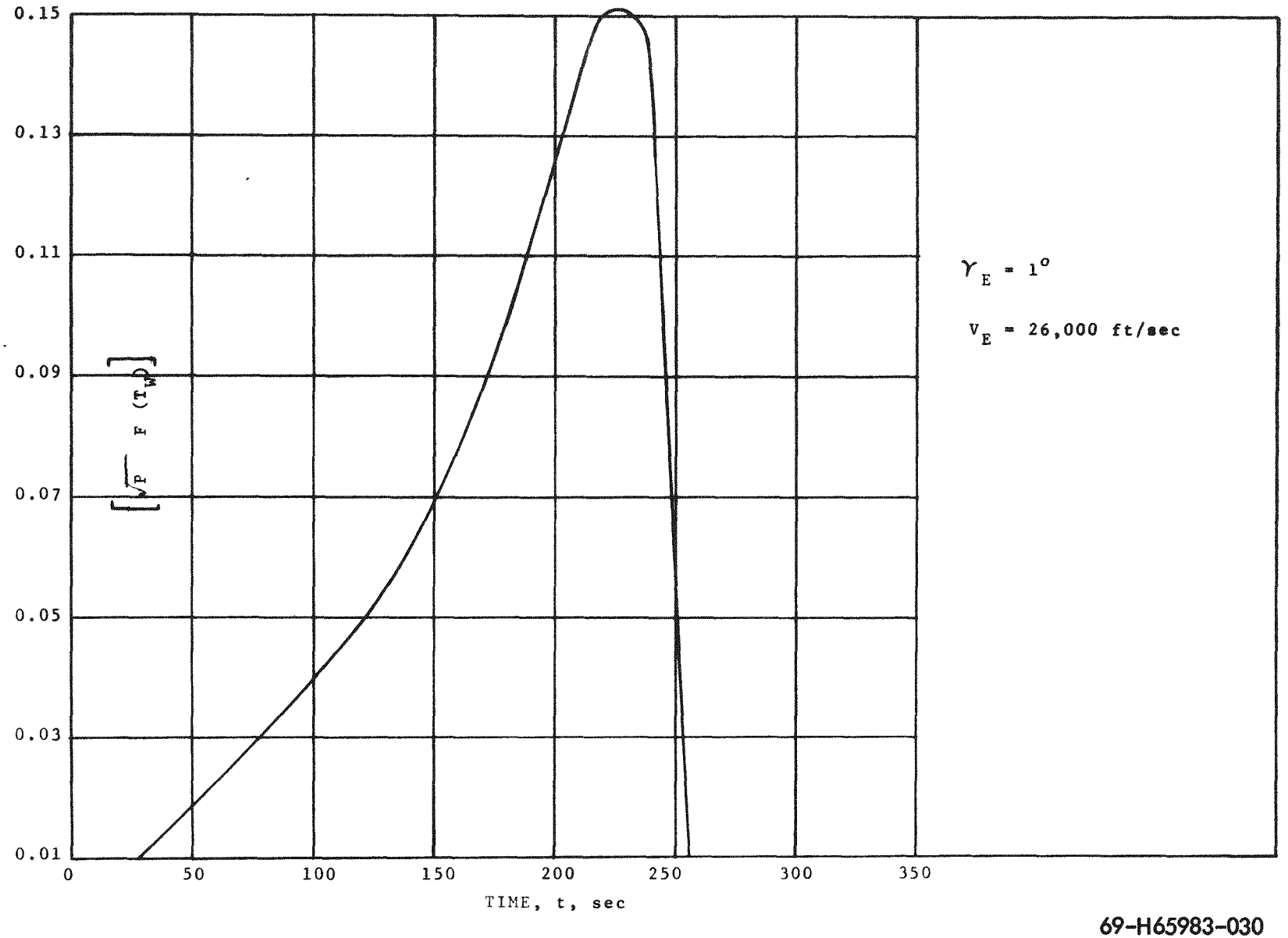

Figure 4-55 Maximum Loss Rate for Spinning SIREN Capsule ($\gamma_E = 1^o$, $V_E = 26{,}000$ ft/sec.

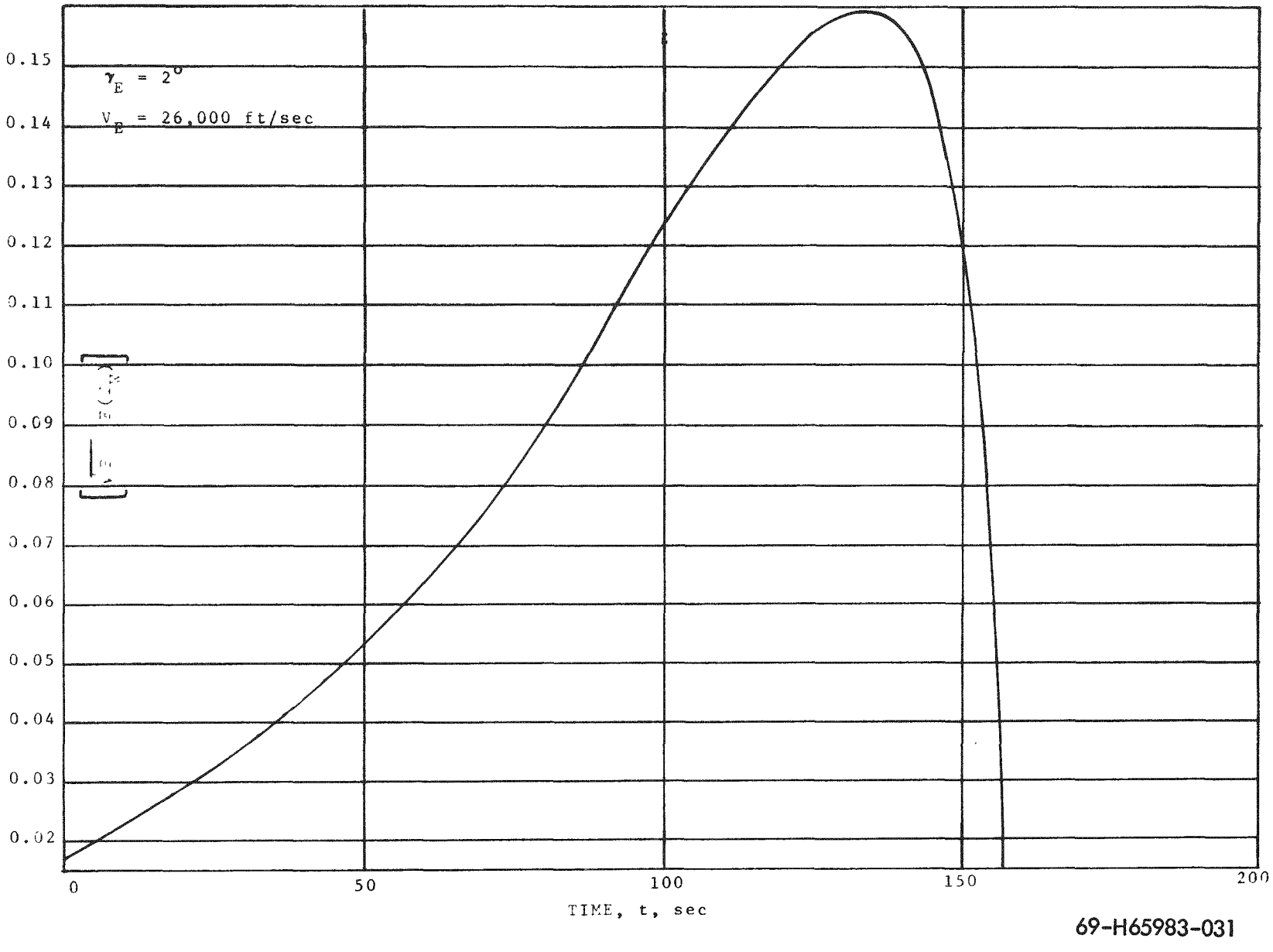

Figure 4-56 Maximum Loss Rate for Spinning SIREN Capsule (γ_E = 2°, V_E = 26,000 ft/sec).

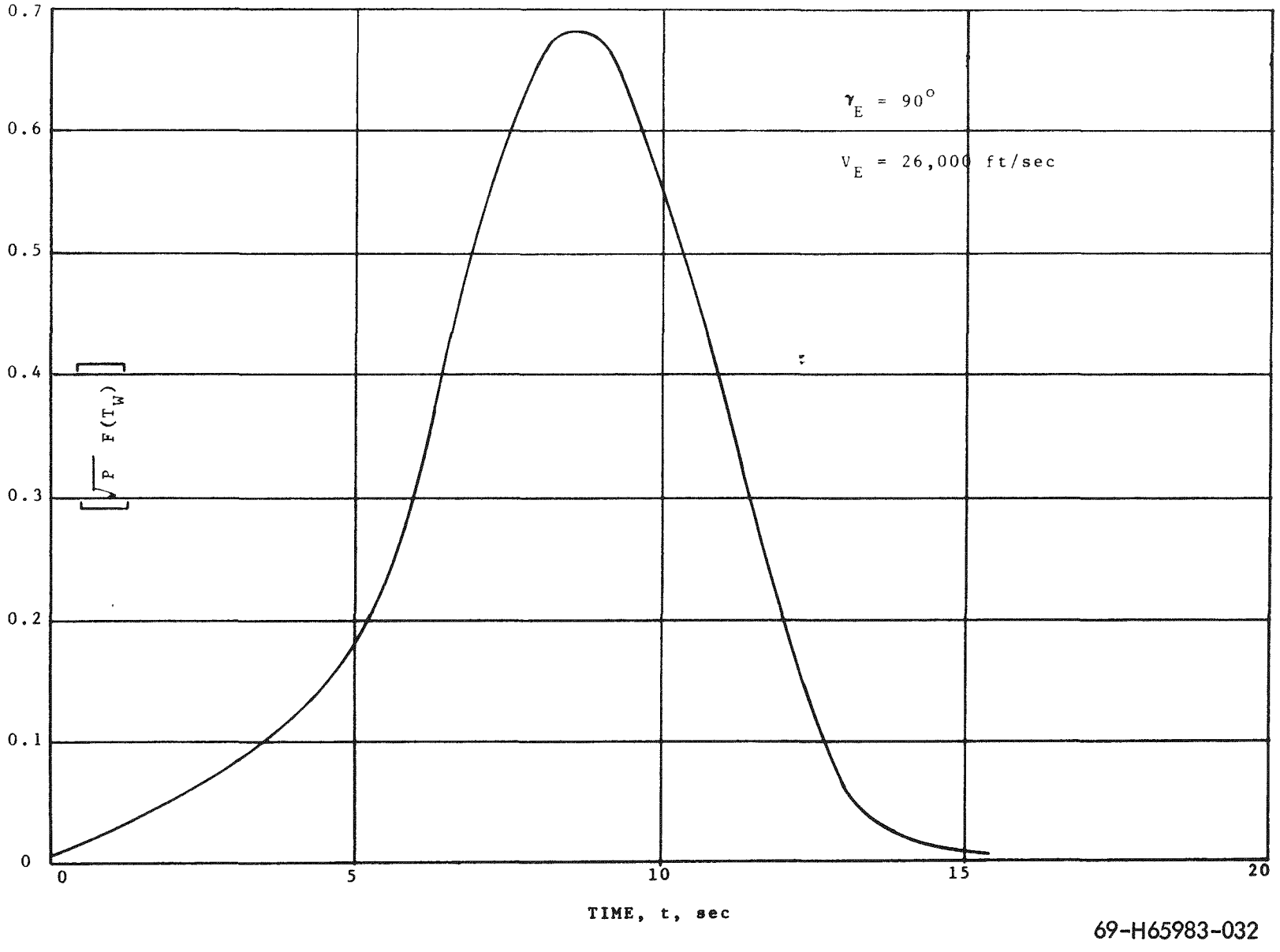

Figure 4-57 Maximum Loss Rate for Spinning SIREN Capsule ($\gamma_E = 90^o$, $V_E = 26{,}000$ ft/sec).

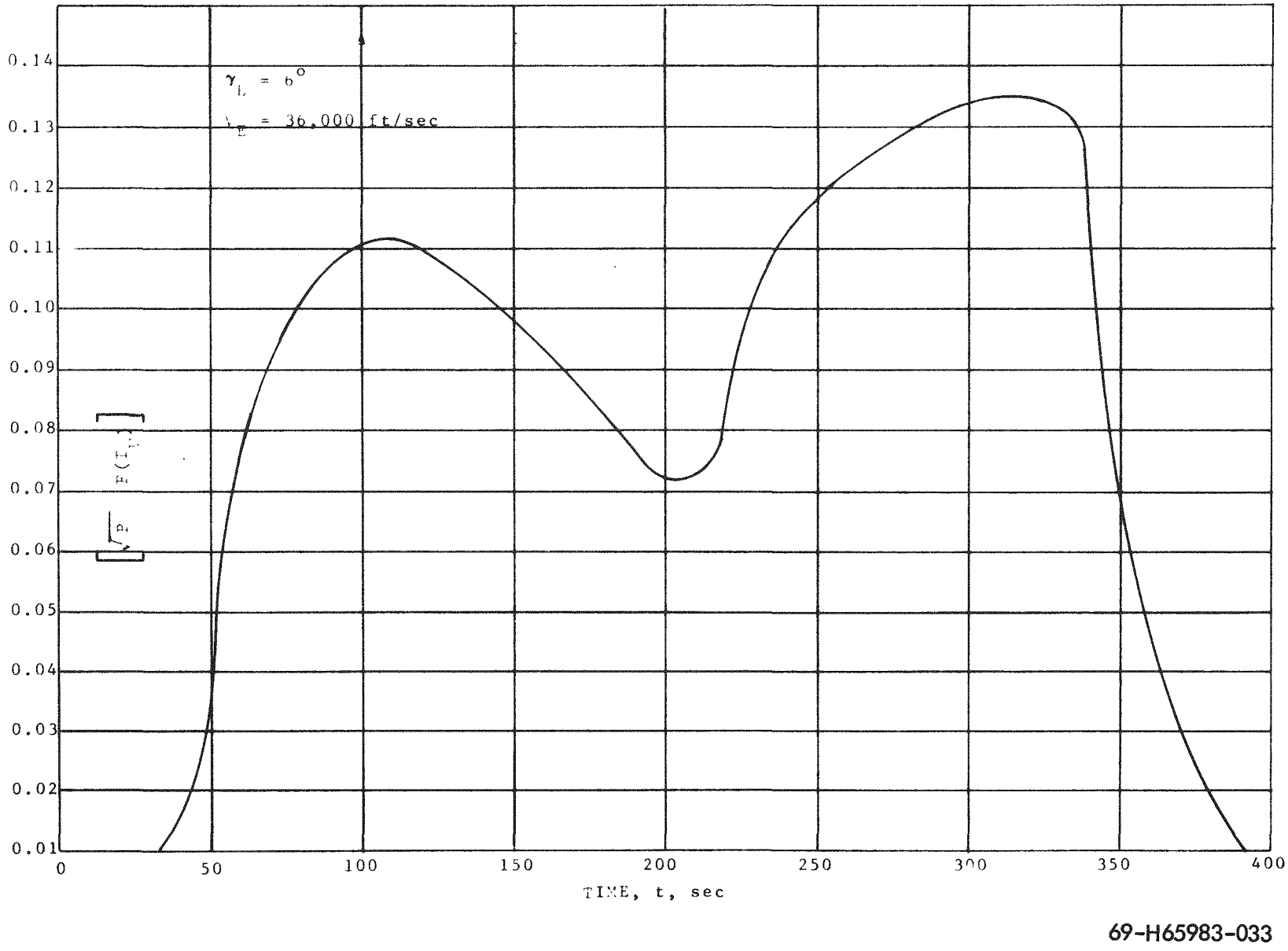

Figure 4-58 Maximum Loss Rate for Spinning SIREN Capsule ($\gamma_E = 6^o$, V_E = 36,000 ft/sec).

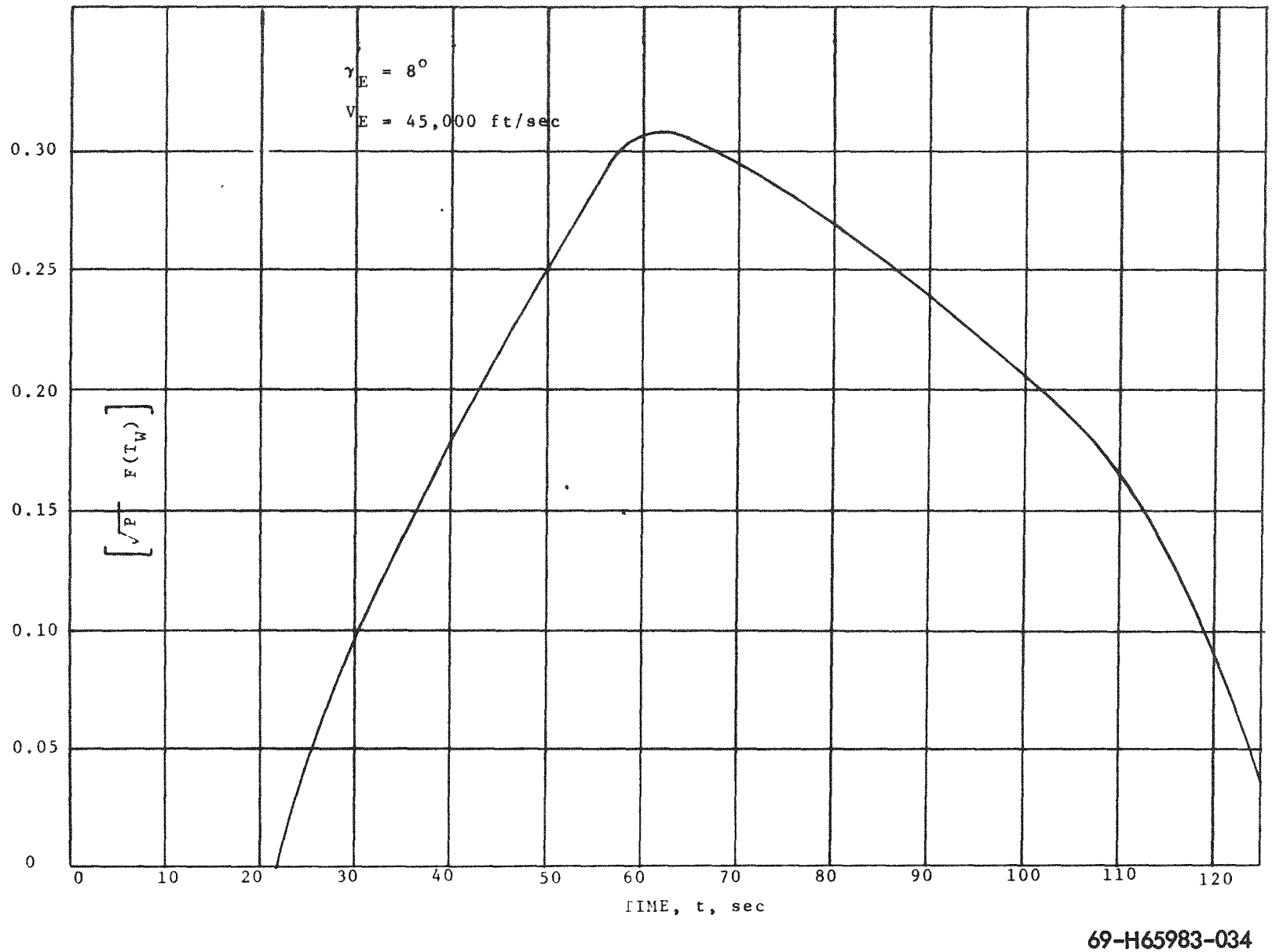

Figure 4-59 Maximum Loss Rate for Spinning SIREN Capsule ($\gamma_E = 8^o$, $V_E = 45{,}000$ ft/sec).

Results are tabulated in Table 4-49. These results are for a spinning capsule. The mass loss rate, total mass loss, and surface recession for the stagnation point of a non-rotating reentry capsule would be increased by a factor of four over that for the spinning capsule.

TABLE 4-49

MASS LOSS FOR SPINNING CAPSULE REENTRY

γ_E (deg)	V_E (ft/sec)	$m = 0.0154 \int_o^{t\,max} F(T_W)\, P_e^{1/2}\, dt$	$(\Delta r) = 12000\ m/\rho_g$ (mils)
0	26000	0.29806 lb/ft^2	35.767
1	26000	0.23672	28.4
2	26000	0.212730	25.52
90	26000	0.05925	7.11
8	45000	0.51516	61.82
6	36000	0.508524	61.

Figure 4-53 indicates that for the SIREN capsule under investigation a terminal velocity anywhere from 245 to 530 ft/sec could be expected, depending upon its relative surface roughness after reentry. Spinning and tumbling motion (resulting from stagnation point ablation) may also affect the drag.

4.4.9 CONCLUSIONS

SIREN capsule surface temperatures during normal orbital reentry conditions for a 3-inch diameter sphere attain radiation equilibrium surface temperature of 1750°K (3150°R) during spinning reentry and approximately 3190°K (5160°R) at the stagnation point during a non-rotating reentry. SIREN capsules reentering under

superorbital conditions of 45,000 ft/sec and 8° experience a spinning surface temperature of 2800°K (5000°R) and a non-rotating stagnation temperature of 4600°K (8200°R). The liner and fuel surface will, with the configuration shown in Figure 4-33, experience temperatures nearly as high as the heat shield. For the superorbital condition the temperature could cause deleterious effects on the integrity of the fuel. It may therefore be necessary to investigate the possible use of a reentry thermal barrier between the heat shield and the fuel liner. Preferably, the thermal barrier would allow sufficient conduction outwardly to allow safe operating temperature during mission life while offering sufficient thermal resistance in the inward direction to insure that the liner and fuel do not exceed degradation temperature levels during reentry. During orbital reentries a thermal barrier may also be required if a steep reentry angle is considered possible. For the shallow orbital reentries it may be possible to achieve reentry without a thermal barrier.

A thermal barrier to solve the superorbital temperature problem could possibly be achieved by simply not impregnating an inner layer of yarn adjacent to the liner. This unimpregnated layer of yarn could also serve as a liner cushion during impact.

For a spinning reentry heat shield surface recession of 61 mils leaves a graphite wall thickness of 439 mils at impact. After a non-rotating reentry the stagnation point wall thickness is 256 mils. Integrity of the fuel capsule after impact at the terminal velocities given in Figure 4-53 can be demonstrated only by impact testing.

This report provides only equilibrium surface temperatures with no consideration of fuel capsule thermal storage capacity and hence does not constitute a complete basis for evaluating the safety of the SIREN fuel capsule. The following topics must be investigated if a sound judgement is to be made:

a. Impact temperatures and optimum ballistic coefficients leading to minimum practical impact velocities, thus allowing impact stress analyses.

b. The effects of internally generated pressure during reentry.

c. Launch pad aborts.

d. Thermal and chemical analyses of a buried heat source.

e. Three-dimensional thermal analysis to allow determination of thermal gradients and thermal stresses.

f. Material degradation and incompatibility at elevated temperatures.

g. Determination of most severe reentry trajectories from the standpoint of maximum temperature and maximum integrated heat load.

h. Thermal barrier design.

4.4.10 REFERENCES

1. Stankevics, J. O. A., "Review of Report RIWA-TM-673/SN; Preliminary Design of a Graphite Spherical Fuel Capsule for Intact Reentry of Microsphere Fueled RIG's", MITHRAS Memo A-644, dated March 6, 1968.

2. Scala, Sinclaire M., and Gilbert, Leon M., "Sublimation of Graphite at Hypersonic Speeds", AIAA Journal, Vol. 3, No. 9, pp 1635 - 1644, September 1965.

3. Metzger, J. W., Engle, M. I., and Diaconis, N. S., "Experimental Evaluation of the Oxidation and Sublimation of Graphite in Simulated Reentry Environments", AIAA Journal, Vol. 5, No. 3, pp 451 - 459, March 1967.

4. Cropp, L. O., "Analytical Methods Used in Predicting the Reentry Ablation of Spherical and Cylindrical Bodies", Sandia Corporation, SC-RR-65-187, 1965.

5. Lovelace, Uriel M., "Charts Depicting Kinematic and Heating Parameters for a Ballistic Reentry at Speeds of 26,000 to 45,000 Ft per Second", NASA TN D-968, October 1961.

6. Allen, H. Julian, and Eggers, A.F., Jr., "A Study of the Motion and Aerodynamic Heating of Missiles Entering the Earth's Atmosphere at High Supersonic Speeds", NACA TN 4047, 1957.

7. Chapman, Dean R., "An Approximate Analytical Method for Studying Entry into Planetary Atmospheres", NASA TR R-11, 1959.

8. Schmidt, J.F.," Laminar Skin-Friction and Heat-Transfer Parameters for a Flat Plate at Hypersonic Speeds in Terms of Free-Stream Flow Properties", NASA TND-8, September 1959.

9. Approximate Theory for Terminal Velocity of a Freely Falling Body. G.D. Stilley, J. of Spacecraft and Rockets, Vol. 4, No. 9, September 1967.

10. Fluid Dynamic Drag, by S.F. Hoerner, 1965.

4.5 POST-IMPACT ANALYSIS

4.5.1 INTRODUCTION

Intact reentry of a heat source capsule and its impact survival defers the final question of capsule integrity to the post-impact period. During this period, where damage by external physical means (rock slides, sand storms, etc.) is assumed negligible, degradation of the heat source containment is the result of thermochemical activity.

Survival of an earth impact can result in a condition where the source is either buried in the ground or is resting on the ground and exposed to the elements. In either case, the environment is significantly different in a number of respects than when the source was deployed in space.

Foremost among the changes is the presence of oxygen which could accelerate the decomposition of the capsule. Since thermal convection is now possible, a lower equilibrium temperature will be established; however, the temperature will increase with time as the surface area of the capsule diminishes through decomposition. In the case of a buried capsule, a host of reactions may take place between the capsule and the surrounding soil. These two situations are considered in detail in the following paragraphs.

4.5.2 CAPSULE ON GROUND SURFACE

The most significant factor influencing reaction of the capsule materials is the equilibrium that will be established under the new conditions. Two situations will be examined. The first assumes the capsule is complete and intact, having an outside diameter of three inches and a capsule thickness of one-half inch. The second assumes a source with a liner only, the result of either capsule parting on impact or its decomposition with time. Intermediate conditions can be assumed to yield intermediate results.

Heat transfer from the source takes place by radiation and convection and is governed by the following equation:

$$Q = (h_r + \bar{h}_c) A_s (T_s - T_a)$$

where

Q = total heat lost, BTU/hr

A_s = surface area, ft^2

T_s = surface temperature, ^oF

T_a = ambient temperature, ^oF

$\bar{h}_c$ = convection coefficient, BTU/hr ft^2 ^oF

h_r = equivalent radiation coefficient, BTU/hr ft^2 ^oF

The convection coefficient is determined as follows:

$$\bar{h}_c = 0.53 (GrPr)^{1/4} \frac{k}{R_s}$$

where

Gr = Grashof number
Pr = Prandtl number
k = conductivity of air

} evaluated at the film temperature

R_s = capsule radius

For the fully encapsulated source, the following conditions are assumed:

$T_s \approx 600^oF = 1060^oR$

$T_a \approx 70^oF = 530^oR$

$$\therefore \quad T_f \approx 335^{\circ}F \left(\text{film temperature} = \frac{T_a + T_s}{2} \right)$$

$$R_s = 1.5 \text{ inches} = 0.125 \text{ ft}$$

$$k = 0.0193 \text{ BTU/hr ft } ^{\circ}F$$

$$Pr = 0.71$$

$$Gr = 0.444 \times 10^6 \times \Delta T \times R_s^3$$

$$\therefore \quad Gr = 0.444 \times 10^6 \times 530 \times (0.125)^3 = 0.459 \times 10^6$$

$$\therefore \quad \bar{h}_c = \frac{0.53(0.459 \times 10^6 \times 0.71)^{1/4} (0.0193)}{0.125} = 1.96 \frac{\text{BTU}}{\text{hr ft}^2 \, ^{\circ}F}$$

The effective radiation coefficient is determined as follows:

$$h_r = \frac{\sigma \epsilon (T_s^4 - T_a^4)}{T_s - T_f}$$

where

σ = Stefan-Boltzman constant, $0.1714 \times 10^{-8} \frac{\text{BTU}}{\text{hr ft}^2 \, F^4}$

ϵ = emissivity, assumed value = 0.8

$$\therefore \quad h_r = \frac{(0.1714 \times 10^{-8}) (0.8) (1060^4 - 530^4)}{(600 - 335)}$$

$$h_r = 6.16 \text{ BTU/hr ft}^2 \, ^{\circ}F$$

Having these heat transfer coefficients, it is now possible to calculate the capsule surface temperature for a representative source at a power level of 240 watts(a nominal power level for a 3-inch diameter capsule).

$$T_s = \frac{Q}{(\bar{h}_c + h_r) A_s} + 70$$

$$T_s = \frac{(240 \times 3.415)}{(1.96 + 6.16)\, 4\pi (0.125)^2} + 70$$

$$\therefore \quad T_s = 515 + 70 = 585^{\circ}F$$

This temperature is in fair agreement with the value assumed ($T_s = 600^{\circ}F$) in establishing material properties; therefore, the assumed value is valid within the limits of the assumptions made for this analysis.

For the case of the heat source resting on the ground in its liner only, the method of analysis is similar but with a somewhat higher temperature due to a reduced heat transfer area.

Assume the following conditions:

$$T_s = 850^{\circ}F = 1310^{\circ}R$$

$$T_a = 70^{\circ}F = 530^{\circ}R$$

$$\therefore \quad T_f = 460^{\circ}F$$

$$R_s = 1'' = 0.083 \text{ ft}$$

$$k = 0.022 \text{ BTU/hr ft}^2 {}^{\circ}F$$

$$Pr = 0.686$$

$$Gr = 0.20 \times 10^6 \times 780 \times (0.083)^3 = 9.06 \times 10^4$$

$$\therefore \quad \bar{h}_c = \frac{0.53(9.06 \times 10^4 \times 0.686)^{1/4} (0.022)}{(0.083)} = 2.20 \text{ BTU/hr ft}^2 {}^{\circ}F$$

As before

$$h_r = \frac{(0.1714 \times 10^{-8})\,(0.8)\,(1310^4 - 530^4)}{(850 - 460)} = 10.12 \text{ BTU/hr ft}^2\,^\circ\text{F}$$

and

$$T_s = \frac{240 \times 3.415}{(2.20 + 10.12)\,4\pi(0.083)^2} + 70$$

$$\therefore \quad T_s = 767 + 70 = 837^\circ\text{F}$$

As another temperature of interest, the interface between the capsule and the liner for the case of an intact capsule should be examined.

The radial temperature rise is given by

$$\Delta T = \frac{(240 \times 3.415)\,(1.5 - 1.0)\,(12)}{4\pi\,2.0(1.5)\,(1.0)} = 132^\circ\text{F}$$

$$\Delta T = \frac{Q(r_o - r_i)}{4\pi k r_o r_i}$$

where

k = capsule conductivity 2.0 BTU/hr ft °F

and

r_i, r_o = graphite inner and outer radii

Therefore, for the intact capsule resting on the ground, the external surface and the capsule liner interface temperatures become 585°F and 717°F respectively at equilibrium.

In summary then, for a source resting on the ground, we have the following conditions of interest:

a. A pyrolytic graphite surface in air at 585°F to 837°F

b. A pyrolytic graphite liner interface at 717°F to 837°F

c. A liner surface in air at 837°F (may or may not be preceded by(b.)

Pyrolytic graphite in air exhibits negligible oxidation at temperatures below 1100°F so that condition (a) can be considered a safe containment situation. Similarly, the liner-graphite reaction to form zirconium carbide for (condition (b)) requires temperatures approaching 4000°F, again indicating negligible containment degradation. Finally, degradation of the liner (i.e., zirconia) in condition (c) requires temperatures above 4500°F, considerably in excess of expected levels. Zirconium-carbide, the aforementioned unlikely product of condition (b) has a threshold oxidation limit of 800°F so that if it were formed prior to condition (c) it would slowly oxidize the liner, ultimately releasing the fuel. Even during reentry, however, critical temperatures for carbide formation are not attained so that this last possibility is extremely remote.

In summary, then, a heat source resting on the ground after impact, whether in its graphite capsule or reduced to its liner, has been shown to exhibit long term stability and is safely contained.

4.5.3 CAPSULE BELOW GROUND SURFACE

A capsule buried in the earth, either upon impact or by post-impact soil shifting, is subject to a different mode of degradation. As a result of temperature increases due to the insulation properties of the earth, corrosion and chemical attack are enhanced by the presence of water vapor, decomposition of soil chemicals, and alteration with time of the local soil envelope.

To estimate the level of chemical reactivity, it is again necessary to estimate the equilibrium temperature of an imbedded capsule under various hypothetical circumstances.

Consider the following possible conditions:

a. A capsule completely surrounded by soil, having good contact and an effective thickness that is large compared to capsule dimensions.

b. A capsule somewhat settled in a cavity and making contact on only half of its surface.

c. A capsule in an enlarged cavity (perhaps due to soil shrinkage) and having only point contact with it.

The above situations might represent gradually changing conditions and can be seen to involve heat transfer by conduction at the outset giving way to convection and radiation in the later stages. Since the time span is not known and indeed may be short compared to the half-life of the source, the heat source is assumed to have its initial value for all of the foregoing analyses.

Condition (a).

The governing relation for a sphere conducting heat to a surrounding material is

$$Q = \frac{4\pi k r_s r_o (T_s - T_o)}{r_o - r_s}$$

where r_o, r_s are the outer and inner radii of the enveloping material. It can be seen that as r_o becomes large compared to r_s, this equation reduces to

$$Q = 4\pi k r_s (T_s - T_o)$$

Thus, since r_s is the source radius and T_o is the soil temperature at a distance from the source, we get

$$T_s = \frac{Q}{4\pi k r_s} + T_o$$

Unfortunately, there exists a broad spectrum of soil compositions and soil conductivities. Furthermore, the value of thermal conductivity tends to increase with temperature but in a different fashion from soil to soil. It will be necessary, then, to make some assumptions about this soil property. Since values between 0.15 and 0.4 BTU/hr ft °F have been reported for various soils and is reasonably constant below 1500°F for most soils, an average of 0.25 is assumed.

Thus,

$$k = 0.25 \text{ BTU/hr ft } ^\circ\text{F}$$

$$r_s = 1.5'' = 0.125 \text{ ft}$$

$$T_o = 50^\circ\text{F}$$

$$T_s = \frac{242(3.415)}{4\pi(0.25)\,(0.125)} + 50$$

$$\therefore \quad T_s = 2100 + 50 = 2150^\circ\text{F}$$

This temperature invalidates the initial assumptions and indicates a more rigorous technique would be required to determine the capsule surface temperature. Such a technique would necessitate a more detailed knowledge of the thermal conductivity as it varies with temperature as well as the selection of an "average soil" upon which to make the determination. Since pure conduction is the basis of the other two conditions, however, it will be assumed that equilibrium exists for some average case at around 1800°F.

Condition (c)

This condition of only minor point contact between the capsule and the cavity is considered at this time because it will simplify the later handling of condition (b). It must be understood that if the cavity is not significantly larger than the capsule then the heat lost by the capsule will result in essentially the same temperature distribution through the soil as in condition (a), subject of course to any changes

in thermal conductivity that might occur. Thus the surface temperature for radiation heat exchange from the capsule is at essentially that temperature arrived at in condition (a). Radiation heat exchange is governed by the following equation:

$$Q = \sigma \epsilon A_s (T_s^4 - T_o^4)$$

Assuming the following values

$$\epsilon = 0.8$$

$$A_s = \pi (0.25)^2 \text{ ft}^2$$

$$T_o = 1800^\circ\text{F} = 2260^\circ\text{R}$$

$$\sigma = 0.1714 \times 10^{-8} \text{ BTU/hr ft}^2 \, ^\circ\text{F}^4$$

$$T_s^4 = T_o^4 + \frac{Q}{\sigma \epsilon A_s}$$

$$T_s^4 = (2260)^4 + \frac{242(3.415)}{0.1714 \times 10^{-8} (0.8) \pi (0.25)^2}$$

$$T_s^4 = 260{,}000 + 7680 = 267{,}680$$

$$\therefore \quad T_s = 2270^\circ\text{R} = 1810^\circ\text{F}$$

Thus, it can be seen that withdrawal from the soil cavity by the capsule with its consequent shift of heat transfer from conduction to radiation imposes no capsule temperature increases of any consequence. And so it is that all three conditions are similar and revolve around the question of soil conductivity. In that regard then, considering the range of soil conductivities, it would appear that equilibrium for a capsule would be established in the range of 1200°F to 2200°F.

As indicated earlier, these temperatures exceed the oxidation threshold for pyrolytic graphite, not to mention the reactivity potential of soil chemicals so that degradation of the capsule will occur with time. However, no conditions appear to favor reaction of the zirconia liner with either the graphite or the soil chemicals so that after oxidation of the capsule, chemical activity will cease and the liner will stabilize at some temperature that is a function of soil composition, possibly even melting the soil and sinking into the earth but without loss of liner integrity.

4.5.4 CAPSULE BELOW WATER SURFACE

A last intact reentry condition involves the possible impact of the capsule in a body of water. Again the equilibrium temperature must be ascertained for the proper evaluation of this particular circumstance.

Using the approach from the case of a capsule resting on the ground, but omitting radiation losses we have

$$Q = \bar{h}_c A_s (T_s - T_w)$$

and again

$$\bar{h}_c = 0.53(GrPr)^{1/4} k/R_s$$

Assuming the following values for the water

$$T_s = 120^\circ F$$

$$T_w = 60^\circ F$$

$$T_f = 90^\circ F$$

$$\therefore \quad k = 0.359 \text{ BTU/hr ft } ^\circ F$$

$$Pr = 5.89$$

$$R_s = 1.5'' = 0.125 \text{ ft}$$

$$Gr = 56 \times 10^6 \times 60 \times (0.125)^3 = 6.57 \times 10^6$$

$$\therefore \quad \bar{h}_c = 0.53(6.57 \times 10^6 \times 5.89)^{1/4}\ 0.364/0.125 = 122 \text{ BTU/hr ft}^2\ ^\circ\text{F}$$

$$\therefore \quad T_s = \frac{Q}{h_c A_s} + T_w$$

$$T_s = \frac{(240)\ 3.415}{(122)\ \pi/4(0.125)^2} + 60$$

$$T_s = 55 + 60 = 115^\circ\text{F}$$

At these temperatures, no reaction with the capsule or liner is expected in either fresh or salt water.

BLANK

4.6 COMPARATIVE ANALYSIS

4.6.1 INTRODUCTION

The stated objective of the Development of the SIREN Fuel Capsule, Phase I, is to evaluate and establish its feasibility within the following design criteria:

- Five-year service life after six-month prelaunch storage
- Minimize stresses on the capsule by helium venting
- Minimum of one year fuel containment after impact in soil or water.

In other sections of this report, test data and analyses are presented on specific aspects of the SIREN capsule's capabilities. It is the purpose of this analysis to discuss the feasibility of the SIREN concept in light of these data, highlighting those areas requiring further development. At this time, feasibility can be discussed only in general terms because:

- The SIREN concept is yet in the preliminary stage of development
- The definition of feasibility is strongly dependent on specific (but undefined) design and mission requirements.

The question of feasibility is discussed in the following paragraphs from four viewpoints:

- Fabricability and fueling of the capsule
- Ability to perform long term mission
- Ability to withstand reentry
- Ability to confine the fuel after impact.

4.6.2 FABRICATION OF THE FUELED CAPSULE

The fabricability of the non-fueled SIREN capsule was demonstrated as part of the Fabrication Task (Section 3) wherein 35 test capsules were successfully prepared. Whereas, the fabrication of a fueled capsule has not yet been demonstrated it has been subjected to analysis. As discussed in paragraph 4.3, the

methods of fabrication and fueling of the capsule are strongly dependent on whether the fuel form is microsphere or solid form such as sintered oxide, solid solution or cermet.

When considering the microsphere fuel form, the capsule would first be fabricated, the fuel then loaded through a fueling port, and then the fueling port sealed. Critical to the success of this approach are:

- The ability to successfully seal the liner (ceramic, cermet, or metallic)
- The ability to fuel and seal the capsule without contaminating the capsule above the acceptable limits.

Several promising approaches to both the sealing and contamination control problem have been devised; however, as yet there have been no actual demonstrations and laboratory evaluations performed.

When considering the solid fuel form, the anticipated fabrication of the capsule would start with the fuel as the capsule core ("hot fabrication"). The fuel would be coated with an inert layer that would serve as an integrally bonded liner. The liner would most probably be either ZrO_2 or ThO_2 depending on the fuel composition and would be applied by a chemical deposition process. The technologies for applying such coating on PuO_2 have been developed and are considered current technology. The graphite yarn would be wound directly on the coated fuel, and subsequently impregnated with pyrolytically deposited carbon. This method of direct fueling/fabrication eliminates the problem of sealing a fueling port as required with the particulate fuel. Also, it appears probable that the existing technology for coating the PuO_2 would result in a surface containing little, if any, contamination. Consequently, the problem of contamination control would be greatly simplified. Critical to the success of the hot fabrication technique would be the development of methods for winding and impregnating a capsule whose

core is both thermally and radiologically hot. Whereas, neither hot winding nor hot impregnation methods have been demonstrated, experience indicates that both processes are technically feasible. Hot winding could be accomplished by modification of the winding machine to provide temperature resistant components, a cooling device, and biological shielding. The required hot impregnation technology is technically related to current methods of impregnation of hollow shapes using the "inside-out-process". In this process, the inside surface of the part is heated initially, and during the course of the impregnation cycle, the hot zone is made to traverse from the inside surface to the outside. Since the carbon is preferrentially deposited on the hotter zones, the impregnation occurs from the "inside to the outside". It appears feasible to use this type of impregnation cycle for "hot" impregnation of the fueled capsule through use of controlled heating rates.

4.6.3 MISSION REQUIREMENTS

Selected properties of the graphite/carbon structure were tested during Phase I to aid the assessment of long term mission capability of the SIREN capsule. The properties tested were oxidation resistance, helium permeability, thermal conductivity, and resistance to solid propellant fire (simulated launch abort). (The generation of test data relating to liner materials, and fuel materials were outside the scope of this program and only limited data from other laboratories are available.)

Oxidation protection of the graphite/carbon structure is required primarily for the prelaunch storage and launch countdown. Based on the test data obtained from the SIREN test capsules and other published data, the following estimated degree of oxidation protection required for a six-month storage in air would be:

STORAGE TEMPERATURE	PROTECTION REQUIRED
Less than 400°F	None
500° to 600°F	Thin surface protection (several mils thick), such as B_6Si or SiC

STORAGE TEMPERATURE	PROTECTION REQUIRED
800° to 1000°F	Thick surface protection and possibly substrate protection, such as B_6Si, SiC or BN
1200°F and above	Developmental surface and substrate protection or canning.

Specific oxidation requirements would be strongly dependent on such parameters as temperature, air flow rate, density and quality of the graphite/carbon structure, and probable surface damage due to handling. Considering the large amount of work already performed on the oxidation protection of graphite in other laboratories, it would be expected that application of known technologies could be successfully extended to the SIREN capsule with a minimum of developmental effort.

The ability of the graphite/carbon structure to vent the helium generated within the fuel was demonstrated by test (see paragraph 5.4). Simply stated, the graphite/carbon structure "leaks like a sieve". Examination of the microstructure of the graphite/carbon indicated two kinds of porosity:

- The carbon impregnant deposited on the graphite yarn but did not completely permeate the filaments of the yarn bundle
- The porosity within the structure lies between and parallel to the lay of the yarn.

Further development of the impregnation process may result in less void volume between yarn lays, but it is doubtful if the impregnation would ever effectively seal the path through the yarn bundle. The introduction of an oxidation protection coating on the surface would be probably offer some resistance to helium flow. However, during prelaunch storage when the fuel would be cool, it is improbable that any significant quantity of helium would be released from the fuel, and even complete sealing of the outer surface of the capsule would cause no significant

helium pressure. At the elevated mission temperatures, the oxidation protection materials would be permeated by the helium at a sufficient rate. In the unlikely case that helium were not to vent through the surface coating at a sufficient rate, the coating would be expected to fissure and vent the gas as the internal pressure increased. Fissuring of the oxidation protection at that period of the mission would be of no consequence. Therefore, based on the available data, there appears to be no problem of venting helium through the graphite/carbon structure.

Measurement of the thermal conductivity of the graphite/carbon structure is an important factor in assessing the long term mission capabilities of the capsule since the conductivity influences the temperatures of the inner components. The temperatures of the inner components affect, among other things, the materials compatibility behavior. The temperature drop across the graphite/carbon was determined to be approximately 130°F; therefore, for a capsule surface temperature of 1800°F, the graphite-liner interface and the liner-fuel interface would be approximately 1930° to 2000°F. The relatively low temperature drop across the capsule wall allows for a higher capsule surface temperature with a correspondingly lower penalty for possible incompatibility at the graphite-liner-fuel interfaces. The demonstration of compatibility of the various capsule components has yet to be performed.

The ability of SIREN capsules to withstand the effects of burning solid propellant was successfully demonstrated with three test capsules. The tests were performed with capsules in proximity of and in contact with solid fuel for burning times to eight minutes. After test, the capsules showed no evidence of oxidation, attack by the fuel residue, thermal shock, or melting of any of the components. Based on these data, it was concluded that the SIREN capsule can successfully withstand solid propellant fires that may occur during mission abort.

4.6.4 REENTRY

The ability of the SIREN capsule to survive the condition imposed by stable (non-spinning) orbital (26,000 ft/sec) or superorbital (36,000 ft/sec) reentry has been successfully demonstrated with plasma air heating rates ranging from 264 B/ft^2-sec to 447 B/ft^2-sec and dwell times ranging from 199 to 300 seconds. The maximum mass loss was approximately 33 grams.

Despite the fact that the SIREN structure ablated at a rate approximately 30 percent higher than that observed in standard graphite reentry heat shields, the material thickness (approximately 0.5 inch) was sufficient to ensure that the center core would remain covered after reentry. The results of scaling the plasma arc test results to hypersonic conditions likewise indicated that core would remain covered.

It is anticipated that improving the density of the SIREN composite (graphite/yarn/pyrolytic carbon or graphite impregnant) structure by optimization of impregnation (or perhaps winding) process would permit the ablation rate to more closely approximate that of graphite reentry heat shields.

It should be noted, however, that the ablation rates for the same test condition would also be lessened if the capsule were spinning during reentry, resulting in a lower stagnation point recession.

4.6.5 IMPACT

To ascertain the feasibility of the SIREN concept relative to post reentry impact, it is required that capsule failure at impact be defined. As stated in paragraph 5.5.3.1, failure is defined for the following fuel forms:

- Microsphere fuel-liner rupture and subsequent dispersal of fuel particulate
- Solid fuel form - production of and subsequent dispersal of fuel fines.

On the basis of these failure criteria, no impact tests were performed which would indicate failure or success of the SIREN to prevent production and/or dispersal of fines from either fuel form. The degree to which the solid Al_2O_3 core simulated a prospective (solid) fuel form is not known principally because the structural properties of the three types of solid $Pu^{238}O_2$ fuel forms are not presently known. If one assumes, however, that the Al_2O_3 core did simulate one of the prospective fuel forms, then it may be concluded that 5 out of 6 impact tests were successful. The core of one capsule shattered at 350 ft/sec and by definition is a failure. A "fines analysis", however, was not performed.

The results of the post impact analysis indicate that considerable improvement of the impact characteristics may be obtained by the use of a high tensile strength graphite yarn (400,000 psi versus 6000 psi presently used). The higher energy absorption characteristic available because of the higher strength yarn would result in a decreased compressive force on the fuel liner.

Additional consideration should be given to impact testing of capsules which have been exposed to reentry conditions and studies made to determine orientation of ablated capsules during impact.

BLANK

SECTION 5
TESTING OF SIREN CAPSULE DESIGN

5.1 INTRODUCTION

Heretofore, the unique properties of graphite/carbon composites have not been tested with respect to the requirements of an isotopic fuel capsule. Therefore, the testing of several properties of the graphite/carbon composite material was included in the overall assessment of the SIREN concept. The tests performed are listed below and reports of the respective tests are given in the following paragraphs:

5.2 Thermal Conductivity Tests

5.3 Oxidation Susceptability Tests

5.4 Helium Permeability Tests

5.5 Impact and Plasma Arc Tests

5.6 Solid Propellant Fire Tests

BLANK

5.2 THERMAL CONDUCTIVITY TESTS

5.2.1 INTRODUCTION AND OBJECTIVES

The high temperatures associated with radioisotopic fuel capsules during reentry as well as during normal operation have necessitated the development of materials which possess high strength and integrity during exposure to extreme thermal environments. The combination of high-strength carbonaceous filaments with a pyrolytically deposited carbonaceous matrix appears to be the correct approach to solving the problems associated with intact after impact reentry of radioisotopic fuel.

Carbon-carbon materials present attractive possibilities for obtaining increased strength and integrity during reentry and after impact. The increased strength, high heat of ablation, thermal shock resistance, and dimensional stability of carbonaceous materials suggest their suitability for reentry of radioisotopic fuel.

This type of material combined with a unique technique of fabrication led to the SIREN concept for fuel capsules. It is the objective of this experimental investigation to determine the thermal conductivity of the SIREN wall structure or heat shield. The SIREN wall structure is believed to be somewhat anisotropic in nature with respect to thermal conductivity because of the yarn winding technique peculiar to the SIREN concept. Of concern in this phase of testing is the radial thermal conductivity only.

Thermal conductivity data obtained in these tests are for temperatures indicative of normal operating conditions; i.e., up to 1800°F.

5.2.2 TEST APPARATUS

Two hollow, three-inch diameter SIREN capsules having a 1/2 inch graphite wall thickness were used as the test specimens. The two capsules were designated as Q-1 and Q-2 and a typical instrumented specimen is shown in Figure 5-1.

SANDERS NUCLEAR CORPORATION

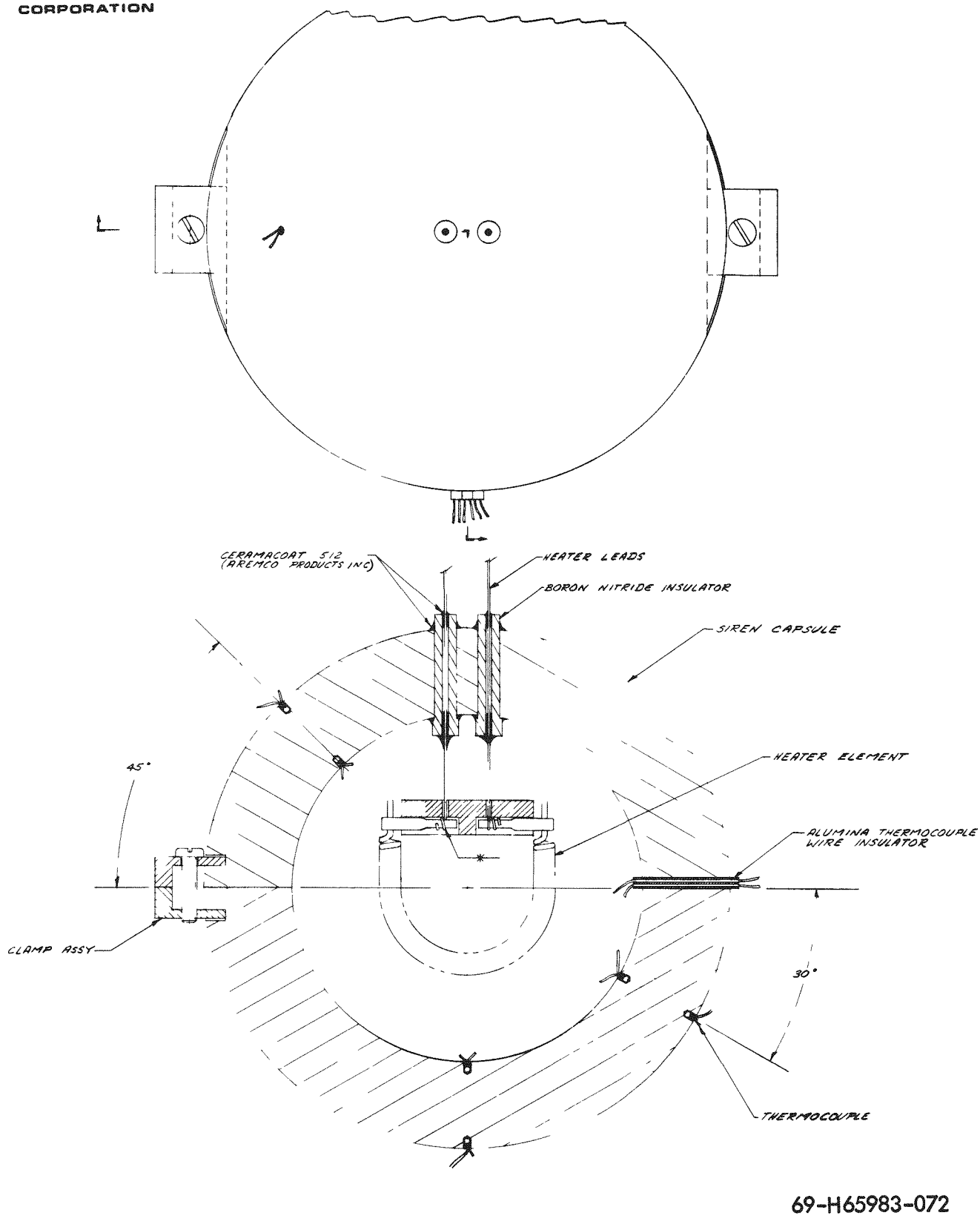

Figure 5-1 Thermal Conductivity Specimen Fully Instrumented.

Determination of thermal conductivity was based on one-dimensional equilibrium heat transfer through the walls of a sphere with internal heat generation. The equation governing the steady-state heat transfer in a sphere is

$$Q = \frac{4\pi K r_1 r_2 (T_1 - T_2)}{r_2 - r_1} \qquad (1)$$

where:

Q = internally generated heat, B/hr

K = thermal conductivity, B/hr ft$^{\circ}$F

r_1 = inner radius, ft

r_2 = outer radius, ft

T_1 = inner temperature, $^{\circ}$F

T_2 = outer temperature, $^{\circ}$F

Rearranging, to solve for K yields

$$K = \frac{Q(r_2 - r_1)}{4\pi r_1 r_2 (T_1 - T_2)} \qquad (2)$$

By placing thermocouples on the inner and outer radius of the graphite wall it was possible to measure the temperature difference across the wall for a specified heat input. Referring to equation 2, K was easily determined by accurately measuring the internal heat input and temperatures. It was also important to determine the exact locations of the thermocouples as well as prevent unaccountable heat losses from occurring.

5.2.3 FABRICATION OF TEST APPARATUS

To allow installation of the internal heater and thermocouples it was necessary to cut the SIREN capsule in half. Once this was done the specimen was

instrumented with six 5 mil diameter chromel-alumel thermocouples. Three thermocouples were affixed to the inside of the capsule wall at a depth of 60 mils. On the outer surface three additional thermocouples were installed at a depth of 60 mils and on the same three radians as the inner thermocouples. The location of the thermocouples is shown in Figure 5-1. It was necessary to embed the thermocouples 60 mils below their respective surfaces so that direct radiation would not influence the thermocouple junction.

Also indicated in Figure 5-1 is the internal heater which was fabricated from 10 mil doubly coiled tungsten wire. The heater leads were 20 mil tungsten wire. Filament and leads were connected via an intermediate tungsten wire with connections being welded. Heater lead wires were electrically insulated from the graphite with boron nitride sleeve type feed-throughs. Diameter of the sleeves was small so that three-dimensional heat transfer would be minimized.

By suspending the instrumented capsule by the two small diameter tungsten lead wires, unaccountable heat losses were reduced to a minimum. In fact, the test apparatus, as shown in Figure 5-2, closely resembles that normally used for calorimetry.

Preliminary estimates of the power required by the internal heater for maintaining the SIREN wall structure at the 1800°F level prompted the use of the radiation barrier shown in Figure 5-2. Without the barrier the power required to raise the capsule to 1800°F in a vacuum was over 2000 watts, exceeding the capabilities of available heaters. By enclosing the capsule within a gold plated radiation shield (emissivity = 0.15) the maximum power requirement placed on the heater when operating in a vacuum environment was reduced to approximately 200 watts. This requirement was higher during the argon and helium tests but never exceeded 600 watts. This was easily achieved with the tungsten heater.

In effect then, the radiation barrier served only to reduce the power input for obtaining a specified wall temperature. Of course, this resulted in reduced ΔT's between the inner and outer thermocouples and hence the accuracy with which

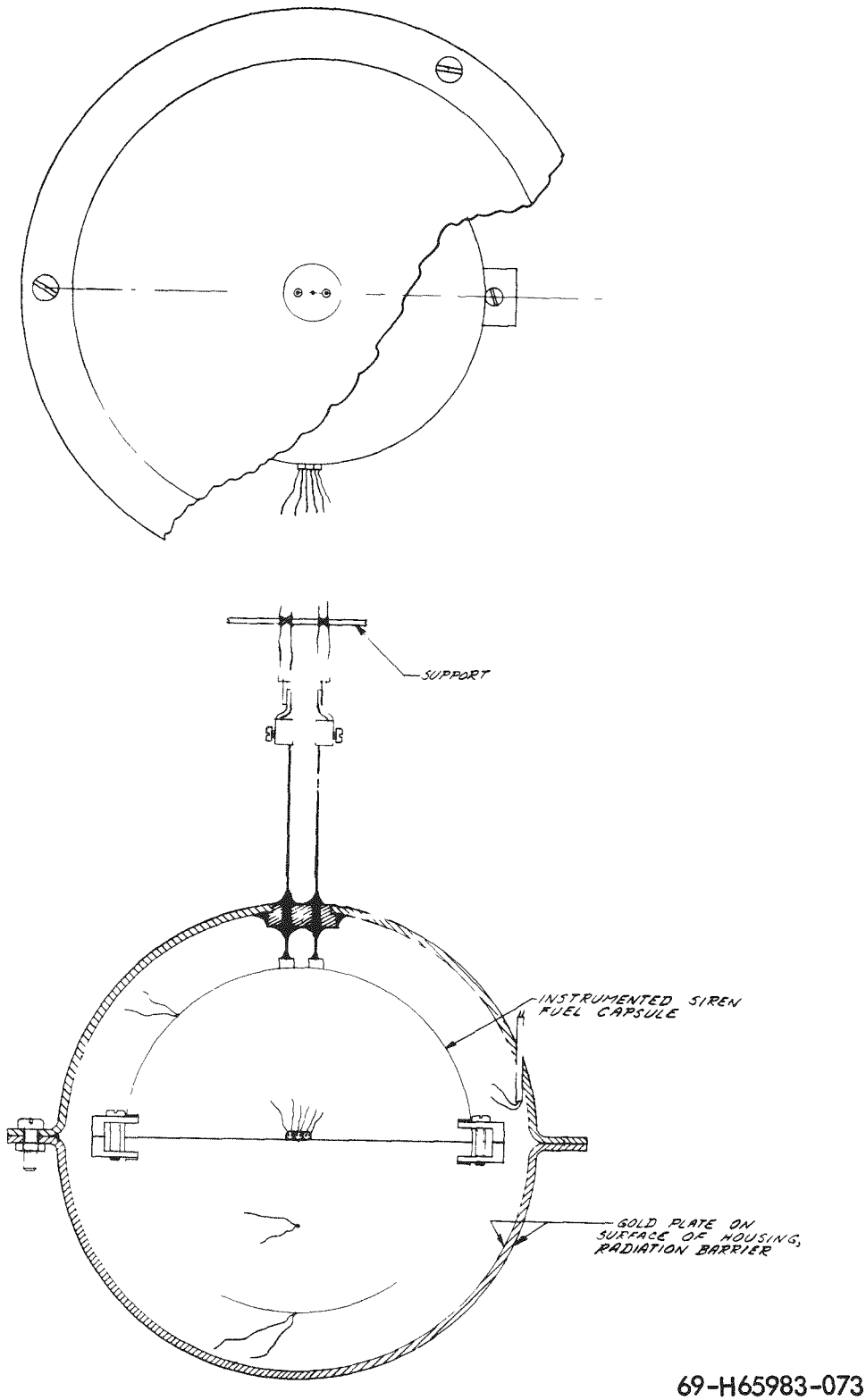

Figure 5-2 Suspended Capsule with Radiation Barrier.

the conductivity could be determined at the lower temperature levels. Combinations used resulted in the optimum tradeoff between heater capability and accuracy of conductivity measurement.

Investigation of the capsule and radiation barrier surfaces indicated no evidence of irregularities which would have caused variations in surface emissivity. Emissivity variations would have led to a 0.24 power variation in temperature.

The clamps holding the two halves of the SIREN capsule together introduced a minor perturbation in the one-dimensional flux near the clamps. The thermocouples were placed a sufficient distance from these perturbations to eliminate any influence on measurements.

Figure 5-3 shows the specimens (with radiation shield) as installed on the test stand.

5.2.4 MEASUREMENT PROCEDURE

It was desired to have thermal conductivity measurements taken at 800°, 1300° and 1800°F in a vacuum ($<10^{-5}$ torr). To determine the effect of gaseous environments on thermal conductivity coefficients, tests were performed in one-third atmosphere each of argon and helium (one-third atmosphere was used so that the bell-jar vacuum system could be maintained under a net positive ambient pressure). With the apparatus installed as shown in Figure 5-2 the pressure in the vacuum chamber was reduced to 10^{-7} torr. During the time of initial evacuation a small amount of power was applied to the heater to promote gasification of entrained volatiles within the specimen.

Once the evacuation procedure was completed, the heater power was increased to a level resulting in an inner capsule wall temperature of $800^{\circ} \pm 50^{\circ}$F. Sufficient time was allowed at this power level to achieve temperature equilibrium. At this point the six thermocouple readings were recorded as well as the power input. The heater power taps were connected to the heater lead wires at the exit

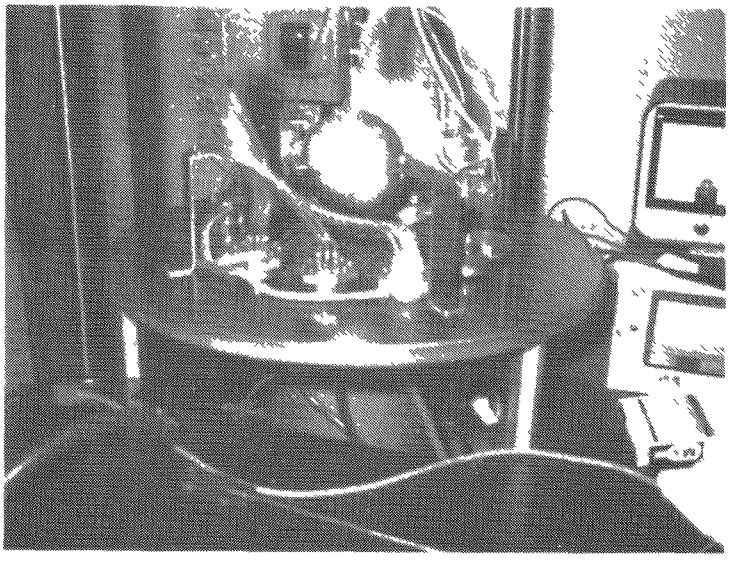

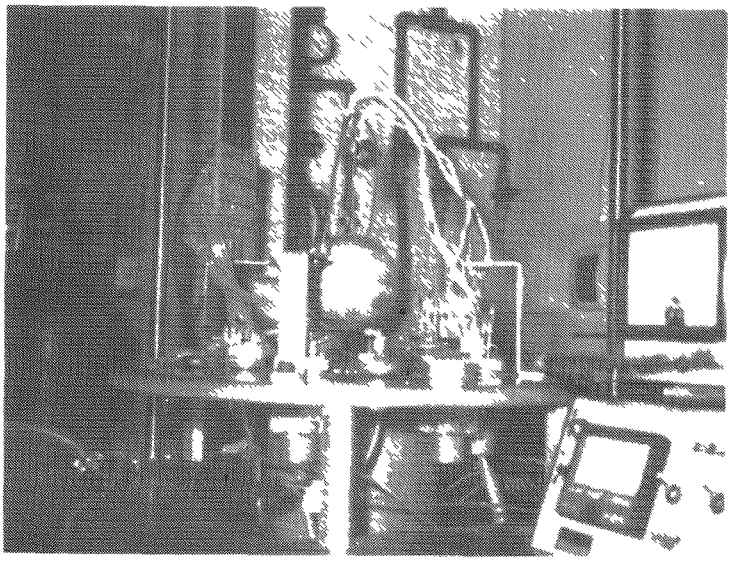

69-H65983-074

Figure 5-3 Test Apparatus.

through the radiation barrier. The power reading therefore represented essentially internal power dissipation. The 1300° and 1800°F measurements were made in a similar manner.

The first specimen, Q-1, was tested only in a vacuum environment (it was not decided to investigate a gaseous environment until after specimen Q-1 had been disassembled). The second specimen, Q-2, was tested in a gaseous environment as well as a vacuum environment. The vacuum test procedure was identical to that of Q-1. After the vacuum measurements were completed, the test system was backfilled with argon to 10 in. of Hg pressure. Measurements were again taken at steady-state conditions at 800°, 1300° and 1800°F. The same procedure was followed using helium.

The thermocouple readings were taken with a Leeds and Northrup millivolt bridge, accurate to the nearest hundredth of a millivolt. A combination Dana, DVM (Model 5400) and Weston AC Ammeter (Model 433) were used to determine power input. Voltage was recorded to the nearest one-tenth volt and current to the nearest one-hundreth ampere. The thermocouples were precalibrated by the manufacturer and had an accuracy over the temperature range of interest of $\pm$0.5 percent.

After the tests were completed, the specimens was dissected so that the exact location of the thermocouple junctions could be established. Thermocouple location played a dual role in determination of conductivity and had to be accurately determined. Photographs of the sectioned pieces showing seated thermocouple junctions are given in Figures 5-4 through 5-7. During the dissection process of specimen Q-1 the thermocouples at station 5-6 were dislocated thereby precluding exact caliper measurement of the thermocouple separation distance. Distance used in the computations for this station was estimated with the aid of installation techniques and examination of the vacant thermocouple wells. Table 5-1 gives the measured distances between thermocouple junctions. Table 5-2 is a tabulation of recorded data.

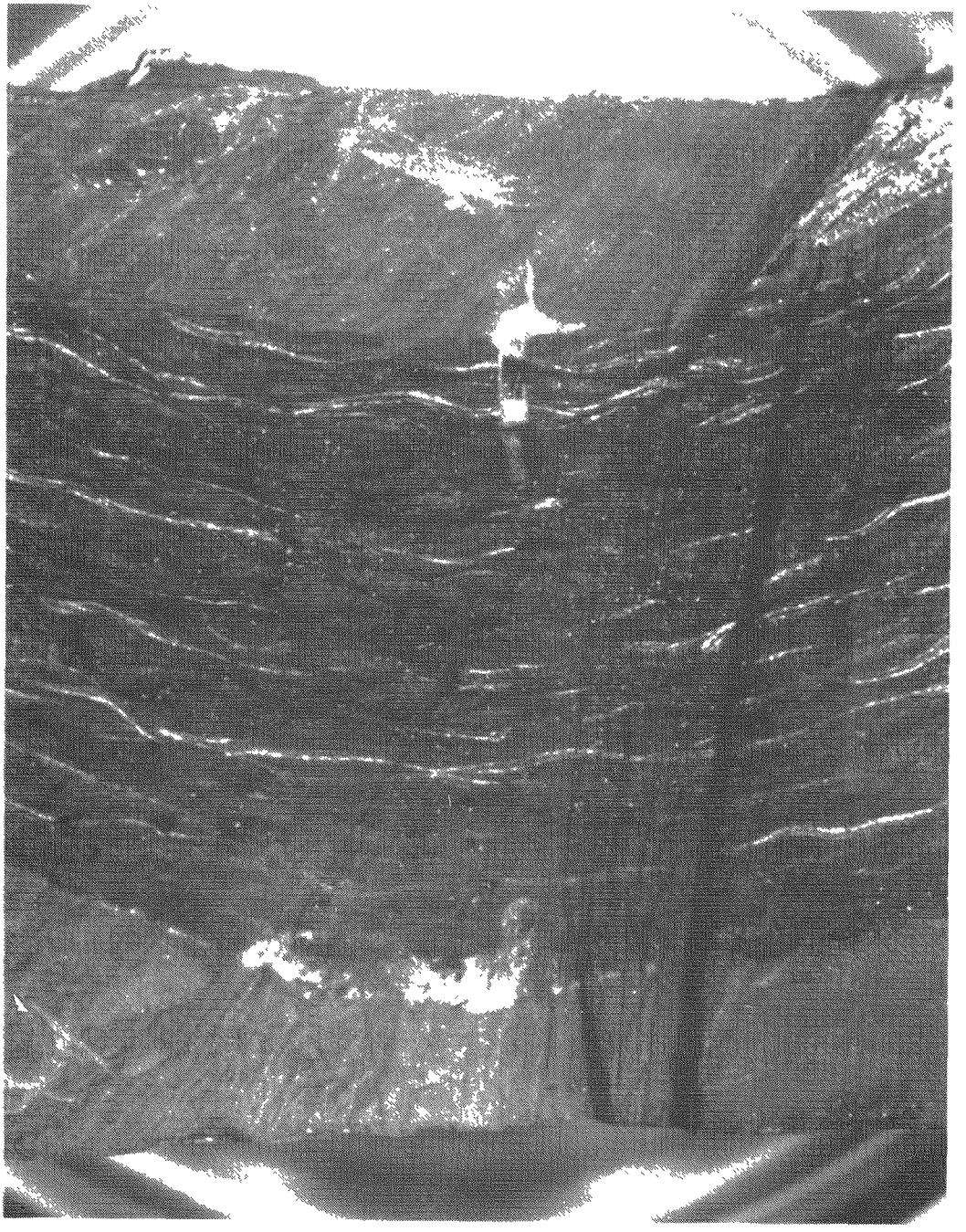

69-584-4

69-H65983-075

Figure 5-4 Dissection of Station 1-2, Specimen Q-1.

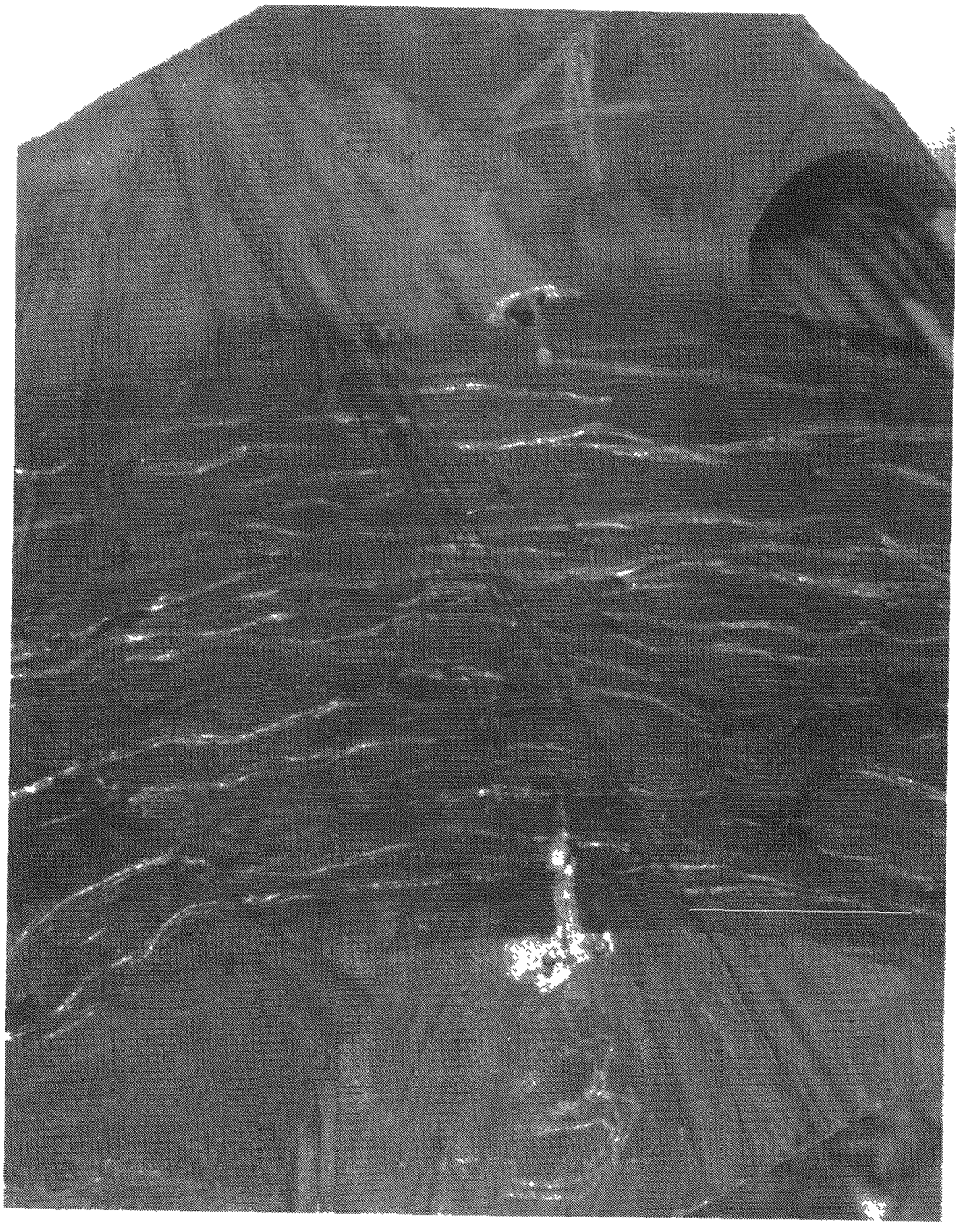

69-584-1

69-H65983-076

Figure 5-5 Dissection of Station 3-4, Specimen Q-1.

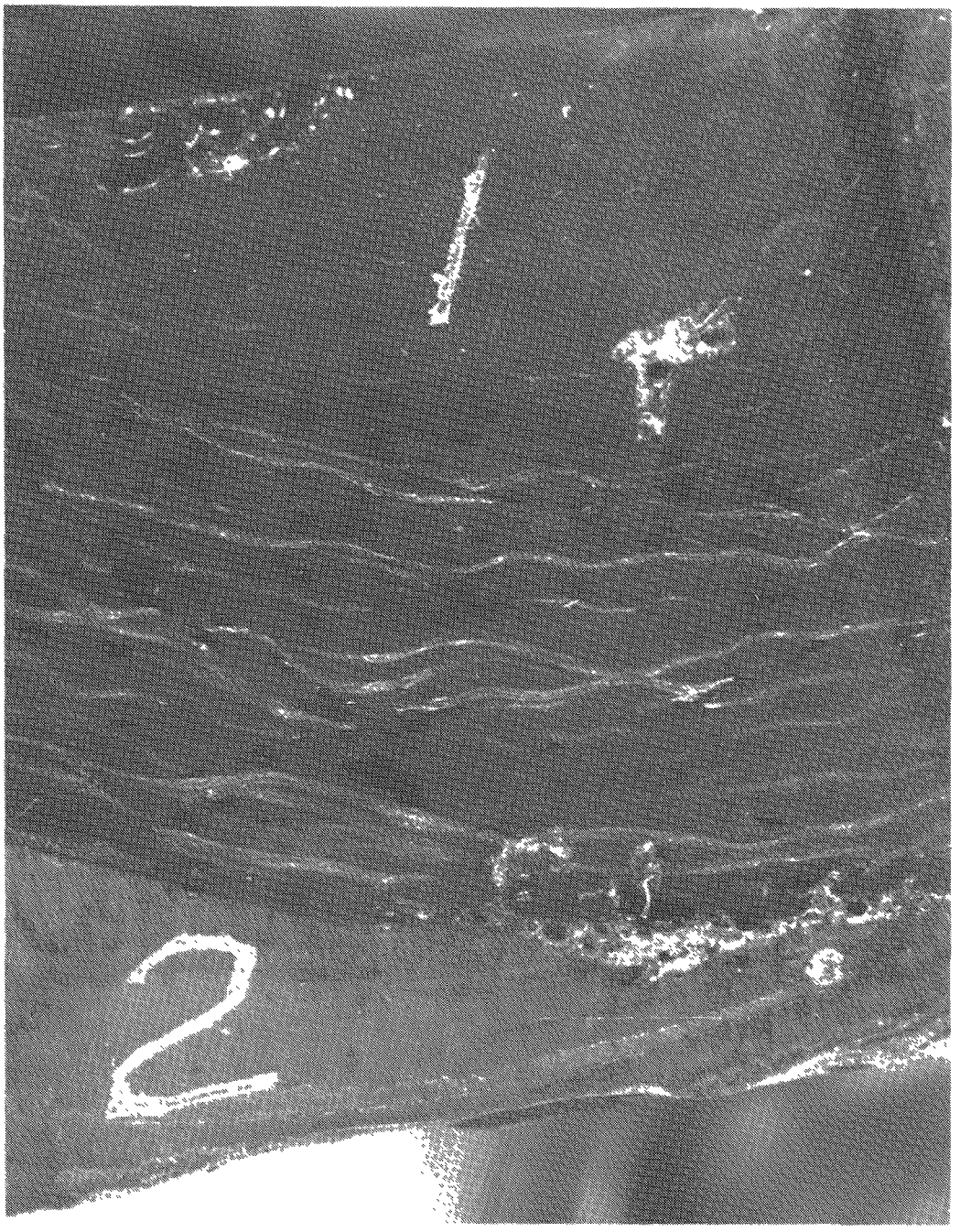

69-584-2

69-H65983-077

Figure 5-6 Dissection of Station 1-2, Specimen Q-2.

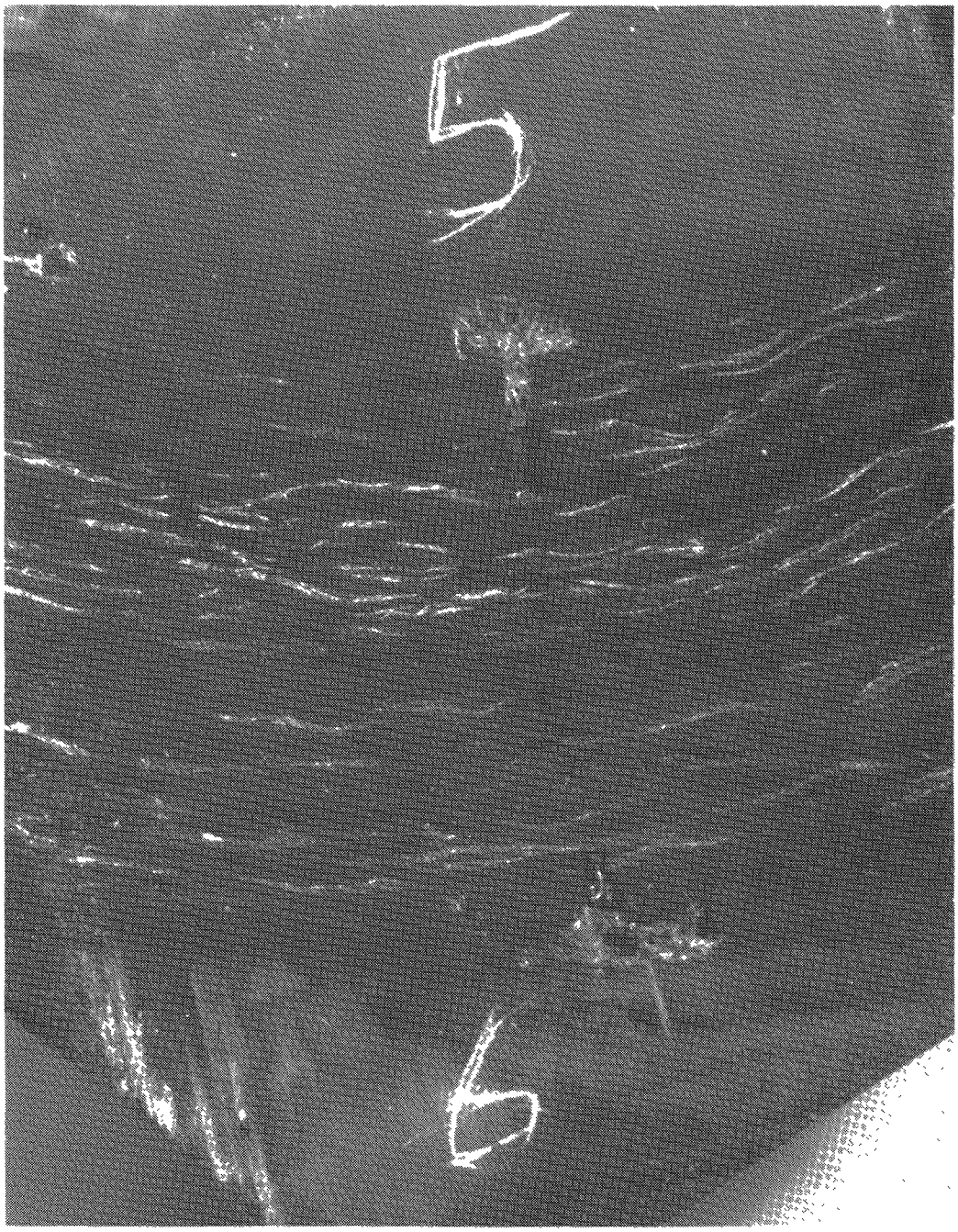

69-584-3

69-H65983-078

Figure 5-7 Dissection of Station 5-6, Specimen Q-2.

Figure 5-8 is a photograph of the test assembly prior to test (Note: the thermocouple leads are make-shift in order to show thermocouple exits - actual leads are 5 mil diameter). Figure 5-9 is a photograph showing the disassembled parts after test.

TABLE 5-1

SPECIMEN DIMENSIONAL CHARACTERISTICS

Specimen	Station	Thermocouple Separation Distance	R_1	R_2
Q-1	1 - 2	0.400 in.	1.100 in.	1.500 in.
	3 - 4	0.400*	1.100	1.500
	5 - 6	0.400	1.100	1.500
Q-2	1 - 2	0.390	1.110	1.500
	3 - 4	Void	Void	Void
	5 - 6	0.370	1.130	1.500

*Estimated

5.2.5 RESULTS

Figure 5-10 is a plot of the experimental results showing conductivity values ranging between 1.9 and 2.5 B/hr ft $^{\circ}$F for vacuum conditions. Even though specimen Q-1 had a higher density than Q2 (see Table 5-3) it has about a 10 percent lower coefficient of thermal conductivity. This is not in general accord with previous published data which indicates increasing thermal conductivity with increasing density. Detailed analysis of the dissected regions near the test stations give some insight into this apparent anomaly. Figures 5-4 and 5-5, dissections of specimen Q-1, show a definite interface between the inner surface of the specimen and the epoxy used for maintaining thermocouple placement during

TABLE 5-2

EXPERIMENTAL DATA

	Temperature												ΔT			Power			Ambient	
	TC-1	TC-1	TC-2	TC-2	TC-3	TC-3	TC-4	TC-4	TC-5	TC-5	TC-6	TC-6								
Specimen	MV	°F	MV	°F	MV	°F	MV	°F	MV	°F	MV	°F	1-2 °F	3-4 °F	5-6 °F	Volts	Amps	Watts	Gas	Pressure Torr
Q-1	17.96	818	17.80	812	18.49	842	18.20	829	18.50	842	18.30	833	6.4	12.8	8.5	10.0	2.00	20.0	Air	1.4×10^{-6}
Q-1	28.29	1256	27.86	1238	29.09	1290	28.44	1262	29.02	1287	28.55	1267	18.4	27.9	20.2	20.0	2.87	57.4	Air	1.1×10^{-6}
Q-1	39.66	1756	37.66	1665	40.45	1792	38.31	1695	40.30	1786	38.55	1705	91.0	97.3	80.0	47.5	4.80	228.0	Air	2.8×10^{-6}
Q-2	18.25	831	18.15	826	18.50	842	18.18	828	18.55	844	18.40	837	4.3		6.4	10.0	2.00	14.4	Air	1.4×10^{-6}
Q-2	29.01	1286	28.69	1273	29.34	1301	28.62	1270	29.41	1304	29.00	1286	13.7		17.6	19.3	2.52	48.6	Air	6.0×10^{-7}
Q-2	39.95	1770	38.68	1711	40.65	1801	38.70	1713	40.70	1804	39.23	1736	58.0		67.0	48.5	4.30	208.5	Air	1.9×10^{-6}
Q-2	18.60	846	18.23	830	18.91	858	18.31	833	18.97	861	18.55	843	15.7		17.8	18.7	2.50	46.9	Argon	254
Q-2	28.33	1257	27.40	1218	29.00	1286	27.65	1229	29.20	1295	28.25	1254	39.9		40.8	35.0	3.60	126.0	Argon	254
Q-2	16.65	763	15.85	729	17.52	800	16.21	744	18.50	820	17.00	778	34.0		42.6	32.0	3.83	122.5	Helium	254
Q-2	28.77	1276	26.90	1197	30.12	1334	27.36	1216	30.73	1361	28.77	1276	80.3		84.2	58.4	4.85	283.5	Helium	254
Q-2	38.85	1719	35.85	1585	40.30	1786	36.10	1596	40.60	1799	37.80	1672	136.0		127.0	90.0	6.00	540.0	Helium	254

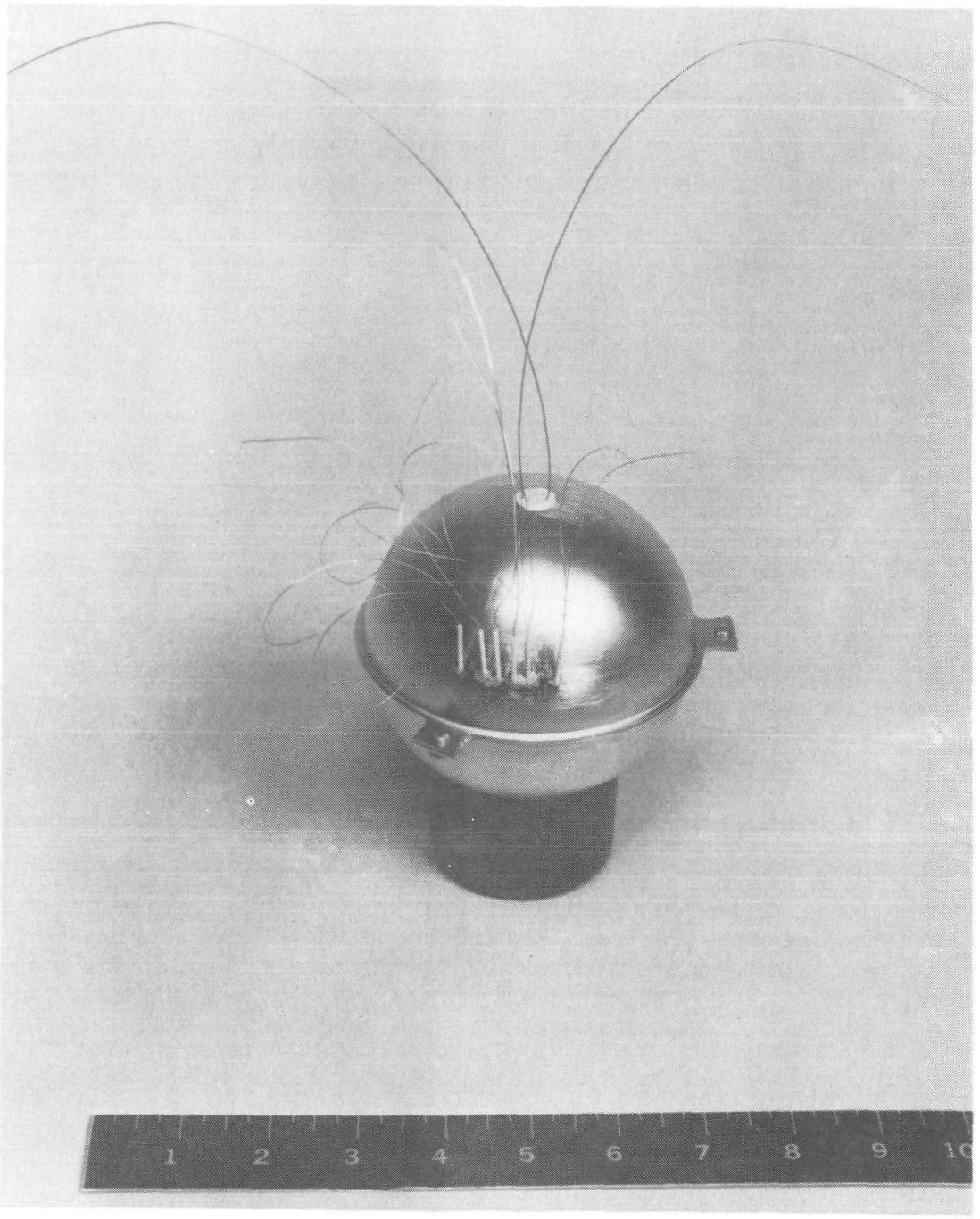

69-543-3

69-H65983-079

Figure 5-8 Radiation Barrier Showing Heater Leads and Thermocouple Leads.

69-543-1

69-H65983-080

Figure 5-9 Disassembly of Specimen Q-1 After Test.

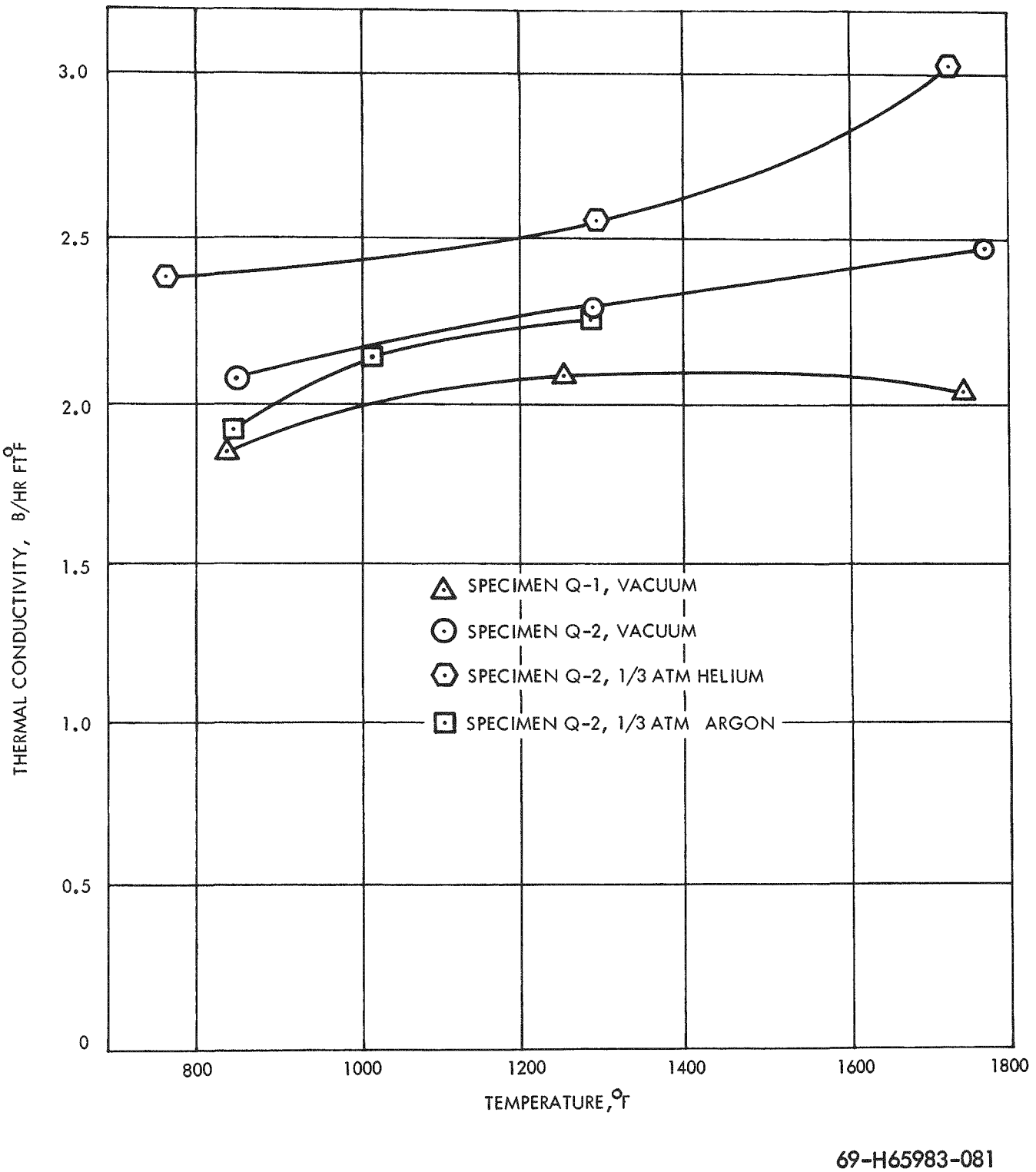

Figure 5-10 Thermal Conductivity of SIREN Carbon-Carbon Matrix.

TABLE 5-3

SPECIMEN WEIGHT SUMMARY

Specimen	Yarn		Impregnation			
			1st Cycle		2nd Cycle	
	Weight gms	Density gms/cc	Weight gms	Density gms/cc	Weight gms	Density gms/cc
Q-1	146.1	0.8138	230.6	1.285	258.1	1.438
Q-2	129.7	0.7224	223.8	1.247	240.1	1.337

dissection. Figures 5-6 and 5-7, dissections of specimen Q-2, however, show no such well defined interface between the inner specimen surface and the epoxy. This implies that the inner layer of yarn for Q-2 was not well impregnated. Even though Q-1 had a bulk density greater than Q-2 it is likely that the density of the carbon-carbon material between the individual station thermocouple junctions was higher for Q-2 than it was for Q-1. The photographs tend to substantiate this belief in that Figures 5-4 and 5-5 (Q-1) show a more coarse region between thermocouples than Figures 5-6 and 5-7 (Q-2).

Also shown in Figure 5-10 is the coefficient of thermal conductivity for specimen Q-2 in the presence of one-third atmosphere of argon and one-third atmosphere of helium. Introduction of the helium into the interstices of the carbon-carbon matrix increased its thermal conductivity by about 15 percent over that for a vacuum while introduction of argon resulted in essentially no change in thermal conductivity. The argon was allowed to penetrate the matrix for 48 hours prior to test.

Figure 5-11 compares the results of the present tests to those of previously published data for materials similar to the carbon-carbon material under test. The Martin-Baltimore company data is for Super Temp Company reinforced

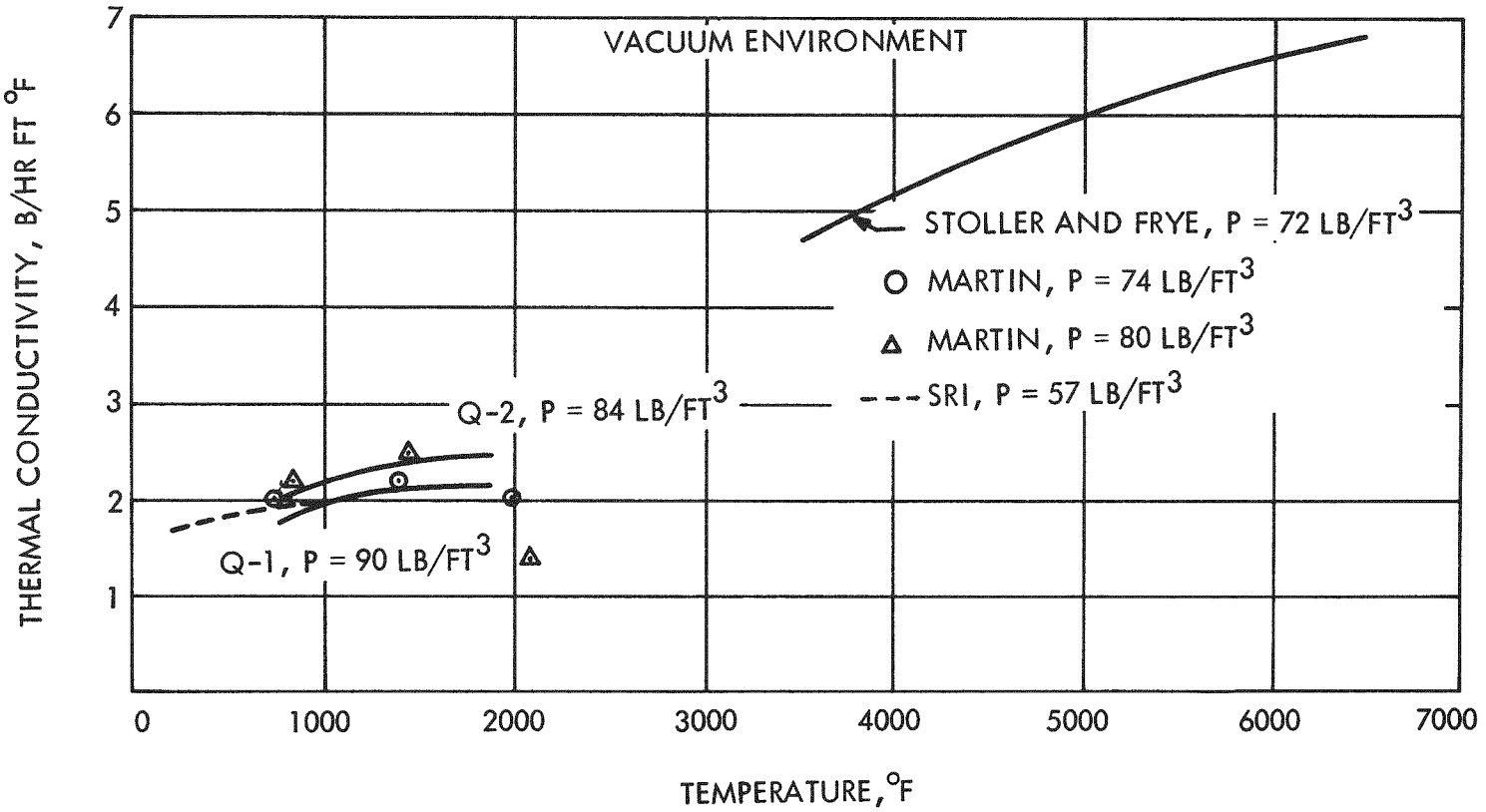

69-H65983-082

Figure 5-11 Comparison of Experimental Data with Published Data.

pyrolytic graphite felt of density as indicated in the graph. The Stoller and Frye[1] data is for material fabricated in a manner very similar to the SIREN technique. The present test data is in good agreement with the data compared.

Figures 5-12 and 5-13 are the plots of the referenced data.

Accuracy of the data gathered during the present tests is estimated to be ±5 percent.

5.2.6 CONCLUSIONS

Thermal conductivity coefficients have been determined for the SIREN carbon-carbon material for the temperature range of 800° to 1800°F. Values ranging between 1.9 and 2.5 B/hr ft°F in vacuum have been shown to be in good agreement with published data on similar materials.

Data presented represents values of thermal conductivity for the radial direction or across the grain only. Future work should be conducted to determine the thermal conductivity in a direction parallel to the filament windings or circumferential direction. Circumferential values of thermal conductivity are necessary to perform accurate analyses on thermal models during operation, reentry, and post operation. Additional measurement techniques will have to be established to perform circumferential measurements since the technique described herein is not applicable to circumferential measurement of thermal conductivity.

Consideration should also be given to determination of thermal conductivity coefficients in the temperature range of 2000°F to 4000°F since this data is not presently available but is required during reentry thermal analyses.

---

[1] H. M. Stoller and E. R. Frye, "Carbon-Carbon Materials for Aerospace Applications", AIAA/ASME 10th Structures, Structural Dynamics and Materials Conference, April 1969.

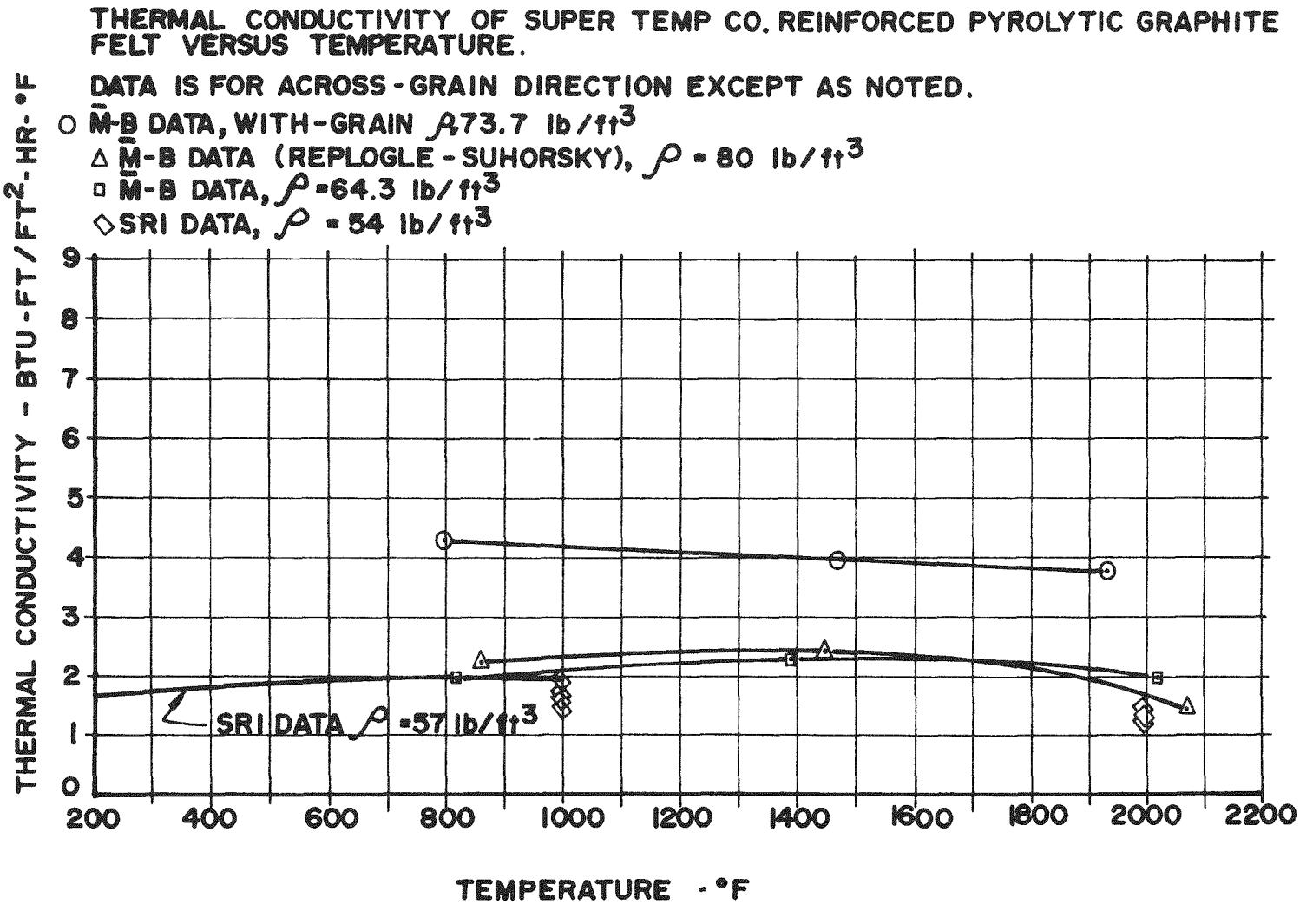

DATA COURTESY OF MARTIN-BALTIMORE CO.

69-H65983-083

Figure 5-12 Thermal Conductivity of Super Temp Company Reinforced Pyrolytic Graphite Felt vs. Temperature.

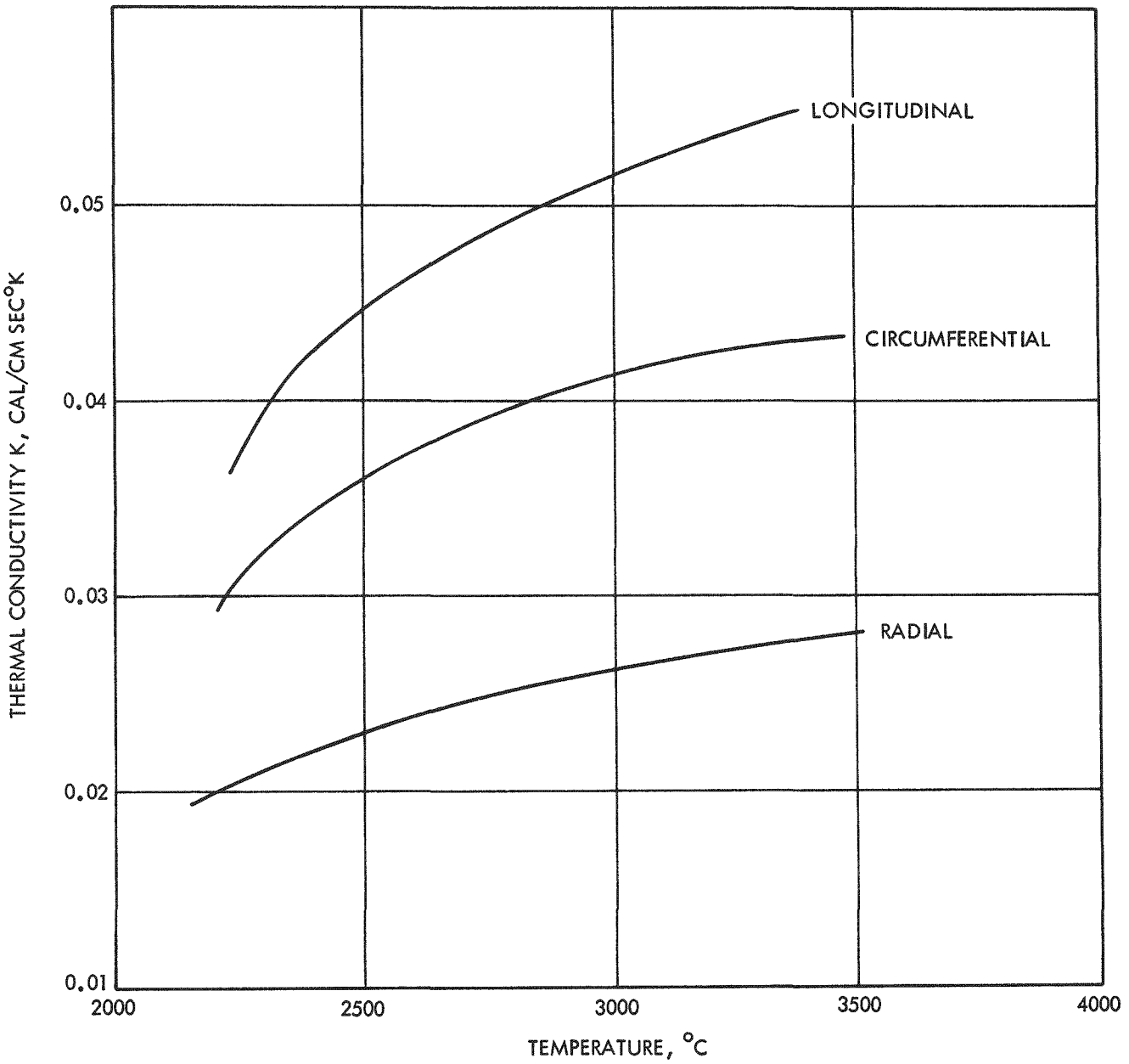

69-H65983-084

Figure 5-13 Data of Stoller and Frye – Thermal Conductivity of Spiral Wrap 1.15 gm/cc.

5.3 OXIDATION SUSCEPTABILITY OF THE SIREN CAPSULE

5.3.1 INTRODUCTION

The objective of the tests discussed in this report was to determine the oxidation susceptability of the SIREN capsule at temperatures above 800° F.

Curves are presented which show the percent weight loss per day as a function of time and for different temperatures. Curves of percent weight loss per day as a function of reciprocal absolute temperature are also presented which show the average performance of the SIREN capsules compared with commercial and pure graphite.

Three capsules were tested at temperatures of 800°F and 1000°F; one B_6Si coated capsule at 800°F; one B_6Si coated capsule at 1000°F; and one uncoated capsule at 800° and 1000°F. The uncoated capsule served as a basis for comparing the effectiveness of the B_6Si coating to prevent oxidation of the graphite structure.

At 1000°F, the oxidation rate of both the coated and uncoated capsule was sufficiently rapid that no meaningful information would be gained by testing at higher temperatures.

The efforts to enhance the oxidation protection afforded by the B_6Si coating are described in this report together with details of the test procedure and equipment.

5.3.2 CAPSULE DESCRIPTION

The SIREN capsules used for the oxidation tests consisted of graphite yarn wound over a 2-inch OD hollow aluminum sphere to a diameter of approximately 3-1/8 inches. Prior to impregnation, the aluminum core was removed by etching, resulting in hollow carbon/graphite spheres.

Four capsules were selected for oxidation testing. Each was prepared in accordance with the procedure outlined in SNP 100029 (see Appendix I) by

drilling and tapping a 1/2-inch 13 thd hole. A hanger was fabricated from nickel wire (12 AWG) and inserted through a threaded (1/2"-13) graphite plug which in turn was screwed into the capsule. The thread area was wetted with furfuryl alcohol to bond the capsule to the plug.

Three of the capsules were plasma flame sprayed with B_6Si, including the seal area and hanger, to a nominal thickness of 0.00125 cm to 0.0074 cm.

The capsule (AL-14) with the 0.0074 cm B_6Si coating was placed in a vacuum chamber along with a thin coated sacrificial capsule and evacuated to approximately 10^{-7} torr and backfilled with argon. The sacrificial capsule was heated by induction to approximately 1300°C (2372°F) for 5 minutes in an air atmosphere. Upon examination, it was evident that the coating was too thin and had pulled back in spots exposing the bare graphite structure. A glassy phase was formed in the intact areas, however, and it was decided to fire capsule AL-14 in a like manner. The attempt was apparently successful since a glassy phase was observed on the capsule. The support hanger for this capsule consisted of "fish spine" ceramic insulators over nickel wire, which in turn was formed in a basket fashion.

Table 5-4 summarizes the physical characteristics of the capsules fabricated for testing.

TABLE 5-4

PHYSICAL CHARACTERISTICS OF OXIDATION TEST CAPSULES

Capsule No.	Weight gms	Density g/cc	B_6Si Coating Weight gms	B_6Si Coating Thickness-cm (Nominal)	B_6Si Coating Fired
AL-3	257.99	1.437	1.6	0.0032	No
AL-6	257.9	1.436	--	--	--
AL-8	265.7	1.480	1.10	0.0021	No
AL-14	265.8	1.480	3.70	0.0074	Yes

5.3.3 TEST PROCEDURE

The test procedure is delineated in Appendix I (SNP 100029). Test program conditions, however, necessitated a slightly different course of action.

5.3.3.1 Test Equipment Description

The test equipment consisted of three essentially identical furnaces, balances, and temperature controllers. A brief description of each major piece of equipment is given as follows:

- Controller; API Temptendor, 0-2000°F, time proportioning
- Power; 0-208 VAC, 16 amp power supply console
- Balance; Torbal, Model ST-1, 0-310 gm capacity 0.01 gm sensitivity;
- Furnace; silica brick, fabricated by Sanders Nuclear.

  Heating elements are Lindberg Model 50731 (nichrome), 950 watts at 115 VAC, 4 Req'd to form cylinder 12" high by 7" ID and connected electrically in series parallel

  The furnace has a shielded air admittance hole at the bottom to maintain the oxygen level as near as possible to normal.

The weighing pans were each weighed and removed, substituting lead weights to equal the tare of the individual pans. A stranded Kanthol A-1 wire (equivalent to 12 AWG) was included in the tare and was used to suspend the capsule within the furnace.

Thus equipped, each furnace/balance assembly becomes a thermogravimetric test facility. The temperatures were controlled to $\pm 2^{\circ}$F. Figure 5-14 shows the furnaces in operation.

69-526-3

69-H65983-060

Figure 5-14 Thermogravimetric Equipment for Oxidation Test.

5.3.3.2 Temperature Profiles

Temperature profiles at selected temperatures were measured for each furnace prior to initiation of oxidation testing. To avoid large error, the profiles were obtained with a single thermocouple along the centerline (vertical) and midway between the centerline and heating element. The zone where the capsules would be suspended was found to vary less than $5^{\circ}F$ and was deemed satisfactory. The temperature controlling thermocouple was positioned slightly above and to one side of the capsule.

5.3.3.3 Basic Procedure

The basic procedure followed for the first round of testing involved the selection and installation of three capsules as follows:

- Furnace No. 1 - $800^{\circ}F$ - Capsule AL-6 (uncoated);
- Furnace No. 2 - $1000^{\circ}F$ - Capsule AL-3 (thin B_6Si coat, unfired);
- Furnace No. 3 - $800^{\circ}F$ - Capsule AL-8 (thin B_6Si coat, unfired).

Each capsule was brought to temperature and allowed to stabilize for one hour. The operating parameters and weights were then recorded. This weight was then taken as the starting weight. All readings were taken and data recorded for each capsule at 24 hour intervals for several days and then at random time intervals thereafter, depending upon the rate of weight change of each capsule.

5.3.4 TEST RESULTS

Tests were performed on two coated B_6Si (unfired) capsules and one uncoated capsule in the first round, and the 0.0024 cm B_6Si coated and fired capsule in the second round.

Table 5-5 is a summary of the test results. Note that the $800^{\circ}F$ test of AL-8 exhibits an average percent weight loss per day of 0.089 while the uncoated

TABLE 5-5

SUMMARY OF TEST RESULTS

Capsule No.	Coated	Temperature	Hours at Temperature	Ave. Wt. Loss (%/day)	Total Wt. Loss %	Total Wt. Loss (gms)
AL-6	no	800 F	67	0.083	0.32	0.71
		1000 F	168	3.4	24.75	65.97
AL-3	yes (unfired)	1000 F	235	3.3	37.07	100.17
AL-8	yes (unfired)	800 F	1144*	0.087	5.35	14.77
AL-14	yes (fired)	800 F	316*	0.042	0.51	1.36

*Test continuing

AL-6 exhibited roughly the same rate of change. At first glance, the coating would appear to provide no protection for the graphite. However, a comparison of the data taken during the first 67 test hours of AL-8 with that of AL-6, reveals the average percent weight loss to be 0.028 vs 0.083 for the uncoated capsule. A similar situation is found to exist for AL-6 and AL-3 at 1000°F; i.e., the coated capsule has a lower rate of weight loss during the early test period.

The average weight loss for capsule AL-14 during the first 316 hours of test time in 0.042%/day and appears to be lower that that for AL-6 and 8.

Figures 5-15 and 5-16 show, in so far as possible, the rate of weight loss (%/day) as a function of time for both the 800 and 1000°F tests. Note that, while some anomalies exist, the trends are quite evident. The data plotted in Figure 5-15 is insufficient to obtain an accurate oxidation rate trend on capsule AL-6 at 800°F except to show that the rate is greater than that of capsule AL-8 and AL-14. This trend is not unexpected. The oxidation rate of capsule AL-8 appears to be decreasing but has not yet become constant. With regard to capsule AL-14, one can draw a curve based only upon the experience with capsule AL-8. The oxidation rate, for identical time periods is lower, but the definite trend has yet to be established.

Referring to Figure 5-16, the oxidation rate of AL-6 (uncoated) is lower above 160 hours of test time than capsule AL-3. Several explanations of this phenomena are possible:

- More surface area available for oxidation in AL-3 structure (lower density)
- Larger opening through plug/hanger seal area.

The most important point, however, is that the oxidation rate for both capsules is sufficiently rapid that no meaningful information would be gained by testing at higher temperatures.

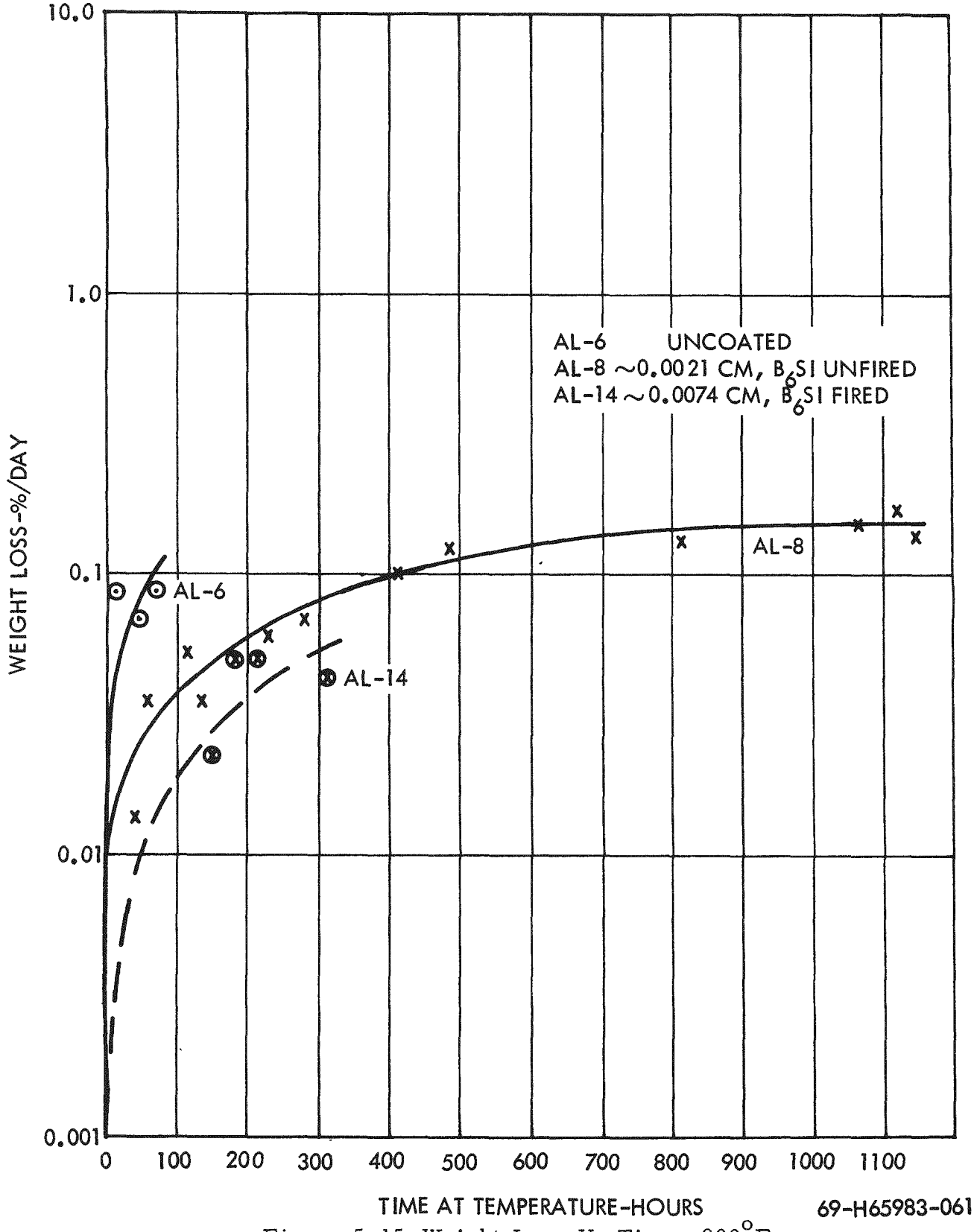

Figure 5-15 Weight Loss Vs Time, 800°F.

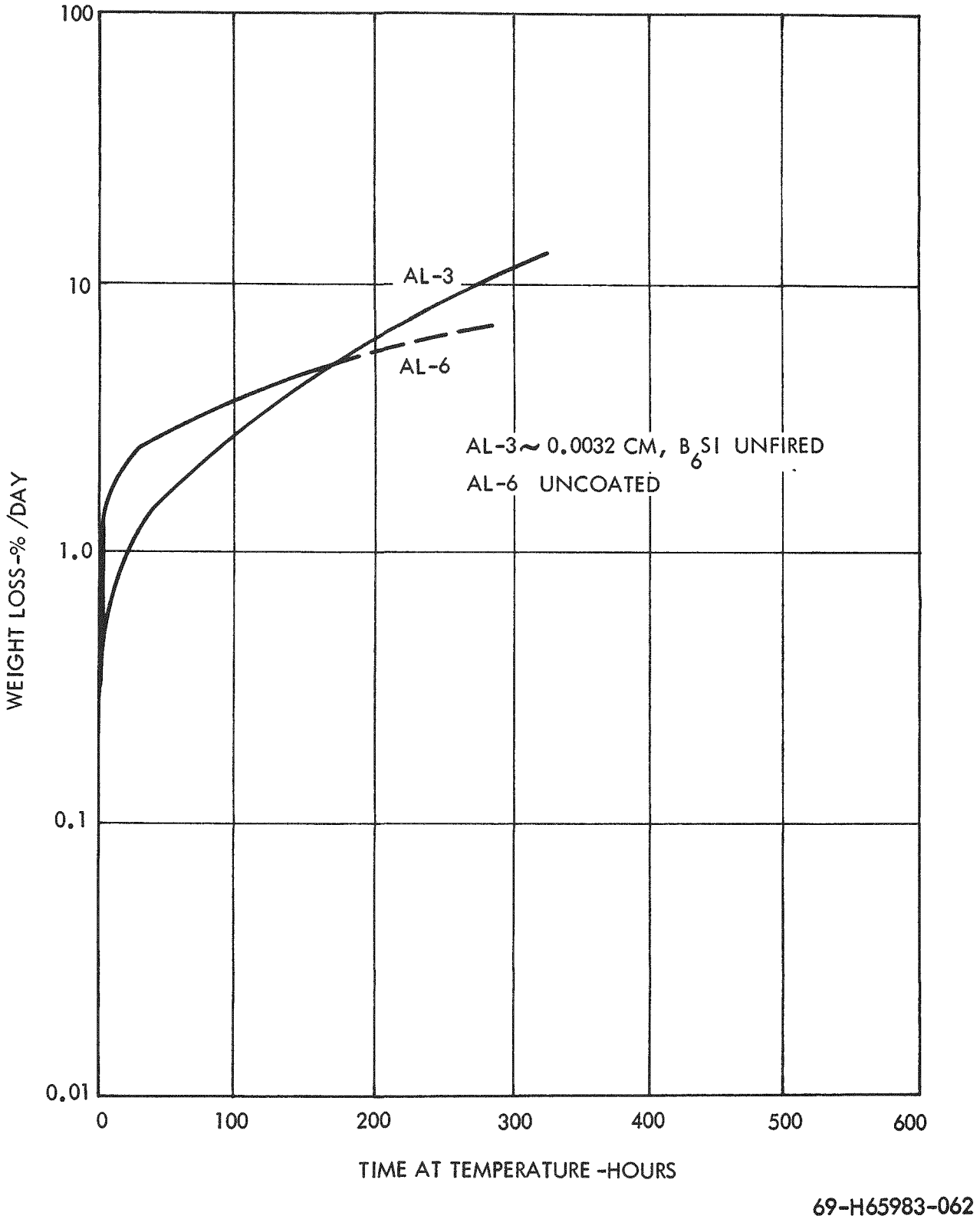

69-H65983-062

Figure 5-16 Weight Loss Vs Time, 1000°F.

Figures 5-17 and 5-18 show the condition of AL-6 and AL-3 after the 1000°F tests (uncoated and coated, respectively).

Two capsules were impregnated with a white epoxy ink, cut and polished for metallographic examination. The capsules used for this examination were AL-6 (no B_6Si coating, tested at 800° and 1000°F) and AL-20 (no B_6Si coating, no oxidation testing). Photomicrographs were taken and are shown in Figures 5-19, 5-20 (AL-6) and 5-21, 5-22 (AL-20).

Referring to Figures 5-19 through 5-22, note that the white epoxy ink is well distributed through the yarn. This suggests that the ink generally followed the yarn wraps, and seeped into the adjacent porous structure (pyrolytic carbon).

5.3.5 DISCUSSION

Referring again to Figures 5-15 and 5-16, the oxidation rates appear to be well established. The increasing rate of oxidation has been attributed to the change (increase) in surface area of the internal SIREN structure as the composite oxidizes. The boron-silicide coating (B_6Si) does generally inhibit this rate as indicated by the curves. The same general trend was exhibited in the 1000°F test also (AL-6 and AL-3), but above 160 hours of test time at temperature, the oxidation rates of the two samples cross over with AL-3 showing the more rapid rate of increase. Differences above this test time can most likely be attributed to differences in density (apparent) and, therefore, available surface area within the structure as indicated below:

Apparent Density (g/cc)

Time	AL-3	AL-6
Test start (0 Hrs)	1.437	1.431
48 Hrs	1.389	1.35
200 Hrs	0.8773	0.983 (from extrapolation)

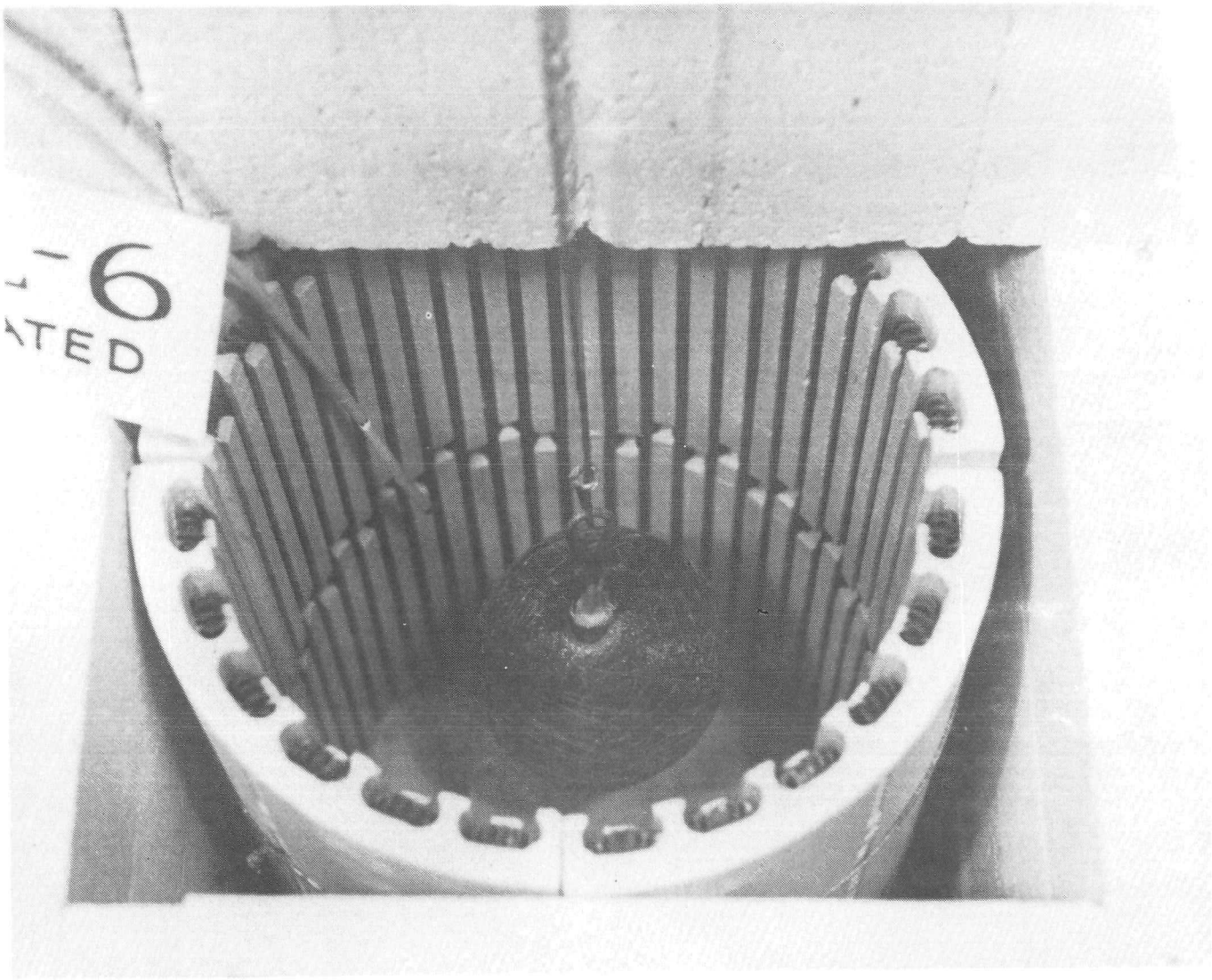

69-526-2

69-H65983-063

Figure 5-17 End of 800° and 1000°F Test on Uncoated Capsule

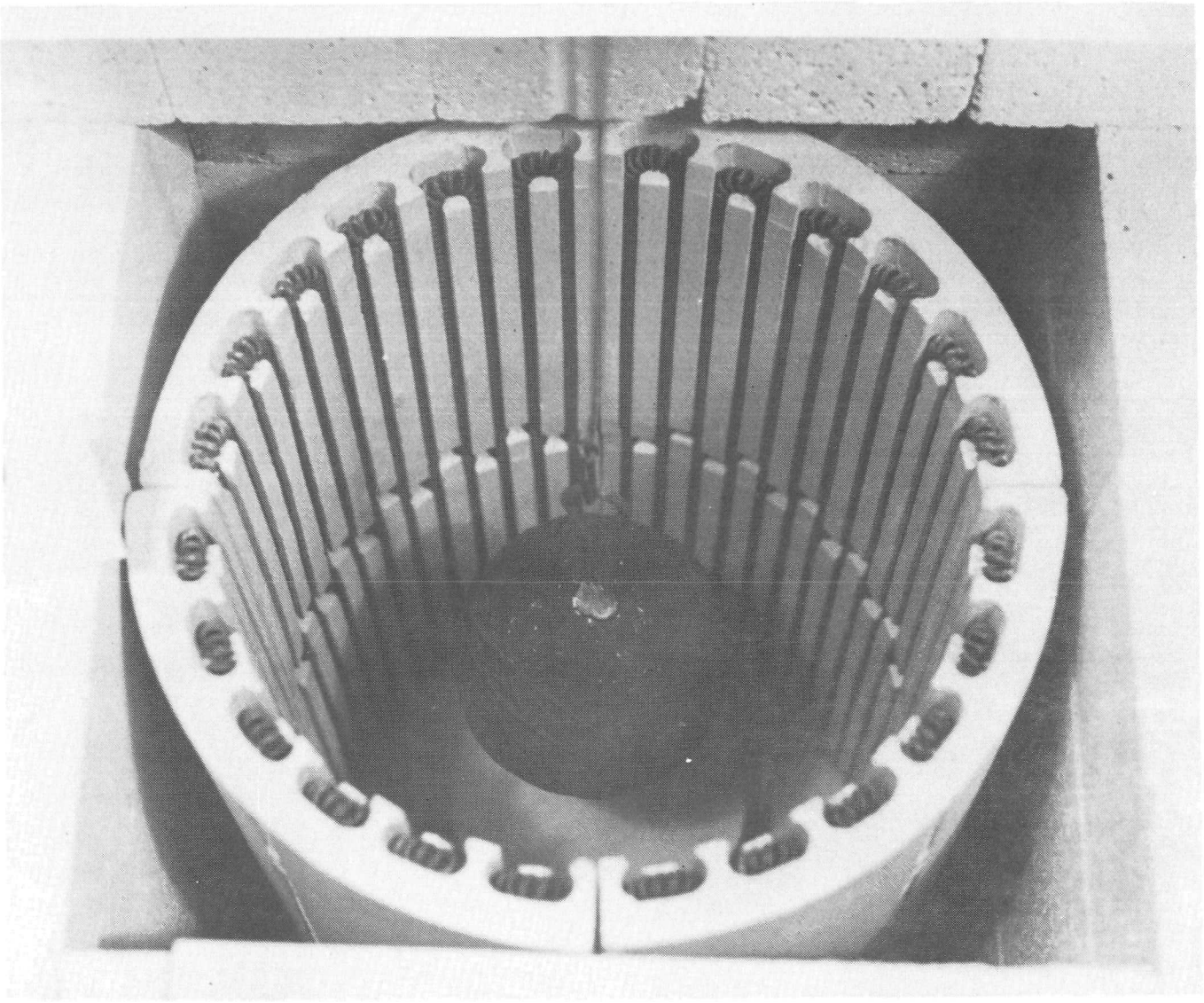

69-526-1

69-H65983-064

Figure 5-18 End of 1000°F Test on 0.0032 cm B_6Si (Coated Capsule, Unfired)

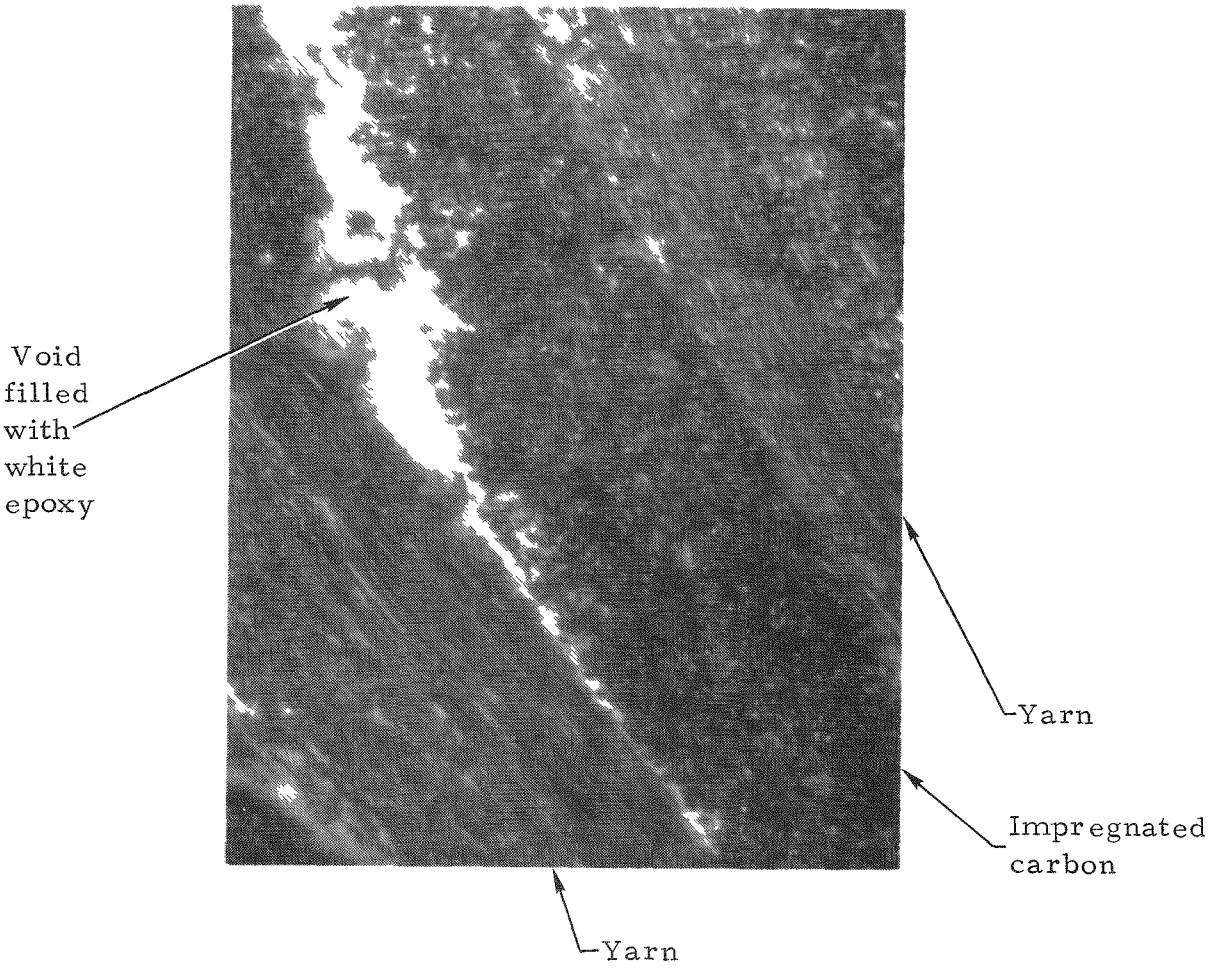

69-H65983-065

Figure 5-19 Section From SIREN Capsule AL-6 ≈ 100X Magnification. Section Shows Graphite Yarn Layer (Upper Right and Lower Left) and Pyrolytic Carbon (Center Section)

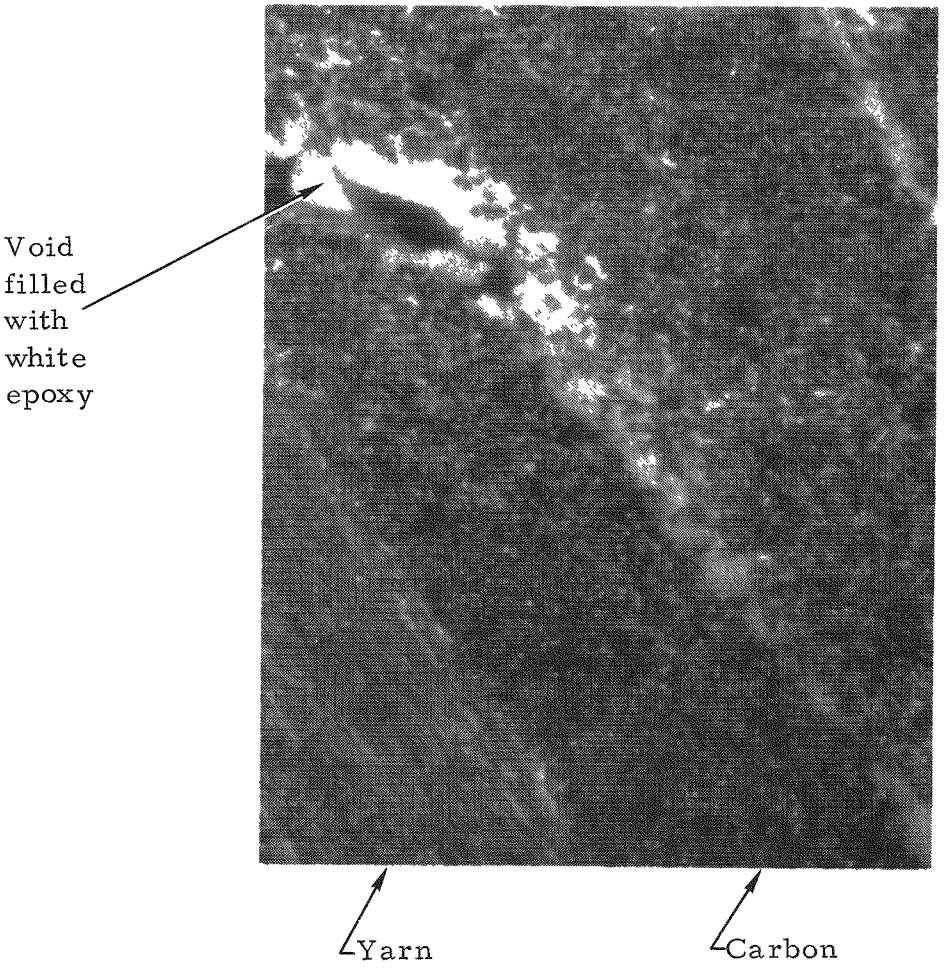

69-H65983-066

Figure 5-20 Section From SIREN Capsule AL-6 ≈ 100X Magnification. Section Shows Graphite Yarn Strands (Lower Left) and Pyrolytic Carbon (Remainder of Picture)

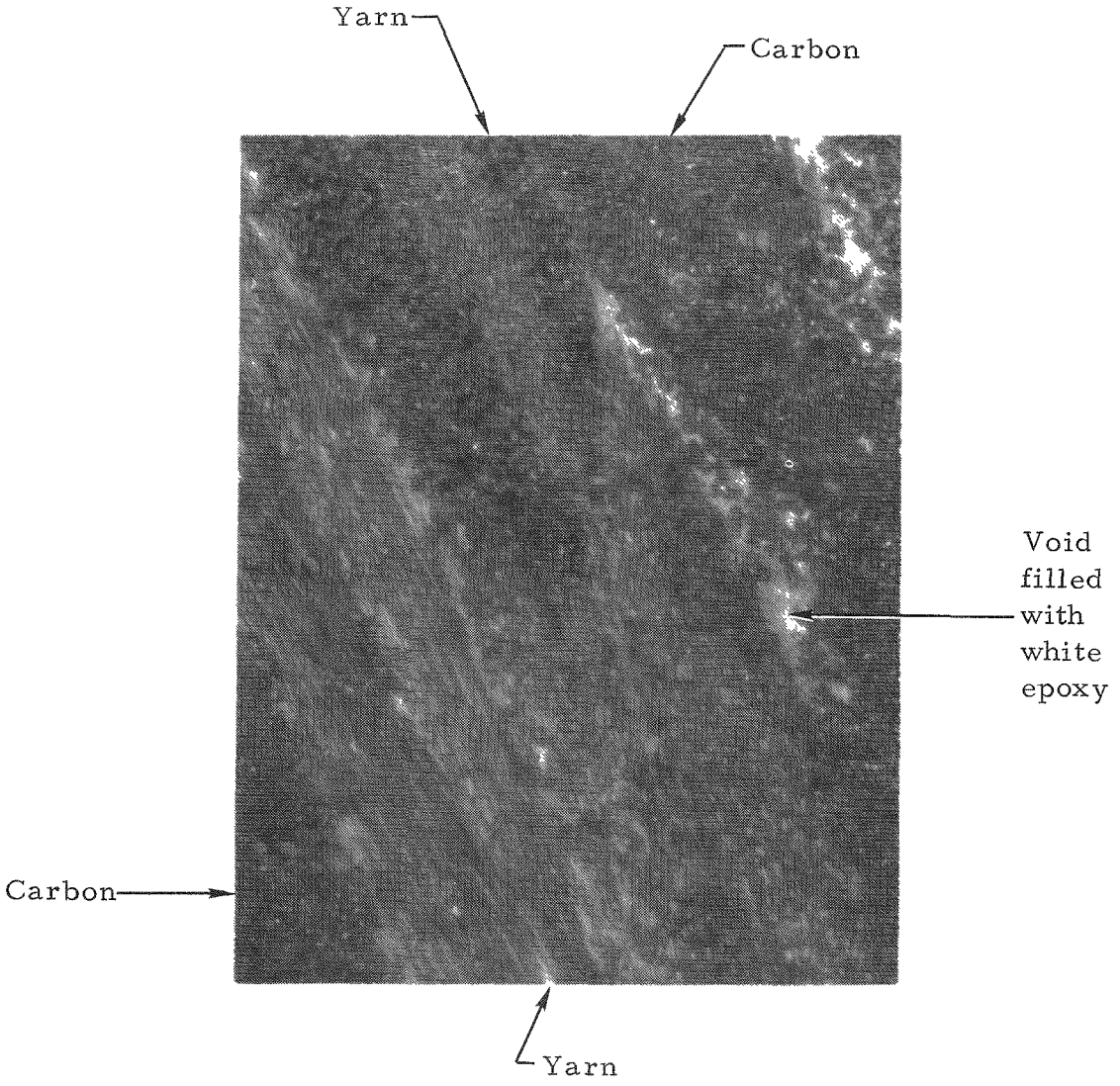

69-H65983-067

Figure 5-21 Section From SIREN Capsule AL-20 ≈ 100X Magnification. Section Shows Graphite Yarn Layers (Left Side and Center) and Pyrolytic Carbon (Lower Left and Upper Right)

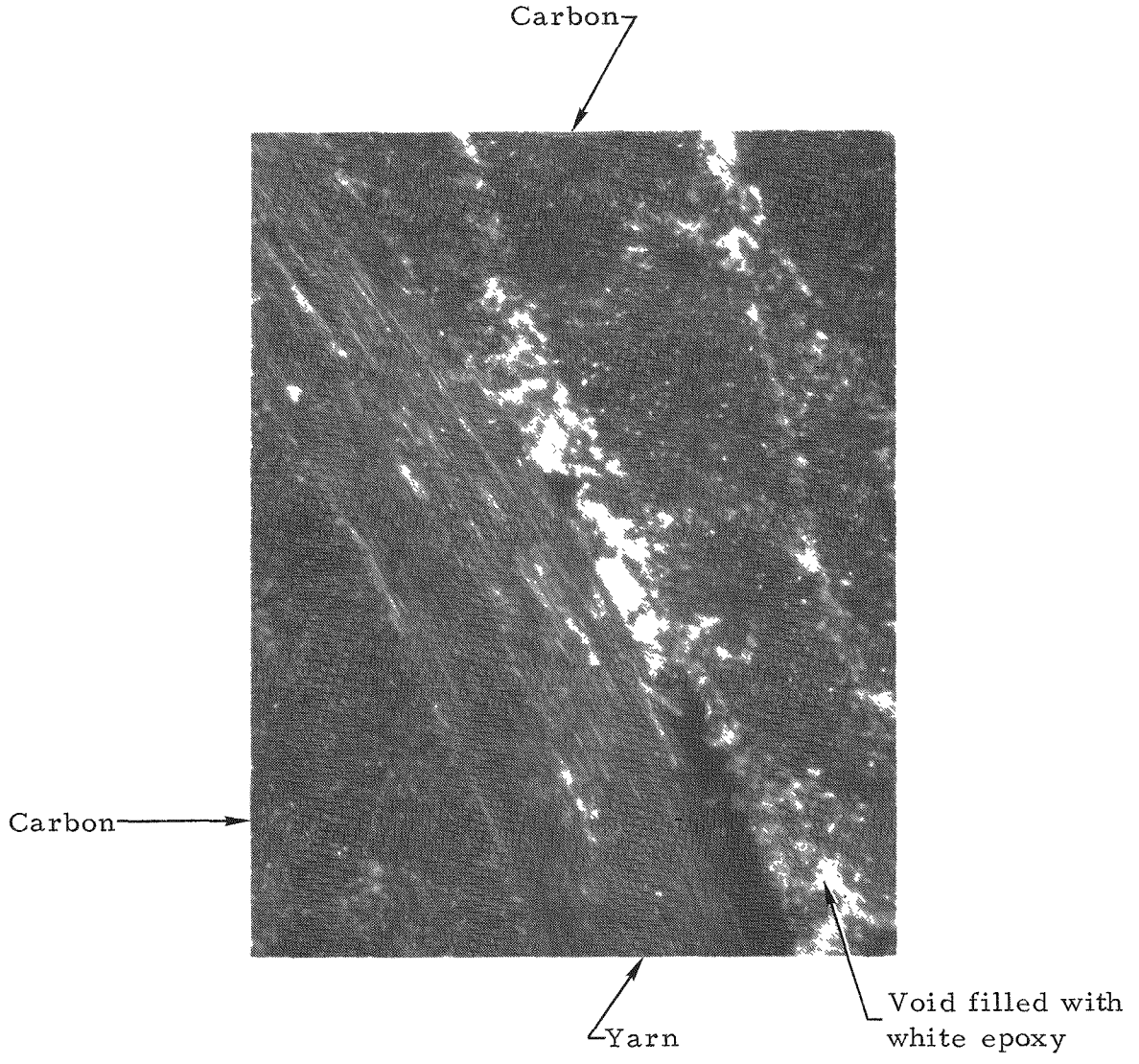

69-H65983-068

Figure 5-22 Section From SIREN Capsule AL-20 ≈ 100X Magnification. Section Shows Graphite Yarn Layers (Upper Left to Bottom Right) and Pyrolytic Carbon (Remainder of Picture)

Upon examining the cross-sections of capsules AL-6 and AL-20, tested and intested respectively, (refer to Figures 5-19 through 5-22), it would appear that there is very little difference in the pore structure and size of the two capsules. Based on these observations it can be assummed that the mass loss due to oxidation was along the original void structure, that is, voids parallel to the lay of the yarn. Also, the data show that the mass loss due to oxidation was not a surface effect, but rather a volume effect.

In Figures 5-17 and 5-18 (note that the seal plug and SIREN capsule structure around the hanger has opened up considerably in the uncoated capsule compared with the coated capsule. It would appear that the effect of the coating has been to give considerable protection to the outer wrap of graphite yarn. The increased degradation around the plug/hanger-capsule interface indicates special attention is required for those capsules containing joined graphite components; i.e., a plugged fueling port.

With regard to capsule AL-14 (0.0074 cm fired B_6Si coating) some oxidation rate is evident as indicated in Figure 5-15. The coating did not provide as complete a seal on the graphite as the literature[1] would seem to indicate. Figure 5-23 is reproduced from Reference 1 to show the effect of a fired B_6Si coating on solid graphite. Each point represents one hour of test time at a specific temperature. Figure 5-24 shows the oxidation rate data of capsules AL-8 and 14 replotted to show the percent weight change relative to initial weight as a function of time. Because of scale differences, small changes in weight will be insignificant when plotted to the same scale used in Figure 5-23. Colton[1] states there was "---no appreciable weight loss on subsequent heat treatments because the protective boron-silicon-oxygen coating had formed." Optimization of the coating and firing technique on the SIREN capsule should achieve oxidation prevention results similar to those experienced by Colton on solid graphite.

Figure 5-25 shows the oxidation rate as a function of temperature for pure and commercial graphites[2] and includes the average %/day weight loss data on

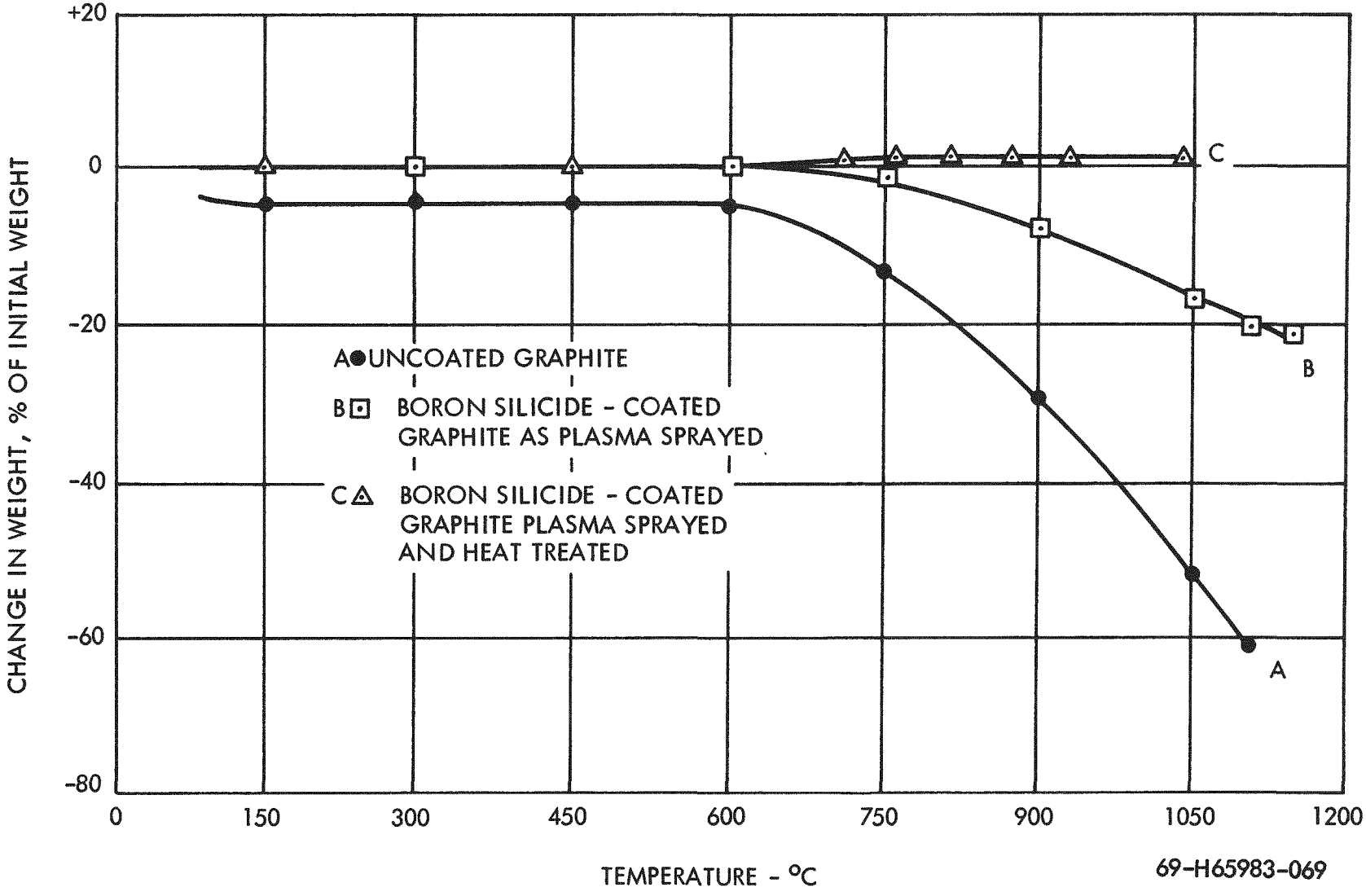

OXIDATION OF GRAPHITE AND BORON SILICIDE (B_6Si) COATED GRAPHITE IN STAGNANT AIR

REPRINTED FROM PATENT 3,275,467 "COATED GRAPHITE AND METHOD OF COATING" E. COLTON

*Figure 5-23 Oxidation Rate of Graphite Coated With B_6Si as a Function of Temperature (°C)

SANDERS NUCLEAR CORPORATION

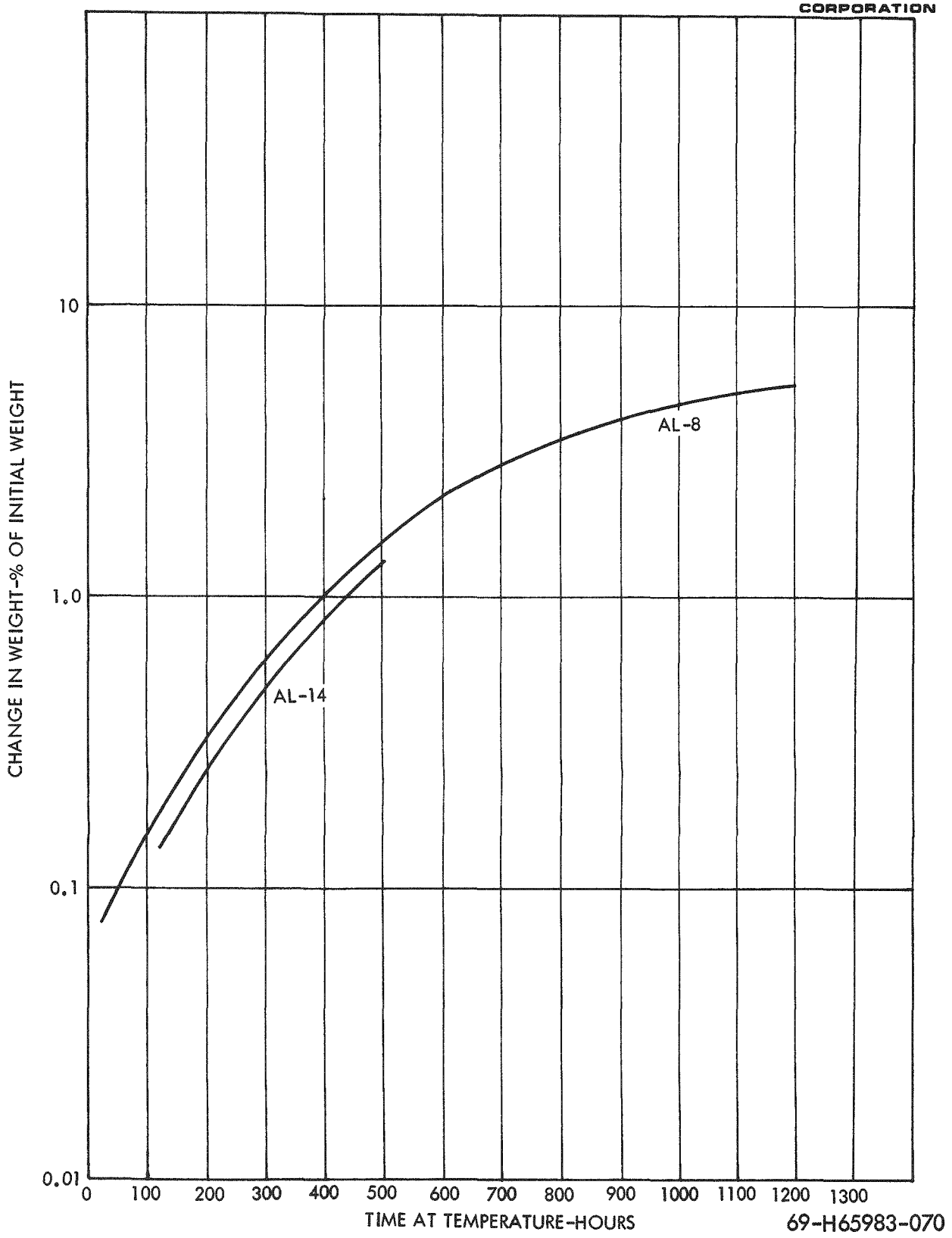

Figure 5-24 Change In Weight Percent of Initial Weight Vs Time at Temperature

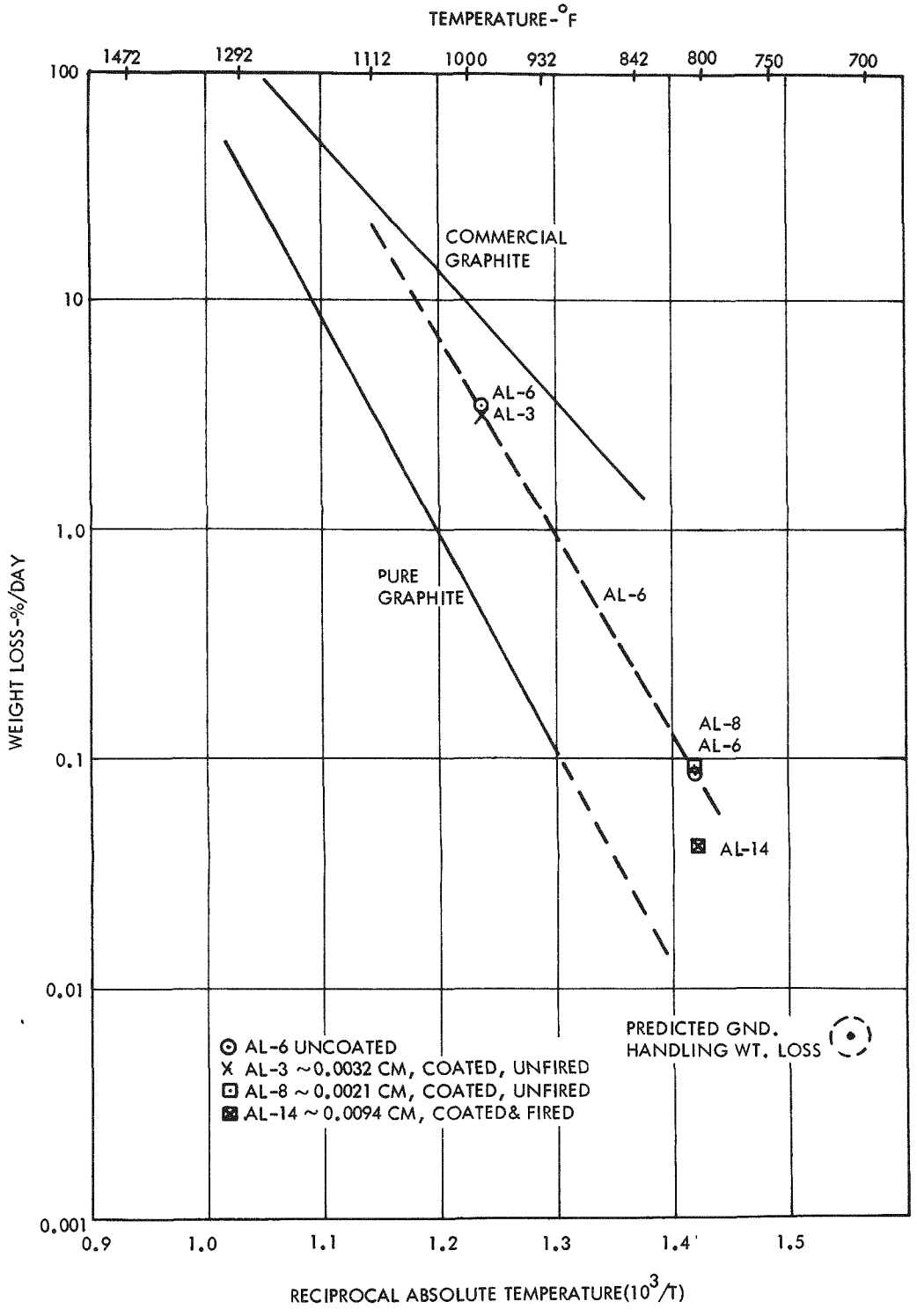

69-H65983-071

Figure 5-25 Comparison of Oxidation Weight Loss (% / Day) Vs Reciprocal Absolute Temperature for Graphites and SIREN.

the uncoated and B_6Si coated capsules for comparison. The similarity of slopes for the AL-16, pure graphite and commercial grade graphite indicates the B_6Si coating had not altered the activation energy of oxidation of the graphite, and hence it can be concluded the coating had not formed a complete seal about the graphite. The data generated by Colton[1] (shown in Figure 5-23) indicates that "complete" protection can be obtained through the use of appropriate thickness and firing of the B_6Si coating. The position of the curve indicates that the uncoated capsule oxidation rate does indeed fall between that of commercial and pure graphites.

In retrospect, it must be noted that the B_6Si coating need only reduce the oxidation rate of the graphite SIREN structure such that the total weight loss is of the order of perhaps 2% or less over a 6 month storage period. Looking at the problem in another way; it is questionable whether an oxidation resistant coating is even required if adequate cooling is provided during storage periods. Assuming the capsule temperature is maintained at or below 700°F during the ground handling portions of the mission Figure 5-24 may be used to approximate the percent weight loss. This rate is 0.0065% per day or 0.2% over a six month period. Such a loss appears to be satisfactory from an operational standpoint.

5.3.6 RECOMMENDATIONS

It is recommended that the present task being conducted on capsules AL-8 and 14 be continued well into Phase II so that accurate comparisons of oxidation rates can be obtained. It is further recommended that sufficient experimentation be performed to optimize the B_6Si coating thickness and firing schedule (using the Colton patent as a basis in both cases) required to achieve an oxidation resistant coating. The oxidation test temperature in future work should be limited to that which calculations show will be the maximum "in air" operating temperature plus some reasonable safety factor.

5.3.7 REFERENCES

1. Patent 3,275,467, "Coated Graphite and Method of Coating", E. Colton, April 26, 1963.

2. Carbon and Graphite Handbook, Mantell, 1968.

5.4 HELIUM PERMEABILITY OF THE SIREN CAPSULE

5.4.1 INTRODUCTION

This section discusses the test procedure, conditions and results of helium, nitrogen and argon gas permeability tests performed on the SIREN graphite yarn wound, pyrolytic carbon impregnated structure.

The requirement for such a test is necessitated by the nature of the fuel ($Pu^{238}O_2$) in that at highly elevated temperatures, helium generated by alpha decay is released. This is particularly true of the condition imposed by the reentry heat pulse.

Because the gas permeation characteristics were completely unknown, the test procedure was written in a manner which gave the test engineer sufficient latitude to modify the test program as necessary in order to carry out the test objectives.

The objectives for this program are to:

- Determine the helium permeation rate in $cc/sec\text{-}cm^2$ for at least two uncoated SIREN capsules
- Determine the effect of SIREN structure density on permeation rate.

The objectives were attained with the addition that one ≈ 0.003 cm B_6Si coated but unfired capsule was tested with helium, argon, and nitrogen.

5.4.2 CAPSULE DESCRIPTION

The SIREN capsules used for the helium permeability test consisted of graphite yarn wound over a 2-inch O.D. hollow aluminum sphere to a diameter of approximately 3-1/8 inches. A small hole was drilled through the winding and aluminum core to permit etching out the aluminum core prior to impregnation with pyrolytic carbon.

Three capsules, fabricated in the manner described above, were selected for the helium permeability tests. One of these was prepared by enlarging the hole (mentioned above) to accept a 3/4-inch copper tube. The tube was cemented in place with epoxy resin as described in test procedure SNP100030. The remaining two were held for testing by whatever final procedure was determined.

One additional capsule was selected after impregnation and plasma flame sprayed with boron silicide (B_6Si) to a thickness of approximately 0.003 cm. The coating was not fired.

5.4.3 TEST DESCRIPTION AND RESULTS

A single SIREN capsule, AL-18, was prepared for trial number 1 in accordance with procedure SNP100030 (see Appendix II) and connected to the CEC leak detector (Model 24-120B) roughing manifold and the roughing pump started. It was impossible to obtain a vacuum because of the extensive influx of air so the test was discontinued.

The capsule was connected by means of the previously installed tubulation to a helium supply for a rough check of helium flow prior to initiating the detailed requirements of trial number 2 as outlined in the procedure. Ample helium flow rates were obtained with relative ease. To determine how the gas was escaping from the capsule, it was immersed in a beaker of water as shown in Figure 5-26 for a bubble test. Figure 5-27 shows the manner in which the gas emerged from the capsule. As indicated in the photograph, the bubbles appear to be generated fairly uniformly around the structure.

The test setup was then modified as shown in Figure 5-28 in order to measure the pressure as well as the flow rate as referenced by procedure SNP100030. Data were then taken to determine the flow rate as a function of pressure. SIREN capsules AL-19 and 20 were then prepared to accept a 3/4-inch pipe by drilling and tapping the capsule structure. A minimum amount of epoxy cement was used to seal the thread area.

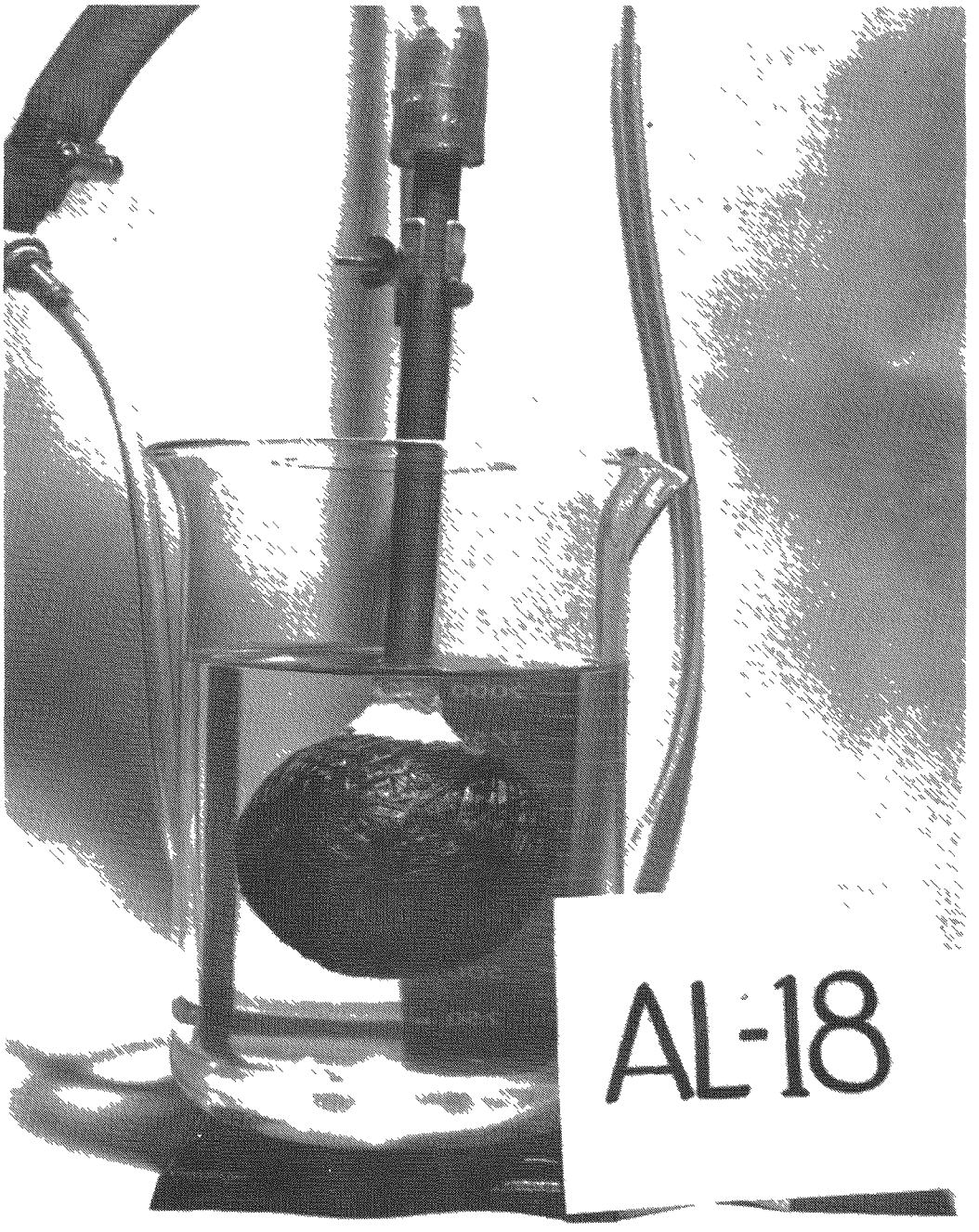

69-444-2

69-H65983-005

Figure 5-26 Helium Bubble Test Setup.

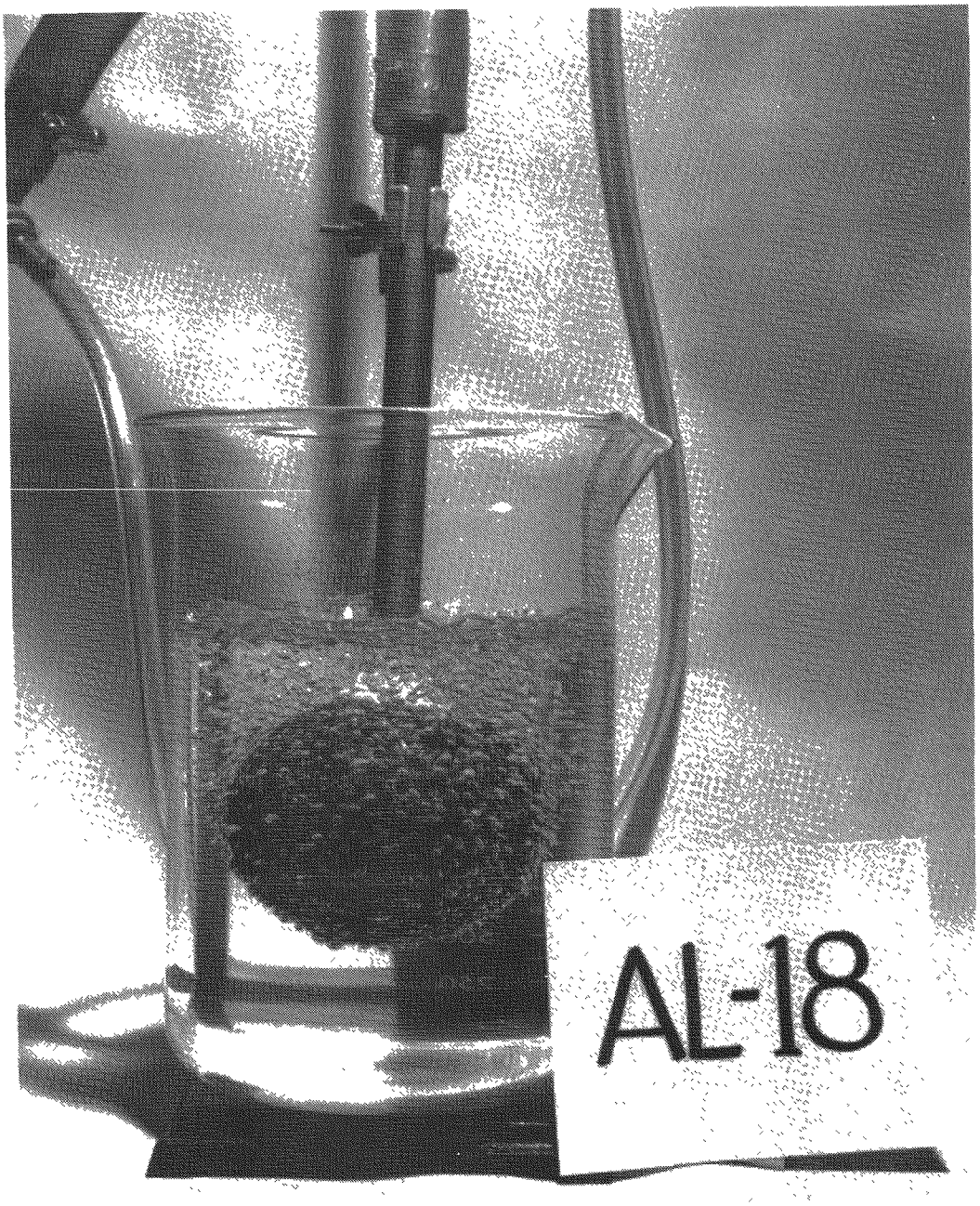

69-444-3

69-H65983-006

Figure 5-27 Helium Bubble Test.

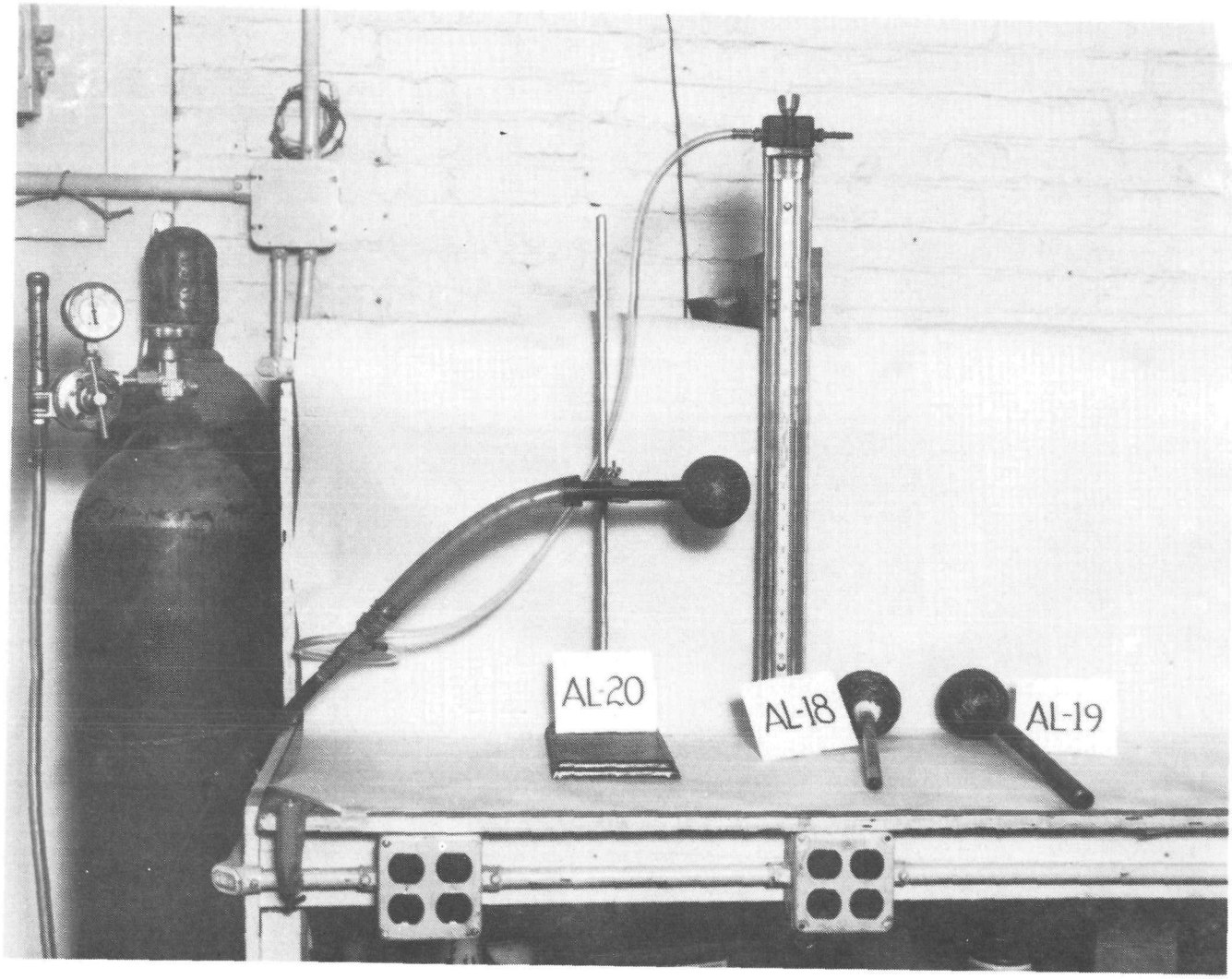

69-444-1

69-H65983-007

Figure 5-28 Helium Permeability Test Setup.

The test data results were plotted and are shown in Figures 5-29 and 5-30 for capsules AL-19 and 20, respectively. Figure 5-31 is a plot of permeation rate versus pressure.

A boron silicide coated capsule (AL-13) (≈0.003 cm coating, unfired) was tested in the same manner as AL-19 and 20 using helium, nitrogen, and argon. The results of this test are depicted in Figure 5-32.

5.4.4 DISCUSSION

Referring to Figures 5-29 and 5-30, one notes that the permeation rates differ. This is due to the differences in capsule density as noted below:

Capsule No.	Slope (SCFH/in. of Hg)	Density (g/cc)
AL-19	3.03	1.53
AL-20	4.55	1.38

The ≈0.003 cm unfired B_6Si coated capsule (AL-13) gas flow rate was measured for three gases. The results, as plotted and depicted in Figure 5-32 or helium, argon, and nitrogen show that the gas permeation rate through the SIREN structure and coating, depends primarily upon the viscosity of the gas. Nitrogen, having a viscosity of 180 micropoise exhibits a higher flow rate for the same pressure than does helium (194 micropoise) or argon (220 micropoise). Secondary effects, relating pore and/or channel geometry in the SIREN graphite structure and type of flow (viscous, viscous with slip, laminar, turbulent, etc.) will alter the relative positions and slopes of these curves.

Making a comparison of the slopes and densities of capsules AL-13 and 19, one finds the following relationships:

Capsule No.	Slope (SCFH/in. of Hg)	Density (g/cc)
AL-13	2.96	1.52
AL-19	3.03	1.53

SANDERS NUCLEAR CORPORATION

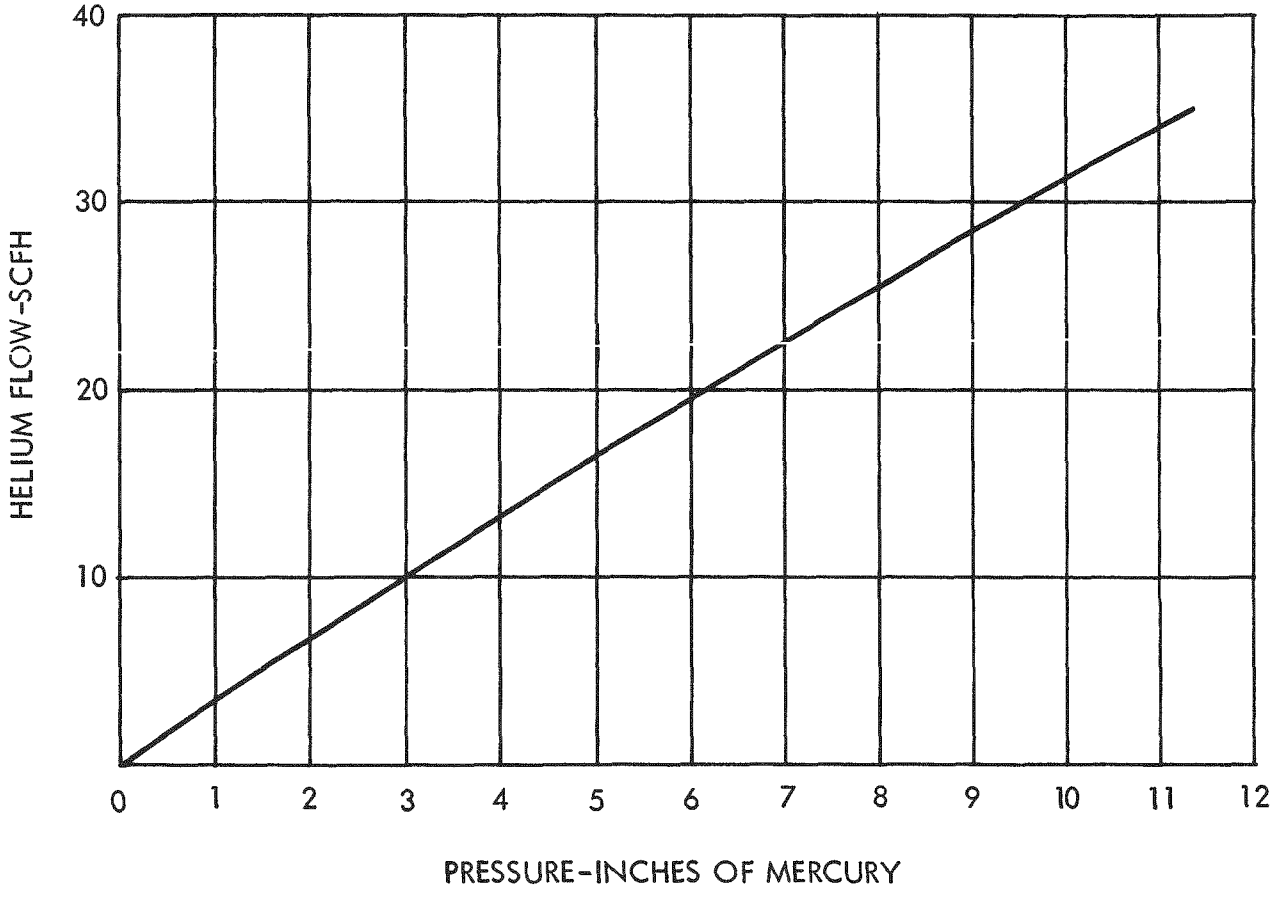

69-H65983-008

Figure 5-29 Helium Permeability Test, SIREN Capsule AL-19, 22 April 1969.

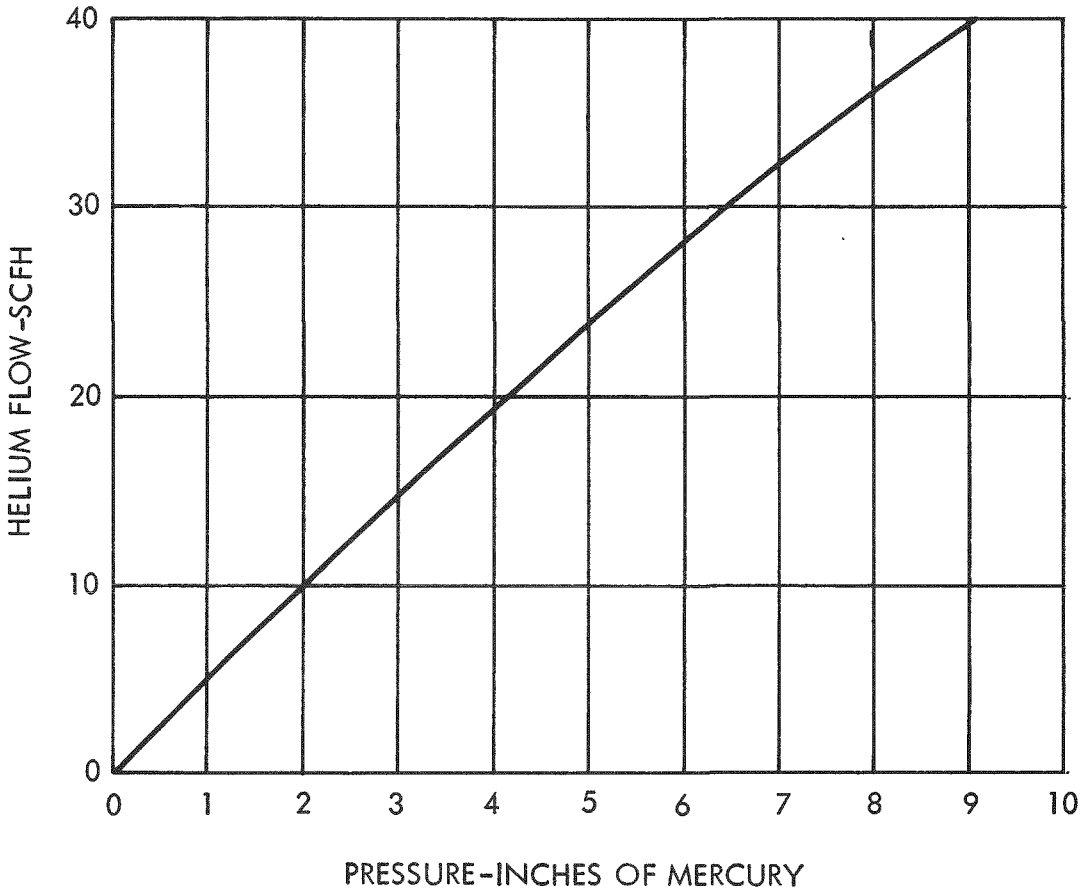

69-H65983-009

Figure 5-30 Helium Permeability Test, SIREN Capsule AL-20, 22 April 1969.

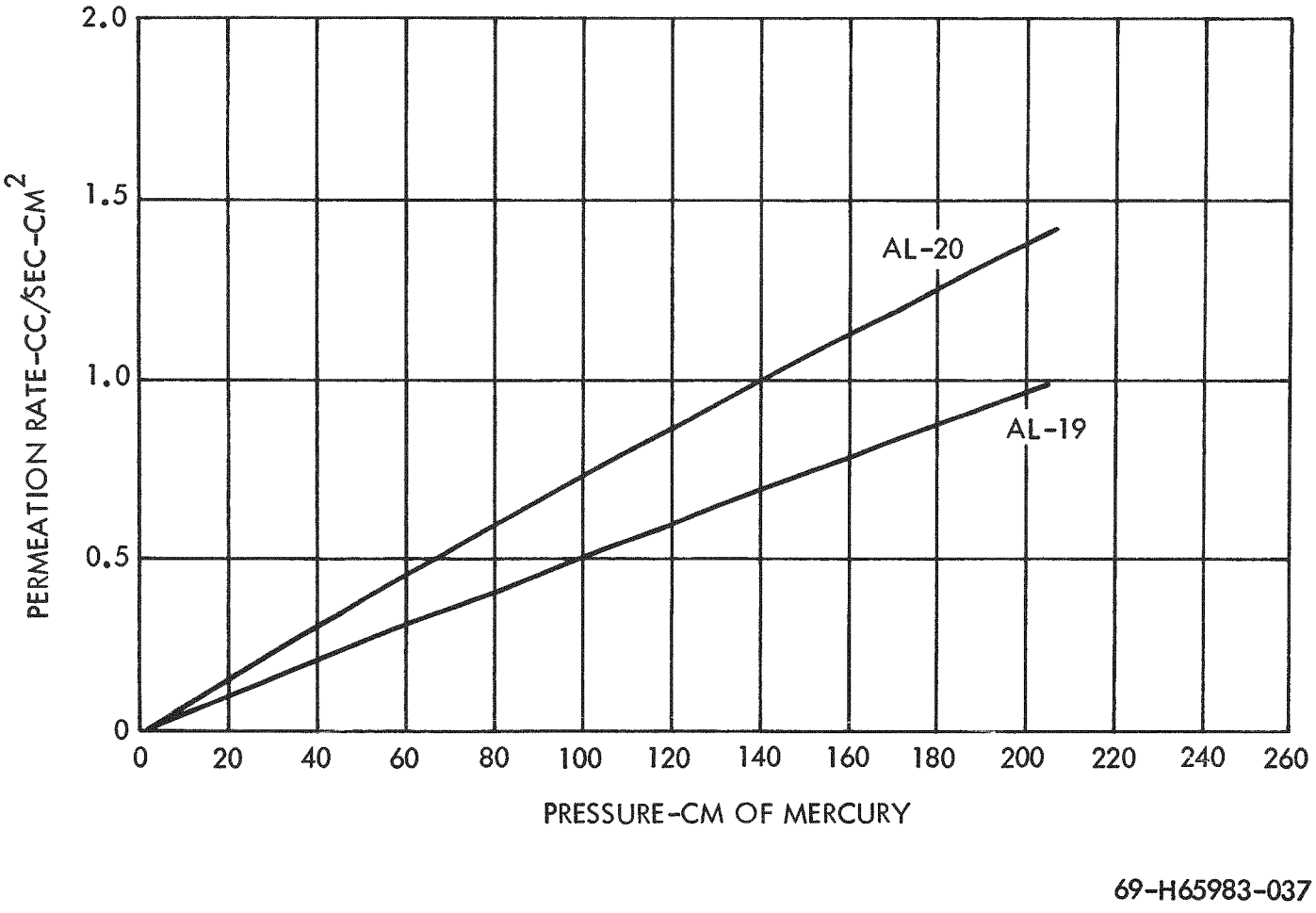

Figure 5-31 Helium Permeability Test, SIREN Capsules AL-19 and AL-20, 12 June 1969.

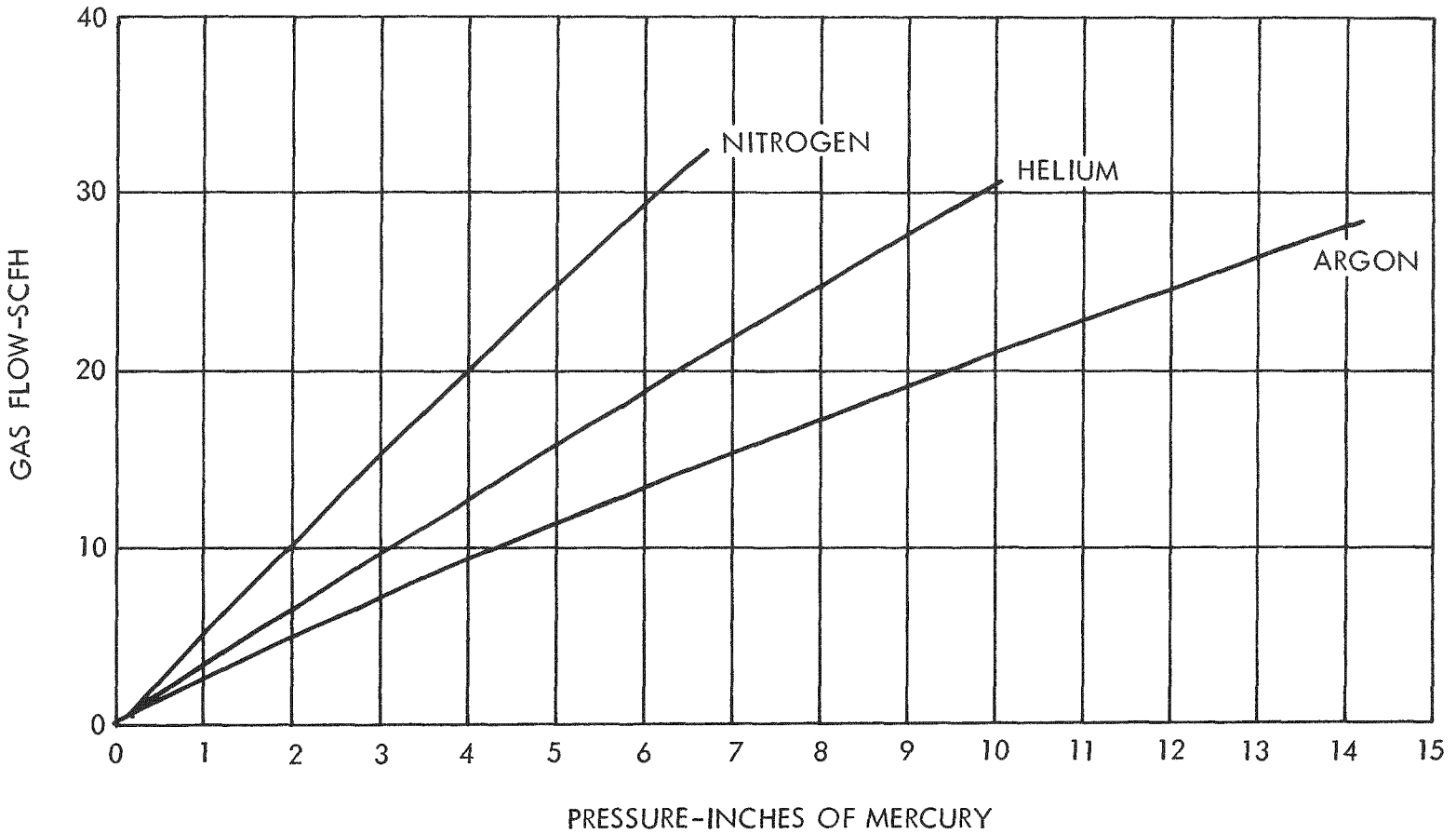

69-H65983-038

Figure 5-32 Permeability Test, SIREN Capsule AL-13, (B_6Si Coating, Unfired), 12 June 1969.

According to the density relationship previously stated, however, capsule AL-13 should have had a slightly higher slope than capsule AL-19 (assuming the density figures are significant). The effect of the unfired coating would appear to be that of impeding the gas flow rate somewhat as exemplified by the lower slope of flow rate versus pressure.

The significant points relative to the helium permeability of SIREN capsule structure are as follows:

- The structure is permeable to helium and other gases; therefore, helium release during the peak heating pulse from reentry condition should present no problem.
- The helium permeation rate is a function of both pressure and SIREN graphite structure density.
- The gas flow rate through the SIREN graphite structure is a function of pressure and gas viscosity.

5.4.5 RECOMMENDATIONS

During the next phases of the SIREN program it is recommended that helium and oxygen permeability studies be performed on improved graphite structures containing candidate liners. Possibly the permeation rate test could be used in the characterization of the combined effect of density and void volume during development of improved graphite structures. Determination of rates of permeation of oxygen through liners would allow prediction of the oxygen stability of the fuel material.

The effect of any oxidation prevention coating on the helium permeability of the structure should be measured at elevated temperatures so that the effect on helium release during reentry conditions can be ascertained.

BLANK

5.5 IMPACT AND PLASMA ARC TESTS

5.5.1 INTRODUCTION

Six SIREN test capsules having Al_2O_3 center cores and 0.5 inch thick carbon/carbon walls were impacted at the Sandia Corporation, Impact Test Facility. Impact velocities ranged between 210 and 352 ft/sec. During impact the graphite was removed from impact area, exposing the Al_2O_3 core. The amount of core exposure increased with increasing impact velocity.

To achieve the required terminal velocities, the Sandia sled-track facilities were employed. A total of eight impact tests were conducted: two on Al_2O_3 spherical center cores and six on SIREN capsules fabricated with the same type of central cores.

The tests were performed by mounting the test specimen at a fixed location above the track and bringing the rocket sled with a 12 in. x 12 in. x 12 in. granite block mounted on it, into contact with the specimen. Because of the recoil velocity of the specimen after impact, an impact angle of five degrees from the normal to the granite surface was specified to prevent capsule escapement after impact. Five degrees from the normal resulted in an actual normal impact velocity of 0.996 of the oblique velocity.

The impact tests characterized the energy absorption capacity peculiar to the SIREN carbon/carbon wall structure as was fabricated for Phase I. Observation of the capsules after impact enabled insight into the mechanism of component failure, thereby defining direction of further development.

Three SIREN capsules, similar to those used in the impact test, were tested in the Sandia Plasma Arc Facility. Test conditions simulated a typical non-spinning orbital reentry and a non-spinning 36,000 ft/sec superorbital reentry at -6 degrees. Capsule test exposure was determined with the aid of data from the reentry analysis. Two capsules were tested at orbital reentry conditions and one at superorbital

conditions. Surface recession data from the plasma arc tests were in good agreement with calculated values. For the orbital reentry condition, stagnation point recession was 0.174 inch and 0.196 inch for the two capsules tested. Superorbital recession was 0.288 inch.

Specifications for the impact and plasma arc tests were arrived at after considerations had been given to the following functions:

- Review of the aerodynamic analysis portion of the SIREN program
- Realization that Phase I was designed to determine feasibility of the SIREN concept
- Time period for Phase I testing after fabrication of the capsules was less than two months
- The capsules that were to be tested did not exactly duplicate weight and structure of a fueled capsule
- Tasks performed under Phase I should be comparable in sophistication
- The three-inch diameter capsules to be tested did not necessarily represent an optimum mission design
- Test facilities were limited to those available at Sandia Corporation.

5.5.2 PROCEDURES AND RESULTS

5.5.2.1 Impact Tests

The characteristics of the capsules tested were:

- SIREN design (see Figure 5-33)
- 3.0-inch outer capsule diameter
- 0.50-inch thick wall made of graphite yarn impregnated with carbon

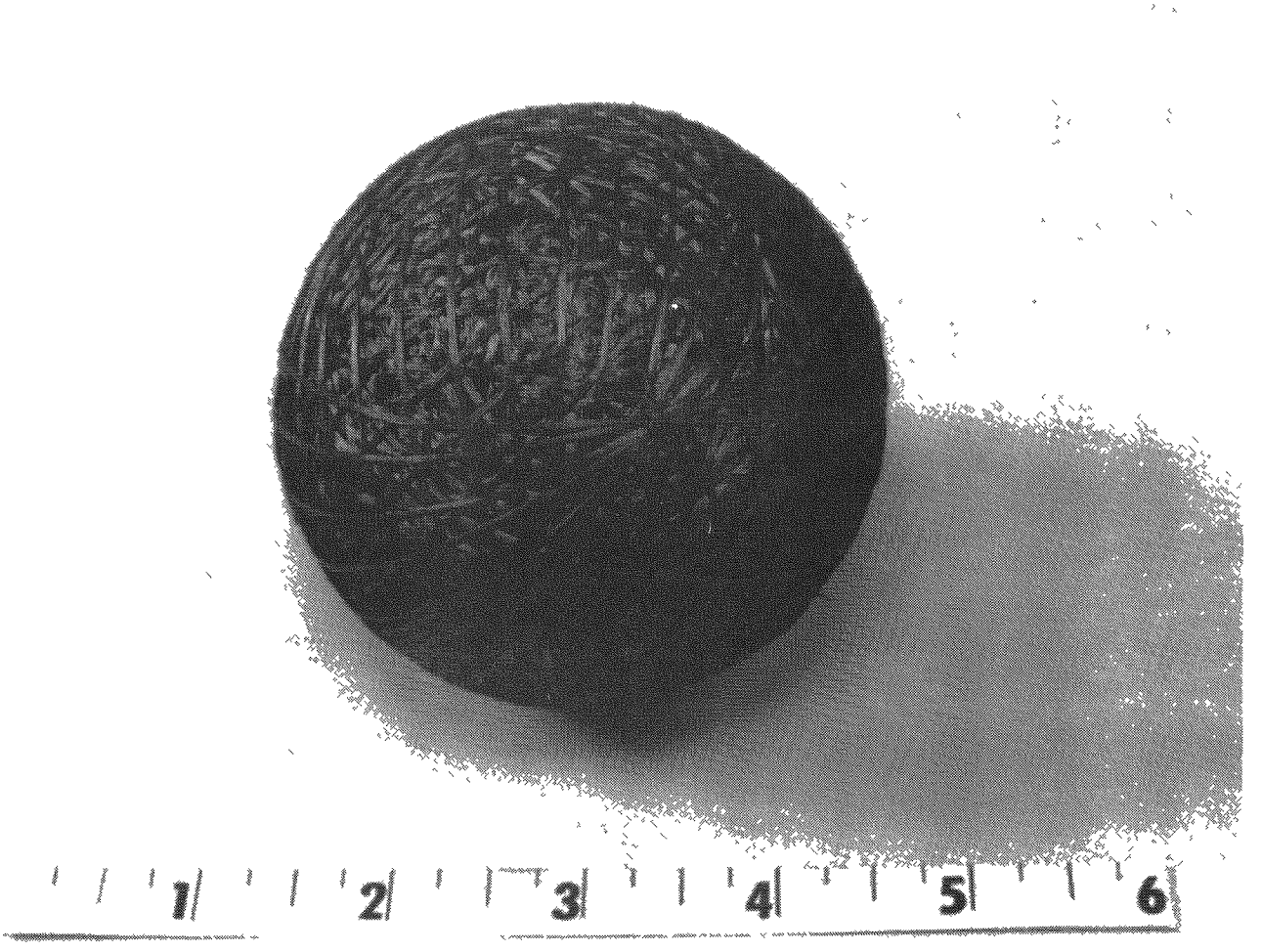

69-311-1

69-H65983-103

Figure 5-33 Three-Inch Diameter SIREN Capsule.

- Al_2O_3 core material of 2.0 inch diameter coated with 0.006 inch of ZrO_2
- Total test capsule weight of approximately 525 grams.

Six SIREN capsules were impact tested at velocities ranging between 210 ft/sec and 352 ft/sec. This velocity range was not necessarily indicative of a 3-inch dimater SIREN capsule; instead, the velocities were chosen because they were more representative of terminal conditions that would occur for SIREN capsules optimized for mission use. That is, an actual mission capsule design should be maintained which will insure the existence of a laminar boundary layer prior to impact. For a 1.60- and 2.50-inch diameter capsule design, the boundary layer remains laminar and thus results in relatively low terminal velocities as indicated in the comparison of Table 5-6. For the 3-inch diameter design, as analyzed during Phase I, the boundary layer could be either laminar or turbulent depending upon the oblateness and surface roughness after reentry. Turbulent flow over the 3-inch diameter capsule could result in terminal velocities as high as 500 ft/sec.

Table 5-7 gives the impact velocities, impact temperature, and the results of impact for the six capsules tested. In addition, the data resulting from impact tests on two Al_2O_3 spheres are presented.

All six capsules had the center core exposed to some degree after impact. In general, the higher the impact velocity the greater the center core exposure after impact. With the exception of Test No. 379, all center cores came through impact undamaged. Impact Test No. 379 (heated to 1500°F) caused the center core to shatter at 350 ft/sec impact velocity.

Both bare Al_2O_3 spheres (one at 255 ft/sec and one at 256 ft/sec) shattered at impact. One sphere was impacted at ambient temperature and one was impacted at 1500°F. Both spheres broke into 5 or 6 large pieces.

TABLE 5-6

SIREN CAPSULE DESIGN CHARACTERISTICS

Capsule Diameter (inches)	Fuel	Graphite Thickness (inches)	Capsule Weight (lb)	Projected Area (ft^2)	C_D	W/C_DA (lb/ft^2)	V_t (ft/sec)
1.6	$Pu^{238}O_2$ microspheres	0.250	0.260	0.01395	0.3	62	230
2.5		0.390	1.210	0.0341	0.27	132	334
3.0		0.500	1.635	0.0492	0.1 to 0.2	332 to 166	300 to 500

TABLE 5-7

SIREN IMPACT TEST RESULTS SUMMARY

Track Test No.	Date	Unit No.	Impact Velocity (ft/sec)	Capsule Temp. at Impact, ^{o}F	Results
373	5-20-69	Al_2O_3 sphere	255	Ambient	Al_2O_3 shattered
374	5-20-69	Zr-6	250	Ambient	Graphite removed from impact area (70^{o} cone angle) Al_2O_3 exposed but unmarked. Graphite cracked on side opposite impact.
375	5-20-69	Zr-8	210	Ambient	Same as Test No. 374 except 60^{o} cone angle. No cracking on side opposite impact.
376	5-21-69	Zr-10	352	Ambient	Same as Test No. 374 except 100^{o} cone angle. Also had back-side graphite lamination and separation.
377	5-21-69	Zr-5 (with plug)	255	Ambient	Same as Test No. 374.
378		Zr-7 (with plug)	250	$1500^{o}F$	Same as Test No. 374. No graphite cracking on side opposite impact.
379		Zr-9	350	$1500^{o}F$	Core shattered - total graphite separation.
380		Al_2O_3 sphere	256	$1500^{o}F$	Al_2O_3 shattered

Figure 5-34 is a photograph showing the Sandia Corporation Sled-Track Facility. The impact area is enclosed within a plexiglass housing. The capsule entry point, slightly larger than the outer diameter of the capsule, appears at the left of the impact chamber and the rocket motors to the right of the sled.

Figures 5-35, 5-36, and 5-37 show the capsule mounting technique for the unheated and heated cases. Radiant heating was used for the heated specimens and was accomplished by lowering the heater enclosure (shown in Figure 5-36) over the specimen. Argon was allowed to flow into the heater enclosure during heating to prevent capsule oxidation. After equilibrium heating had been accomplished the heater enclosure was removed and the specimen impacted.

Figures 5-38 through 5-43 are photographs of the six SIREN capsules after impact. Figure 5-44 shows the four unheated capsules after impact. Capsule Zr-5, in Figure 5-44, had a graphite plug placed 180 degrees from the impact point. The plug duplicated to some degree a plug that may be required after fueling with microspheres. The carbon/carbon material showed small cracks around the plug after impact, but the plug remained firmly intact.

Examination of the six impacted capsules suggested that the kinetic energy absorbed by the capsule at impact manifested itself in three unique regions within the carbon/carbon material. Directly after impact the capsule assumes a shape similar to that shown in Figure 5-45. In this condition, the volume of the carbon/carbon material is approximately the same as the volume of the material prior to impact. Consequently, the surface area per layer of material increases to accommodate the geometrical diversion from the spherical shape. As a result, the entire volume of carbon/carbon material experiences circumferential tensile stresses. Region I also experiences radial compressive stresses which, for the tests performed, are sufficiently large to pulverize the matrix carbon and thus render it useless in maintaining inter-yarn integrity. The material of Region I, however, remains intact in its crushed condition during the compression interval.

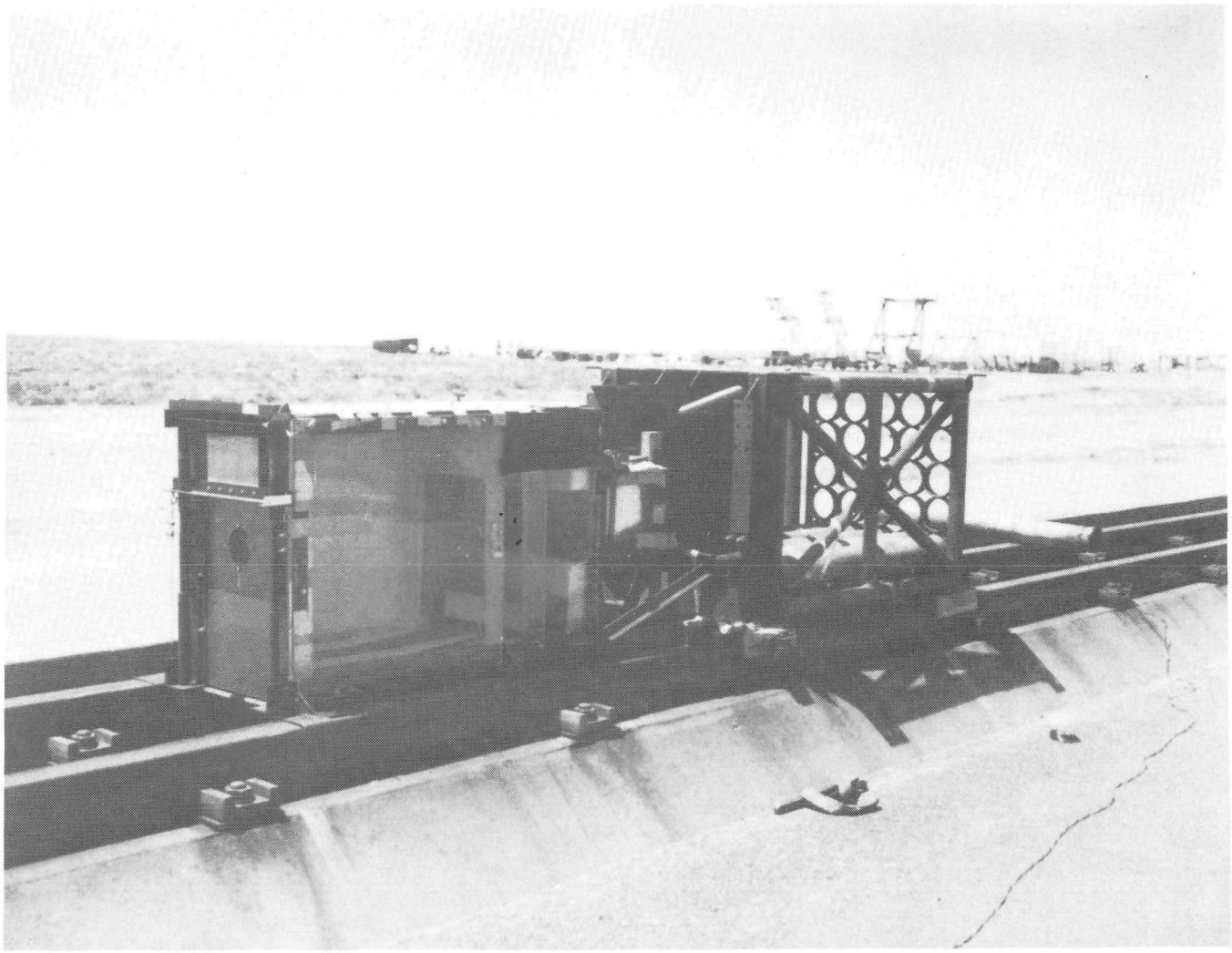

Sandia D69-11312
69-H65983-104

Figure 5-34 Sandia Corporation Sled-Track Facility.

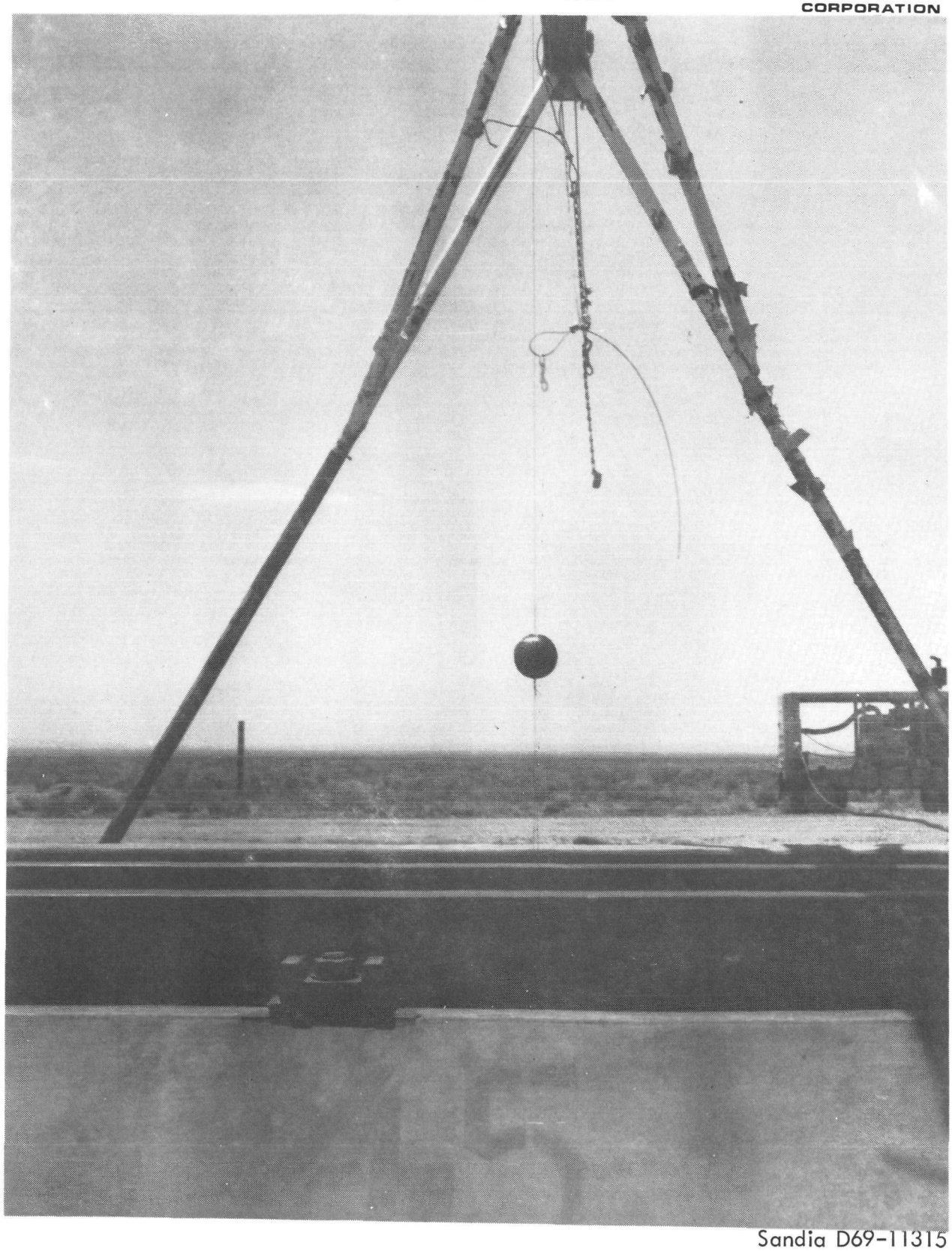

Sandia D69-11315

69-H65983-105

Figure 5-35 Unheated Capsule Suspended Above Test Track.

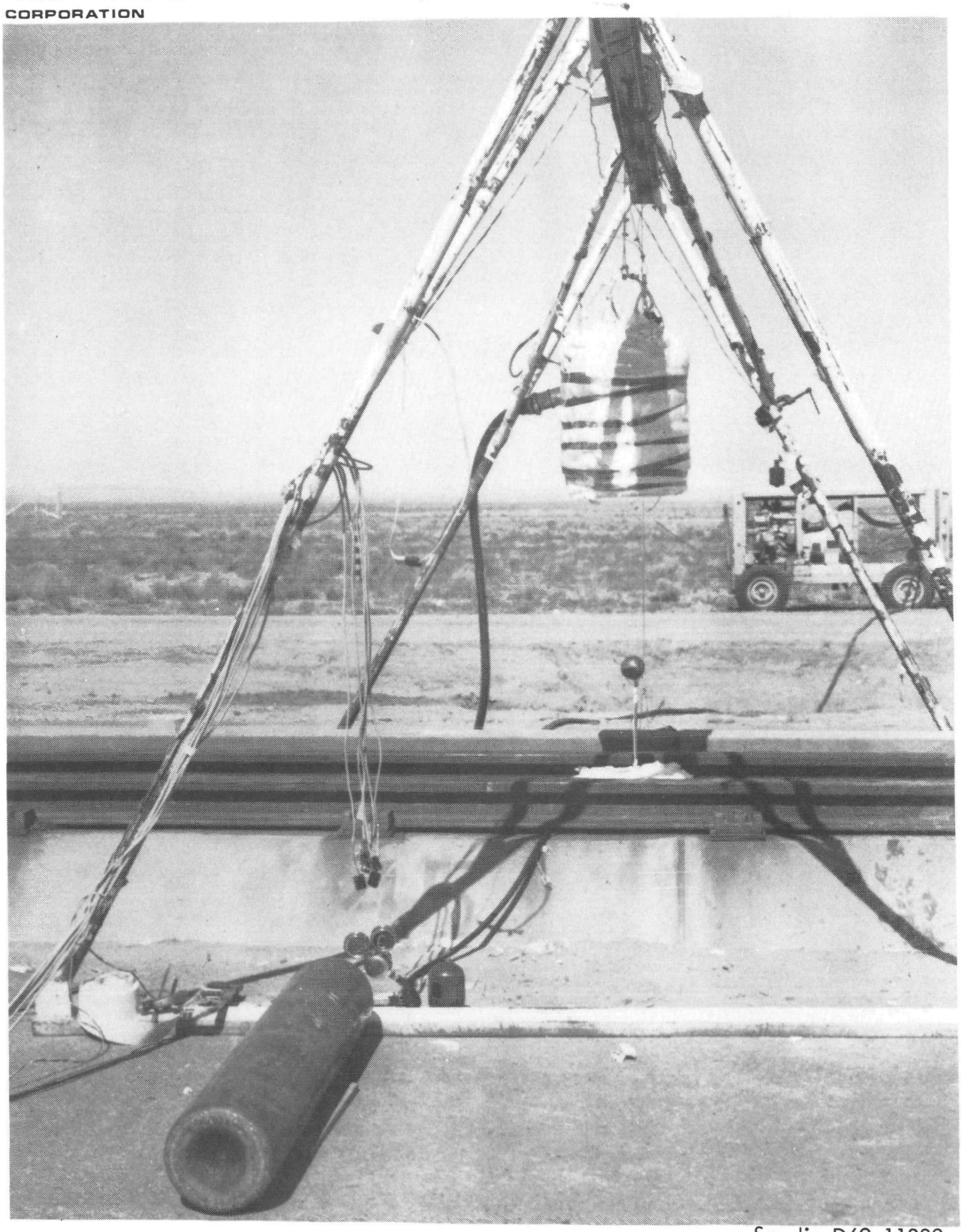

Sandia D69-11338

69-H65983-106

Figure 5-36 Heater and Capsule Mounted Above Test Track.

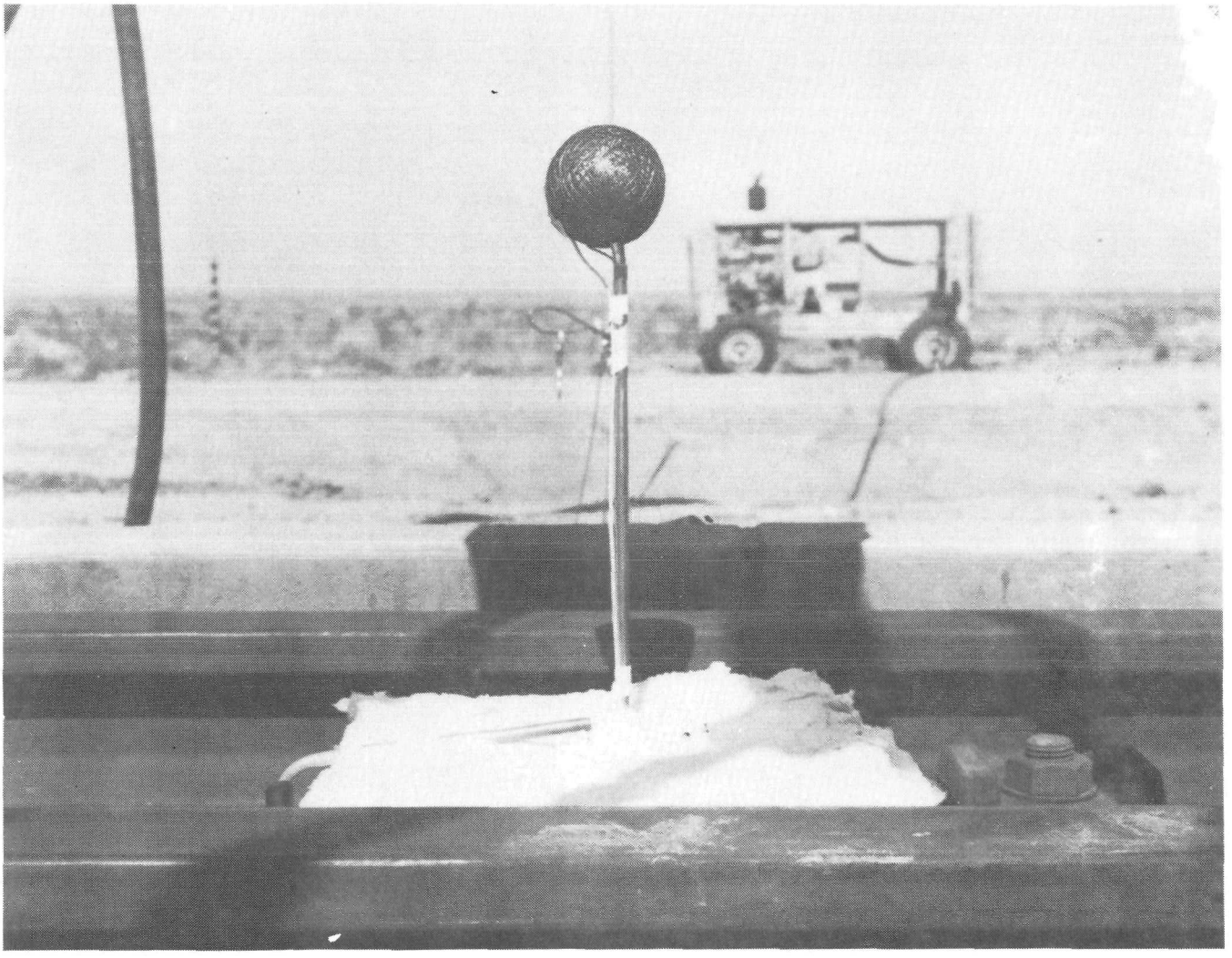

Sandia D69-11337

69-H65983-107

Figure 5-37 Mounting Technique for Heated Capsule.

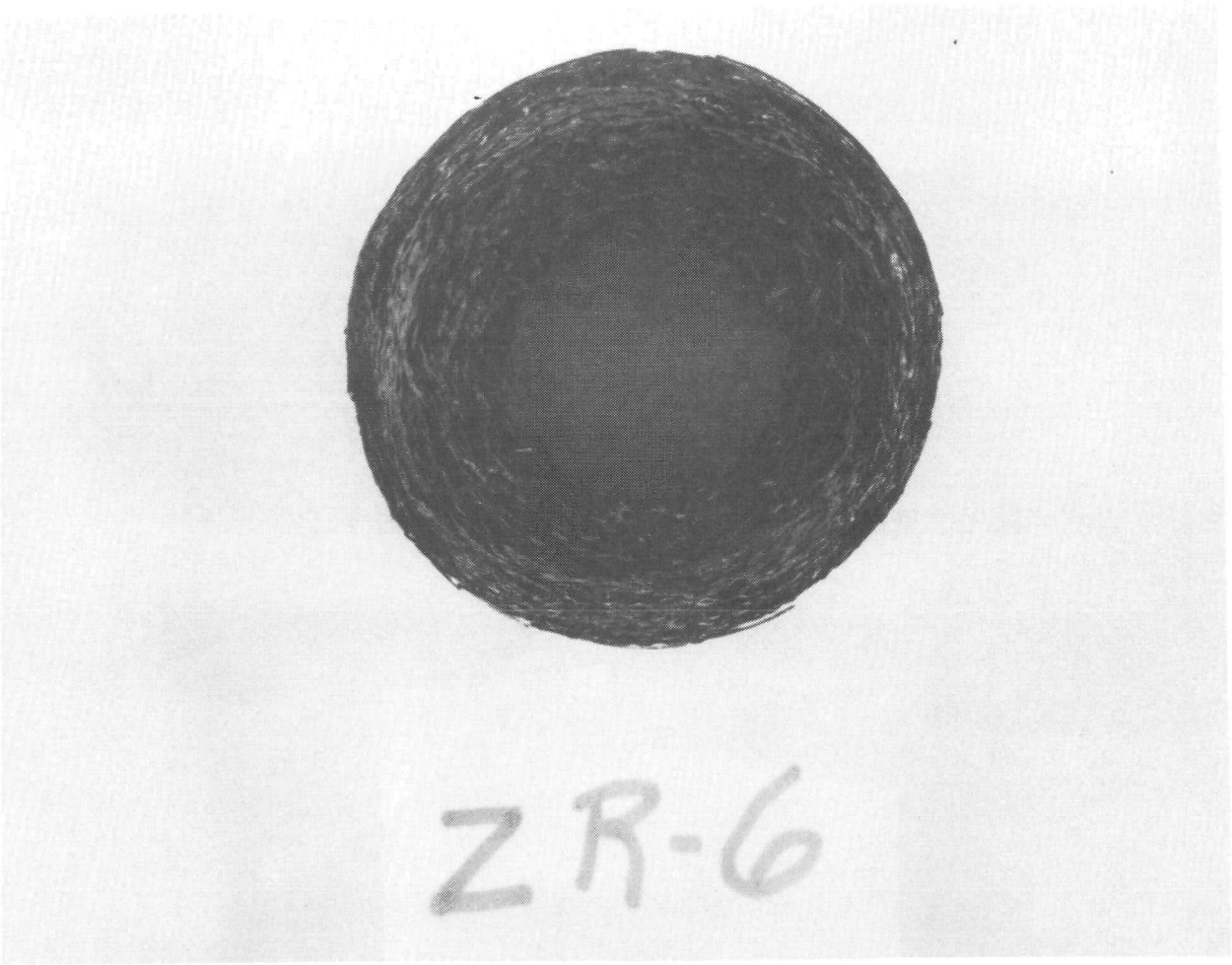

Sandia D69-11318

69-H65983-108

Figure 5-38 SIREN Capsule Impacted at 250 ft/sec, and at Ambient Temperature.

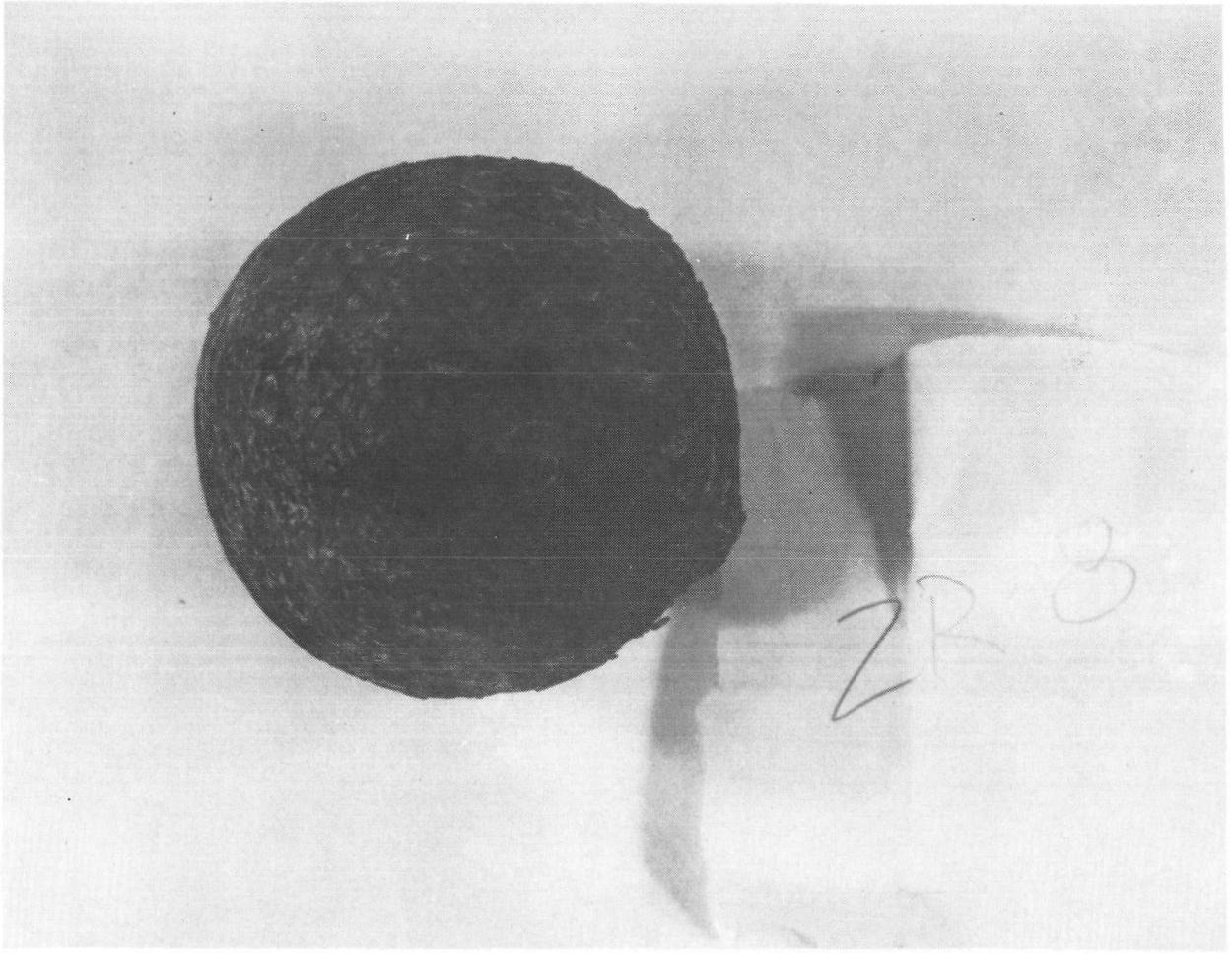

Sandia D69-11319

69-H65983-109

Figure 5-39 SIREN Capsule Impacted at 210 ft/sec, and at Ambient Temperature.

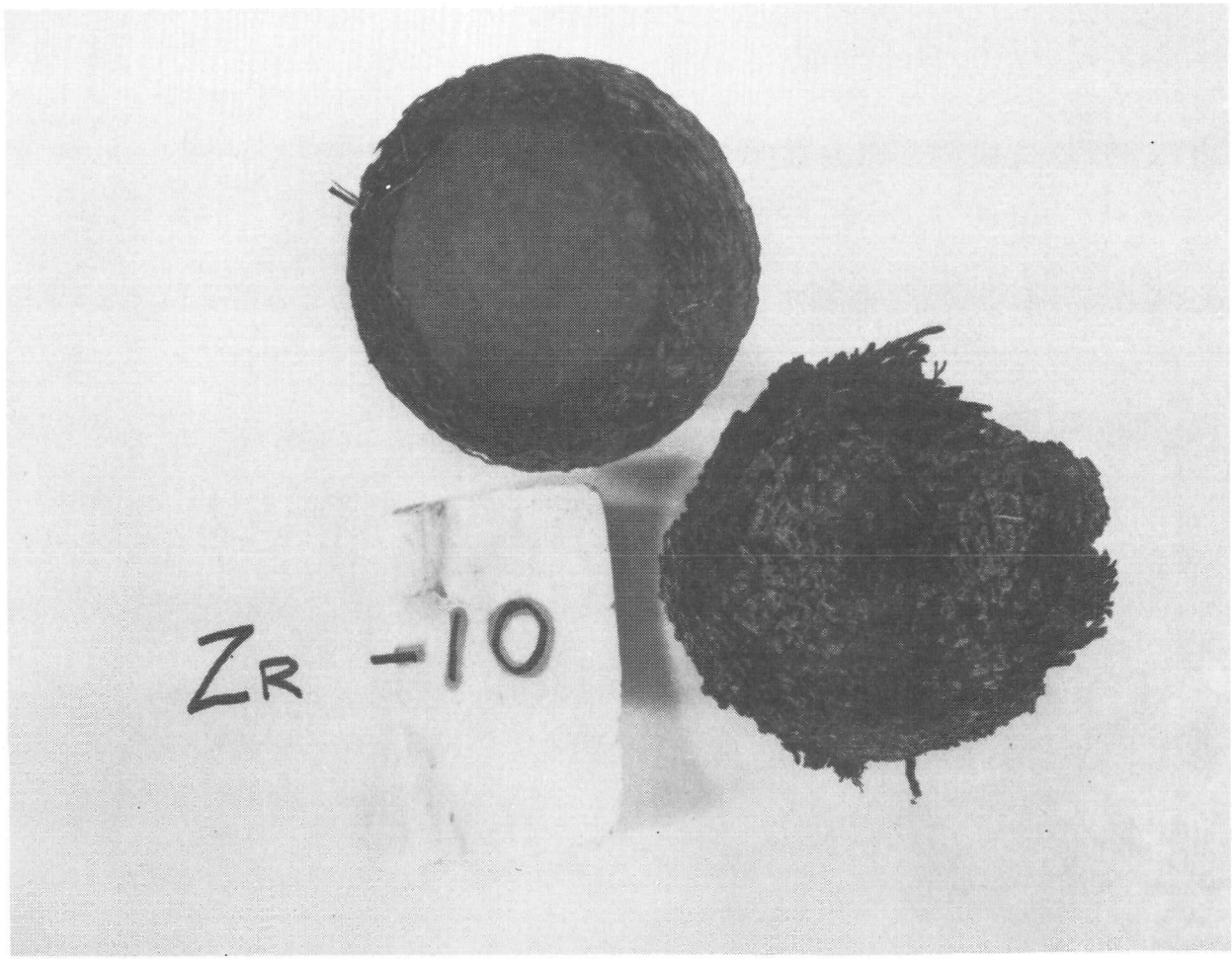

Sandia D69-11317

69-H65983-110

Figure 5-40 SIREN Capsule Impacted at 352 ft/sec, and at Ambient Temperature.

Sandia D69-11316

69-H65983-111

Figure 5-41 SIREN Capsule Impacted at 255 ft/sec, and at Ambient Temperature.

Sandia D69-11340

69-H65983-112

Figure 5-42 SIREN Capsule Heated to 1500°F and Impacted at 250 ft/sec.

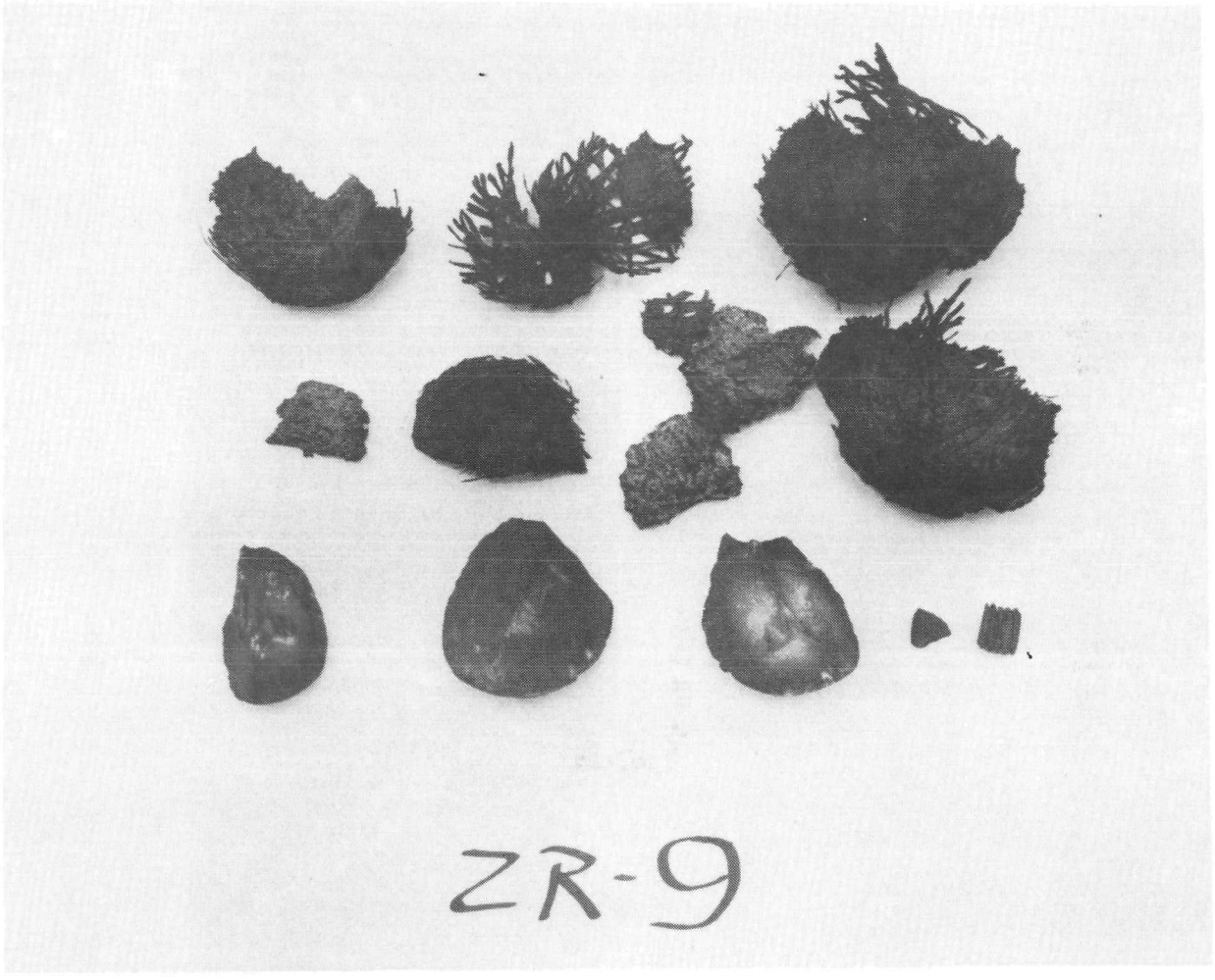

Sandia D69-11339

69-H65983-113

Figure 5-43 SIREN Capsule Heated to 1500°F and Impacted at 350 ft/sec.

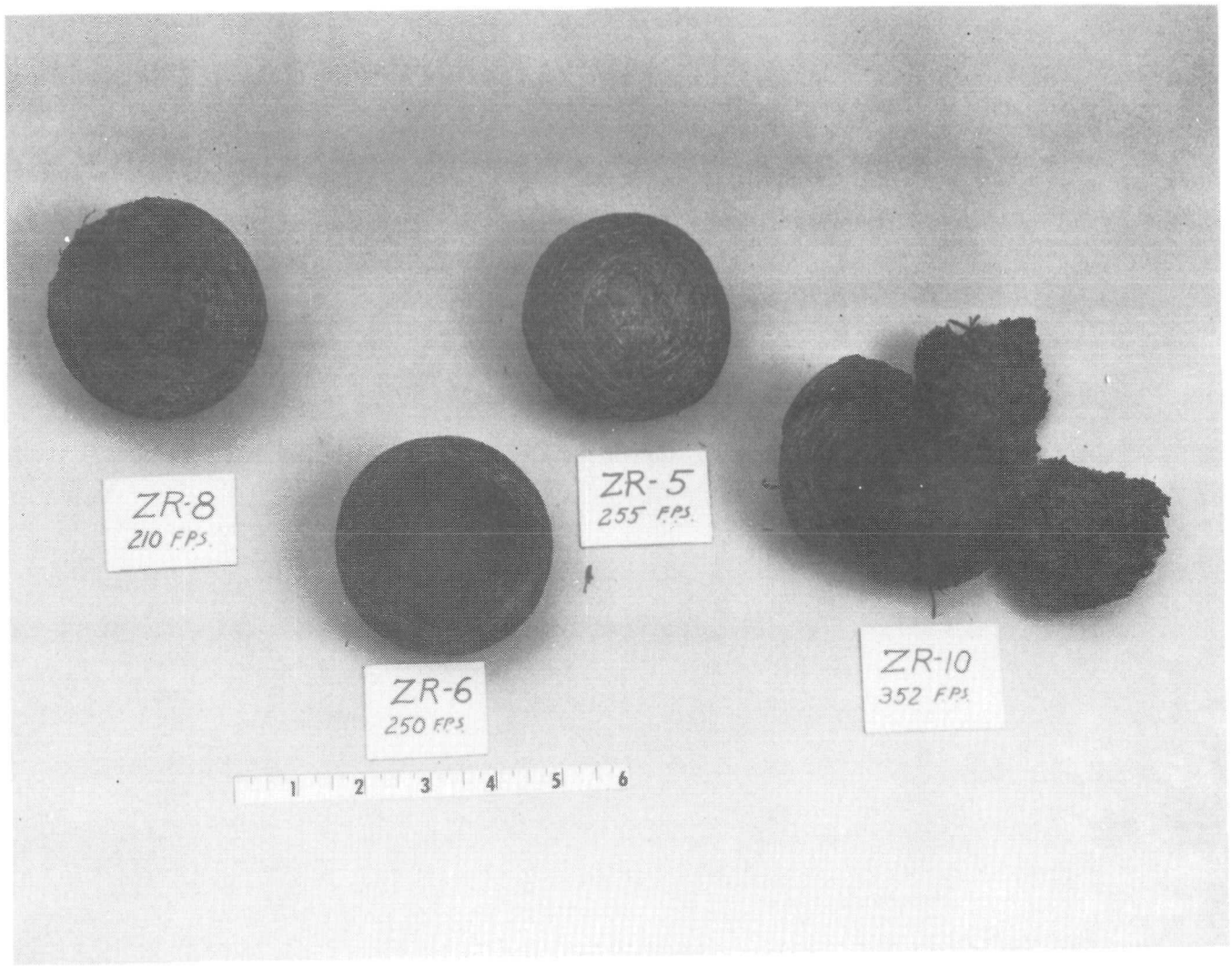

69-623-2

69-H65983-114

Figure 5-44 Unheated SIREN Capsules After Impact.

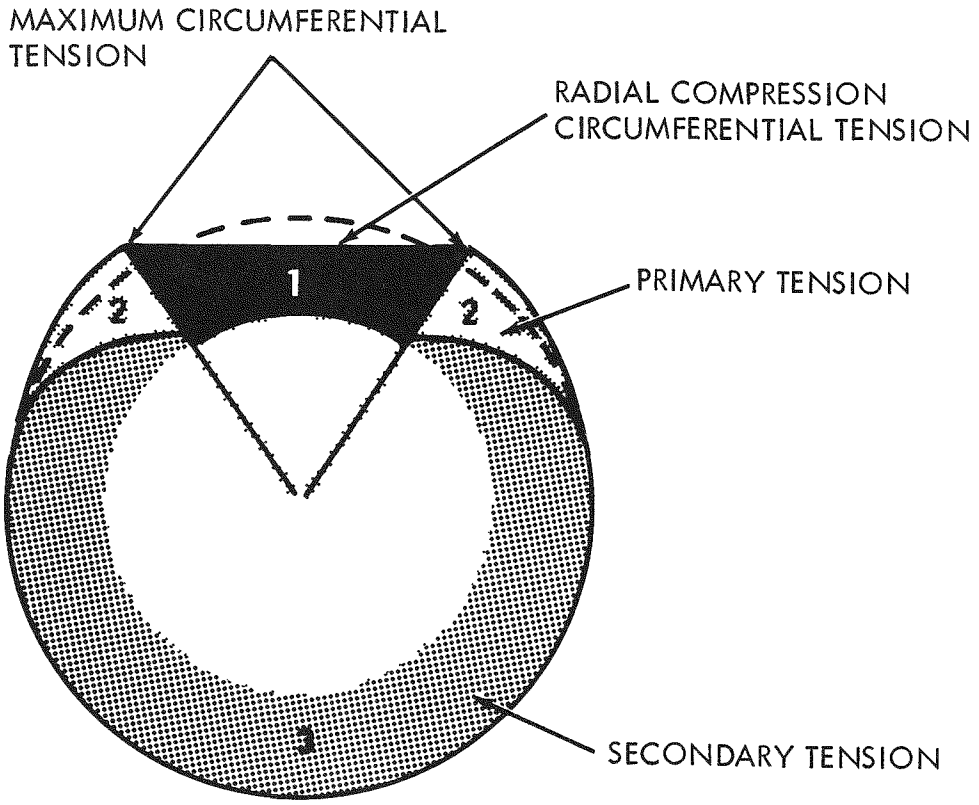

69-H65983-115

Figure 5-45 Stress Zones Established During Impact.

Region 2 experiences both radial and circumferential tension with the maximum circumferential tensile stresses and the minimum radial tensile stresses occurring at the boundary between Regions 1 and 2. As a result of radial tension in Region 2 and radial compression in Region 1, the interface separating the two regions experiences zero radial stress. However, the interface between Regions 1 and 2 experiences the highest circumferential stress in the matrix material and is thus the likely area to rupture during impact. During capsule separation from the granite impact block, the material leaves Region 1; the matrix material because it was crushed to powder during impact, the yarn because it was torn in tension at the interface of Regions 1 and 2.

Region 3 also experiences tension but to a lesser degree than Region 2. At the higher impact velocities it is sufficient to cause hairline cracks in the material of this region.

Higher kinetic energies at impact result in a larger included conical angle for Region 1, which in turn leads to a larger center core exposure after impact. Higher kinetic energies also lead to greater circumferential tensile stresses in all regions which tend to cause more pronounced cracking in Regions 2 and 3.

5.5.2.2 Plasma Arc Tests

The SIREN capsules tested at the Sandia Plasma-Arc Facilities were identical to those described for the Impact Test with the exception that a B_6Si oxidation resistant coating had been added. Three capsules were tested: capsules Zr-1, Zr-3, and Zr-4. Table 5-8 lists the conditions under which the capsules were tested. The tabulated values of pressure, heat rate, and test interval were intended to duplicate the reentry parameters which have the major effect on capsule mass loss.

Run numbers 1 and 2 simulated an orbital reentry condition, whereas Run number 3 simulated a 36,000 ft/sec superorbital reentry at minimum skip angle (-6 degrees). Both tests assumed a non-spinning stable reentry.

TABLE 5-8

PLASMA-ARC TEST CONDITIONS FOR SIREN CAPSULE

Run No.	Model No.	$\dot{q}$ (BTU/ft. -sec.) (R = 3 in.)	P_{T_2} (atm.)	Model Dwell Time (sec.)	Recession at Stagnation Point (in.)	Mass Loss (gms)	Maximum Surface Temperature (^{o}F)	
							ϵ = 1.0	ϵ = 0.85
1	Zr-4	264	0.060	199	0.174	13.50	3230	3390
2	Zr-3	272	0.062	199	0.196	13.45	3250	3410
3	Zr-1	447	0.083	300	0.288	33.14	3820	4010

During tests on each of the three capsules the stagnation-point surface temperature was measured using optical techniques. Table 5-8 gives the maximum surface temperature recorded at the stagnation point.

The exit of the plasma-arc nozzle had a diameter of 4.0 inches resulting in approximately a 4.0-inch diameter plasma stream directly in front of the capsule. The ratio of the nozzle exit area to the nozzle throat area was 10.0. This resulted in a Mach number of 3.9 in front of the oblique shock.

The capsules were modified at Sanders Nuclear Corporation to accommodate the Sandia test fixtures (i.e., drill and tap for stingers, etc.). The stinger was made of 0.50-inch diameter carbon rod and was threaded to the capsule at a point 180 degrees from the stagnation zone.

Stagnation point recessions, as presented in Table 5-8, were 0.174 inch and 0.196 inch for test conditions duplicating orbital reentry at zero degrees reentry angle. For the 36,000 ft/sec superorbital condition, the recession was 0.288 inch at the stagnation point. Table 5-9 allows comparison of the plasma-arc test data with the calculated surface recession from the aerodynamic analysis. The last column in Table 5-9 gives the plasma-arc surface recession after scaling to hypersonic conditions. Scaling procedures are given in detail in Appendix III. Results indicate that calculated values of surface recession averaged about 30 percent less than were actually experienced during the plasma-arc tests.

With the exception of surface heat flux, the test conditions were similar to the conditions used to theoretically calculate surface recession. The level of heat flux contributes a minor influence on the SIREN surface recession as long as it is sufficient to maintain the stagnation surface temperature within the diffusion-controlled regime for graphite (diffusion-controlled regime lies between 2240°F and 7000°F).

Figures 5-46 through 5-48 are photographs of the SIREN capsule after exposure to simulated reentry conditions. Figures 5-49 and 5-50 are photographs that allow comparisons of surface recession between the three tested capsules.

TABLE 5-9

SIREN CALCULATED AND PLASMA-ARC REENTRY CONDITIONS

Sample	Trajectory	Reentry Mode	Calculated Reentry Conditions				Plasma-Arc Conditions at Mach No. = 3.9				Surface Recession After Scaling of Plasma-Arc Tests to Hypersonic Conditions (inches)
			Air Pressure (ATM)	Stagnation Point Heat Rate ($B/sec\ ft^2$)	Model Dwell Time (sec)	Stagnation Point Recession (inches)	Air Pressure (ATM)	Stagnation Point Heat Rate ($B/ft^2\ sec$)	Model Dwell Time (sec)	Stagnation Point Recession (inches)	
Zr-4	$V_o = 26,000$ ft/sec $\gamma_o = 0.1^o$	Stable	0.06	360	200	0.143	0.060	264	199	0.174	0.202
Zr-3	$V_o = 26,000$ ft/sec $\gamma_o = 0.1^o$	Stable	0.06	360	200	0.143	0.062	272	199	0.196	0.228
Zr-1	$V_o = 36,000$ ft/sec $\gamma_o = 6.0^o$	Stable	0.08	868	300	0.244	0.083	447	300	0.288	0.334

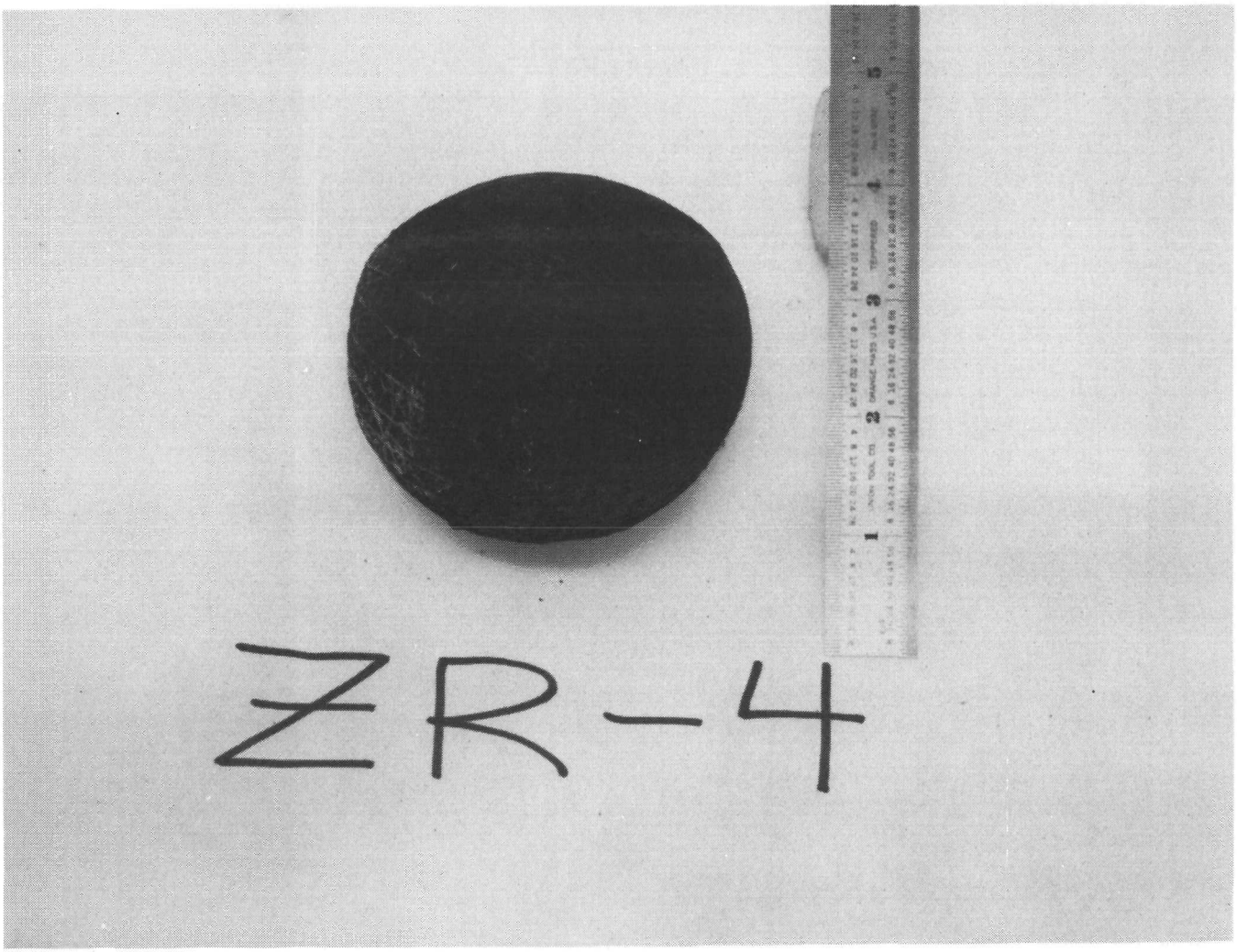

Sandia D69-12223
69-H65983-116

Figure 5-46 Simulation of Orbital Reentry, Run Number 1.

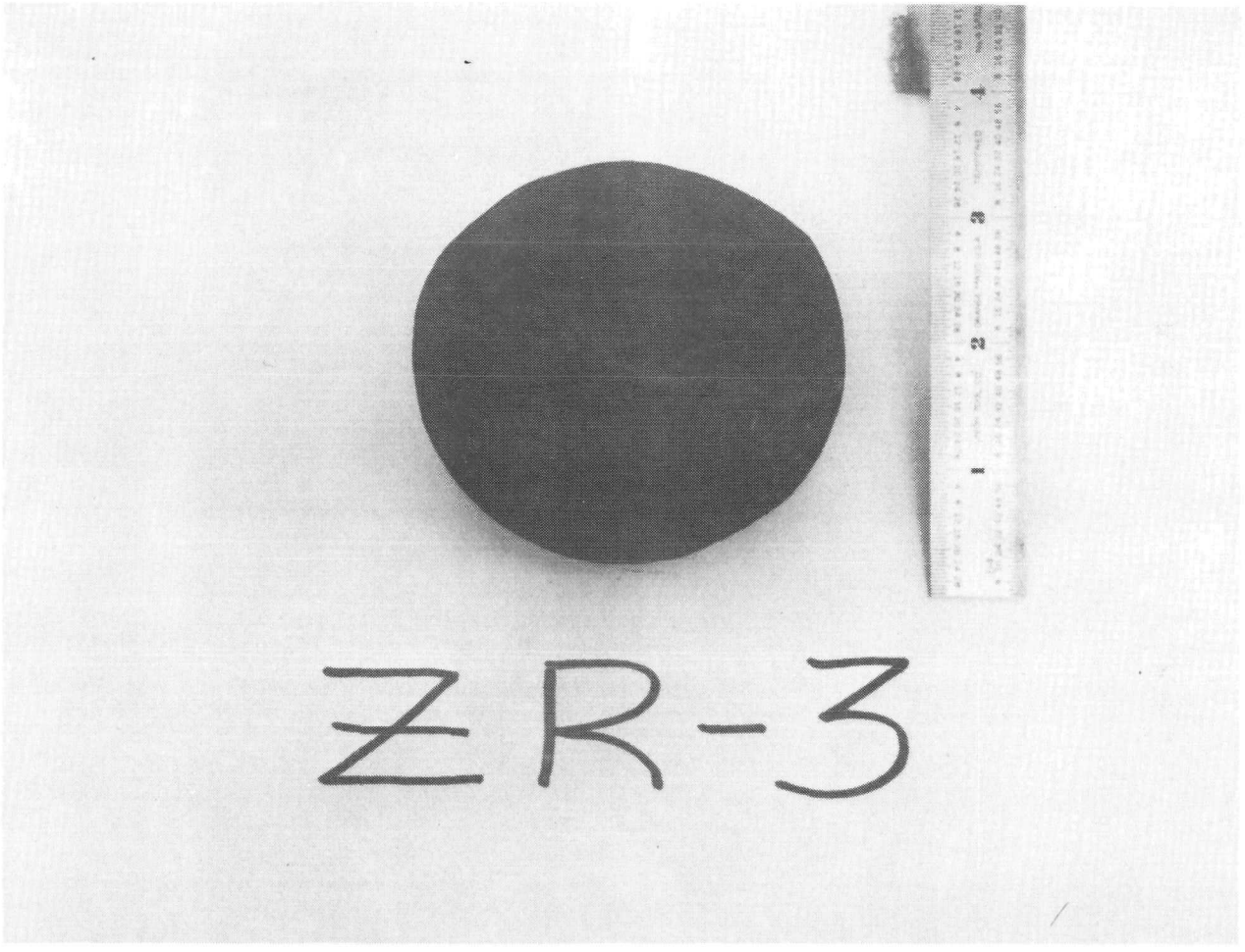

Sandia D69-12222
69-H65983-117

Figure 5-47 Simulation of Orbital Reentry, Run Number 2.

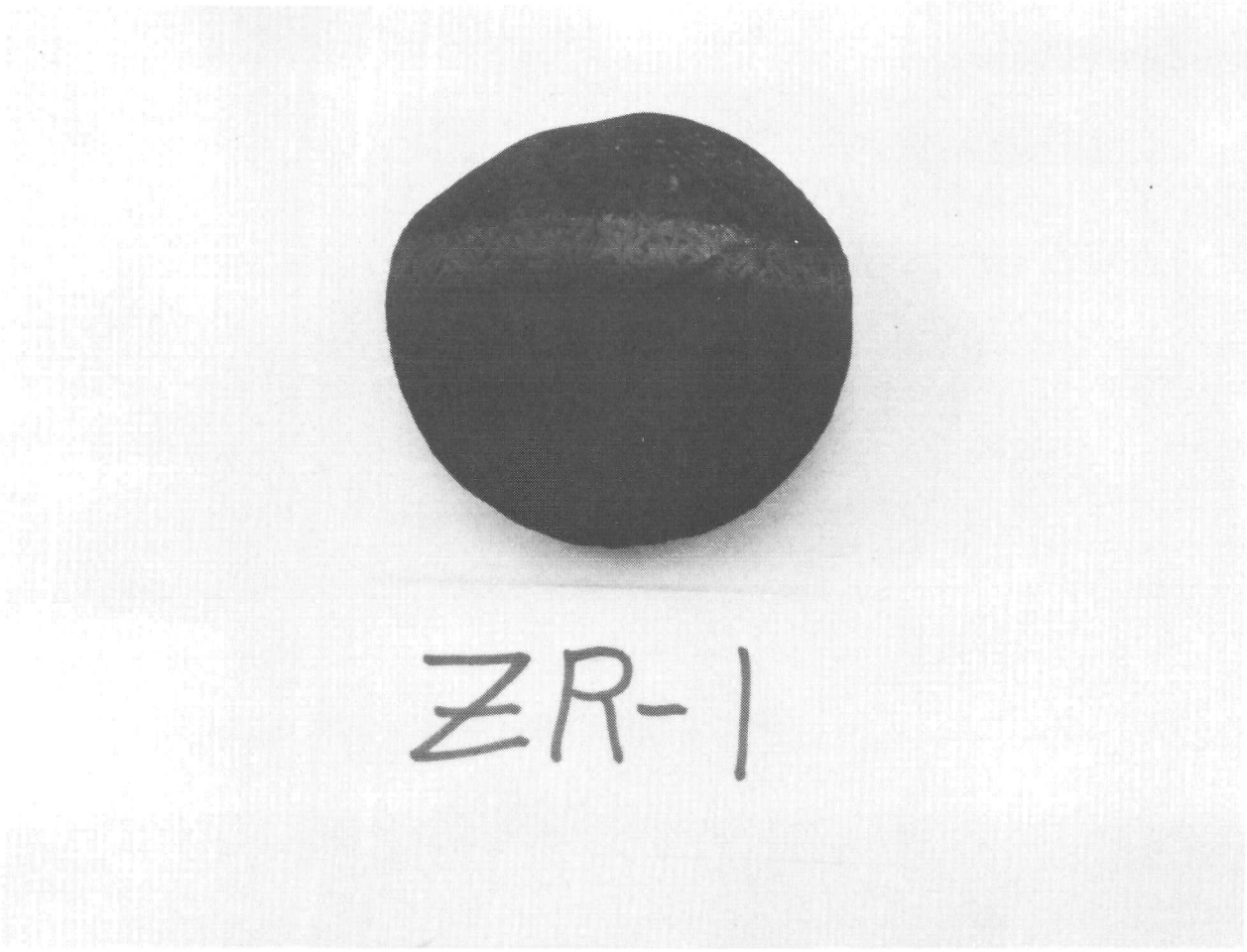

Sandia D69-12225

69-H65983-118

Figure 5-48 Simulation of Superorbital Reentry, Run Number 3.

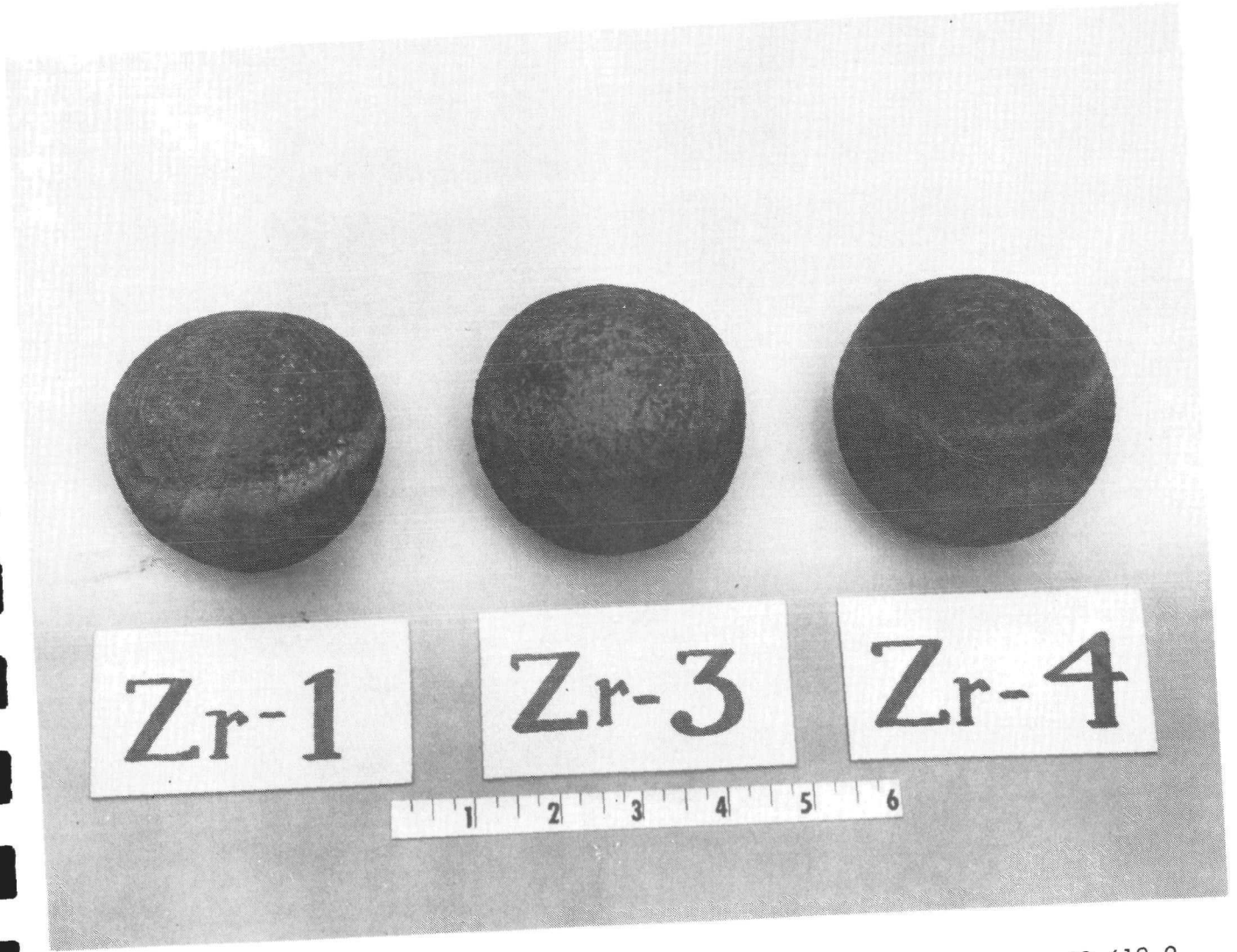

69-618-2

69-H65983-119

Figure 5-49 Comparison of SIREN Capsules After Simulated Reentry in Sandia Plasma-Arc Facility (Oblique View).

SANDERS NUCLEAR CORPORATION

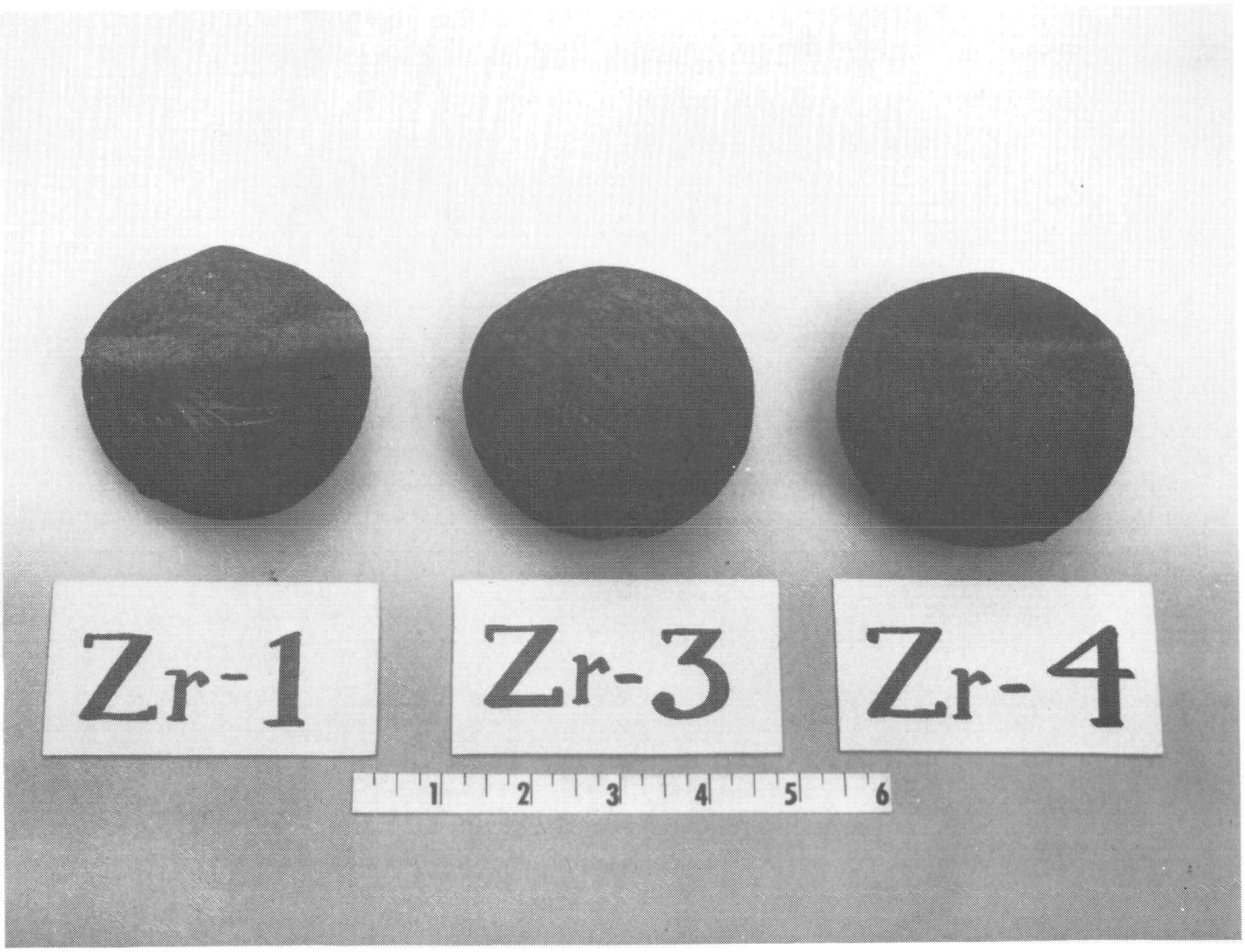

69-618-1

69-H65983-120

Figure 5-50 Comparison of SIREN Capsules After Simulated Reentry in Sandia Plasma-Arc Facility (Profile View).

The irregularity of surface recession which occurred for Zr-1 was a result of improper alignment in the plasma stream. The misalignment was verified by films taken during test runs. Figures 5-51 through 5-53 are photographs of the capsules during each of the three tests. Figure 5-54 is a photograph of Zr-1 taken during the cooling cycle immediately after the test and provides an excellent thermograph of the various lays of the graphite yarn.

5.5.3 CONCLUSIONS

5.5.3.1 Impact

To discuss the feasibility of the SIREN concept to withstand impact, a definition of capsule failure is required. Therefore, capsule failure at impact, for the purpose of discussion, is defined for the following fuel forms as:

- Microsphere fuel form - fuel liner rupture and subsequent dispersal of fuel
- Solid fuel form - production of and subsequent dispersal of fuel fines.

No impact tests were performed which would indicate success or failure of the SIREN capsule to contain a microsphere fuel form. Six impact tests were performed which would indicate the success or failure of the SIREN capsule to prevent the production and subsequent dispersal of fines from a solid fuel form (assuming Al_2O_3 has properties similar to solid fuel forms). No tests were performed to test for the success of SIREN when impacting with an actual solid fuel form.

All of the impact tests were performed with center cores of Al_2O_3 to simulate a prospective fuel form. It is not presently known to what degree the Al_2O_3 core simulates a prospective fuel form. The main reason for the uncertainty in simulation is that the structural properties of the three types of solid PuO_2 fuel forms are not known at present.

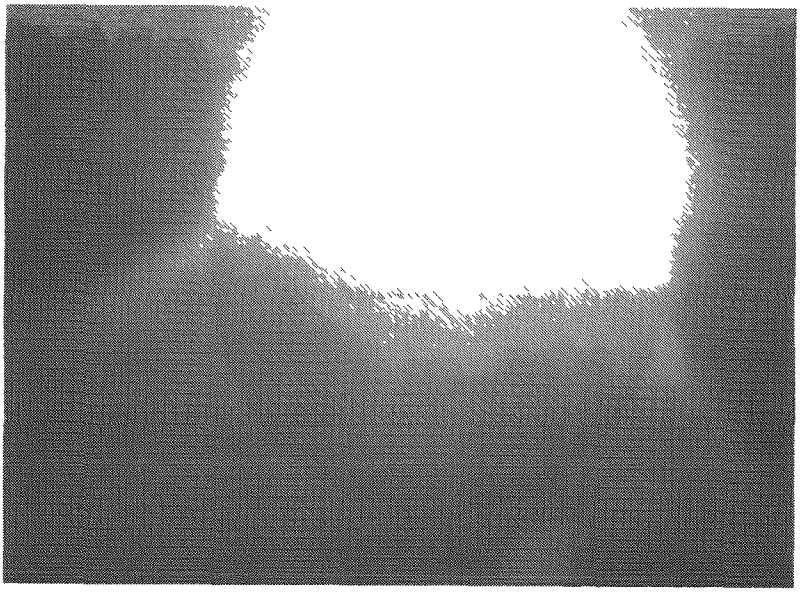

69-H65983-121

Figure 5-51 Capsule Number Zr-1, Approximately 200 Seconds into Test.

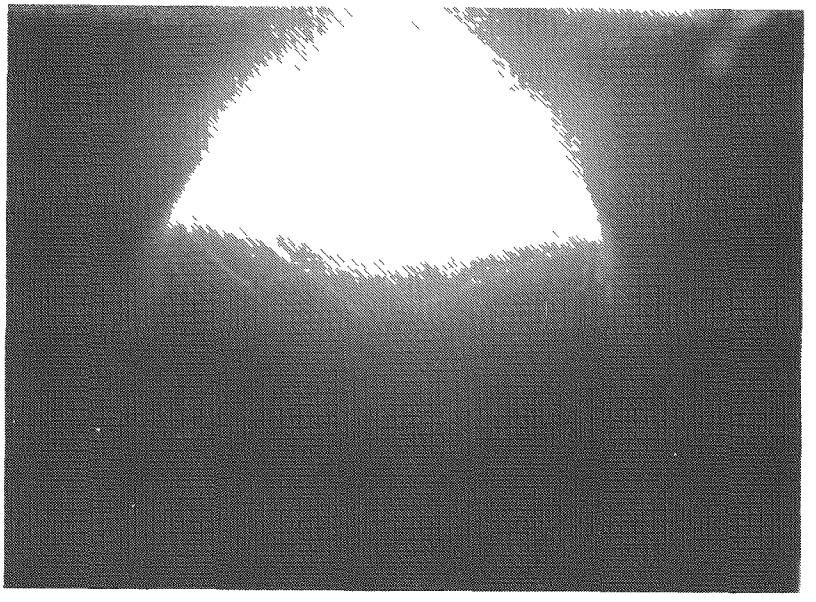

69-H65983-122

Figure 5-52 Capsule Number Zr-3, Approximately 125 Seconds into Test.

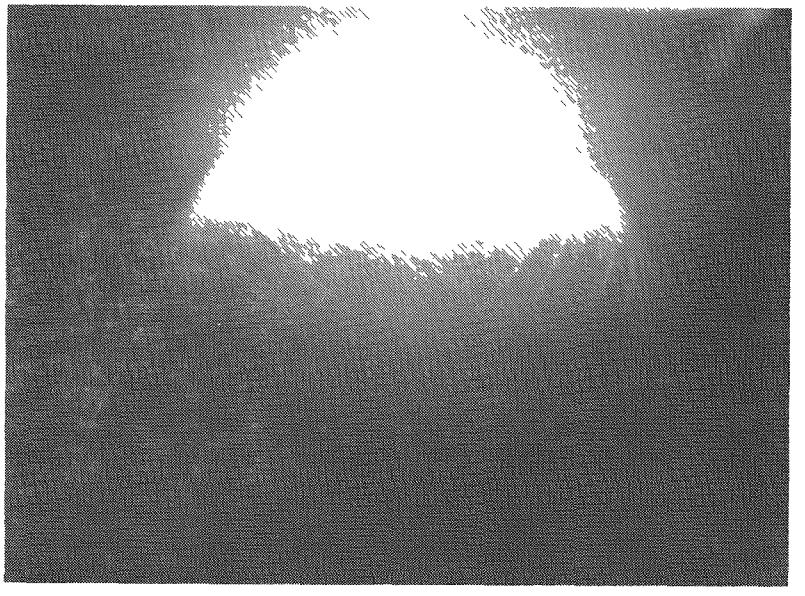

69-H65983-123

Figure 5-53 Capsule Number Zr-4, Approximately 125 Seconds into Test.

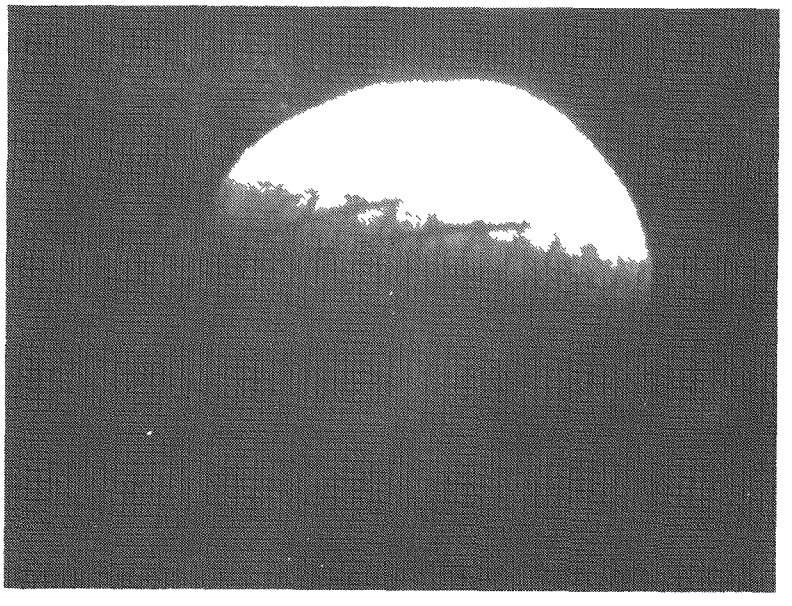

69-H65983-124

Figure 5-54 Capsule Number Zr-1, A Few Seconds After Completion of Test.

Assuming that the Al_2O_3 core did simulate a fuel form, then it may be concluded that five out of six impact tests proved to be a success. One capsule had the center core shatter at 350 ft/sec and could be considered a capsule failure by definition. No attempt, however, was made to measure or detect the "fines" produced.

For all six capsule impact tests, considerable compressive forces were transmitted through the carbon/carbon material to the surface of the Al_2O_3 core. For the capsule design tested, it is highly improbable that a ceramic liner surrounding a microsphere fuel form would have remained intact after impact. However, it is likely that the fluid motion peculiar to microspheres would have distributed the energy of impact throughout the carbon/carbon material, and thus resulted in a fuel capsule that had a shattered liner and intact carbon structure. The use of a metallic liner with a microsphere fuel form may be required if there exists a need for greater strength and containment. A cushion layer between the liner and the carbon/carbon material to prevent transmission of the concentrated compressive forces is also a possibility to enhance the impact resistance of a capsule containing microspheres.

Efforts to determine the mechanical properties of proposed fuel forms should precede future SIREN impact tests. Once the fuel forms have been mechanically characterized, the development of a fuel simulant should follow which will allow more meaningful impact test data to be obtained.

Additional impact testing should then be carried out on the present SIREN construction as well as on SIREN capsules which have been improved as a result of information gathered during this phase or subsequent phases of the SIREN effort. A possible improvement which became apparent after analyzing the results of the present phase is to use a high tensile strength fiber (400,000 psi as compared to the 6000 psi presently used) to enhance the carbon/carbon energy

absorption characteristics during impact. Higher energy absorption in the carbon would result in a decreased compressive force on the center core or fuel liner.

Additional areas of investigation should include trade-offs between ablation characteristics, impact energy absorption, and ballistic coefficient as a function of carbon/carbon density. Investigation would not necessarily be directed only toward homogenous density variations, but also to density gradients in the radial direction.

Impact tests should also be performed on capsules which have been exposed to reentry conditions. Studies should be made to determine orientation of these ablated capsules during impact.

5.5.3.2 Plasma Arc

Plasma arc tests indicated that the carbon/carbon heat shield of the SIREN ablates in a manner and at a rate approximately 30 percent greater than standard graphite reentry heat shields. The 0.5 inch thickness of material used on the feasibility design was sufficient to insure carbon coverage of the center core after reentry, even for the superorbital condition. The 4000°F temperature produced no visible degradation as a result of thermal shocks.

BLANK

5.6 SOLID PROPELLANT FIRE TESTS

5.6.1 INTRODUCTION

Three test SIREN capsules were subjected to solid propellant fires to determine the effects of the fire on the specimens. None of the capsules contained radioisotopic fuel. The fire tests were conducted at the facilities of Isotopes, Inc., in Baltimore, Maryland, April 10 and 14, 1969, in accordance with Isotopes' Test Plan Number 466A3322084. Isotopes, Inc., prepared two test configurations; the "proximity test" in which the capsule was positioned between two blocks of propellant placed side-by-side, and the "contact test" in which the capsule was positioned directly on the top of the propellant block. Sanders Nuclear provided three 3-inch diameter test capsules complete with thermocouples. The primary data anticipated from the test were the effect the flame and temperature environment would have on the capsule. Other data to be obtained would be measurement of the temperature profile during test at different positions within the capsule. As discussed in subsequent paragraphs, the SIREN capsules successfully withstood both fire tests as demonstrated by:

- No observable loss of material by burning, melting or erosion
- Complete mechanical integrity was maintained - neither cracking nor spalling due to thermal effects was observed
- None of the component parts experienced temperatures above their melting points
- All component parts exhibited excellent compatibility and thermal stability.

5.6.2 PREPARATION OF SIREN TEST CAPSULES

The three capsules used for the fire tests were "extras" in the lot of capsules being prepared for evaluation under contract AT(29-2)-2708 (inclusion

of the fire test was not anticipated at the beginning of the contract). The three capsules were 3-1/8 inches in diameter and contained a 5/8-inch thick outer layer of wound graphite yarn impreganted with carbon. Two of the capsules were prepared with hollow centers, and the third with a solid center of Al_2O_3 over-coated with ZrO_2 (the ZrO_2 is a compatibility layer between the graphite and Al_2O_3). Due to the press of the testing schedule, the capsules received only one of two of the carbon impregnation cycles and consequently had a somewhat lower density than was desired. Prior to testing, the surface of each capsule was plasma sprayed with B_6Si for additional oxidation resistance.

The capsules were instrumented internally with 30 gage W-Re thermocouples. For the hollow capsules a 1/2-inch diameter entrance hole was drilled through the capsule and redundant thermocouples placed approximately diametrically opposite at 1/16 inch from the outside surface, 1/2 inch from the outside surface and at the center of the capsule. After insertion of the thermocouples, the central cavity was filled with ZrO_2 powder (fuel analog) and the entrance hole plugged with a support stinger (a graphite rod). The solid core capsule was instrumented by drilling a 1/2-inch hole through the graphite and placing the thermocouples tangent to the Al_2O_3 core. Dimensions and weights of the three capsules prior to test are given below.

Capsule Number	Outside Diameter (inches)	Total Weight (gms)	Graphite/Carbon Weight (gms)	Graphite/Carbon Density (gm/cc)
Al-4 (hollow)	3-1/8"	245	245	1.4
Al-2 (hollow)	3-1/8"	220	220	1.3
Zr-2 (solid Al_2O_3 core)	3-1/8"	492	223	1.2

5.6.3 FIRE TESTS

The fire tests were performed with blocks of ALGOL II B Scout Rocket propellant. For the proximity tests two blocks of propellant were placed about 18 inches apart on a sand bed with the capsules placed between the blocks. Flame retardant was applied to all but the facing sides of the propellant block to direct the flame towards the capsules. For the contact tests, one capsule was laid directly on the propellant surface and the second capsule suspended by the stinger several inches above the surface of the propellant. This second position was selected to obtain complete flame engulfment of the capsule. The position of the capsules prior to test are shown in Figures 5-55 and 5-56.

The duration of the tests was 4 and 8 minutes for the proximity and contact tests respectively. The test personnel were unable to obtain a reliable measure of the flame temperatures because of smoke; their estimate based on optical pyrometer readings was 3700°F. Subsequent tests using pyrometric cones indicated the flame temperature was probably about 4500°F which is closer to the manufacturer's reported temperature of 4800° to 5000°F.

The testing facilities were limited to only one available instrument channel per test. For the proximity test another manufacturer's capsule was afforded the instrument channel leaving the SIREN capsule without any thermocouple readout. However, for the contact test one of the SIREN capsules was connected with the instrument channel. Unfortunately, during the test a lead counter weight supporting the instrumentation leads melted and shorted all the thermocouple extension leads well away from the capsule and thereby terminated temperature measurement. The maximum temperature obtained in the capsule before the thermocouples were shorted was approximately 1000°F.

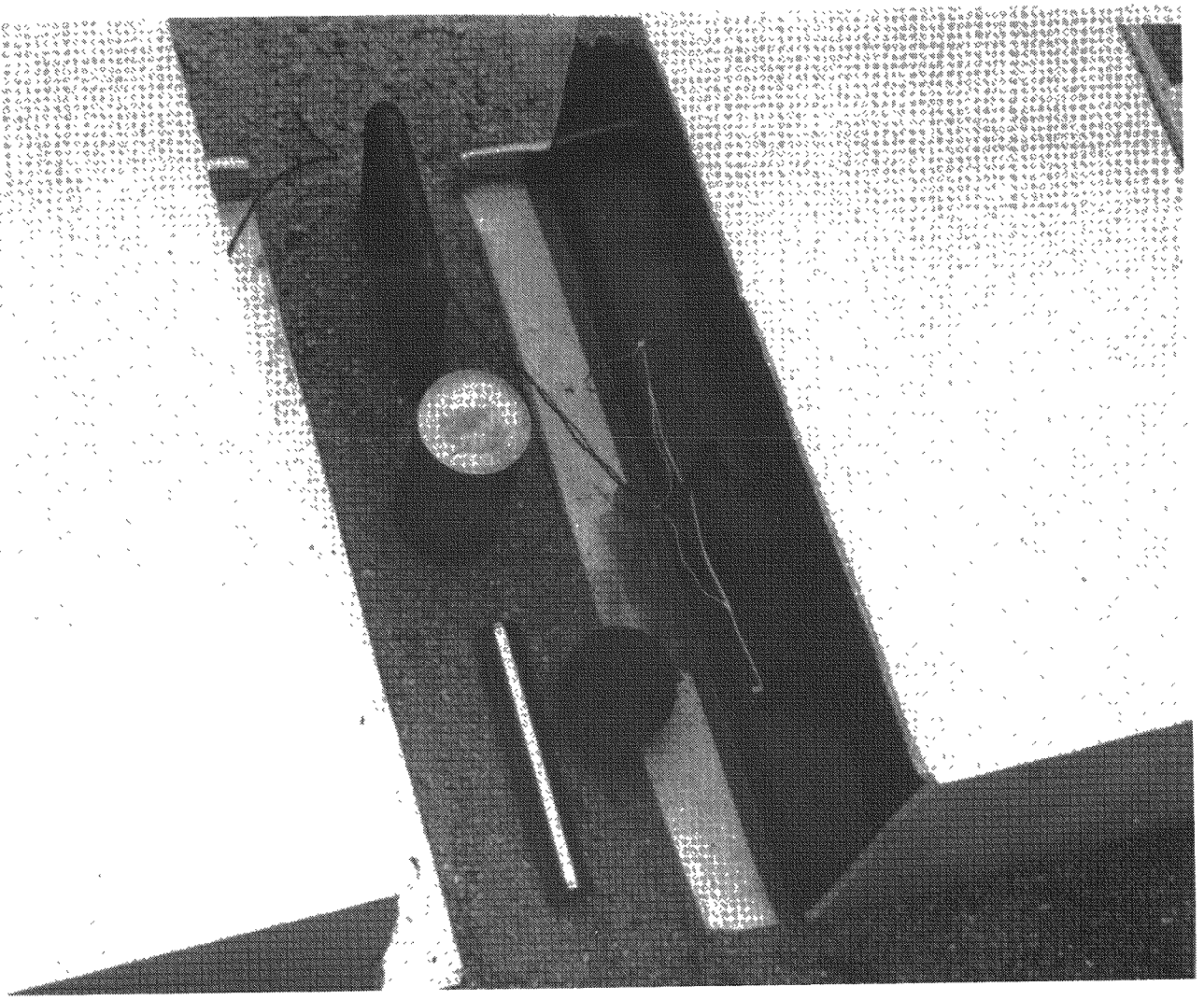

69-525-1

69-H65983-126

Figure 5-55 Proximity Fireball Test, 10 April 1969, Before Firing.

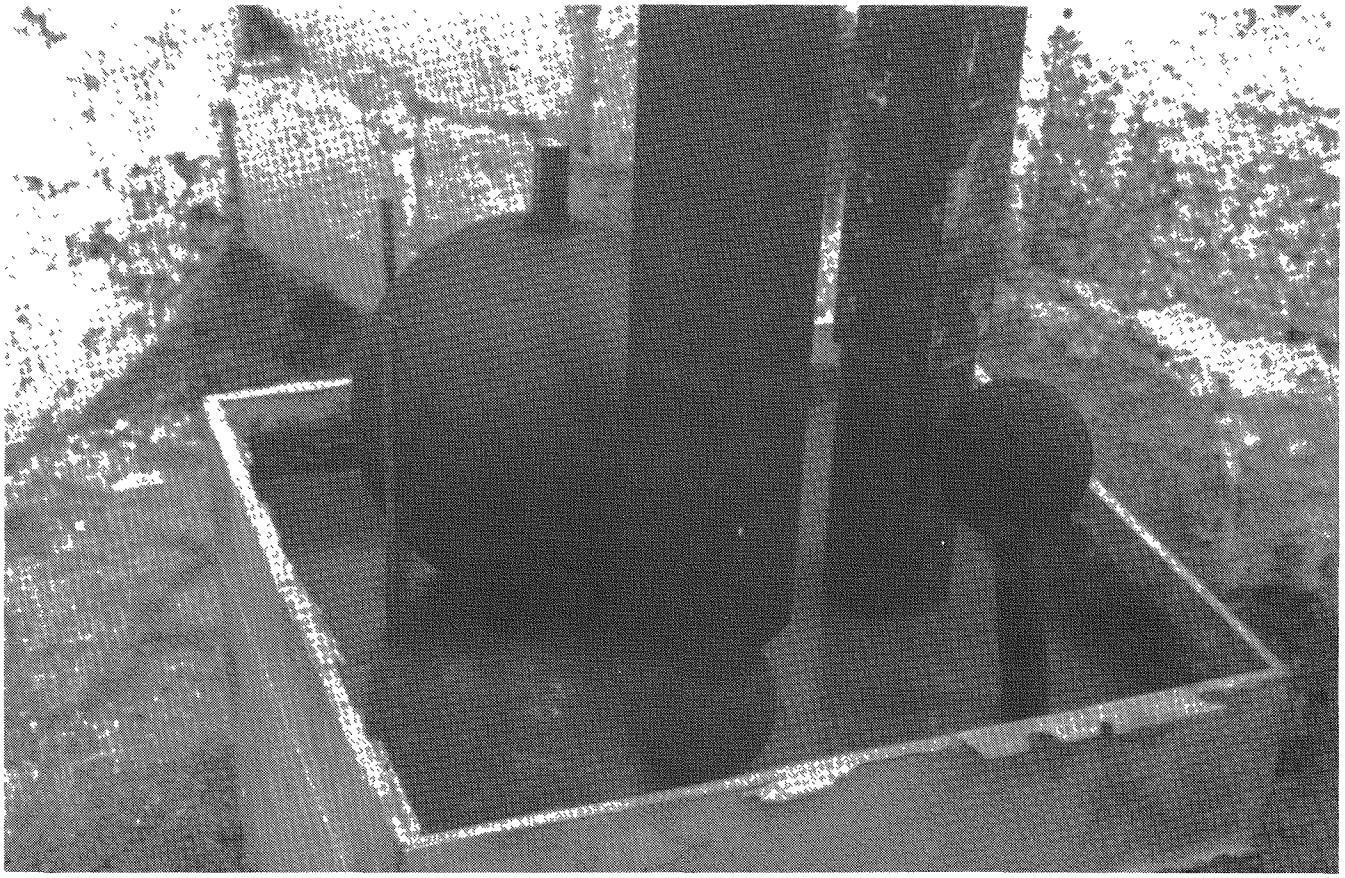

69-525-4
69-H65983-127

Figure 5-56 Contact Fireball Test, 14 April 1969, before Firing.

5.6.4 EVALUATION OF SIREN CAPSULES AFTER TEST

The condition of the capsules immediately after fire testing is shown in Figures 5-57 and 5-58. Heavy white deposits of aluminum compounds formed on the capsules during exposure to the flame. As shown in the more detailed views of the tested capsules, Figures 5-59, 5-60 and 5-61, the outer surface of the capsules appeared unaffected by the tests as indicated by the condition of the graphite yarn. Combustion products deposited from the flame adhered to the surface but did not penetrate the graphite structure. As shown in Figure 5-61 a portion of the deposit was removed and several layers of the graphite yarn adhered to the deposit; the deposit did not penetrate below that thickness. No evidence of cracking or spalling was observed on any of the three capsules.

The capsule containing the solid Al_2O_3 core was cross-sectioned after the contact fire test; the sections are shown in Figures 5-62 and 5-63. Examination of the sections revealed the following:

- The Al_2O_3 ceramic core showed no evidence of melting, cracking or spalling (the melting point of Al_2O_3 is about 3700°F)
- The graphite and ceramic core remained compatible during the test as evidenced by the absence of any reaction and bonding between the two materials
- Essentially none of the graphite structure was lost while in contact with the flaming propellant as shown by the uniform and full thickness of the graphite
- No internal cracks or separations were observed within the graphite structure
- Neither the graphite structure nor the ceramic core were dimensionally distorted during the test.

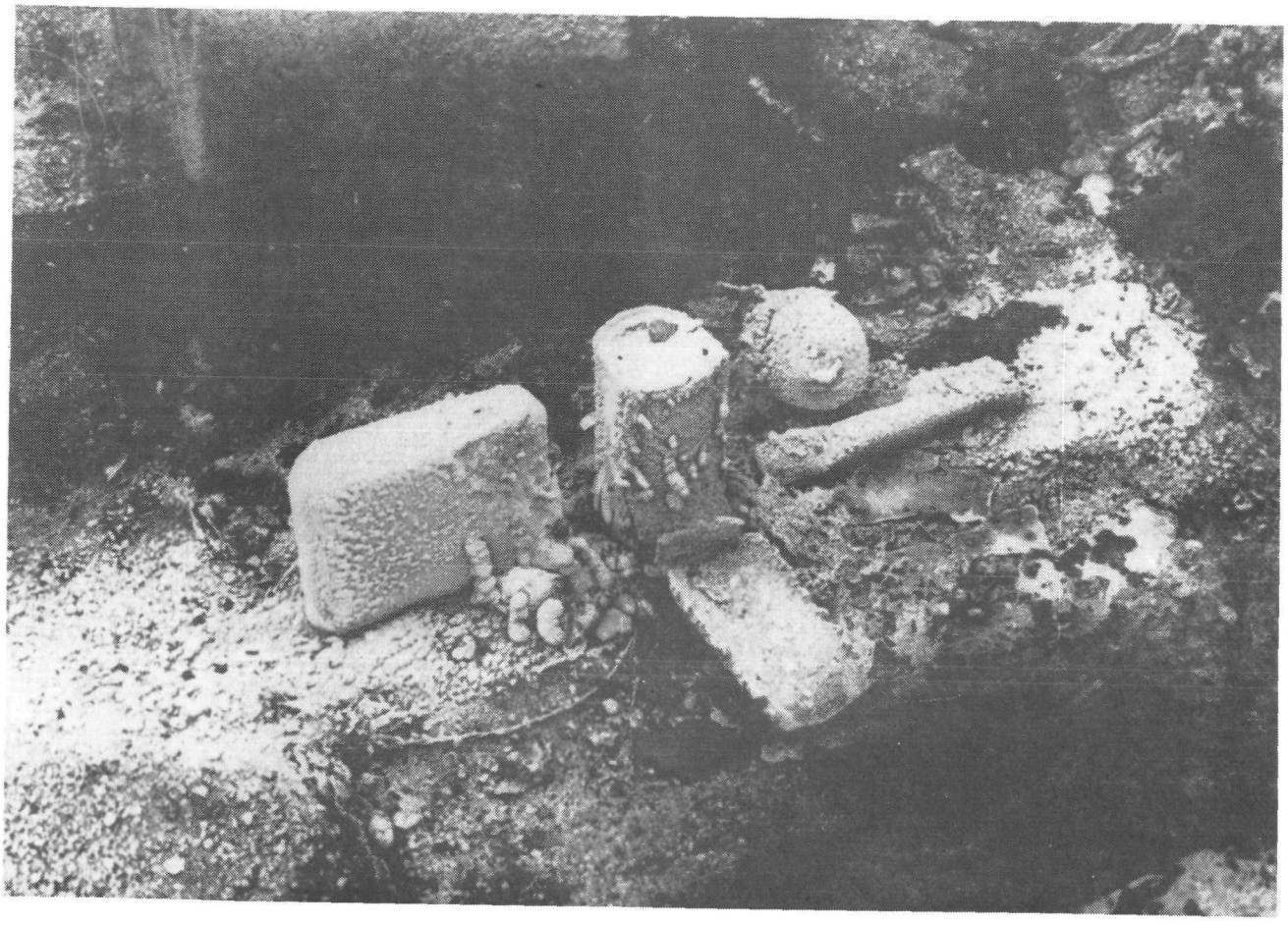

69-525-3

69-H65983-128

Figure 5-57 Proximity Fireball Test, 10 April 1969, After Firing.

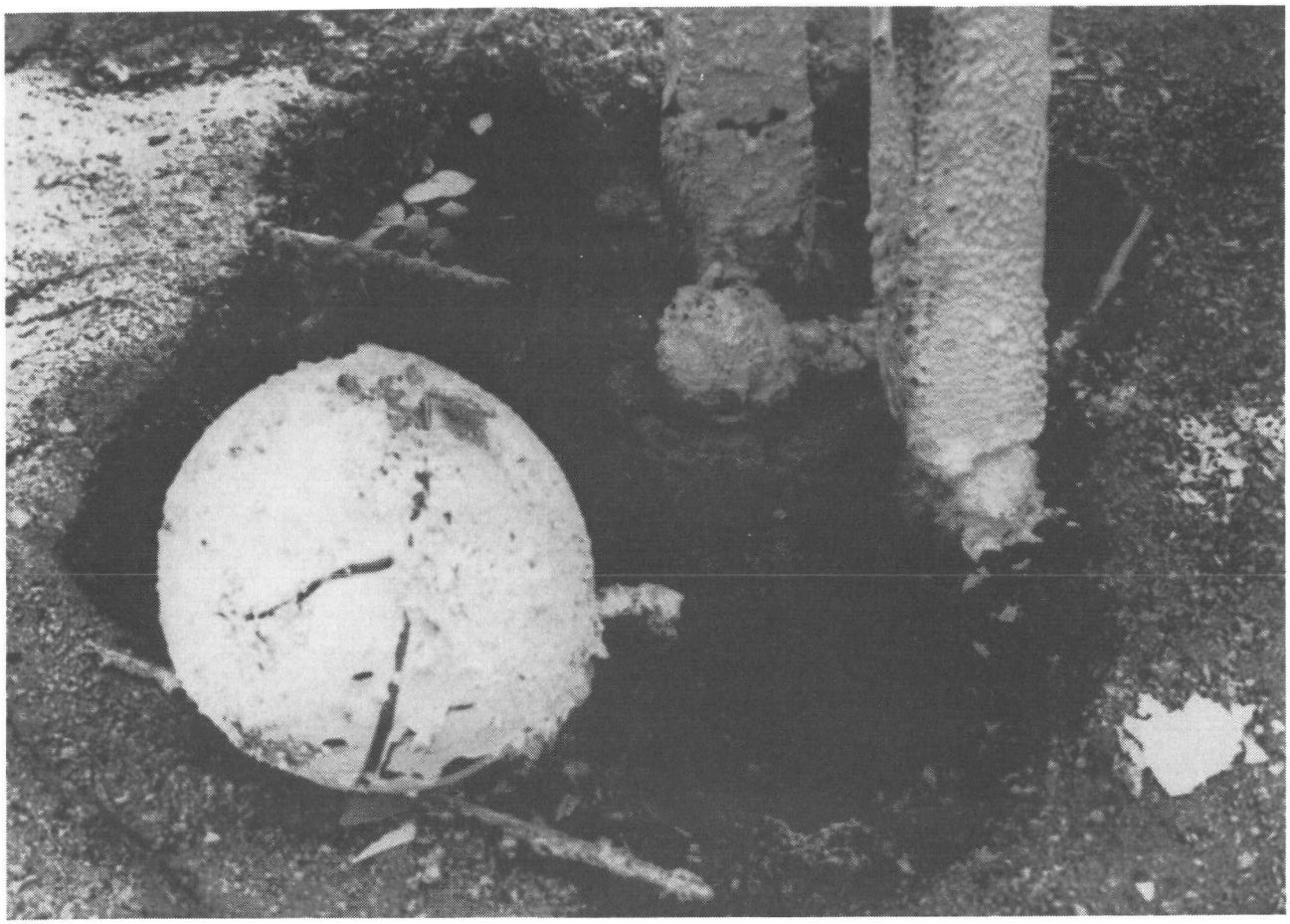

69-525-2

69-H65983-129

Figure 5-58 Contact Fireball Test, 14 April 1969, after Firing.

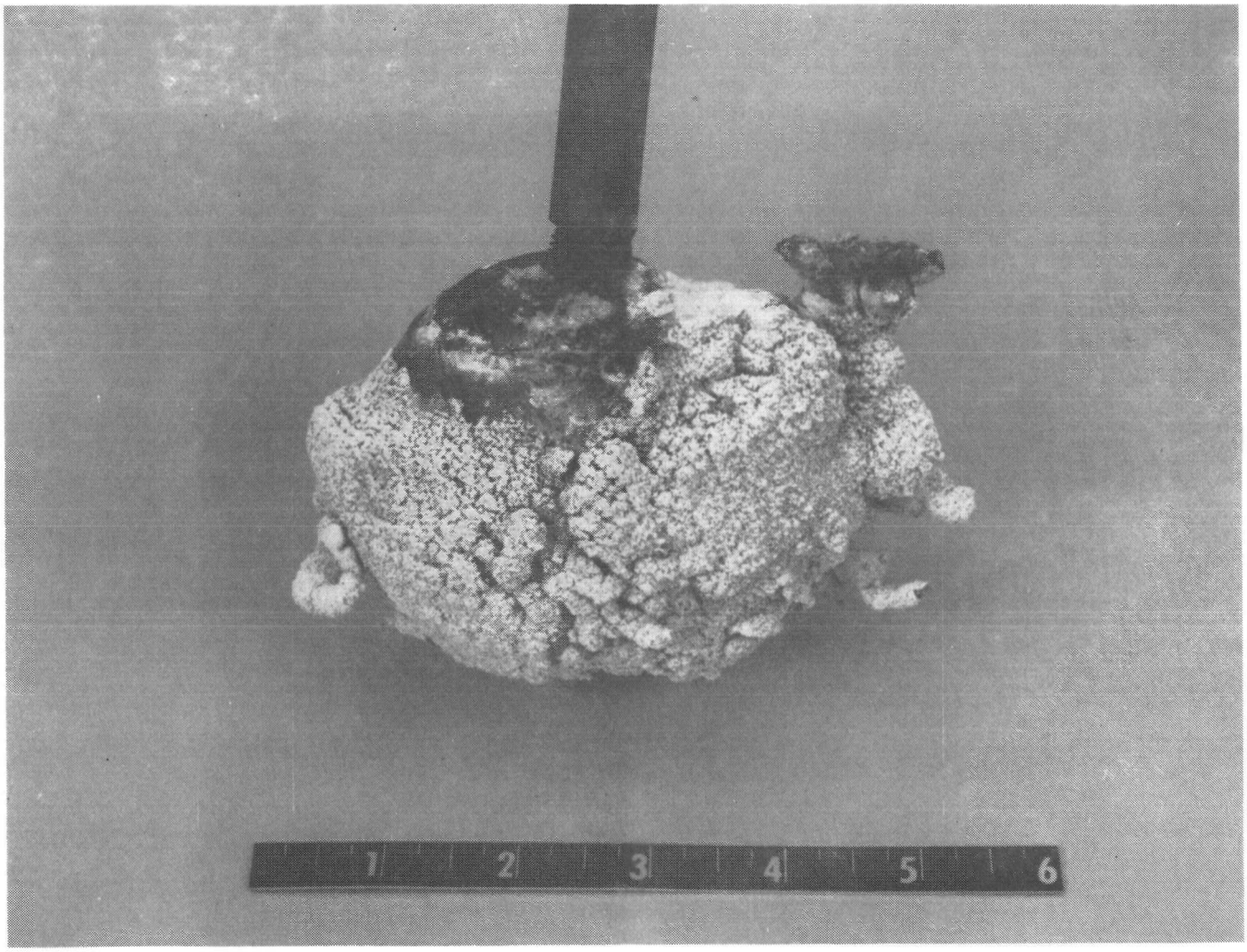

69-404-3

69-H65983-130

Figure 5-59 Proximity Test Showing Flame Deposited Material.

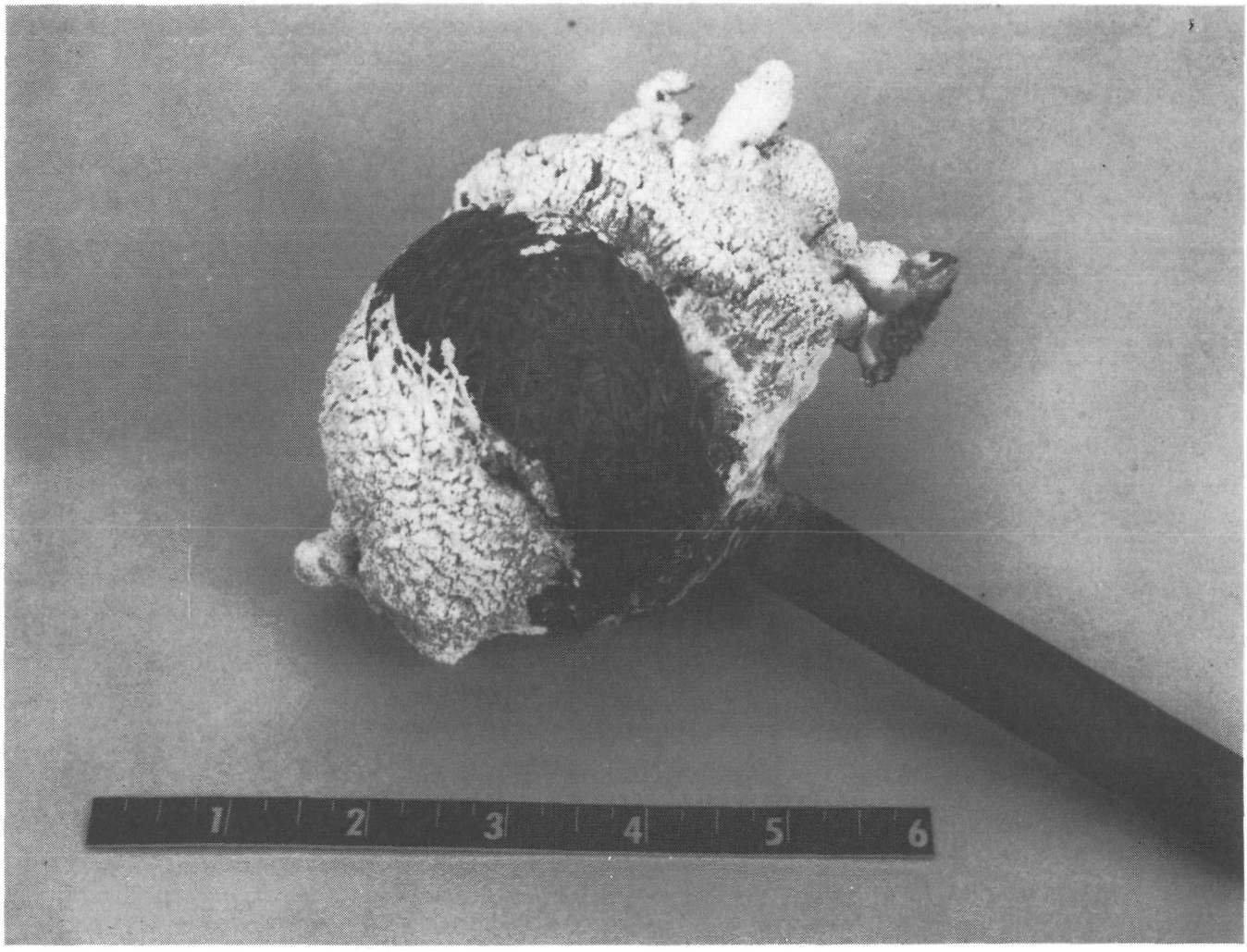

69-404-2

69-H65983-131

Figure 5-60 Proximity Test - Note Excellent Condition of Graphite Winding.

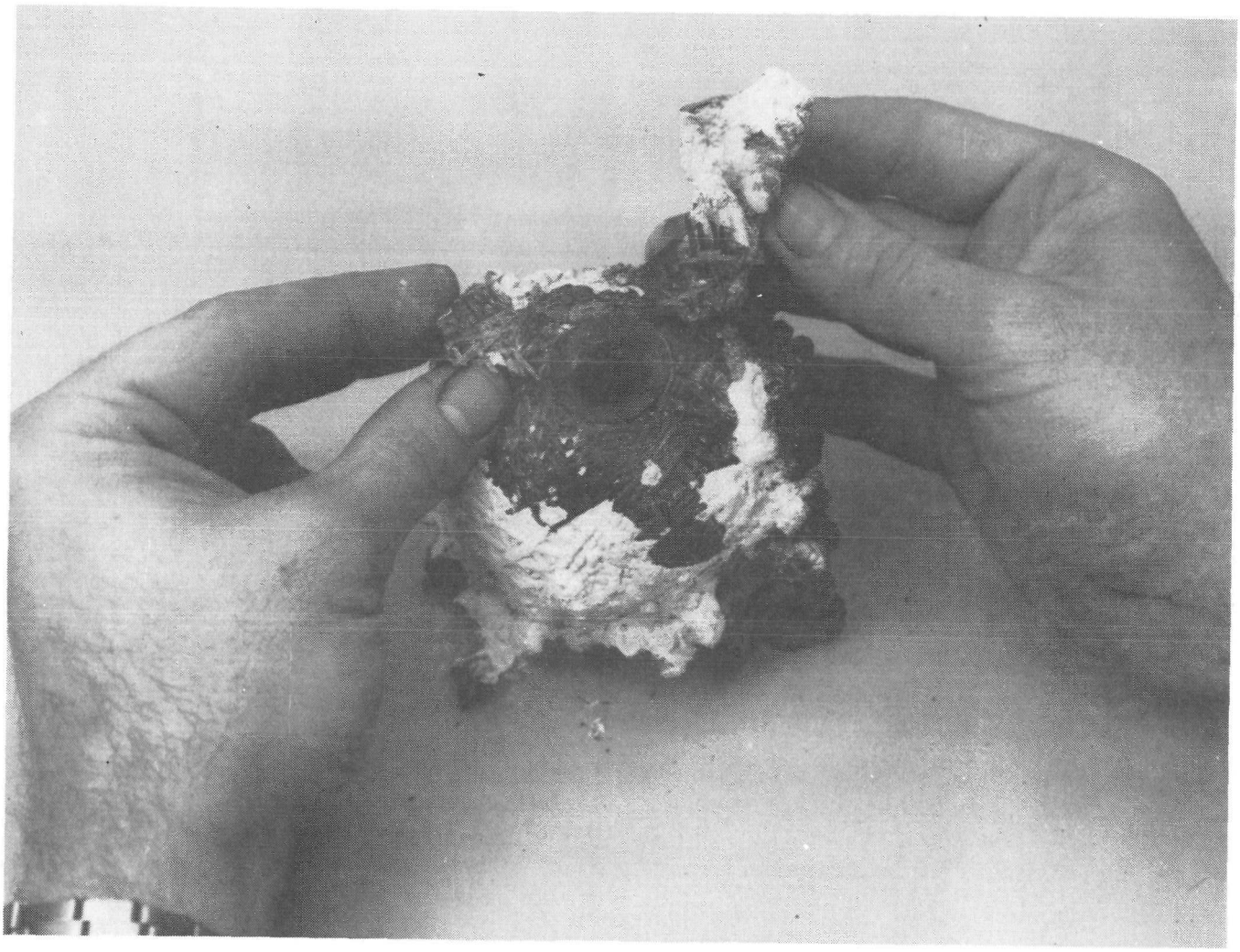

69-414-2

69-H65983-132

Figure 5-61 Contact Test.

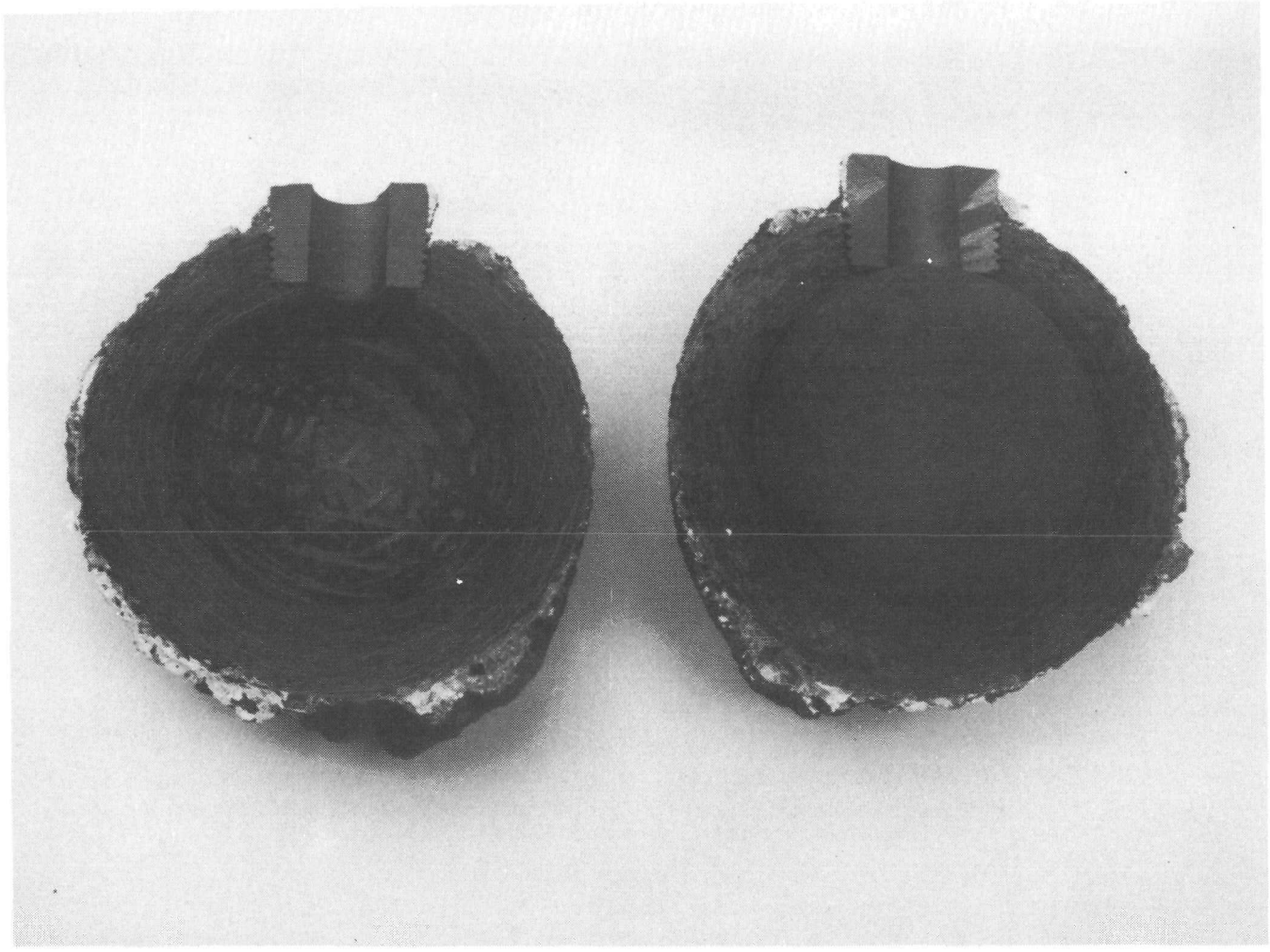

69-524-2

69-H65983-133

Figure 5-62 Sectioned Capsule After Contact Test.

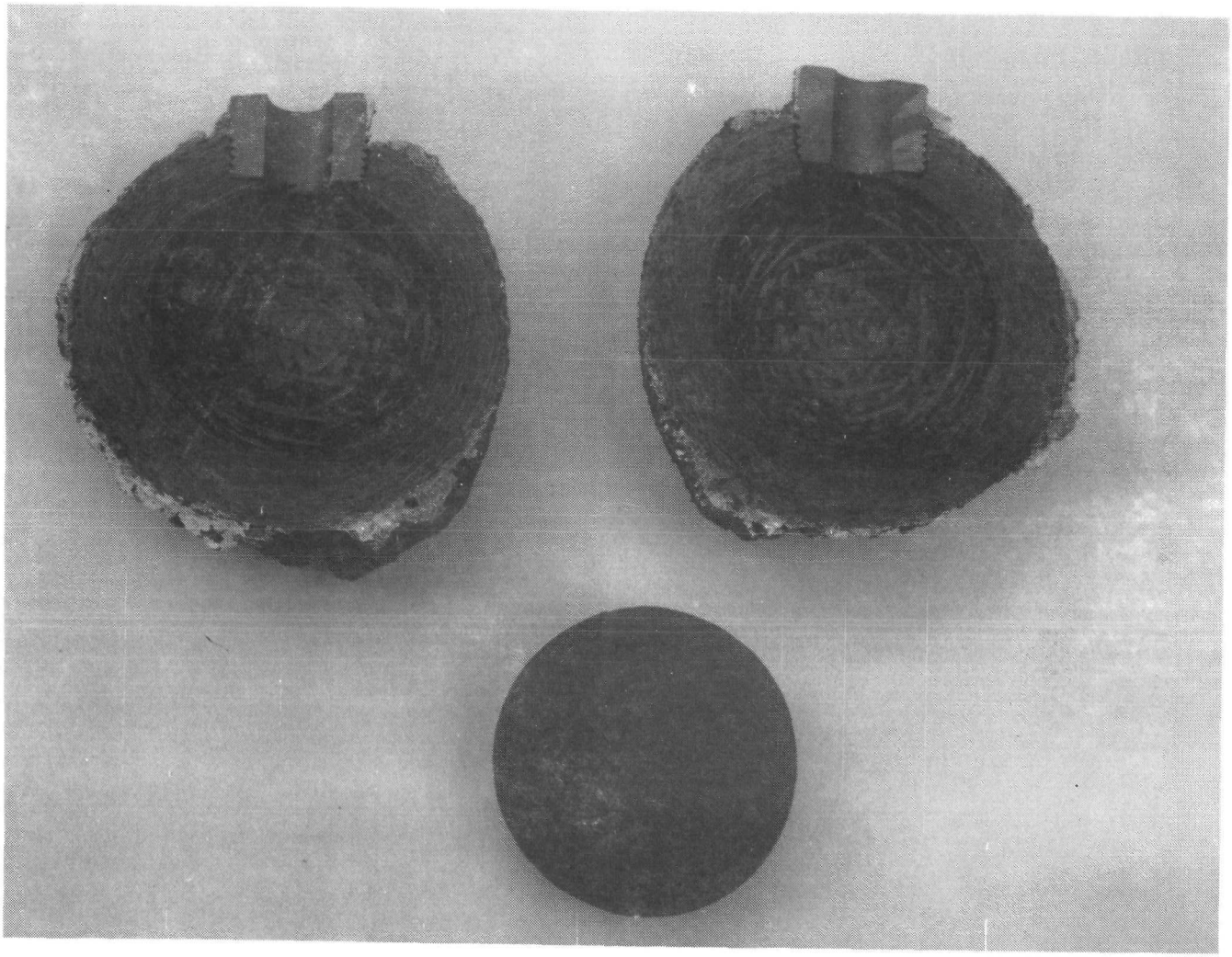

69-524-1

69-H65983-134

Figure 5-63 Sectioned Capsule After Contact Test, Core Removed.

5.6.5 CONCLUSIONS

Based on the testing of three capsules, it can be clearly concluded that the SIREN capsule successfully withstood the effects of flaming solid propellant for times up to eight minutes. The capsules were unaffected by the thermal and flame environments and it can be reasonably assumed that they could survive an even more severe environment.

APPENDIX I

SANDERS NUCLEAR

TEST PROCEDURE

SNP 100029

SIREN CAPSULE

OXIDATION TESTS

I-2

REVISION STATUS OF EACH SHEET															
SHEET			1	2	3	4	5	6	7	8	9	10	11	12	13
REVISION															
14	15	16	17	18	19	20	21	22	23	24	25	26	27	28	29
30	31	32	33	34	35	36	37	38	39	40	41	42	43	44	45

NOTES
1 SHEET ONE REVISION LETTER IS THE IDENTIFYING REVISION FOR THIS MULTISHEET DWG
2 SYMBOL ‡ INDICATES VENDOR ITEM – SEE SPEC/SOURCE CONTROL DWG
3 INTERPRET DWG PER 815002

REVISIONS			
LTR	DESCRIPTION	DATE	APPROVED

SANDERS NUCLEAR CORPORATION

CONFIDENTIAL

CONFIDENTIAL

		CONT NO	SANDERS NUCLEAR CORPORATION, Nashua, New Hampshire
		DR L. Gifford 3/4/69 DATE	
		CHK	SIREN Capsule Oxidation Tests
		ENG DEV / MECH/ELEC	
		PROJ	SIZE A; CODE IDENT NO 28428; SNP 100029
NEXT ASSY	USED ON		SCALE; SHEET 1 OF 7
APPLICATION			

OP 276 REV–

SANDERS NUCLEAR CORPORATION

REVISIONS			
LTR	DESCRIPTION	DATE	APPROVED

1.0 INTRODUCTION

The tests outlined in this procedure will be performed on six (6) B_6Si coated SIREN capsules for the purpose of determining the oxidation rate as a function of temperature. The time span for these tests is 1.5 months or approximately 1080 hours. The test temperature will range between 800 and 1800°F.

Refer to Figure No. 1 for flow chart of test program.

2.0 OBJECTIVE

The objective of the tests described herein is to establish the oxidation rate of the B_6Si coated SIREN Capsule as a function of temperature.

3.0 TEST REQUIREMENTS

3.1 APPLICABLE DOCUMENTS

Paragraph IV-C of the Statement of Work
Contract AT(29-2)-2708
Furnace and Setup Drawing Nos.

3.2 TEST CONDITIONS

3.2.1 Environment

The tests will be conducted in an air atmosphere, inside a furnace operating at selected temperatures.

3.3 REQUIRED MEASUREMENTS

Each capsule will be weighed prior to furnace heat up and during exposure period at discreet intervals.

The weight of each capsule will be determined to the nearest 0.1 gms or better.

SIZE	CODE IDENT NO	
A	28428	SNP 100029
SCALE		SHEET 2 OF 7

OP 909 REV-

REVISIONS			
LTR	DESCRIPTION	DATE	APPROVED

Weighing will be performed on a schedule delineated later in this procedure.

A thermal profile of each furnace will be obtained at 800°F, 1000°F, 1200°F, 1400°F and 1800°F, with thermocouples centered in the cylindrical opening and spaced every 2" vertically.

3.4 TEST FAILURE CRITERIA

Failure of the coated capsules shall be deemed to have occurred when the weight has decreased 10% from the initial "at temperature" weighing.

3.5 REPORTS

Summary type progress reports shall be furnished in time for the program monthly report submittal. In addition, a final report shall be written which presents and discusses the data obtained.

4.0 PROCEDURE

4.1 CAPSULE PREPARATION

Prior to coating the six capsules with B_6Si, the hole used to caustic etch out the aluminum liner will be drilled and tapped ½" - 13. A matching plug shall be fabricated from a spare capsule.

The capsule shall be suspended by means of a nickel hook and assembly made as shown in Figure No. 2 (page 7). Twisting of the two wires to form the suspension hook external to the capsule shall be accomplished after the plug is in place.

The entire capsule, including hook, will be flame sprayed with B_6Si prior to test in accordance with established procedures.

NOTE: One of the six capsules will be withheld from the flame spray procedure, i.e., not coated.

SIZE	CODE IDENT NO	
A	28428	SNP 100029
SCALE		SHEET 3 OF 7

OP 909 REV-

REVISIONS			
LTR	DESCRIPTION	DATE	APPROVED

4.2 TEST SETUP AND OPERATION

C A U T I O N : Do not chip coating on capsules or hook during weighing process. Handle coated capsule with clean nylon gloves.

4.2.1 Weigh each of three capsules (one uncoated, 2 coated) and record capsule number and initial weight.

4.2.2 Fabricate support rod from Kanthal or Nichrome wire (3 or 4 twisted strands) of sufficient length to support the capsule at the mid point (vertical) of the furnace. Tag and weigh each rod.

4.2.3 Install each capsule in a furnace, at the furnace midpoint, close top, and adjust balance. Total weight should be the same as the sum of the support bar and capsule weights.

4.2.4 Apply 300 watts of power to each furnace, setting controllers at the following temperatures:

Uncoated Capsule - 800°F
Coated Capsule - 800°F
Coated Capsule - 1000°F

Bring furnace to temperature in a 4 hour time period by increasing the power input.

4.2.5 Note whether the balance reading changes due to convection heating currents in the furnace during the heat up process. If so, record new data and rebalance as necessary.

4.2.6 When furnace temperature has been stable at the set point temperature for at least one (1) hour, reweigh each capsule, recording both time and weight in the log.

4.2.7 Weighing Schedule

4.2.7.1 Uncoated Capsule

The uncoated capsule will be tested at 800, 1200, 1400, 1600 and 1800°F for time periods sufficient to obtain a significant weight change (1 to 2%). At

SIZE	CODE IDENT NO.	
A	28428	SNP 100029
SCALE		SHEET 4 OF 7

OP 909 REV-

REVISIONS			
LTR	DESCRIPTION	DATE	APPROVED

least three data points (time and weight) shall be obtained for each temperature.

4.2.7.2 Coated Capsules

Reweigh each of the coated capsules every working day for the first calendar week of test operation. If the weight change at 800°F and/or 1000°F is less than 0.1%/day continue testing for an additional 10 days, repeating this procedure for a total of 30 calendar days.

Should either of the coated capsules exhibit no measurable weight change in 20 calendar days, shut down the furnace(s) and replace the capsule(s) with one of the remaining units, following the procedure outlined in Paragraphs 4.2.1 - 4.2.7. Set the temperature for this test 200°F higher than the test it replaces.

At the completion of the uncoated capsule tests, a coated capsule will be installed for test at 200°F higher than the then currently highest test temperature.

4.3 DATA REDUCTION

A curve of weight change rate in per cent/day as a function of reciprocal absolute temperature times 10^3 shall be generated for the uncoated and coated capsule tests.

4.4 POST TEST ANALYSIS

At the conclusion of the test program the remains of the uncoated capsule and at least two other coated capsules will be metallographically sectioned for examination and comparison with a coated but untested capsule. Photo micrographs will be taken of each section for comparison with the untested capsule and included in the test report.

SIZE	CODE IDENT NO.	
A	28428	SNP 100029
SCALE		SHEET 5 OF 7

OP 909 REV-

SANDERS NUCLEAR CORPORATION

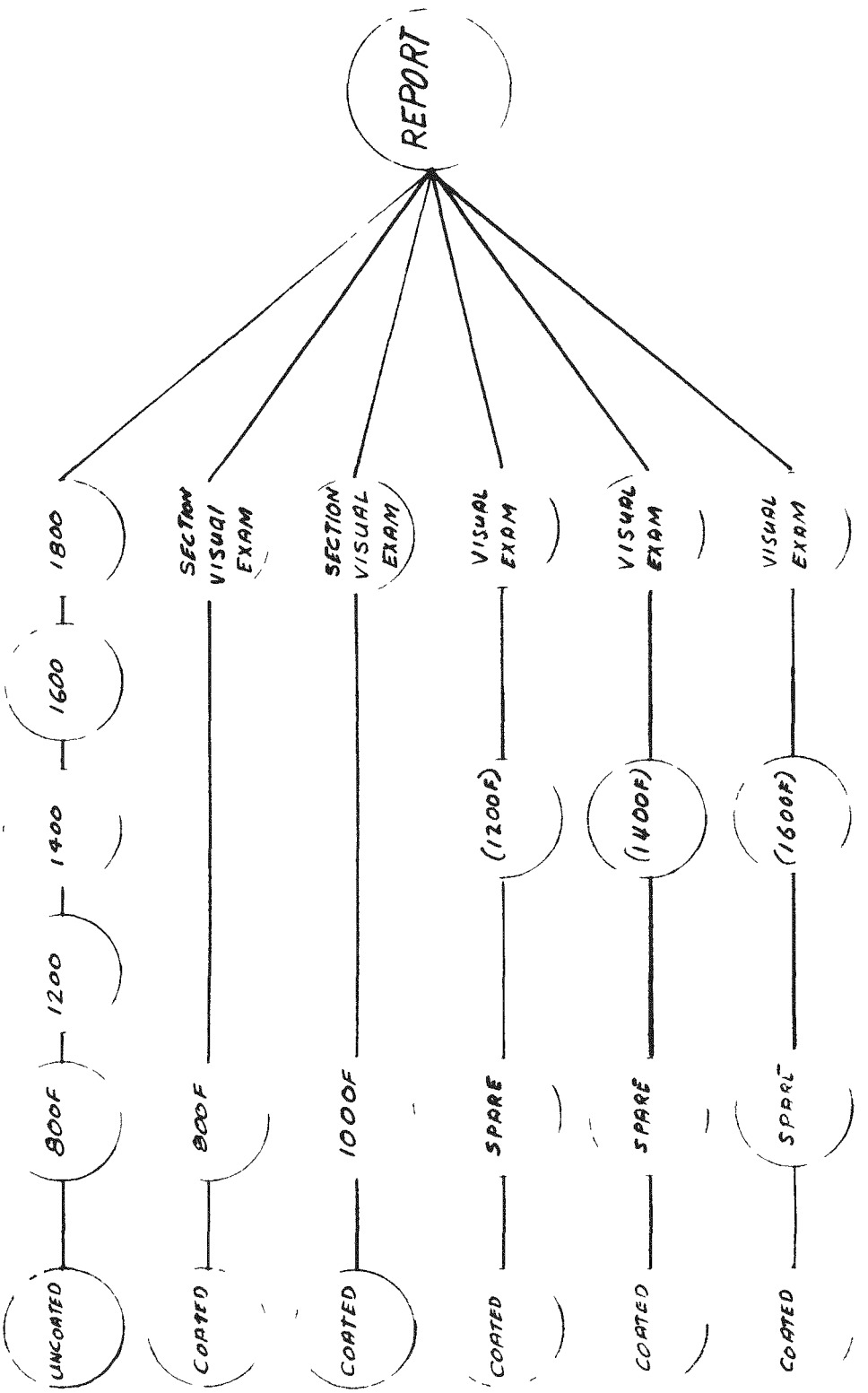

FIGURE No. 1 TEST PROGRAM FLOW CHART

SANDERS NUCLEAR CORPORATION

~~CONFIDENTIAL~~

REVISIONS			
LTR	DESCRIPTION	DATE	APPROVED

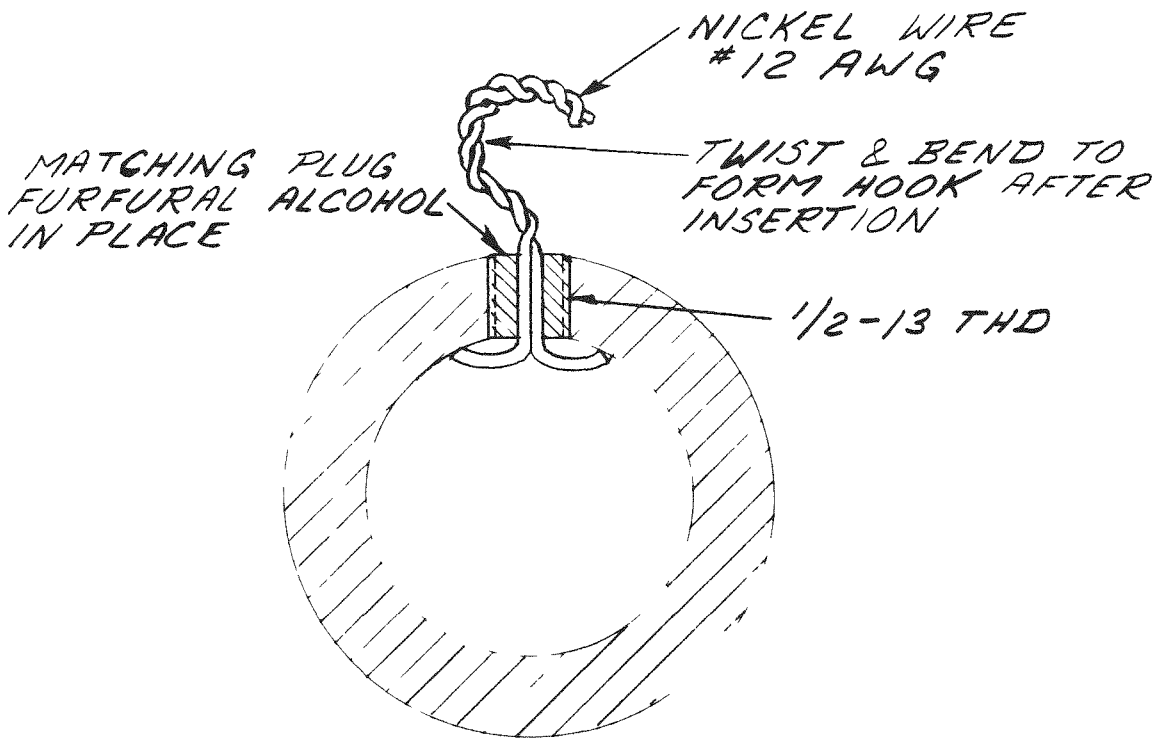

SIZE	CODE IDENT NO	
A	28428	SNP 100029
SCALE		SHEET 7 OF 7

OP 909 REV-

APPENDIX II

SANDERS NUCLEAR

TEST PROCEDURE

SNP 100030

HELIUM PERMEABILITY TEST OF SIREN CAPSULE

REVISION STATUS OF EACH SHEET															
SHEET			1	2	3	4	5	6	7	8	9	10	11	12	13
REVISION															
14	15	16	17	18	19	20	21	22	23	24	25	26	27	28	29
30	31	32	33	34	35	36	37	38	39	40	41	42	43	44	45

NOTES
1 SHEET ONE REVISION LETTER IS THE IDENTIFYING REVISION FOR THIS MULTISHEET DWG
2 SYMBOL ‡ INDICATES VENDOR ITEM – SEE SPEC/SOURCE CONTROL DWG
3 INTERPRET DWG PER 815002

REVISIONS

LTR	DESCRIPTION	DATE	APPROVED

SANDERS NUCLEAR CORPORATION

CONFIDENTIAL

CONFIDENTIAL

CONT NO

DR H.R. Safford 3/4/69 DATE

CHK

ENG DEV

ENG MECH/ELEC

PROJ [signature] 3/6/69

NEXT ASSY | USED ON

APPLICATION

SANDERS NUCLEAR CORPORATION
Nashua New Hampshire

Helium Permeability Test of
SIREN Capsule

SIZE	CODE IDENT NO	
A	28428	SNP 100030

SCALE | SHEET 1 OF 7

OP 276 REV–

REVISIONS			
LTR	DESCRIPTION	DATE	APPROVED

1.0 INTRODUCTION

The tests outlined in this procedure will be performed on three (3) SIREN Capsules for the purpose of determining the helium permeability rate of the outer capsule structure. The capsules will not have a liner material of any type.

Because of the porous nature of the SIREN outer structure, it will be necessary to perform some experimentation in order to arrive at a usable test method. The test engineer will, therefore, be permitted considerable latitude in making "on the spot" modifications to this procedure in order to accomplish the test objective.

One of two basic test methods will be used. The first will involve an attempt to evacuate the internal void volume. If pressures of the order of a few microns are achieved, standard helium leak rate determinations will be made. If a vacuum cannot be satisfactorily obtained, the capsule will be pressurized and flow rate observed using standard gas flow equipment and techniques.

2.0 OBJECTIVE

The objective of the tests delineated in this procedure is to determine the helium permeability rate of the SIREN Fuel Capsule.

3.0 PROCEDURE

This procedure has been written to provide some latitude in the actual manner in which the tests shall be conducted.

3.1 SAMPLE PREPARATION

Prepare only one of the capsules initially. The remaining two units will be prepared after the procedure has been established in order to permit modification, if necessary, of the means of access to the capsule internal void volume.

3.1.1 Drill 11/16" diameter hole on the capsule diameter.

SIZE	CODE IDENT NO	
A	28428	SNP 100030
SCALE		SHEET 2 OF 7

SANDERS NUCLEAR CORPORATION

REVISIONS			
LTR	DESCRIPTION	DATE	APPROVED

3.1.2 Smear hole sides with clear epoxy cement, insert 12" long 5/8" OD copper tubulation, rotate to cover inserted portion with epoxy and remove. Clear the tubulation opening of any epoxy, reinsert and allow epoxy to harden in accordance with Manufacturer's instructions before proceeding with the next step.

3.2 TRIAL NO. 1

3.2.1 When step 3.1.2 is completed, connect the capsule tubulation to the CEC Model 24-120B leak detector roughing manifold and determine whether or not the capsule can be evacuated to any significant low pressure (less than 100 microns of Hg). If it can, continue evacuation, cutting in leak detector manifold as appropriate and proceed with step 3.2.2. If not, skip to step 3.3.

3.2.2 If throttling of L.D. is necessary, utilize a calibrated leak attached to the capsule tubulation to determine sensitivity and minimum detectable leak (MDL). See Figure No. 1 for sketch.

If throttling is not necessary, use sensitivity and MDL determined prior to capsule evacuation with CEC Standard Leak.

3.2.3 Examine capsule with helium gas jet for specific leak points. If leaks are detected in tubulation seal area, vent test articles, seal leaks with small amount of epoxy and retest when epoxy is hard.

3.2.4. If no leaks are detected or none can be specifically located, bag capsule and pressurize bag with helium for gross leak rate determination.

3.2.5 When step 3.2.4 is complete, replace capsule in original identification container and repeat steps 3.1 and 3.2 for the two remaining units. Record results of all measurements.

3.3 TRIAL NO. 2

In the event Trial No. 1 is unsuccessful, i.e., the leak rate is too large for the CEC leak detector to handle, connect capsule

SIZE	CODE IDENT NO	
A	28428	SNP 100030
SCALE		SHEET 3 OF 7

OP 909 REV-

REVISIONS			
LTR	DESCRIPTION	DATE	APPROVED

tubulation to a low range flow meter (range to be determined by experimentation) and low range manometer in a manner which will permit measurement of helium flow through the capsule and helium pressure within the capsule as shown in Figure No. 2. Instrumentation will have to be determined by trial and error.

3.3.1 Measure the flow rate as function of pressure and record results for at least four internal helium pressures.

4.0 TEST DATA CALCULATIONS & REPORT

4.1 TRIAL NO. 1

When using the CEC standard leak, the following equations apply:

$$1)\quad S_{LD} = \frac{LR_{SL}}{DIV_{LRM} \times Atten} \times Temp\ Corr_{SL}$$

where S_{LD} is the leak detector sensitivity; LR_{SL} is the leak rate as specified on the standard leak in atm cc/sec; DIV_{LRM} is the number of divisions indicated on the leak rate meter; and Atten is the multiplier; and $Temp\ Corr_{SL}$ is the temperature correction, shown at standard leak (1.5%/^{o}F).

$$2)\quad LR = S_{LD} \times DIV_{LRM}$$

where LR is the leak rate; S_{LD} and DIV_{LRM} as previously defined.

$$3)\quad MDL = S_{LD} \times Div\ Noise_{LRM}$$

where MDL is the minimum detectable leak in atm cc/sec; S_{LD} as defined previously; $Div\ Noise_{LRM}$ is the no. division indicated on LRM as spurious outputs multiplied by 2. (NOTE: Noise specification is 2% FS peak to peak, therefore, $Div\ Noise_{LRM} = 4$.)

SIZE	CODE IDENT NO	
A	28428	SNP 100030
SCALE		SHEET 4 OF 7

OP 909 REV-

REVISIONS			
LTR	DESCRIPTION	DATE	APPROVED

4.2 TRIAL NO. 2

The standard gas laws will be used in determining the helium leak rate and referred to STP.

4.3 PERMEATION RATE

The helium permeation rate through any material generally is given in terms of volume per unit time per unit area, therefore, the test results of either Trial No. 1 or No. 2 will be calculated to reflect this nomenclature.

The internal and external average surface area will be determined for each capsule. The average of these two numbers will then be used to determine the permeation rate as follows:

$$\text{Permeation Rate} = \frac{\text{Leak Rate (cc/sec)}}{\text{Surface Area } (cm^2)} = cc/sec/cm^2$$

4.4 ERROR ANALYSIS

Perform a simple error analysis to determine the error limits for the data obtained.

4.5 REPORT

Prepare a final report, disclosing the test method used and test results. If Trial No. 2 is the method used, include a curve showing flow rate vs pressure for each capsule so tested.

SIZE	CODE IDENT NO	
A	28428	SNP 100030
SCALE		SHEET 5 OF 7

OP 909 REV-

SANDERS NUCLEAR CORPORATION

REVISIONS			
LTR	DESCRIPTION	DATE	APPROVED

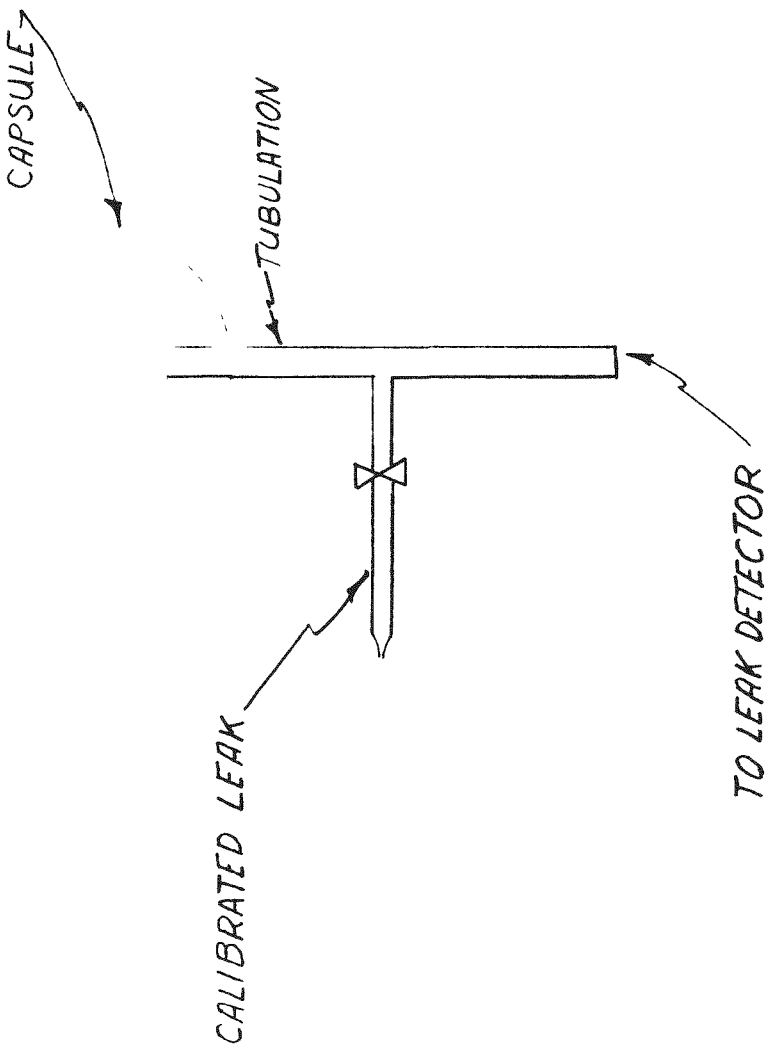

FIGURE NO. 1

SIZE	CODE IDENT NO	
A	28428	SNP 100030
SCALE None		SHEET 6 OF 7

OP 909 REV-

SANDERS NUCLEAR CORPORATION

~~CONFIDENTIAL~~

REVISIONS			
LTR	DESCRIPTION	DATE	APPROVED

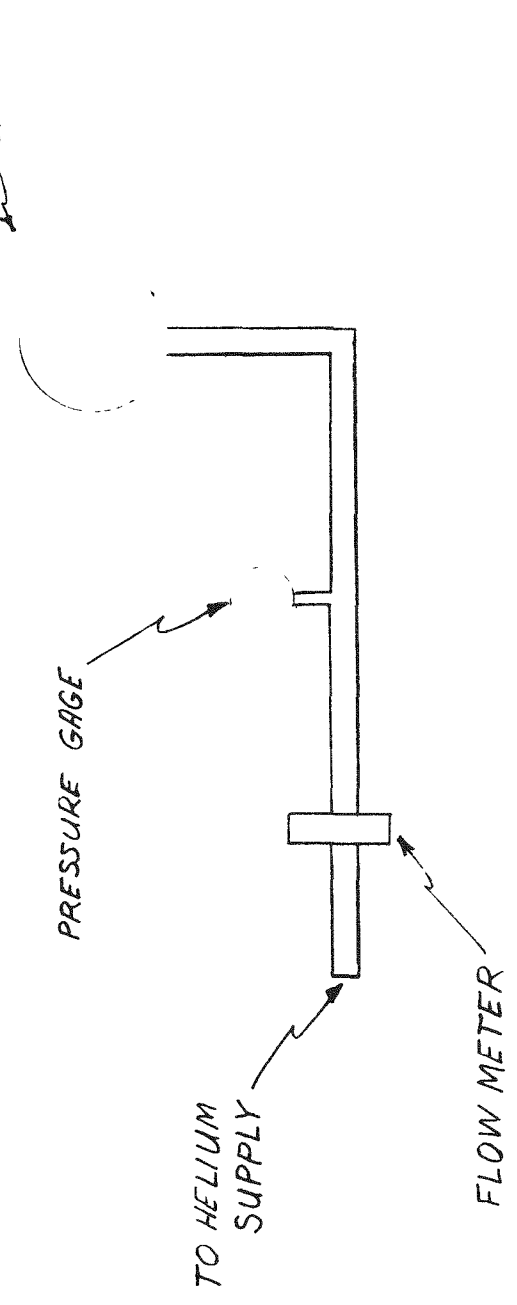

FIGURE NO. 2

SIZE	CODE IDENT NO.	
A	28428	SNP 100030
SCALE		SHEET 7 OF 7

OP 909 REV-

APPENDIX III

SCALING OF PLASMA-ARC TESTS TO HYPERSONIC FLIGHT CONDITIONS

APPENDIX III

SCALING OF PLASMA-ARC TESTS TO HYPERSONIC FLIGHT CONDITIONS

In hypersonic reentry the diffusion-controlled rate of graphite loss is written[1], [2]

$$\dot{m}_D^o \, (R_N/P_e)^{1/2} = 0.00635 \text{ lb ft.}^{-3/2} \text{ atm}^{-1/2} \text{ sec}^{-1} \qquad (1)$$

at the stagnation point of a sphere. This expression has been derived from a correlation of numerical boundary layer solutions on the basis of various aerodynamic and thermodynamic relationships appropriate to hypersonic flow. In particular, it has been assumed that:

$$H_e \approx u_\infty^2 / 2 \qquad (2)$$

$$(R_N/u_\infty) \; (du_e/ds) \approx (2\epsilon)^{1/2} \qquad (3)$$

where ϵ is the density ratio across the bow shock and du_e/ds is the velocity gradient along the spherical surface.

On the other hand, from a more fundamental point of view, the mass transfer should be expressible as the product of a diffusion coefficient times a concentration gradient, or density difference divided by boundary layer thickness. On this latter basis:

$$\dot{m}_D^o \propto \left[\rho^* \mu^* \, du_e/ds \right]^{1/2} \qquad (4)$$

with fluid properties evaluated at some point in the boundary layer. Scaling to conditions where conditions a) and b) are not valid must be accomplished in this fundamental frame of reference.

The fundamental formula (2) may be expressed in a practical form by noting that the fluid property $\rho^* \mu^*$ may be approximately expressed in the form:

$$\rho^* \mu^* \approx P_e \; f(H_e/H_{ref}) \tag{5}$$

With this kind of a correlation in mind, Gilbert and Scala have published the graphite mass loss formula in a form equivalent to:

$$\dot{m}^o_D (R_N/P_e)^{1/2} \tag{6}$$

$$= 0.00635 \; (u_\infty{}^2/2H_e)^{1/4} \left[(2\epsilon)^{1/2} (u_\infty/R_B) \; (ds/du_e) \right]^{1/2}$$

If the flow is sufficiently hypersonic, the factors in the brackets are essentially unity and we have the familiar expression

$$\dot{m}^o_D (R_N/P_e)^{1/2} = 0.00635 \tag{1}$$

At moderate supersonic Mach numbers the factors can be computed from gas tables and the correlation of stagnation point velocity gradient given in Reference 3. The result is illustrated in the Figure where the ratio of $\dot{m}^o_D$ to its asymptotic value is plotted versus Mach number. As an example, in a test conducted at M = 2.5, the mass loss expected is about 80% of that calculated from the simple expression (1).

SANDERS NUCLEAR CORPORATION

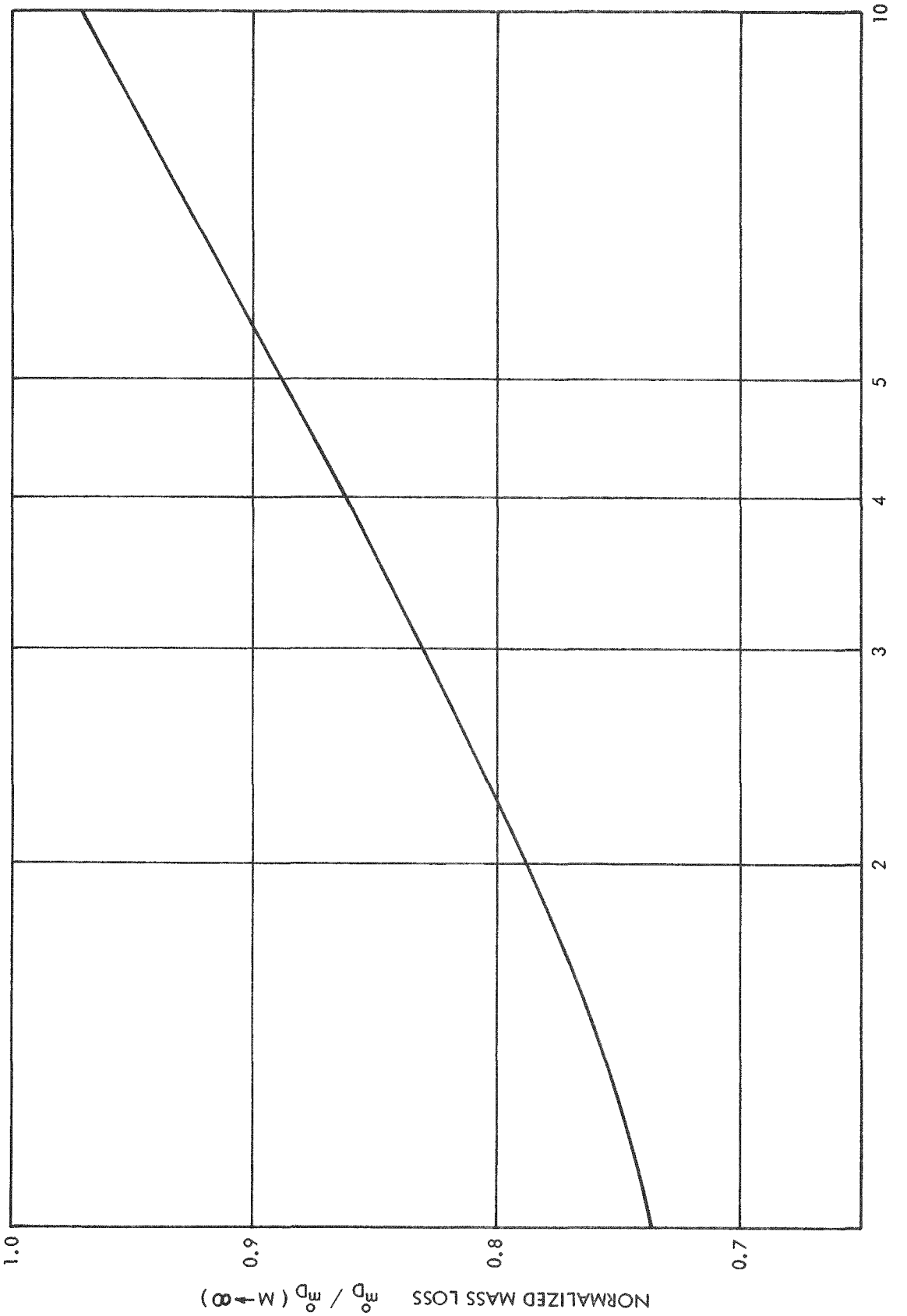

69-H65983-125

Scaling Factor as a Function of Mach Number.

REFERENCES

1. Metzger, J. W., et al, "Oxidation and Sublimation of Graphite in Simulated Reentry Environments", AIAA Journal, Vol. 5, No. 3, March 1967.

2. Gilbert, L. M. and Scala, S. M., "Combustion and Sublimation of Cones, Spheres, and Wedges at Hypersonic Speeds", AIAA Journal, Vol. 3, No. 11, November 1965.

3. Romig, M. F., "Stagnation Point Heat Transfer for Hypersonic Flow", Jet Propulsion, Vol. 26, No. 12, December 1956.

BLANK